THESIS AND ABSTRACT

The role of ultraviolet light in the image and non-image forming visual systems of mice

Thomas Scarth Watson

Brasenose College, Oxford

Nuffield Department of Clinical Neurosciences

Nuffield Laboratory of Ophthalmology

Thesis submitted in fulfillment of the requirements for the degree of Doctor of Philosophy, University of Oxford

Word count: 48,909

Trinity Term 2014

Abstract

The role of ultraviolet light in the image and non-image forming visual systems of mice

Thomas Scarth Watson

Thesis submitted in fulfillment of the requirements for the degree Doctor of Philosophy, University of Oxford, Trinity Term 2014

Long thought to be absent from mammals, UV sensitivity has now been established in many species, including mice, where it has been found to provide visual sensitivity and drive circadian responses. Compared to closely related species, the murine UVS cone photopigment is both in relatively high abundance and is associated with a unique expression gradient across the retina, raising questions concerning the function of UV sensitivity that may be relevant to other mammals. Here we investigate the non-image and image forming roles of UV light in mice. Phase-shifting sensitivity changes in rod and cone photoreceptor mutants/ transgenics indicated a significant contribution by cone photoreceptors to this assay of photic-entrainment under UV light. Generation of an *Opn1sw* knockout lacking the UVS opsin gene confirmed a critical role of UVS cones in the non-image forming system of the mouse, differing from that established for the middle-wave sensitive (MWS) cone opsin, and confirmed that UV light could be used for visual tasks in a visual adaptation of the novel-object recognition assay. Finally, examination of retinal c-fos induction found evidence of an inhibitory influence of the cone pathway linked to short-wavelength sensitivity. That the contribution of UVS opsin was significantly greater than similar experiments have found for MWS cones, despite widespread cone opsin co-expression, may indicate a distinct role for the UVS-only s-cones in the non-image forming visual system. Overall these data suggest that the role of ultraviolet light in the circadian system of the mouse may be central to its unique cone opsin characteristics and provides new insight concerning this critical research model relevant to its use in the investigation of human biology.

Author's Publications

Hughes, S., **Watson, T.S**., Foster, R.G., Peirson, S.N., and Hankins, M.W. (2013). Nonuniform distribution and spectral tuning of photosensitive retinal ganglion cells of the mouse retina. Curr. Biol. CB *23*, 1696–1701.

Van Oosterhout, F., Fisher, S.P., van Diepen, H.C., **Watson, T.S**., Houben, T., VanderLeest, H.T., Thompson, S., Peirson, S.N., Foster, R.G., and Meijer, J.H. (2012). Ultraviolet light provides a major input to non-image-forming light detection in mice. Curr. Biol. CB *22*, 1397–1402.

Acknowledgments

While amazed I'm suddenly approaching the end of my degree, I'm so thankful for the opportunity to realise what was truly a lifelong goal of studying at Oxford. Thinking of who to thank from the best four years of my life is extremely difficult but firstly thank-you to the Clarendon Fund and Brasenose College for the funding and support that made this time possible.

Thank-you as well to the whole of the Nuffield Department of Clinical Neuroscience and in particular the Nuffield Laboratory of Ophthalmology for your support. Thanks to Jovi, Jess and David, fellow DPhil students who helped make the lab such a positive and fun place to work. As well to Eric Tam for his help setting up the Novel Object experiments, being always happy to give advice and help run experiments while somehow balancing all that with a new baby and another on the way! Thanks to my co-supervisor Dr. Sumanthi Sekaran for her great help in bringing me to the UK and getting me settled in the lab. Similarly to Dr. Stuart Peirson for constantly being available for experimental advice, data analysis, literature questions and (of course) reading over many many drafts of this thesis! I'm sure I wouldn't have got to this stage without your help. Huge thank-you to Dr. Steven Hughes (who I probably bothered more than any other) for putting up with my endless requests and questions about immunohistochemistry protocols, antibodies, confocal imaging and much more. You always found time to help and your sense of humour made the time in the lab so much more enjoyable. Thanks to Professor Hankins for his advice throughout my degree and especially for his help in the final stages of this thesis. Finally to the rest of the group, Aarti, Lawrence, Lindsay, Violetta, Simona and everyone else in the department support staff.

I'm so grateful to all the many and life-long friends I've made along the way from Brasenose, the department and the wider Oxford community. As well to all the members of the OUBC, too many to name, who have played an integral role in my amazing Oxford experience. To my roommates at 40 Henley Street and all those I've trained and raced with, thank-you.

My family is always such a big part of my life and this degree has been made possible through the love and constant support of my parents always encouraging me to dream big and then helping to make those goals possible. Of course to my best friend and twin brother Alec with whom I've been able to share this experience and to my sister Maryann for being on call whenever things got stressful (and whose shark research has been a great reminder of how tame my work really is).

Last, but certainly not least, to my supervisor Professor Russell Foster whose constant positivity has made my time in the department such a pleasure. From my initial e-mail out of the blue to securing funding to my pursuits in and out of the lab I've always known I had your full support. The encouragement and trust you've shown me to manage my project has been invaluable and I'd hope to be able to emulate some portion of your enthusiasm in all my future exploits. Your contributions to circadian research are inspiring and I know you'll continue to inspire many others in the years ahead.

Abbreviations

ABCR	- ATP binding cassette transporter
AII	- type A II amacrine cells
Alpha (phase)	- activity phase
AMPA/KA	- AMP-activated protein kinase alpha
ANOVA	- analyses of variance test
AOP	- accessory optic pathway also AOS-accessory optic system
ARP	- acidic ribosomal protein
atRDH	- all-*trans* retinol dehydrogenase
B2M	- β2 Microglobulin
BMAL1	- brain and muscle ARNT (Aryl hydrocarbon receptor nuclear translocator) -like 1
B-Gal	- beta-galactosidase
CaMK	- Ca^{2+}/calmodulin dependent protein kinase
11cRDH	- 11-*cis* retinol dehydrogenase
CKI	- casein kinase I
cl	- attenuated diphtheria toxin fused to cone opsin promotor
CLOCK	- circadian locomotor output cycles kaput
CNG	- cyclic nucleotide gated (channel)
Cpd	- cycles per degree
CRALBP	- cellular retinaldyhyde binding protein
CRBP	- cellular retinoid binding protein
CRE	-cyclic AMP (adenosine monophosphate) response element
CREB	- CRE binding protein
CRTC1	- CREB-related transcription coactivator 1
CRY	- cryptochrome
CT	- circadian time
DAG	- diacylglycerol
DAPI	- 4',6-diamidino-2-phenylindole
DD	-constant dark

dLGN	- dorsal LGN
DT-A	- diphtheria toxin subunit A
Egr1	- Early growth response 1
ENU	- N-ethyl-N-nitrosourea
ER	- endoplasmic reticulum
ERG	- electroretinogram
EWN	- Edinger-Westphal nucleus
EYFP	- enhanced yellow fluorescent protein
Gapgh	- Glyceraldehyde 3-phosphate dehydrogenase
GC	- Guanylyl cyclase
GCL	- ganglion cell layer
(c)GMP	- (cyclic) gaunosine monophosphate
GNAT1	-guanine nucleotide binding protein (G protein), alpha transducing activity polypeptide 1
hr	- hour
IC50	- half maximal irradiance
IF (visual system)	- image forming (visual system)
IGL	- intergeniculate leaflet
INL	- inner-nuclear layer
IP_3	- inositol triphosphase
IPL	- inner plexiform layer
IR	- infra-red
IRBP	- interphotoreceptor retinoid binding protein
IRC	- irradiance response curve
KO	- knockout
LD (cycle)	- Light/Dark (cycle)
LED	- light emitting diode
LGN	- lateral geniculate nucleus
LH/AH	- lateral/ anterior hypothalamus
LL	- constant light
LRAT	- lecithin retinol acyl transferase

LWS	- long-wave sensitive (cone opsin)
M-cells	- parasol ganglion cell, also magnocells
MAPK	- mitogen activated protein kinase
mGluR6	- metabotrophic glutamate receptor 6
min	- minute
mRNA	- messenger-RNA
MWS	- middle-wave sensitive (cone opsin)
N^2	- liquid nitrogen
NIF (visual system)	- non-image forming (visual system)
NIR	- near infrared
NOR	- novel object recognition
NOT	- nuclei of the optic tract
NPAS2	- neuronal PAS domain-containing protein 2
NR4A1	- nerve growth factor 1B
OKR	-optokinetic response
ONL	- outer-nuclear layer
OPL	- outer plexiform layer
Opn1mw	- MWS opsin gene
Opn1sw	- UVS opsin gene
Opn1sw KO	- refers to *Opn1sw*$^{tm1(KOMP)Vlcg}$ model generated as described in Methods Chapter 2
Opn4	- melanopsin gene
OPN4L	- long-isoform of melanopsin
OPN4S	- short-isoform of melanopsin
P-cells	- midget ganglion cell or parocells
PACAP	- pituitary adenylate cyclase activating peptide
PBS	- Phosphate Buffered Saline
PCR	- polyermerase chain reaction
PDE	- phosphodiesterase
PER	- period
PFA	- paraformaldehyde

PI3K	- phosphoinositide 3-kinase
PIP_2	- phosphatidylinositol biphosphate
PKA	- protein kinase A
PLCβ4	- Phospholipase C Beta4
PLR	- pupillary light response
PON	- pretectal olivary nuclei (also OPN- olivary pretectal nuclei)
POS	- photoreceptor outer-segment (layer)
PP	- protein phosphatase.
(i)pRGC	- (intrinsically) photosensitive retinal ganglion cell
rd	- mutation of rod photoreceptor cGMP-phosphodiesterase β subunit
Rdta	- rhodopsin targeted diphtheria toxin gene
RF	- receptive field (of cell)
RGC	- retinal ganglion cell
Rho	- Rhodopsin gene
Rho (phase)	- rest phase
RHT	- retinohypothalamic tract (RHT)
ROR	- retinoid-related orphan receptor
RPE	- retinal pigment epithelium
RPE65	- retinal pigment epithelium-specific protein 65kDa
RT	- room temperature
s	- second
SC	- superior colliculus
SCN	- suprachiasmatic nucleus or nuclei
SEM	- standard error of the mean
Sik1	- Salt inducible kinase 1
SPZ	- subprarventricular zone
Tau	- period
TKO	- triple-knockout (of cones, rods, melanopsin)
TRPC	- transient receptor potential channel
TRβ	- thyrioid hormone receptor beta
TTFL	- transcription/ translation feedback loop

UV	- Ultra-violet
UVS	- Ultraviolet-sensitive (cone opsin)
V1	- primary visual cortex or Striate Cortex
VEP	- visual evoked potential
VLPO	- ventralateral preoptic nucleus
VOCC	- voltage-operated calcium channel
VS	- violet sensitive cone opsin
WT	- wildtype
ZT	- zeitgeber time

Chapter 1: **General Introduction**

1.1 Retinal Structure and Function

The vertebrate retina is the light sensitive layered neural tissue in the eye. It is made up of two separate structures, the neural retina and the retinal pigment epithelium (RPE). Both are derived from the optic vesicle which, for humans, appears by 4 weeks into development (Forrester et al., 2002a). The critical layered organization of the neural retina begins to be recognizable from 7 weeks but cell types continue to develop and migrate with photoreceptor outer segments beginning to form around 5 months post-fertilization (Forrester et al., 2002a).

The mature retina has 10 layers (Figure 1.1) that can be classified from the back of the eye out towards the lens and cornea as consisting of the RPE, the photoreceptor layer, the external limiting membrane, the outer nuclear layer (ONL), the outer plexiform layer (OPL), the inner nuclear layer (INL), the inner plexiform layer (IPL), the ganglion cell layer (GCL), nerve fiber layer and the inner limiting membrane. Retinal Ganglion Cell axons run in the nerve fibre layer to exit the eye at the optic nerve head. At the optic nerve head, the ophthalmic artery enters the eye supplying the inner retinal layers. Blood vessels are also found within the pigmented choroid, supplying outer retina, ciliary body and iris (Forrester et al., 2002b). The organization can be alternatively described as 5 alternating layers of nerve cell bodies and synapses (Purves, 2001a). The cell bodies in the INL, ONL and GCL are spaced by the synaptic processes in the two plexiform layers. In terms of cell types, the neuronal cells include photoreceptors, bipolar cells, ganglion cells, amacrine and horizontal

cells, and these are supported by three types of glial cell comprising astrocytes in the optic nerve fiber layer, microglial cells in the INL and Müller cells found across the retina (Haverkamp and Wässle, 2000). One example of an important role for retinal glial cells is the tight and adherent junctions both between Müller cells and with photoreceptors that form the retinal barrier termed the external limiting membrane that separates the photoreceptor cell bodies in the ONL from the protein-rich fluid matrix in the interphotoreceptor space surrounding the outer segments (Omri et al., 2010).

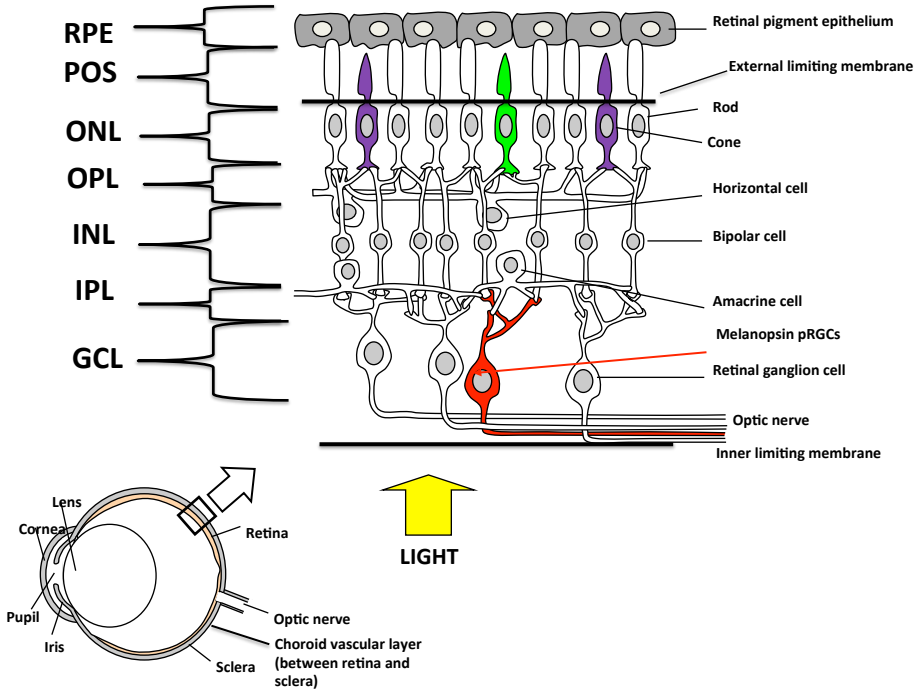

Figure 1.1 The Mammalian Retina: Structure and Layers The mammalian retina consisting of the Retinal Pigment Epithelium (**RPE**), the photoreceptor outer segment layer (**POS**), the external limiting membrane, the outer nuclear layer (**ONL**), the outer plexiform layer (**OPL**), the inner nuclear layer (**INL**), the inner plexiform layer (**IPL**), the ganglion cell layer (**GCL**), nerve fiber layer to optic nerve (note also entry point for blood supply to inner retina) and the inner limiting membrane. The direction of light entering the retina is also depicted and major retinal cell types labeled on the right.

The Photoreceptors

The photoreceptors contain light absorbing photopigment proteins. In the presence of light, the process of phototransduction triggers the change in cell membrane potential that is essential to vision (Forrester et al., 2002c). Photoreceptors require the support of the RPE, which has many key roles in the retina including immunoregulation, maintaining the blood-retinal barrier and retinoid metabolism. Perhaps its most vital, however, is in photoreceptor renewal where it actively recycles the tips of outer-segments to maintain photoreceptor function (Forrester et al., 2002c). The two classic categories of vertebrate visual photoreceptors are rods and cones. While rods contain the photopigment rhodopsin, maximally sensitive to 497-500nm light in most land dwelling vertebrates (Soucy et al., 1998; Toda et al., 1999), vertebrate cones may express any one of 4 different types of visual pigment named according to their maximal absorption from long-wave sensitive to ultraviolet sensitive. Humans have long-wave sensitive (LWS), middle (MWS) and short wave sensitive (SWS) cone classes. Sequence analysis has revealed that while LWS and MWS cones have 98% similarity they only share 40% homology with the SWS opsin gene. This points to an ancient division between the L/MWS and SWS genes while the LWS and MWS division may have occurred far more recently (Nathans et al., 1986). Mice, by contrast, have only two cone opsins, a MWS cone with peak absorption at 508nm and an ultraviolet-sensitive cone (UVS) at 360nm (Jacobs et al., 1991; Nikonov et al., 2006).

The cell membrane opsin proteins are covalently linked through a Schiff base to a chromophore to constitute the visual pigment. The major steps in the phototransduction

process in rods and cones are shown in Figure 1.2. Light absorption by the G-protein coupled receptor opsin causes the chromophore (vitamin A derived 11-*cis*-retinal for birds or mammals or vitamin A2 derived 11-*cis*-3,4 dihydroretinal in certain fish, reptiles and amphibians (Hunt et al., 2001a)) to photoisomerize from 11-*cis* to all-*trans*. The resulting instability leads to the opsin shifting to a metarhodopsin II intermediate, activating the G-protein coupled to the receptor, transducin. Transducin activation lowers the cyclic gaunosine monophosphate (cGMP) concentration and the drop in cGMP closes cGMP gated cation channels in the cell's plasma membrane so that the photoreceptors hyperpolarize. Closure of voltage-gated Ca^{2+} channels results in a reduction in the release of the major retinal neurotransmitter, glutamate. Glutamate is released at high levels in the dark but the graded hyperpolarization response to light in photoreceptors decreases glutamate at the synapses with bipolar cells and this causes different responses depending on the type of bipolar cell being synapsed too (Forrester et al., 2002d).

Figure 1.2 Summary of Phototransduction in Rods and Cones Following light absorption by the photopigment (Step 1), a conformational shift of the chromophore isomerizing to all-*trans* activates the receptor consisting of 7-transmembrane domains (R to R*). The activated receptor associates with an inactive

G-protein resulting in the release of GDP and the binding of GTP by the α-subunit (Gα) (Step 2), which activates the G-protein. Note that the R* is not altered and can diffuse to contact another inactive G-protein and repeat the process. In the case of rods the photopigment receptor is rhodopsin and in cones the receptor is one of the cone opsins. The G-protein is Transducin for both rods and cones. Two activated transducin G-proteins bind to the inhibitory γ subunits of the enzyme cGMP phosphodiesterase (PDE) to activate it (Step 3). Activated PDE catalyze the hydrolysis of cGMP to GMP (Step 4). cGMP is a cellular messenger normally maintained at a steady level in the dark between its synthesis by guanylyl cyclase (GC) and hydrolysis through residual PDE activity, and the decrease in its concentration closes cGMP gated cation channels (CNG channels, CNGA1/B1 in rods (Weitz et al., 2002), A3/B3 in cones (Peng et al., 2004)) in the membrane (Step 5). The closed channels result in a reduction in the cation influx into the photoreceptor outer-segment, which contains the discs that house the opsin G-protein coupled receptors, and membrane hyperpolarization. Hyperpolarization results in reduced glutamate release at the photoreceptor/ bipolar cell synapse and a light response being passed through the retina. Inactivation of the photopigment occurs with phosphorylation of the receptor and Arrestin protein binding (Kühn and Wilden, 1987; Wilden et al., 1986). For a detailed review of vertebrate phototransduction see (Pugh and Lamb, 2000), figure from (Lamb and Pugh, 2006).

Bipolar Cells

Bipolar cells may be classed as either OFF or ON depending on the effect of glutamate binding. ON-bipolar cells express mGluR6 metabotropic receptors which, when bound by glutamate maintain the cells in a hyperpolarized state (Masu et al., 1995). When glutamate release from the photoreceptor drops following phototransduction, the ON-bipolar cell depolarizes due to Na+ channels opening and the cell transmits a signal. By contrast, in the OFF-bipolar cell glutamate binding to AMPA/KA ionotropic receptors (Hack et al., 2001) maintains a depolarized state thus the effect of the decreasing glutamate release from photoreceptors induces hyperpolarization and the cell stops signaling (Forrester et al.,

2002d). While initially there were thought to be only five types of bipolar cells (Forrester et al., 2002d), ten different types have now been identified in the mouse retina, one rod bipolar cell (ON-type) and nine types of cone bipolar cell (four OFF type and five ON) (Ghosh et al., 2004) which may make contact with one (miget bipolars) or many (diffuse bipolars) cones (Forrester et al., 2002d).

Retinal Ganglion Cells

From bipolar cells the visual signals are passed to retinal ganglion cells (RGCs) which, like bipolar cells, are present in a wide range of morphological classes with at least 22 distinct subtypes now identified in the mouse (Coombs et al., 2006; Völgyi et al., 2009) and 20 across primate species (Field and Chichilnisky, 2007). These RGC classes also have functional significance as different RGCs project to different brain regions and subtypes of RGC have been shown to encode separate types of visual information concerning direction of motion, edges and background motion context (Barlow et al., 1964; Ölveczky et al., 2003; van Wyk et al., 2006). However, the signal path is not often direct from photoreceptor to bipolar to ganglion cell as horizontal and amacrine cells are also involved in the signal transmission as discussed below.

Photoreceptors greatly outnumber the number of RGCs in the retina with peak RGC density in the mouse at 8,000 cells/mm^2 (Dräger and Olsen, 1981) while peak rod and cone densities are 100,000 and 16,000 cells/mm^2 respectively (Jeon et al., 1998). Horizontal cells are situated post-synaptic to the photoreceptors in the INL/ OPL and each horizontal cell

receives signals from a large number of photoreceptors, averaging the input before passing the processed signal back to the photoreceptor synapses and on to bipolar cells (Leamey et al., 2008). The network of horizontal cells are connected by gap junctions and these connections can be regulated by dopamine release from amacrine cells thus allowing for neural adaptation through modification of cone sensitivities as well as the sensitivity area (or receptive field, RF) of both bipolar and ganglion cells. Vertebrates may have either two (most species including humans) or only one (rodents including mice) type of horizontal cell (Peichl and González-Soriano, 1994).

Amacrine Cells and Rod/Cone Signaling Pathways

As mentioned above, amacrine cells also act to modulate the visual signal. They may do this indirectly through neurotransmitter release or directly as they receive inputs from bipolar cells and connect to ganglion cells (Leamey et al., 2008). Some of the many amacrine cell types also have particular roles in signalling pathways. For example, the AII amacrine cell, first described in the cat retina (Kolb, 1979), is central to the rod signaling pathway as the main target of rod- bipolar cells (Strettoi et al., 1992). The ON-rod bipolar cells make few, if any, connections directly to RGCs but instead connect to the AII cells. These in turn couple to both the ON and OFF- cone bipolar cell types and make use of the existing cone-signaling pathway. While this may be the dominant method of rod-signal transduction, there is evidence for both direct connections from rods to OFF cone-bipolar cells (Hack et al., 2001; Soucy et al., 1998) and rod to cone gap junction connections (Nelson, 1977; Raviola and Gilula, 1975). However, the primary rod path through AII cells is up to 1 log unit more

sensitive to light (Völgyi et al., 2004). See Figure 1.3 for an illustration of Rod/ Cone signaling pathways from (Soucy et al., 1998).

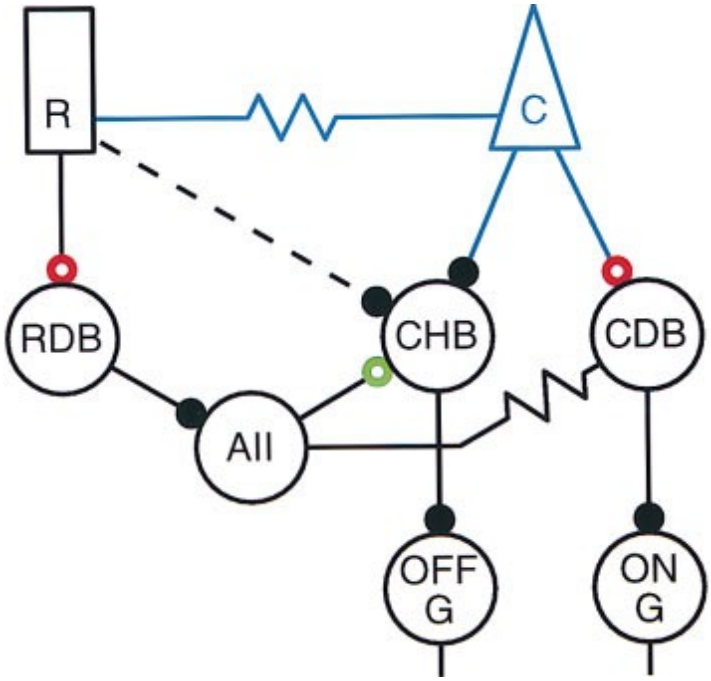

Figure 1.3 Representation of Rod/ Cone signaling pathways in the mammalian retina Rods (R), cones (C), Depolarizing Rod (RDB) and Cone (CDB) Bipolar Cell types, Hyperpolarizing Cone Bipolar Cell (CHB), AII amarine cell (AII), ON (ON G) and OFF (OFF G) ganglion cells. Filled circles indicate sign-preserving synapses, open circles sign-inverting. Figure from (Soucy et al., 1998).

In the cone-signaling pathway in the retina, the graded hyperpolarization light responses from the photoreceptors may be passed to a large variety of cone bipolar cells. As an overarching rule, the axons of ON-bipolar cells make contacts in the deeper sublamina of the IPL while OFF-bipolar cells terminate in the outer third of the IPL which indicates a separation of these information streams (Strettoi, 2008). Some bipolar cell types may also be specialized for a given cone type as in the case of the blue cone bipolar cells which are also found in the mouse retina (Haverkamp et al., 2005).

Finally, the light response is passed to ganglion cells for signal transmission out of the retina. Ganglion cells may have large (eg magnocells, M cells, parasol cells) or small (eg parvocells, P cells or Midget cells) receptive fields of bipolar and amacrine cell connections and project to different regions of the brain through the optic nerve (Forrester et al., 2002d).

The Retinal Pigment Epithelium

While the signaling pathway through the retina has been discussed, one key retinal layer whose function deserves discussion in further detail is the Retinal Pigment Epithelium (RPE). The RPE is located nearest to the back of the eye, adjacent to the photoreceptor outer-segments (See Figure 1.1) and is a monolayer of cells that extends across the entire retina (Forrester et al., 2002b). As mentioned in the photoreceptor section above, the RPE has a variety of critical roles in the eye including supporting retina attachment, serving as a selectively permeable barrier to the retina, absorption of light to prevent scattering, storage of key ocular nutrients (including Vitamin A which is vital for opsin synthesis) and recycling of outer-segments (Forrester et al., 2002b). The diurnal cycle of outer-segment renewal that is critical to vision occurs with the shedding of outer-segment tips containing the photopigment discs, and these are then phagocytosed by the RPE cells. Cone outer-segment removal is significantly slower but the process is generally similar. Regeneration of the photopigment also occurs in the RPE cell cytosol where retinyl-ester isomerase converts all-*trans*, which is transported into the RPE, to 11-*cis* retinol before 11-*cis* retinol dehydrogenase changes 11-*cis* retinol into 11-*cis* retinal (See Figure 1.4 for a summary of

the classic visual cycle of photopigment regeneration). As retinol isomerase is only found in the RPE, damage or separation from the RPE means the breakdown of this regenerative cycle (Forrester et al., 2002c) and disruption of the RPE has been found to result in photoreceptor functional abnormality and degeneration (Longbottom et al., 2009). While rods are thought to recycle chromophore solely through the classic visual cycle with the RPE, evidence now suggests that cones also use a cone-specific retina visual cycle involving Müller cells that is key to cones' ability to signal under bright light conditions (Wang and Kefalov, 2011).

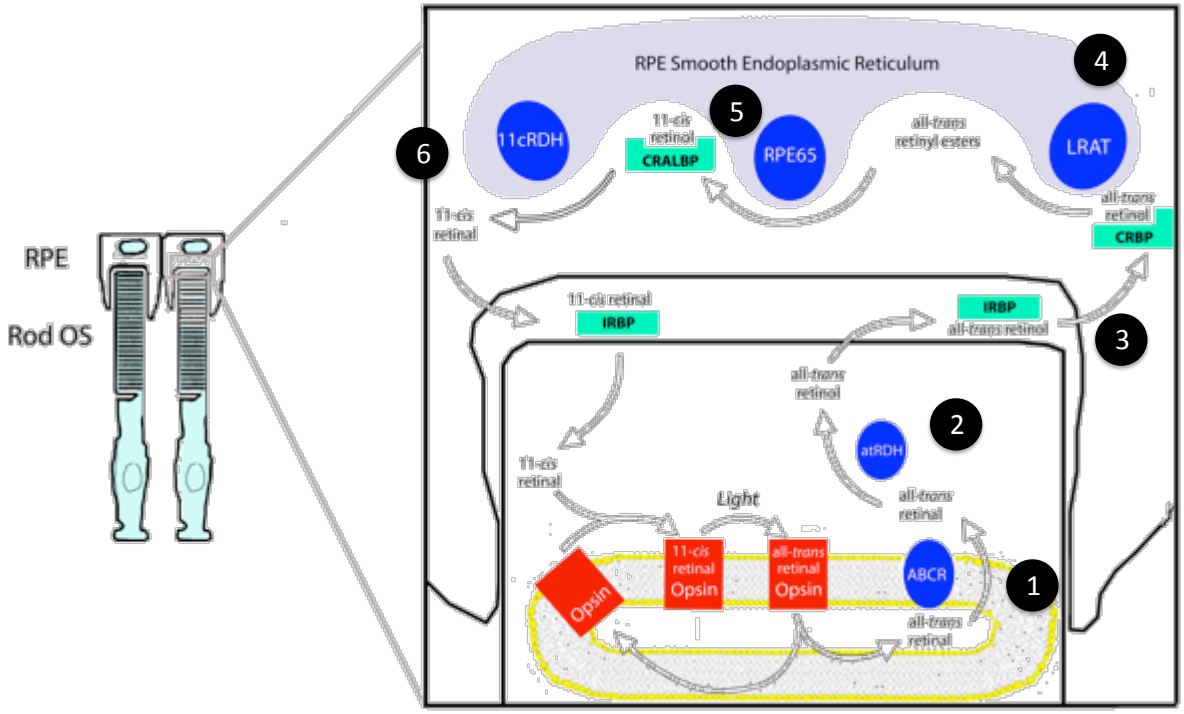

Figure 1.4 The Classical Visual Cycle for regeneration of 11-cis retinal The photoisomerization of 11-cis to all-trans retinal starts the process of phototransduction but, for the regeneration of 11-cis retinal, all-trans retinal must be transferred to the RPE. First, all-trans is transferred from the inner leaflet of the disc by ATP binding cassette transporter (ABCR) to the cytoplasm (Step 1) (Liu et al., 2000). All-trans retinal is then reduced to all-trans retinol by all-trans retinol dehydrogenase (atRDH) (Step 2) (Haeseleer et al., 1998). Next,

the all-trans retinol binds to interphotoreceptor retinoid binding protein (IRBP) and transported to the RPE where it is transferred to cellular retinoid binding protein (CRBP) (Step 3) (Saari et al., 1982). The all-trans retinol is converted to all-trans retinyl esters through esterification by lecithin retinol acyl transferase (LRAT) (Step 4) (Saari and Bredberg, 1989) and retinal pigment epithelium-specific protein 65 kDa (RPE65) hydrolyses and isomerises the retinyl esters to 11-cis retinol (Step 5) (Redmond et al., 2005). Finally, the 11-cis retinol binds cellular retinaldyhyde binding protein (CRALBP), is converted to 11-cis retinal by 11-cis retinol dehydrogenase (11cRDH) and transported back to the outer-segment by IRBP (Step 6) (Saari et al., 2001). Figure adapted from (Crouch, 2009).

1.2 Image-Forming Visual Pathways

Retinal ganglion cells project to various brain areas for different visual functions. In humans, the electrical signals conveying light information from the photoreceptors pass through the retina to ganglion cells then down their axons making up the optic nerve, through the optic chiasm then end up in the thalamus region called the lateral geniculate nucleus (LGN) (Forrester et al., 2002d). Neurons from the LGN then relay the visual signals on to the visual cortex in the occipital lobe. This is termed the primary visual or retinogeniculostriate pathway (See Figure 1.5) and in mammals is accompanied by an accessory optic pathway (Giolli et al., 2006; Hayhow et al., 1960) and a retinohypothalamic pathway (Hendrickson et al., 1972).

Figure 1.5 Major central projections of retinal ganglion cells in humans Axons from RGCs project to the Lateral Geniculate Nucleus (LGN), from where LGN axons fan out as optic radiations to carry visual information to the primary visual cortex or Striate Cortex in the primary visual pathway. RGC also have major projections to the superior colliculus (SC), the pretecum and down the retinohypothalamic tract (RHT) to the hypothalamus. Figure from (Purves, 2001b).

The main target of the LGN visual signals is the area known as the primary visual cortex, area V1 or the Striate Cortex. The V1 receives the information from the visual field into a highly organized map maintained from the signal origin through the LGN allowing for a remarkable separation of visual signals. An illustration of topographic separation of visual information is in the magnocellular and parvocellular pathways. Organised into different layers of the LGN, the magnocellular pathway allows rapid transmission of light information while the slower parvocellular signals transmit spatial and colour information (Forrester et al., 2002d). These signals are combined with input from many other cortical areas to give visual perception. V1 is linked to associated cortical areas called prestriate regions or V2-V5

and each have specific functions. For example, directional motion processing in area V5 augments the motion detection in V1(Born and Bradley, 2005).

However, there is considerable variation in the target of RGC projections with differing balances of subcortical targets identified in several mammalian species (Ling et al., 1998). In primates, as described above, most RGC projections are made to the dorsal LGN while only a few project to other areas of the mid-brain including the pretectal area and superior colliculus (SC) (Rodieck and Watanabe, 1993). In carnivores, as demonstrated in the cat, about half of the RGCs project to the SC while 77% were found to project to the LGN (about a quarter of RGC project to both LGN and SC) (Illing and Wässle, 1981). In other small mammals such as rodents, almost all RGCs project to the SC as demonstrated in the rat (Dreher et al., 1985), hamster (Chalupa and Thompson, 1980) and mouse (Hofbauer and Dräger, 1985).

In primates, the SC has a significant role in generating the rapid reflexive eye correction and locking-on movements (saccade) involved in vision (Reviewed in Stein and Wallace, 1996) while also being a key site of multisensory integration (Stein et al., 2002).

While it does not receive direct retinal input, the cerebellum is also involved in visual control, mainly in the vestibular-ocular reflex that uses information from the vestibular apparatus to make the small eye movements required to stabilize light on the retina during motion (Blazquez et al., 2003; Ito, 1982). A related ocular response associated with support of the accessory optic pathway (AOP) is the optokinetic reflex which involves both smooth

tracking and saccade movements of the eye to follow objects moving through the visual field without requiring larger head movements (Krause et al., 2014). Further details of the optokinetic response are discussed in the introduction to Chapter 5.

While visual functions have naturally been a large focus in the study of RGC projections, there is also a retinohypothalamic tract (RHT), as mentioned above, consisting of a subpopulation of retinal ganglion cells, that make connections to hypothalamic brain areas including the anterior hypothalamic area, lateral hypothalamus and the superchiasmatic nuclei. These projections are vital to non-visual light functions including the coordination of the body clock and circadian rhythms (Panda, 2008) as discussed in the next section.

1.3 Circadian Rhythms

Energy from the sun powers life on Earth and many of the key behaviors and functions of organisms revolve around the 24-hour solar rhythm. The anticipation and adjustment to daily solar time may influence behavioral decisions on food intake, avoiding predator interactions, environmental damage (Lowrey and Takahashi, 2004) and seasonal breeding behavior (Goldman, 2001) while vital processes such as metabolism, body temperature, alertness, the secretion of many hormones and the sleep/wake cycle demonstrate strong 24 hour fluctuations (Czeisler et al., 1995; Foster and Hankins, 2002; Fu et al., 2005; Hastings et al., 2007). An organism is thus able to synchronise or ‘entrain’ its daily ‘circadian’ (Latin ‘around a day’) rhythm to its temporal environment and coordinate its physiology and behavior to an appropriate phase. Two illustrations of the importance of this coordination are

from evolutionary trends and disease. That a method of circadian entrainment has evolved independently across the three domains of life (Bacteria, Archaea and Eukaryota) from bacteria to fungi to plants and animals (Dunlap, 1999) indicates that circadian regulation is fundamental to life on Earth. A second indication of the significance of these rhythms is that the effects of ongoing circadian disruption are thought to cause or contribute to several pathological neurodegenerative disorders (reviewed in (Hastings and Goedert, 2013)), metabolic syndromes, sleep disorders and increased risk of cancer (Ellenbogen, 2005; Straif et al., 2007; Waterhouse and DeCoursey, 2004).

A key feature of these circadian rhythms is that they are maintained under constant conditions. That is, they do not depend on solar or external interaction but demonstrate ongoing, strong oscillations on a near 24-hour basis (Aschoff, 1984; Czeisler and Klerman, 1999). However, most circadian rhythms do not have a period length of exactly 24 hours so, when left in isolation, the oscillations 'free-run' and drift over time with respect to the 24 hour solar day. Thus to maintain coordination, both an internal time-keeper (or clock) is required as well as a mechanism of input for external stimuli (called zeitgebers), in order to indicate the external environmental phase and keep the clock's rhythm in sync.

The Clock: Interlocking Transcription/ Translation Feedback Loops

The molecular mechanism of the mammalian clock depends on two interacting transcription/ translation feedback loops (TTFLs) (See Figure 1.6). The first 'core' loop involves two activator proteins, CLOCK and BMAL1, and two repressors, PER (Period) and CRY

(Cryptochrome). CLOCK and BMAL1 combine as subunits to form the transcription factor CLOCK:BMAL1 (Huang et al., 2012) which is then able to activate the transcription of PER and CRY via E-box enhancers. PER and CRY similarly link to form the PER:CRY repressor and this heterodimer moves from the cytoplasm to the nucleus to inhibit their own transcription by acting on the CLOCK: BMAL activator. However, to limit this inhibition, PER and CRY proteins are acted on by ubiquitin pathways (Busino et al., 2007; Godinho et al., 2007; Reischl et al., 2007; Shirogane et al., 2005; Siepka et al., 2007) and degraded, thereby relieving the repression of *Per* and *Cry* and resulting in fluctuating levels of the PER and CRY proteins with a period of about 24-hours (Reppert and Weaver, 2002).

Of course, for entrainment the clock must not only cycle but also allow modification of the rhythm based on external input. This control involves many additional proteins, some of which interact with the core TTFL and others that form the second TTFL. In association with the core TTFL, are a number of casein kinases (CKI delta and epsilon), which affect the rate of PER:CRY degradation and transport, as well as defined phosphatases, which regulate the kinases: PP1 for CKI-δ (Lee et al., 2011) and PP5 for CKI-ε (Partch et al., 2006). The second TTFL helps to stabilize the core loop against noise and disruption by interacting with the core *Cry1* gene and introducing a delay mechanism in its transcription that is vital to the adjustment of the clock (Ukai-Tadenuma et al., 2011). This TTFL involves the activator proteins ROR-α (retinoid-related orphan receptor alpha), ROR-β and ROR-γ (Sato et al., 2004) and their interaction with the repressors REV-ERB-α and REV-ERB-β (Preitner et al., 2002). Together, the ROR-REV loop also helps to strengthen the rhythmic transcription of *Bmal1* but this has been found to be non-essential to the core clock (Liu et al., 2008).

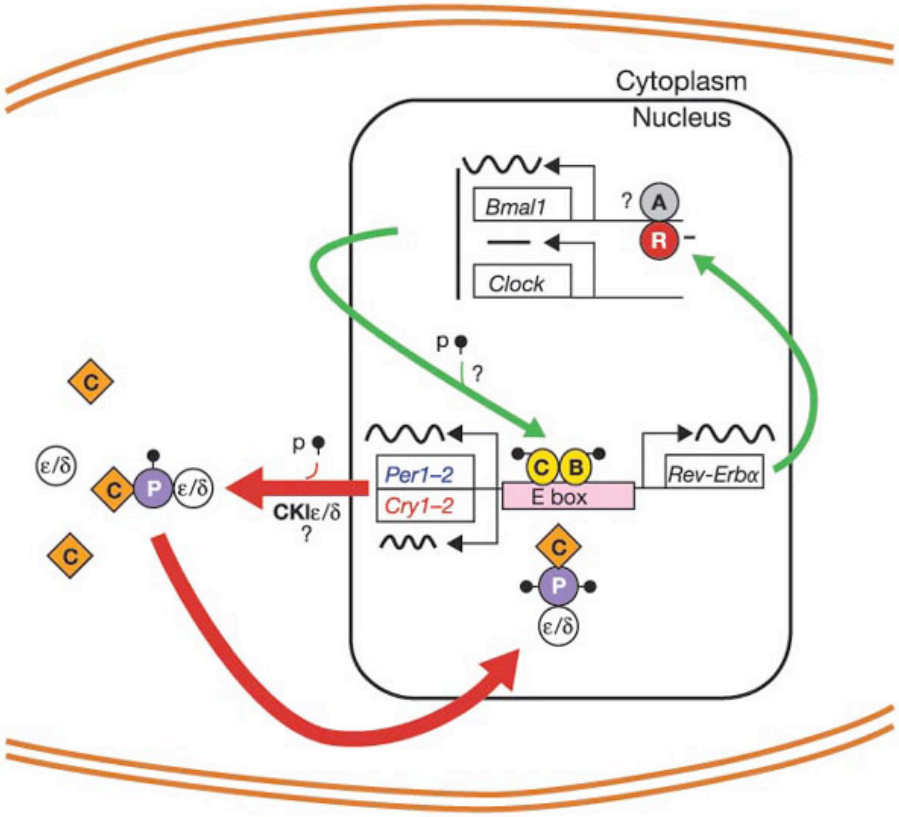

Figure 1.6 Mammalian circadian clock TTFLs The major elements of the interlocking TTFLs of the central clock are shown with CLOCK (C, oval), BMAL1 (B) acting through E-box enhancers on *Per, Cry* and *Rev-Erb*. PER (P) and CRY (C-diamond) complex along with CKI-δ/ CKI-ε and are phosphorylated. This complex acts on CLOCK-BMAL1 to inhibit further transcription. REV-ERB-α (R) interacts with Rev-Erb/ ROR elements in the *Bmal1* promotor to repress transcription, which is in turn opposed by ROR activators (A). Figure from (Reppert and Weaver, 2002).

Clock mutants and the Roles of the Clock Genes

The roles of the various clock genes can be deduced to some extent through examination of the effect of targeted gene disruptions in animal models. Mice with mutations in the *Clock*

gene become arrhythmic under constant darkness and have reduced amplitude and strength in the core clock (Gekakis et al., 1998; King et al., 1997; Vitaterna et al., 1994, 2006). It has since been discovered that the related protein NPAS2 can link with BMAL1 and partially compensate for the loss of CLOCK (DeBruyne et al., 2007). *Per* and *Cry* mutations have also been investigated. The *Period* gene family contains *Per1*, *Per2* and *Per3* while the *Cryptochrome* genes are *Cry1* and *Cry2*. Individual knockouts missing any one of these genes do not lose clock function. *Per1* (Bae et al., 2001; Cermakian et al., 2001; Zheng et al., 2001) and *Per2* (Bae et al., 2001; Zheng et al., 2001) mutants displayed short periods and disrupted activity rhythms in the dark. Clock gene levels were also reduced in *Per2* mutants (Bae et al., 2001). *Cry1* mutant mice display shorter periods while *Cry2* mice have 1 hour longer periods (van der Horst et al., 1999; Vitaterna et al., 1999). However, mutants for either both the *Per1* and 2 or both *Cry1* and 2 genes show severe effects with complete rhythm loss in the clock (Bae et al., 2001; van der Horst et al., 1999; Vitaterna et al., 1999; Zheng et al., 2001) indicating significant redundancy in PER and CRY functions. *Per1/Per2* double knockout mice were also found to have significant changes in their retinal structure and altered cone gene expression indicating the importance of clock function in development (Ait-Hmyed et al., 2013). *Per3* mutants display few circadian abnormalities while both *Per1/Per3* and *Per2/Per 3* double mutants do not differ significantly from the *Per1* or *Per2* single mutants indicating that *Per3* does not play a critical role in the clock function (Bae et al., 2001; Shearman et al., 2000).

Thus a central theme can be seen as, while circadian effects are evident, no single mutation in any of the *Per, Cry, Clock* or *Rev-Erb-alpha* genes results in a complete loss of the core

clock (Ko and Takahashi, 2006). Only disruption of *Bmal1* is sufficient on its own to cause complete rhythm loss (Bunger et al., 2000). This stability and redundancy built in to the central clock mechanism indicates how important circadian rhythm is to an animal's survival as evolutionary selection has resulted in a clock that is extremely robust.

The Suprachiasmatic Nuclei (SCN)

This central clock mechanism in mammals is located in the paired suprachiasmatic nucleus (SCN) of the hypothalamus. SCN damage results in a loss of rhythm and related circadian disruption while introduction of prenatal SCN-tissue into animals with SCN lesions can restore rhythm (Ralph et al., 1990; Weaver, 1998). Indeed, isolated SCN neurons each display the central gene cycles and firing rhythms (Aton et al., 2005; Liu et al., 2007; Welsh et al., 1995). The SCN clock regulates hundreds of SCN genes involved in key neuronal and metabolic activity (Panda et al., 2002a). However, the SCN is not the only region to contain a clock. In fact, peripheral tissues also contain rhythmic expression of many of the central clock genes (for a recent review of peripheral clocks see (Richards and Gumz, 2012)) although there are some tissue-dependent differences in expression patterns (Ko and Takahashi, 2006). These peripheral clocks, of which primary examples include those in the heart, liver, kidney and muscle, are coordinated by the central clock and regulate a significant portion of the genome (around 10% of all genes expressed, see review (Duffield, 2003)) and tissue specific arrays of clock-regulated genes move peak gene expression to the optimum time in the day for a given function (Partch et al., 2014). An indication of tissue-specific clock roles may be seen in the varied effects of the BMAL1 mutation in mice. In

addition to the breakdown of the circadian clock, these mice display lower weight, infertility, arthritis and reduced lifespan and these varied effects have been taken to indicate tissue-specific clock roles in various pathways from glucose metabolism to adipogenesis through the body (Bunger et al., 2000, 2005; Rudic et al., 2004; Shimba et al., 2005). There is also an independent retinal clock that can generate circadian rhythms in retinal gene expression independent of the SCN and persists following photoreceptor degeneration (Ruan et al., 2006; Sakamoto et al., 2000).

Clock Adjustment for Entrainment

As mentioned before, an animal not only needs a clock but also an input mechanism to coordinate the clock with the environment. For mammals, the primary entertainer or zeitgeber is light (See Figure 1.7 below for illustration of the process from light exposure to clock adjustment described in this section). Retinal projections to the SCN are through the retinohypothalamic tract (RHT) and light activation results in neurotransmitter release of glutamate and PACAP (Hannibal et al., 2000) which activates a calcium-dependent signaling cascade involving a number of kinases such as PKA, CaMK and MAPK (Meijer and Schwartz, 2003). This cascade results in the phosphorylation of the calcium/ cyclic AMP response element (CRE)-binding protein (CREB) at Ser133 (Ginty et al., 1993) and Ser 142 (Gau et al., 2002) to activate it. CREB then binds and induces expression in SCN genes that contain CREs including *Fos*, *Nr4a1*, *Egr1* (Lin et al., 1997; Morris et al., 1998; Porterfield et al., 2007), a number of kinases (Doi et al., 2007), several micro-RNAs (Cheng et al., 2007) and, most critically, *Per1* and *Per2* as this allows for adjustment of the circadian clock

(Albrecht et al., 1997; Schwartz et al., 2011). The direction of the effect due to light-induced *Per* is importantly clock-dependent in that if the increased expression occurs when *Per* levels are rising in the late circadian night, the rise will be accelerated and the rhythm will be advanced, but if *Per* is falling in the late circadian day/ early night then induction will delay the clock (Hastings et al., 2007). Thus light adjusts the mammalian clock in a clock-gated manner. Recent work has pointed to the existence of a further layer of the clock mechanism shown in Figure 1.7, as CREB-related transcription coactivator 1 (CRTC1) activates CREB, which in turn induces *Per1* and salt inducible kinase 1, *Sik1,* expression. SIK1 phosphorylates CRTC1, deactivating it and thereby down-regulating *Per1* providing a mechanism to limit the effect of light exposure on the clock providing a negative feedback on light input (Jagannath et al., 2013).

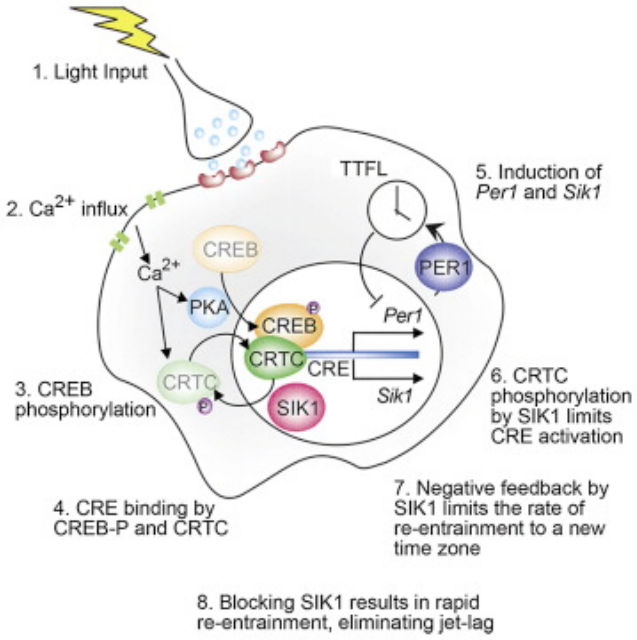

Figure 1.7 Photic Regulation of the Clock This schematic illustrates the basic steps from light input through CREB activation that affects the transcription of key clock genes such as *Per1* as well as the negative feedback loop involving SIK 1 that acts to suppress the light impact on the clock. From (Jagannath et al., 2013).

1.4 Melanopsin and pRGCs in the Mammalian Retina

One of the most exciting areas of circadian research in the last two decades has been the study of the photoreceptors responsible for the light signals to the SCN as the results have revolutionized the view of the non-image forming (NIF) system in mammals. The initial assumption was that it was likely to be rods and cones signaling through the known visual pathways, however investigation has since found evidence that indicates that this is not the case. Firstly, the circadian system is less sensitive than the visual system by a factor of over one-thousand which is difficult to explain if the photopigments and pathways involved were the same. The discovery of a unique subset of retinal ganglion cells projecting down the RHT to the known site of the core clock, the SCN, gave further support for the idea of a separate system (Moore et al., 1995) and the pupillary constriction action spectrum of mice without rods or cones was found to rely on a photopigment with maximum sensitivity at 479nm (Lucas et al., 2001). Finally, the loss of rod and cone photoreceptors did not prevent the ability of light to influence circadian behaviors in either mice or human patients, and only removing the eye could cause the loss of these functions (Foster, 1998; Freedman et al., 1999; Lucas et al., 1999; Nelson and Zucker, 1981; Zaidi et al., 2007).

A central part of the explanation for these inconsistencies was found with the discovery of photosensitive retinal ganglion cells (pRGCs) (Berson et al., 2002) containing the photopigment melanopsin (Gooley et al., 2001; Hannibal and Fahrenkrug, 2002; Hannibal et al., 2002; Hattar et al., 2002, 2003; Lucas et al., 2003; Provencio et al., 1998a, 2002). It is now clear that input from rod, cone and melanopsin pRGC components all play a role in

circadian responses. pRGCs receive input from the outer retina (Belenky et al., 2003; Dacey et al., 2005; Perez-Leon et al., 2006; Viney et al., 2007; Wong et al., 2007) and knocking out melanopsin does not result in a loss of circadian light response, though there are effects on the magnitude of pupil response and phase-shifting (Lucas et al., 2003; Panda et al., 2002b; Ruby et al., 2002). Triple mutants without any of the three classes of photoreceptor no longer display visual or circadian light responses, so between them, rods, cones and pRGCs are responsible for all visual input of light (Hattar et al., 2003; Panda et al., 2003). Evidence also suggests that pRGCs form the only conduit of light-signals to the circadian brain centers. Ablation of pRGCs themselves has the same impact as the triple rod/cone/melanopsin knockout on entrainment and pupil response while the animals retained normal visual responses (Göz et al., 2008; Güler et al., 2008; Hatori et al., 2008).

Characteristics of the Melanopsin Photopigment

The melanopsin gene appears to be more similar to rhodopsin from invertebrates than to the vertebrate gene (Panda, 2008) and forms a photopigment that is most sensitive to 480nm blue light through binding to retinaldehyde, like the rod and cone photopigments, to activate a G-protein signaling cascade leading to a depolarizing current (Fu et al., 2005; Melyan et al., 2005; Newman et al., 2003; Panda et al., 2005; Qiu et al., 2005) (See Figure 1.8 for illustration of melanopsin phototransduction cascade). There is also evidence that the melanopsin photopigment may be unique among vertebrate photopigments in being bistable (Melyan et al., 2005; Mure et al., 2007). pRGCs are less sensitive than rods or cones, encoding the intensity of external illumination with tonic responses having latencies of

almost a minute, and are resistant to bleaching (Berson et al., 2002; Dacey et al., 2005; 2008) as shown by a recent study where pRGCs were shown to be able to signal continuously for ten hours (Wong, 2012). The exact intracellular signaling mechanisms in pRGCs remain to be fully understood although there have been recent advances (outlined in (Hughes et al., 2012a)). In each pRGC, the melanopsin content is very low when compared to opsin expression in rods and cones with an average of 3 melanopsin molecules per μm^{-2} in the cell wall of pRGCs compared to 25,000 opsin molecules per μm^{-2} in rod and cones (Do et al., 2009). Thus, pRGCs capture a small number of photons, leaving most to pass through the retina to rods and cones, but highly amplify those that are absorbed with slow sustained responses (Schmidt et al., 2011).

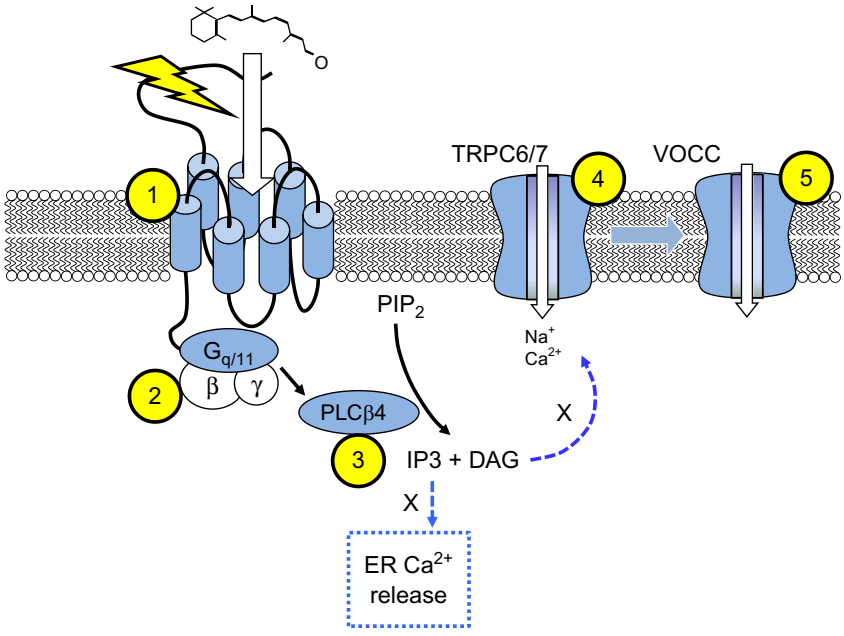

Figure 1.8 Melanopsin phototransduction Illustration of the current knowledge concerning the signaling pathway of melanopsin. Light activation of the photopigment melanopsin (step 1) activates a $G_{q/11}$ G-protein (step 2) which in turn activates Phospholipase C Beta4 (PLCβ4) (step 3) which, through currently unclear steps that have been shown not to involve inositol triphosphase (IP3) mediating Calcium release or diacylglycerol

(DAG), results in the opening of TRPC6/7-type channels (step 4) leading to voltage-operated calcium channel (VOCC) activation and a depolarizing current. PIP_2- phosphatidylinositol biphosphate, ER-endoplasmic reticulum. From (Hughes et al., 2012a).

pRGC Projections and Subtypes

pRGCs in the mouse project to 6 major sites. These include the SCN, site of the central clock, the ventral LGN, the main visual relay, the intergeniculate leaflet (IGL) in the thalamus, which connects to the SCN and plays a vital part in entrainment responses, the SC, an established visual center, the nucleus of the optic tract (NOT), which along with the accessory optic tract terminal nuclei are thought to play key roles in driving optokinetic nystagmus, and the pretectal olivary nuclei (PON or olivary pretecal nuclei, OPN), the site of the pupil response (Edelstein and Amir, 1999; Gall et al., 2013; Gooley et al., 2003; Hannibal and Fahrenkrug, 2004; Hattar et al., 2003, 2006). See Figure 1.9 for central projections of pRGCs. The paired nuclei of the SCN are located at the bottom of the hypothalamus, above the optic chiasm and each nuclei has a dorsal 'shell' region which contains the central clock and a 'core', located ventrally, which is where pRGCs project and connections are made to other key circadian brain areas such as to the pineal gland for light regulation of melatonin (Hastings and Herzog, 2004; Larsen et al., 1998; Teclemariam-Mesbah et al., 1999). The SCN is also linked to the ventrolateral preoptic nucleus (VLPO), a key brain area in sleep regulation, and light signals from pRGCs have been shown to control light induction of sleep (Altimus et al., 2008; Lupi et al., 2008; Tsai et al., 2009). Together this collection of key physiological outputs driven through pRGC connections to the brain areas mentioned above makes up what is termed the non-image forming (NIF) visual system.

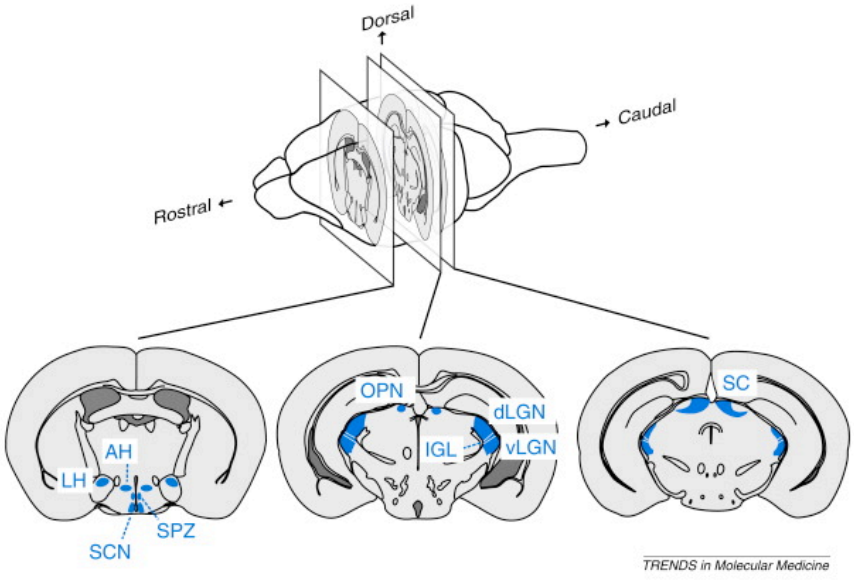

Figure 1.9 Central projections of pRGCs in the mouse pRGC axons have been found to project to the Suprachiasmatic nucleus (SCN), lateral hypothalamus (LH), anterior hypothalamus (AH), subparaventricular zone (SPZ), olivary pretectal nucleus (OPN or PON), intergeniculate leaf (IGL), dorsal lateral geniculate nucleus (dLGN), ventral lateral geniculate nucleus (vLGN) and the superior colliculus (SC). From (Hatori and Panda, 2010).

Though they play such a key role in physiology, pRGCs make up a relatively small proportion of the total RGCs in the retina with percentages from 0.2-0.3% in humans to 2.6% in the rat (Hattar et al., 2002) and about 1% in the mouse (Panda, 2008). At birth, however, pRGCs are found at high densities of 200 pRGCs/mm^2 that are capable of transmitting light signals to the SCN. This density declines rapidly after birth as the retinal cells differentiate so that by two weeks three-quarters of the pRGCs have been lost with the remaining cells spaced across the retina to form a dendritic net contacting bipolar and amacrine cells in the IPL (Belenky et al., 2003; Sekaran et al., 2005; Tarttelin et al., 2003; Tu et al., 2005). This pattern of high cell density at birth followed by a period of

programmed cell death is not unique to pRGCs as other types of RGC, and indeed amacrine, bipolar cells and photoreceptors, also show significant early loss with the degree as well as the timing of pRGC cell death matching that of the larger RGC population (Guerin et al., 2006; Vecino et al., 2004). This process is thought to be critical in developing specific RGC connections with only correctly targeted cells surviving to adulthood (Guerin et al., 2006). While there was initially assumed to be only one type of pRGC, at least 5 classes termed M1 to M5 have now been identified by their dendritic morphology and projections (Barnard et al., 2006; Berson et al., 2010; Hankins and Lucas, 2002; Müller et al., 2010; Sekaran et al., 2003; Tu et al., 2005; Viney et al., 2007; Vugler et al., 2007; Zhang et al., 2008). M1 cells stratify in the OFF sublamina of the IPL while M2 connect in the ON sublamina and M3 in both layers (Schmidt and Kofuji, 2011; Schmidt et al., 2008). M1 cells are smaller with less complex branching dendrites than M2s and the latter show different electrical properties with lower input resistance, lower light sensitivity and lower maximal responses than M1s (Schmidt and Kofuji, 2009). One explanation for the lower photosensitivity of M2 cells is that melanopsin protein density is higher in M1s (Berson et al., 2010; Ecker et al., 2010; Schmidt and Kofuji, 2009). M1 and M2 pRGCs have also been found to differentially express two isoforms of the melanopsin protein with M1s expressing both the long and short isoforms (OPN4L and OPN4S) but M2s only express the long-isoform (Hughes et al., 2012b; Pires et al., 2009). Two more categories of pRGC have been identified based on their morphological characteristics. Cells with dendrites ramifying in the ON sublamina and possessing large soma and long dentrites have been identified as M4, and those with highly branched and smaller dendrites as M5. Both of these cell types have lower melanopsin densities and lower direct light sensitivity than M1/M2s (Ecker et al., 2010).

The different categories of pRGCs also appear to have separate functional roles. The classes project differentially to NIF brain centers and contribute to different NIF light responses (Baver et al., 2008; Chen et al., 2011; McNeill et al., 2011). The M1 pRGC in particular is thought to be the critical subtype for entrainment and the PLR (Ecker et al., 2010; Güler et al., 2008; Hatori et al., 2008) while the other cell types with lower melanopsin expression rely on greater outer retina input from rods and cones (Schmidt et al., 2011) and may play roles in spatial and motion analysis (Zhao et al., 2014). In fact, subtypes of M1 pRGCs have been identified by expression of the Brn3b transcription factor with Brn3b negative cells driving entrainment in the SCN and Brn3b positive cells driving the PLR in the PON (Chen et al., 2011). See Figure 1.10 for illustration of pRGC subtypes and their main projections.

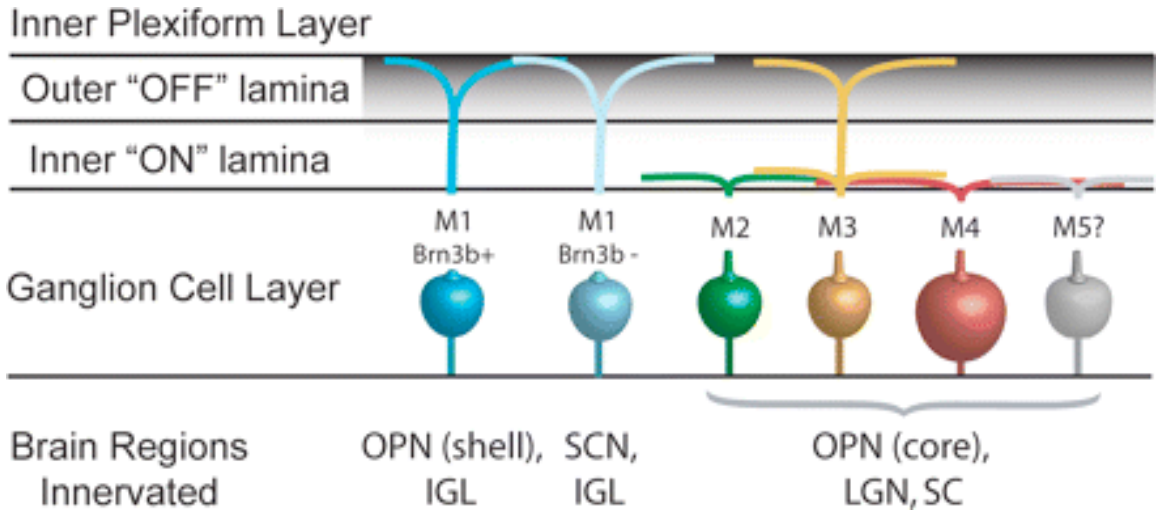

Figure 1.10 pRGC subtypes in the mouse The morphologic and molecular differences that define the pRGC subtypes M1 to M5 including the subtypes of M1 *Brn3b* negative and positive. Current evidence for the differential projections to the OPN (PON), IGL, SCN, LGN and SC are listed. From (Sexton et al., 2012).

Adding to the complexity of the different subtypes of pRGCs is the contribution of rods and cones. They signal through all types of pRGCs to varying extents (Güler et al., 2008; Hatori et al., 2008; Zhao et al., 2014) to contribute to both PLR (McDougal and Gamlin, 2010) and entrainment (Lall et al., 2010). Interestingly, evidence thus far has indicated that rods, but not cones, make a significant contribution to entrainment under normal light conditions, being the main driver for entrainment at very low light intensities and signaling through cones at higher intensities (Altimus et al., 2010). Both rods and cones have been implicated in the PLR (Allen et al., 2011; Lall et al., 2010). It has been suggested that rods and cones may input through different classes or subtypes of pRGC to make these varying contributions and even that the different types of cones may play different roles in NIF functions (Allen et al., 2011). A study of the threshold of NIF behavioral outputs found that the threshold for entrainment was much lower than that for masking responses or the PLR, which supports the idea that separate mechanisms must be involved (Butler and Silver, 2010).

Melanopsin and Vision

There is also evidence from human patients and animal models lacking rods and cones that melanopsin may be able to provide visual input for brightness perception and sensitivity through pRGC projections to the dorsal LGN, the main relay to the visual cortex, and a melanopsin-dependent persistent firing of dLGN neurons has been identified (Brown et al., 2010; Ecker et al., 2010; Zaidi et al., 2007). However, determination of a behavioral

significance for this contribution of melanopsin irradiance signals to the visual thalamus awaits further studies.

1.5 Unique cone gradients in the mouse retina

While the mouse has often been used as a model of the mammalian image and non-image forming visual systems it should be noted that there are certain aspects of the structure of the mouse retina that are quite unique. Like many mammals, the mouse retina is rod dominated with 97% of photoreceptors being rods (Leamey et al., 2008), but the mouse has a significantly higher peak RGC density than other nocturnal rodents (Dräger and Olsen, 1981; McCall et al., 1987; Métin et al., 1995) being much more similar to diurnal carnivores like the cat (Stone, 1978). Like other non-primate mammals, the mouse retina does not have a cone dominated fovea at the center of the retina but rod, cone and RGC densities do peak in the central retina and decrease peripherally (Jeon et al., 1998). The anatomy of scotopic and photopic visual pathways are also broadly similar in the mouse but cone opsin expression is not.

Immunohistological studies of the mouse retina have shown the presence of two cone opsins, a middle-wave sensitive MWS opsin with peak sensitivity at 508nm and an ultraviolet-sensitive UVS opsin with a peak at 360nm, the two cone opsins also found in other rodents such as the rat (Jacobs et al., 1991; Nikonov et al., 2006) (See Figure 1.11 for photopigments in the mouse retina). However, it was also noted that the opsin expression was organized in a stark gradient with UVS opsin dominating the ventral retina and MWS expression highest in

the dorsal retina (Szél et al., 1992). While it was initially assumed that this gradient would correspond to cones expressing one or the other opsins, it was determined that most mouse cones express both UVS and MWS and it is the varying expression levels in the same cone that produce the gradient (Röhlich et al., 1994; Szél et al., 1996). Co-expression of opsins in the same cone is observed during development in several species such as the rat and gerbil but in mice the co-expression persists into adulthood (Röhlich et al., 1994). Functional evidence of this co-expression in mice was established from electroretinogram (ERG) recordings where responses to short wavelength UV light stimulating the UVS opsin was suppressed by a long-wavelength adapting stimuli in a manner consistent with co-expression of the UVS and MWS opsins in the majority of cones (Lyubarsky et al., 1999). It is now established that mice possess a very atypical cone expression amongst mammals with opposing gradients of cone opsin co-expression with a dorsal-ventral gradient of increasing UVS expression and a ventral-dorsal MWS gradient (Applebury et al., 2000). Unlike most mammals where the longer wavelength cone opsins are the most highly expressed (Neitz and Neitz, 2001), UVS expression is significantly greater than MWS in the mouse (Szél et al., 1996) with three times more UVS mRNA than MWS (Applebury et al., 2000). The reason behind this co-expression has been suggested to be an alternation to a gene switch that, in rats, causes most of the UVS cones abundant during development to switch off UVS in favor of MWS (Neitz and Neitz, 2001). Why this mutation might be selectively maintained through mouse evolution is not clear.

However, not all mouse cones co-express both opsins as 3-5% of the total cone population only express UVS opsin and represent a true s-cone population, evenly spaced across the

retina and contacted by a dedicated blue-cone bipolar cell (Haverkamp et al., 2005). The presence of a second distinct cone type could provide an explanation for the observation that mice were found to show colour discrimination despite the widespread MWS/UVS opsin-co-expression, an ability which should require two different cone inputs (Jacobs et al., 2004).

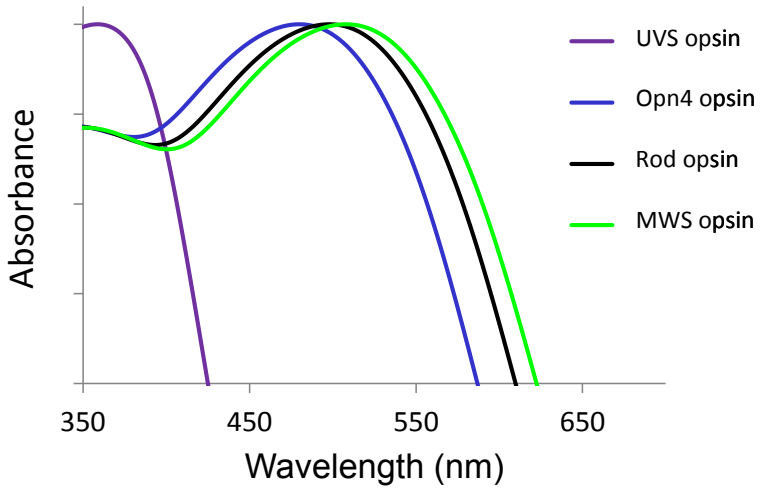

Figure 1.11 Photopigments in the mouse retina Absortion spectra for photopigments present in the mouse retina**,** ultra-violet sensitive UVS cone opsin (λmax=360nm), melanopsin *Opn4* (λmax=480nm), *rhodopsin* (λmax=498nm) and middle wave sensitive MWS cone opsin (λmax=511nm).

1.6 Ultraviolet Sensitivity and Functions Review

Ultraviolet light definition and discovery

The ultraviolet (UV) is defined as a band of wavelengths from 100-400nm in the electromagnetic spectrum, just shorter than the band from 400-700nm that is said to be 'Visible Light' according to the limits of human visual sensitivity. The presence of the ultraviolet spectrum as a category of light outside of that visible to humans was discovered by Polish scientist Johann Ritter in 1801 but it was not until British scientist John Lubbock's work with ants in 1883 that it was realized that some animals could perceive light below the limits of human senses.

Ultraviolet light is further divided into categories of UV-A, 400-315nm, UV-B, 315-280nm, and UV-C, below 280nm. However, all of UV-C and about 90% of UV-B radiation is absorbed by oxygen and oxygen radicals in the stratospheric ozone layer leaving UV-A as the most available of the UV wavelengths to natural processes (Madronich et al., 1998).

UV sensitivity across the animal kingdom

Following Lubbock's work with ants, the ability to perceive UV radiation was found in other insects including bees, wasps and fruit flies (Frisch, 1924; Lutz, 1920). The sensitivity to UV for vision has been identified in crustaceans, birds, reptiles as well as some fish, mammalian and amphibian species (Honkavaara et al., 2002; Hunt et al., 2001a).

The origin of UV sensitivity is thought to be in early archaebacteria that existed during the period before formation of the ozone layer when significant amounts of the damaging UV-C and UV-B shorter wavelengths reached the earth's surface. Early UV tuned photopigments would have allowed archaebacteria in the oceans to avoid the peak of this dangerous UV radiation during the day and ascend for photosynthesis at dusk (Neitz and Neitz, 2011). Reviews of photopigment genetics have pointed to the ancestral pigment as being ultraviolet-sensitive (UVS).

In vertebrates, cone photopigments are classed into 4 general opsin categories: long-wave sensitive (LWS) with a peak absorption between 500 and 570nm, middle-wave sensitive (MWS) 480-520nm, short-wave sensitive (SWS) 415-520nm and finally violet (VS) or ultra-violet sensitive (UVS) which absorb maximally between 355 and 435nm (Hunt et al., 2001a). All share the common structure of vertebrate photopigments previously discussed and are tuned to the various absorption maxima with small changes at specific amino acid sites. For the VS/ UVS proteins, sensitivity in either the violet or ultraviolet wavelengths has been shown to be controlled in birds by a single change from Serine to Cysteine at site 90 in the second transmembrane helix (Yokoyama et al., 2000).

While in insects the UVS photopigment has been retained throughout evolution, phylogenetic analysis suggests that in most vertebrate species other than teleost fish, the UVS opsin was lost with mutations shifting absorptions to longer wavelengths to produce a VS opsin (Hunt et al., 2001a). As mentioned above, many species of birds have regained the UV photopigment through the Ser90 to Cys90 switch and further tune spectral sensitivity

with a system of oil droplets (Bennett and Cuthill, 1994; Lind et al., 2013). Opsin sequence analysis has also indicated that, in mammals, the cone complement was reduced to only LWS and VS/UVS in a nocturnal ancestor. The multiple cone classes in some primates and humans is due to replication of the LWS gene to a MWS opsin while our SWS cone is more accurately a VS opsin (Hunt et al., 2001a).

Study of this subject has often sought to paint UV vision as a unique adaptation yet, looking across the animal kingdom, the lack of UV sensitivity in a species seems more rare than its presence. In fact, more intriguing questions would seem to those concerning the rarity of far-red sensitivity (Briscoe and Chittka, 2001) or indeed why humans and several other species have lost the ability see into the UV.

Given how common a feature UV vision is across the animal kingdom, it follows that there must be costs associated with UV vision that resulted in adaptive pressures leading to the loss of UV sensitivity in some species. There are indeed several negative impacts associated with UV vision. Firstly, transmission of shorter wavelengths to the retina results in increased chromatic aberration and decreased visual resolution. Passage through the lens results in a degree of scattering in all wavelengths but this effect is much larger for shorter wavelengths thus there is a tradeoff between greater spectral vision and decreased visual acuity (Hut et al., 2000). Secondly, ancestral archaebacteria would have relied on the first UVS photopigments to avoid exposure to intense UV in early earth because short-wavelength radiation can be extremely damaging to organisms and cause significant genetic mutations. In the ocular context, UV exposure has been linked to a number of corneal dystrophies,

ocular cancers and lens cataract formation in humans (Yam and Kwok, 2014). Retinal damage resulting from light exposure in rats has been shown to increase sharply moving into the ultraviolet wavelengths (van Norren and Schellekens, 1990). For animals with longer life spans, like humans, accumulated retinal damage from UV exposure would be a costly trade off for UV sensitivity in vision.

To block UV wavelengths from reaching the retina and prevent UV retinal damage and the visual costs, many diurnal mammals including humans, monkeys, squirrels as well some species of fish rely on a variety of molecular compounds in the lens that absorb wavelengths below 400nm. The most common of these is l-3-hydroxykynurenine *O*-β-d-glucoside, the main product of tryptophan metabolism to kynurenine in the lens (Bova et al., 1999).

As a final point on UV sensitivity, it is important to note that photopigments other than UVS may provide UV sensitivity due to absorption spectrums extending into the UV (See Figure 1.11 above for an example in mouse photopigments). Indeed, if it were not for kynurenine and related compounds in the lens, the human blue cone, which is in fact of the VS cone class having a maximal absorption at 420nm, would allow humans to experience sensitivity into the UV range (Hunt et al., 2001a). There are also non-rod, non-cone photopigments that could provide UV sensitivity. It has been suggested that OPN5 might be able to form a UV sensitive photoreceptor in mouse and humans (Kojima et al., 2011). Kojima et al. reported OPN5 was detected in the mouse retina, brain and skin as well as in human skin, brain and testis and was able to form a functional photopigment, able to activate Gi signaling, with a maximal absorption at 380nm. There is no in-vivo evidence for OPN5 function in mouse or

humans but this is an illustration that while we are concerned here with UV visual sensitivity there are many other light responses and certainly other mechanisms of UV sensitivity present in humans other than the visual. For example, rhodopsin expressed in skin cells and melanocytes helps to regulate melanin synthesis in the tanning response that protects the skin from UV light induced damage (Natarajan et al., 2014).

Functions of UV Vision

Though humans have evolved a mechanism of blocking UV transmission to the retina and we have lost our ancestral UVS opsin there is no doubt from the prevalence of UVS cones in other species that there are selective advantages to UV vision for many animals. In fact, a number of bird species have been found to have their greatest electrophysiological sensitivity below 400nm (Bennett and Cuthill, 1994). Studies have found a large number of functions for UV vision that can be grouped into general categories of navigation/ migration, feeding/ foraging and communication.

In terms of navigation/ migration, Monarch butterflies travel thousands of miles from the United States and Southern areas of Canada to Mexico each fall. Froy et al. have shown that the butterflies rely on sensitivity to ultraviolet light for orientation (Froy et al., 2003). Similarly, bees have been shown to use light vibration vectors (e-vectors) of UV light to determine the sun's position from any view of the sky by using the natural scattering of short-wavelengths (von Frisch, 1967; Wehner, 1989). Songbird species are similarly able to orientate to the sun even when it is fully obscured by clouds and there is evidence in some

species that this is through a similar mechanism to bees (Bennett and Cuthill, 1994). Finally Reindeer provide a good example of evolutionary adaptation to UV vision to fit their environment. Though other closely related species in family Cervidae do not extend their visual range in the UV, reindeer have evolved increased ocular media transmission that allows increased sensitivity to wavelengths below 400nm (Hogg et al., 2011). The reason for this shift is explained by the artic environment where the low sun angle for much of the year results in higher scattering and with the increased reflection off snow, UV wavelengths make up a greater portion of the available light than at lower latitudes so reindeer have adapted to make use of this spectral range.

There have also been a number of studies showing functions for UV vision in foraging behaviors. Studies examining birds of prey including kestrels and buzzards have indicated that they may use the UV reflectance of the urine of prey species such as the vole to determine prey densities in areas they are hunting (Rajchard, 2009). This hypothesis has been called into question by evidence that the UV reflectance of urine in natural settings such as fields would be low, but ultimate resolution awaits further behavioral studies (Lind et al., 2013). Some varieties of fruit and flower show stronger contrast to their background under UV light as compared to visual light which may aid herbivorous birds during foraging (Honkavaara et al., 2002; Martin Schaefer et al., 2007; Rajchard, 2009). UV sensitivity in fish has been suggested to aid in the detection of plankton in the shallower water where young fish feed and interestingly many species lose UVS cones as they grow older and move to deeper water where UV vision may be less important (Bowmaker and Kunz, 1987; Hunt et al., 2001a; Loew et al., 1993).

Inter and intra-species communication is an area where there is a large variety of evidence for functions involving UV sensitive vision. One area where a large role for UV sensitivity has been found is in mating displays or sexual selection. Many species have unique markings that are only visible in the UV range such as on the beak horn of king penguins (Dresp and Langley, 2006) and the dewlap of anoline lizards (Fleishman et al., 1993). In both species, these features are thought to play a significant part in mating displays and mate selection. Blue tits appear to humans as monochromatic with little difference between genders but it was found that males have a number of markings outside of the visual spectrum and how female blue tits rate potential mates depends largely on the UV reflectance of their crown feather (Hunt et al., 1998). Similarly, male common blue butterflies assess female nutrition statuses using the UV reflectance on their wings during mate selection (Knüttel and Fiedler, 2001). There are also examples of communication regarding predator/ prey interactions in the UV. As many species of raptor have only a VS photopigment (perhaps tuning the VS/UVS opsin away from shorter wavelengths for visual acuity benefits) they are less sensitive to the shorter wavelengths of UV light. Songbird species with UVS photopigments thus have adapted to use displays that reflect more strongly in the UV range which is less visible to their predators (Lind et al., 2013). Many caterpillar species use a different tactic as the bird species that prey on them have UVS photopigments that mean that their greatest light sensitivity is to shorter wavelengths. These caterpillars have developed markings that reflect very strongly in the UV to warn of poison and deter the predators (Honkavaara et al., 2002). Finally, in species where egg parasitism is common, there is evidence that some host

species could rely on UV reflective marking on eggs to differentiate between their eggs and those of the parasitic species (Rajchard, 2009; Underwood and Sealy, 2008).

Thus, while we can't see the UV, as discussed above, the vast majority of species can (Kevan et al., 2001) and there is a wide range of functions in which species make use of this expanded visual sensitivity. Several authors have pointed out that, despite the great interest in the subject, these species are simply using UV as another part of the light spectrum and the temptation to exaggerate the importance of UV light or label UV a 'special channel' or adaptation is an example of anthropocentrism.

Circadian role of UV

Apart from the visual functions there is also evidence of other important roles for the retinal sensitivity to UV light. In 1973 it was noted that exposure to UV light of 360nm could induce a phase shift in the body temperature rhythm of rats (McGuire et al., 1973). Canaries were found to entrain to increasing additions of UV light (Pohl, 1992) and bees in the arctic have been found to entrain to daily variation in UV light during the constant-light conditions of the arctic summer (Chittka et al., 2013). Thus there is growing evidence for the input of ultraviolet light to the non-image forming visual system.

1.7 Ultraviolet Function in the Mouse

Rodentia are significant in the study of how animals utilize ultraviolet light as they are one of the few mammalian orders where many species have regained a UVS opsin in their retina. Rats were one of the first species in which UV light was demonstrated to be able to alter daily rhythms (McGuire et al., 1973). In 1991, Jacobs et al. used electroretinogram (ERG) recordings to determine that mice had a sensitivity peak in the UV light range at 360nm suggesting a specialized UV detection mechanism. Further behavioral tests confirmed that mice could see UV light (Jacobs et al., 1991). Neither was this a phenomenon restricted to mice as Jacobs found that the rat, gopher and gerbil also have UV peaks in ERG sensitivity pointing to a wider and previously unknown UV system in this group. This was especially surprising given that it was thought to be an established fact at the time that no mammals had any of the UVS photopigments known to exist in the retina of other vertebrates and further that rodents had monochromatic vision with only one cone class. Investigation into this finding confirmed a UVS cone class in the mouse retina in addition to the known MWS cone opsin (Szél et al., 1992).

Hypotheses concerning the reason for UV sensitivity in a largely nocturnal group such as rodents have been varied. It is known rodent urine reflects in the UV (Desjardins et al., 1973) and it was suggested that perhaps UV sensitivity allowed for intra-species communication and territorial control which would have favored the evolution of UV vision (Chávez et al., 2003). It could also be that the second class of cone allows for color vision and that this provides an adaptive advantage. Behavioral forced choice discrimination tests

in mice have suggested that they are capable of discriminating color, an ability that can only be explained by contributions from both cone classes (Jacobs et al., 2002) but the co-expression pattern of MWS and UVS in the same cells in the retina seem a very poor arrangement for color vision (Gouras and Ekesten, 2004). There is also the possibility that it is a circadian role that is the most significant for the UVS pigment. UV is known to be able to induce phase shifts in mice and induce melatonin suppression (Brainard et al., 1994; Provencio and Foster, 1995; Sharma et al., 1998) and this might explain the large gradient in UVS expression towards the sky-facing ventral part of the retina. Furthermore, undermining all these theories with regards to explaining the presence of UV cones has been the suggestion that it might not be the UVS cones that are responsible for all of the behavioral demonstrations of UV sensitivity but that secondary absorption from rods or MWS cones might play a role. The Syrian Golden Hamster was found to phase shift to UV light at a level comparable to light in the visible spectrum despite the hamster being a monochromat with only a MWS cone (von Schantz et al., 1997). This interesting observation led to the suggestion that it may be the beta-band or secondary peak absorption from one of the other photopigments that allows UV sensitivity and this issue has not been comprehensively resolved. There is also the possibility that ultraviolet-induced visible flouresence may play a role. UV or near-UV light is known to induce blue-green light fluorescence when absorbed by certain materials including the lens of mammalian species including humans and other primates (Zuclich et al., 2005). This fluorescence would be at a much lower irradiance than the incident light but it is possible that this could be absorbed by photopigments sensitive to visible light and induce a behavioural response.

1.8 Main Thesis Aims

As outlined in this introduction, mice have been found to possess a sensitivity to UV light that seems to provide input to both visual (Jacobs et al., 1991) and circadian (Brainard et al., 1994) systems, as well as a retina with a unique organization of ultraviolet sensitive opsin (Neitz and Neitz, 2001). While the mouse is known to have a UVS cone opsin, the pattern of co-expression has called into question how much of a role ultraviolet sensitivity might have in mouse vision. At the same time cones are thought to make only a limited contribution to non-image forming functions like circadian entrainment. The purpose of the research presented in the following chapters was threefold,

i) to confirm the photoreceptor responsible for the behavioral ultraviolet sensitivity identified in mice
ii) to investigate the extent and basis of ultraviolet contributions to both the image and non-image forming visual system
iii) to develop a hypothesis to explain why the mouse has a retina with a unique organization and extensive ultraviolet sensitivity.

Using models of photoreceptor loss as well as targeted photopigment gene knockouts, a number of image and non-image forming assays were employed to assess responses to ultraviolet light in the mouse. These data define a significant contribution of the UVS cone opsin to the non-image forming system of the mouse and a novel *Opn1sw* knockout model was generated to confirm and expand on these observations.

Chapter 2: **Materials and Methods**

2.1 Animal housing

Mice were bred and housed in the Department of Biomedical Services, University of Oxford in individually ventilated, filter-top cages and fed *ad libitum*.

Prior to experiments, mice were housed in cages isolated from possible confounding external stimuli in light-tight ventilated chambers and entrained to a 12h:12h L:D cycle for a minimum of 7 days. Light-dependent resistors connected to a ClockLab interface (Actimetrics, Wilmette, IL, USA) were used to record the light/dark conditions at all times. Ambient temperature was maintained at 20 ± 2 °C and food and water were available *ad libitum*. All aspects of animal work were carried out under Home Office personal (PIL: 30/9262) and project licenses (30/2812) in accordance with the Animal (Scientific Procedures) Act 1986 (UK) and the Oxford Policy on the Use of Animals in Scientific Research and approved by the Home Office (UK) Animals Prodcedures Department (ASPD). All procedures were performed in a designated establishment.

2.2 Breeding and Opn1sw model generation

Rod, cone and melanopsin photoreceptor models

Transgenic rodless (*rd/rd*), rodless coneless (*rd/rd cl*) and coneless (*cl*) animals were maintained on a C3H background while *Opn4* $^{-/-}$ mice were maintained on a C57BL/6 background. non-*rd* C3H animals (used to refer to wildtype C3H mice used as controls for

rd/rd line) were maintained as a separate homozygous line for control animals. The *rd/rd* and *rd/rd cl* lines were maintained as one line homozygous for the *rd/rd* mutation and heterozygous for the *cl* mutation. The *cl* line was derived from crossing *rd/rd cl* with the C3H wildtype mice. Lines were backcrossed onto commercially available C3H (Harlan Laboratories) on a yearly basis to minimize genetic drift. All transgenic animals on a C3H background were 80-100 days old prior to being used in experiments. *Opn4* $^{-/-}$ lines were maintained as *het/ het* breeding pairs. Genotyping methods are described below.

Opn1sw knockout (*Opn1sw*$^{tm1(KOMP)Vlcg}$) model

Opn1sw knockout animals were recovered at The Wellcome Trust Center for Human Genetics (University of Oxford) by Dr. Ben Davies using embryonic stem cell material obtained from the Knock-Out Mouse Project (KOMP) repository at the University of California, Davis (https://www.komp.org/).

Two embryonic stem cell clones were obtained from KOMP (10640A-F7 and 10640A-H6) both containing a full gene ablation of the *Opn1sw* allele so that no coding sequence of the *Opn1sw* gene remained. The full name for the allele and this model is *Opn1sw*$^{tm1(KOMP)Vlcg}$ but the model is referred to as *Opn1sw* KO in this thesis for simplicity. The complete coding sequence has been replaced with a ZEN-UB1LacZ reporter cassette where the endogenous ATG present in exon1 has been fused to a *LacZ* reporter gene (Figure 2.1). The ZEN-UB1 consists of a *LacZ* reporter with exogenous polyA sequence and a *loxP* flanked UBC-Neomycin-pA selection cassette; full details of the sequence of the reporter/selection cassette and the regions of flanking DNA can be found at

http://www.velocigene.com/komp/detail/10640. The 2498bp deleted sequence is copied below and Figure 2.2 shows the BLAST alignment of the deleted region with the *Opn1sw* gene on chromosome 6 of the mouse genome (http://blast.ncbi.nlm.nih.gov/Blast.cgi).

Full Deleted Sequence in *Opn1sw* KO:

tcaggagaggatgacttttacctgtttcagaatatctcttcggtggggccctgggatgggcctcagtaccaccttgctcctgtctgggccttccgcctccaggcagccttcatgggattt
gtcttctttgtggggaccccactcaatgccatagtgctggtggccacactgcattacaaaaagttgcgacagcccctcaactatattctggtcaatgtatccctcgggggcttcctcttct
gcatcttctctgtcttcacagtcttcatcgccagctgtcacggatacttcctctttggtcgccatgtttgtgctctggaggccttcttgggctctgtagcaggtactgaaggcaacctgggct
agagagagggggcccttaattatcctgagcagttggacctctaacaatgggctgtgtgagcattaaactccattccaactctctggacttgctcaattacacctatattccactccaggctc
agggagtctgtctaccccattcttttcacatttgctgcaggtctagtgacaggatggtcattggctttcctggcttttgaacgctacgttgtcatctgtaaaccttcggcagcatccgcttc
aactccaagcatgcactgatggtggtcctggctacttggattattggtatcggggtgtccatcccaccctttttggctggagcaggtgagaggatagggcagtgctctgatgtgggac
gagagattgggtataacctttattctttgacctgagttggtagagtaaggaggaaaggggccgctggagacatcaatggttactctgccattgtaactactgtagtgtcttctggcatt
cttccaactggagaagccaatccagaagctaagcccattcttccagttctcggaatgaatgtttggtccttttcaggttcatccctgagggcctgcagtgctcctgtggcccagactggt
acactgtgggcaccaagtatcgaagcgagtactacacctggttcctcttcatcttctgtttcatcattcctctttccctcatctgcttctcctactcccagttgctgaggactctcagagctgt
gagtgggttttgagaggggcaggtaggagtaactcaggaggccccaggagagacagtatatatcttcctcaggatacgtctagaatatccgtggtcagataggagtattggggaag
ggggagtgaaaacgctgttacaacttattggtagagcacttacctagcaggtgtgaggtactgggttccatcttctgcacaagaggtagtgggcgaaggaccagagagaggaggg
gacaaggatgggatcttttctagtgtcagagctgaggacgcccttcatgatgcctccctcaagggaaagccaaactcagccaggagagagagggctttgacccttgtgctcaattcc
aggtggcagctcagcagcaagagtctgctacgacacaaaaggctgaacgggaggtgagtcatatggtggtggtgatggtgggatccttctgtctctgctacgtgccctatgctgccc
tggccatgtacatggtcaacaatcggaaccacgggctggacttacggcttgtcaccatccccgccttcttttccaagagctcctgtgtctacaaccccatcatctactgcttcatgaataa
gcaggtaaagcggtctatctacattcccacgaggttctggtccattagaccctggttcttccgctattgatgtctttgtgactcagcaccctggcctccacacagggcttatagatgagga
aagccagagtagtccaagcaggccaggatgctcttggtaggcacatgaacccagagtatggttcctaaaatactggaacaaggggaggctagaccttgagccagaaaaatcaaatt
gaaagagtgggaaaggatgggaaatgcccccacctacttcatttagcaatggcagagatggagcaaagggcctttcacatgctcggcaaatatccgcatcactgagttatatatacat
catccctactctttctgtcttggtggaaaataacatcaacagtaacaggtgtctagctttttttcttttttaaagatagggtctgagtaacactagctgtcctggaactcatatggaaaccaggc
tgtccttgaactcaagaggtggtcctgcctcctatcccgagtgctggagtcaaaagatgtgtaccagcacataagtccagccttctgcaaaccttttaatccagtccttttaaagtttagcct
gcaggagcaaggagttaaaggtggagtttaggtagtcttcagggtaaggataataaacacttctctttccagttccgggcttgcattctggagatggtgtgcaggaagcccatggcag
acgaatctgacgtgtctggctctcagaaaacagaagtttctactgtctcttctagcaaagttggccctcactgaggcccctcagctggcctgctagcagca

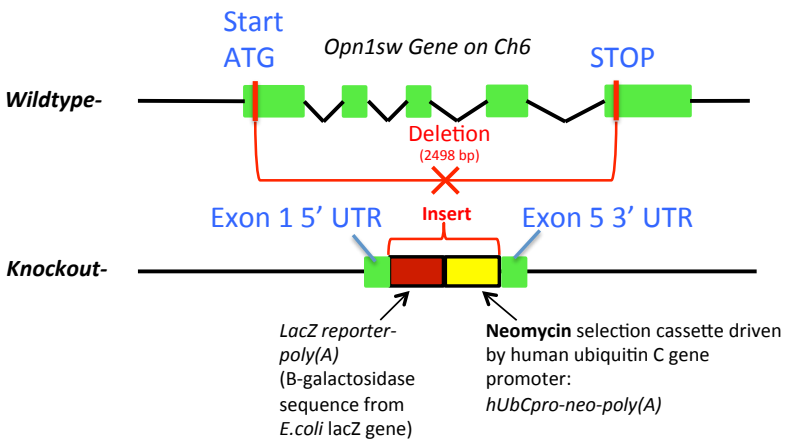

Figure 2.1: *Opn1sw* knockout construct- Top panel shows the wildtype *Opn1sw* gene structure based on the ENSMUST00000080428 transcript. The bottom panel shows the complete replacement of the coding region of the *Opn1sw* gene in the knockout by the ZEN-UB1 cassette consisting a *LacZ* reporter with exogenous polyA sequence and a *loxP* flanked UBC-Neomycin-pA selection cassette.

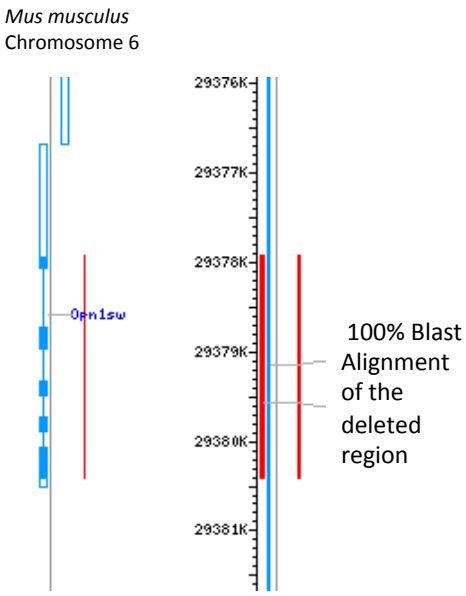

Figure 2.2: Deleted sequence in Opn1sw knockout- BLAST alignment (http://blast.ncbi.nlm.nih.gov/Blast.cgi) of the deleted sequence in the *Opn1sw* KO (above) with the wildtype *Opn1sw* gene on chromosome 6 of the mouse genome.

To summarize the procedure performed by Dr. Ben Davies and The Wellcome Trust Center for Human Genetics (University of Oxford), the ES cell clones were thawed and cultured before 12-16 ES cells were injected into individual blastocysts from 3 week old albino C57BL/6J female mice that had been superovulated and mated with albino C57BL/6J male mice. Embryos were flushed from the uterus of successfully mated mice on day 3.5 of pregnancy and cultivated for 2 - 3 hours until the majority of obtained embryos were at the expanded blastocyst stage.

Blastocysts for which successful injection occurred were then implanted into 2.5 day pseudo- pregnant foster CD1 mice. Offspring were judged for percent contribution of ES cells by appearance of black patches on the white albino coat. As ES cell karyotype was XY, chimeric male mice showing a high proportion of ES cell contribution were then moved from The Wellcome Trust Center to the Department of Biomedical Services, University of Oxford and bred with albino C57BL/6J females to check for germ line transmission.

As the ES cells obtained from the KOMP (VGB6) were from a C57BL/6N background and thus wild-type at the tyrosinase locus, germline presence of the chimeria/ albino pairings was indicated by pups heterozygous for the C2-J albino mutation and showing black coats. Black-coated pups were obtained for the 10640A-H6 ES cell line and genotyping (detailed below) determined two pups were indeed heterozygous (*het*) for the *Opn1sw* deletion. These *hets* were then bred with wildtype C57BL/6J mice (Harlan Laboratories) and *het* offspring from these used to establish *het/het* breeding pairs and trios so that littermate wildtype animals could be used as controls. Mice were all healthy and we did not observe any overt adverse phenotype associated with the deletion.

2.3 Genotyping

Genotyping was performed using tissue taken via ear punch. The tissue was digested in 50mM NaOH for 90 minutes at 95^{o}C before neutralization with a 1M Tris-HCl Buffer (pH 5) and storage at -20^{o}C or used directly for PCR.

PCR reactions were performed using the DNA from the digested ear punches in 20µl total volume with specific procedures details below:

rd/rd Genotyping-

Reagents

Primer RD 3 5'- TGA CAA TTA CTC CTT TTC CCT CAG TCT – 3'

Primer RD 4 5' – GTA AAC AGC AAG AGG CTT TAT TGG GAA – 3'

Primer RD 6 5' – GCA TTA ATT CTG GGG CGC ATG G – 3'

Stocks 100mM

AmpliTaq Gold polymerase (Applied Biosystems)

10X PCR Gold Buffer

25mM $MgCl_2$

dATP, dCTP, dGTP, dTTP

PCR grade water

PCR mix for 25µl volume

AmpliTaq Gold	0.25 µl
10X PCR Gold Buffer	2.5 µl
25mM $MgCl_2$	2.5 µl
10mM dATP, dCTP, dGTP, dTTP	0.5 µl
Primer 20mM	0.5 µl each
Genomic DNA	1.0 µl
PCR grade water	17.25 µl
	25.0 µl

PCR cycling conditions

Step 1. 95°C	5 min. x 1 cycle	
Step 2. 94°C	30 sec.	}
Step 3. 60°C	30 sec	x 40 cycles
Step 4. 72°C	1 min.	
Step 5. 72°C	10 min.	

Expected product sizes:

The RD3/RD6 pair of primers amplify a 0.4 kb PCR product from the wild-type *Pdeb* allele whereas the RD3/RD4 primer pair amplify a 0.55 kb product from the mutant *Pdeb* ^{rd1} allele. Both of these bands should of course be present in the heterozygous mice. See Table 2.1.

Table 2.1 *rd/rd* genotyping expected results

Primer Set	Product size	Wildtype non-*rd*	Het	*rd/rd*
RD3/RD6	0.4kb	+	+	-
RD3/RD4	0.55kb	-	+	+

cl Genotyping

PCR mix

		ul	*MM x 10*	*Final conc.*
Buffer		2.5	25	x 1
$MgCl_2$		1	7.5	2mM
dNTPs		0.5	12.5	200 µM each
Primers:	DTA +	0.5	5	0.5 µM
(25 µM)	DTA -	0.5	5	0.5 µM
H_20		14.75	142.5	
Taq		0.25	2.5	
DNA		5	-	
		25 µl	Total	20 µl each

Add 2.5 µL of Taq polymerase (diluted 1in 5) to each MM x10 aliquoat used.

For 10µL Taq 1 in 5 dilutionuse:

2µL Taq DNA polymerase

1µL NH_4 Buffer

7µL H_2O

Add 20µl of MM per tube, then 5 µl of DNA. Run PCR with annealing temperature at 60°C.

Primers:

Dta + GTACCACGGGACTAAACC

Dta - ATACTCATACATCGCATCTTG

PCR Cycle:

94°C for 3mins

94°C for 15s
62°C for 30s
72°C for 30s } x 35 cycles

72°C for 5mins

Expected Result: Dta transgene in the *cl* should produce a 486bp product with these primers and no product in wildtype samples.

Opn4 $^{-/-}$ *Genotyping-*

Reagents

Primers:

Opn4 forward exon 3: 5'- AGA AGT GGC TCT TTG GGG AGA C – 3'

Opn4 reverse exon 4: 5'- GCA GAA GGC ATA GAA CTC GCA AC – 3'

LacZ forward: 5' – AAG CAG TCA GCA GCC CAA AG – 3'

LacZ reverse: 5' – TGT CAC CCT CCT GGT CTT GC – 3'

Sybr Green PCR master mix

PCR grade water

Protocol

PCR mix for 20µl

Sybr Green	10 µl
Primer	0.5 µl each
H_2O	8.0 µl
	19 µl

Make master mix and transfer 19µl to each well in the plate. Add 1µl of the lysate containing the genomic DNA to each well and apply foil to plate.

PCR cycling conditions

Holding stage

95 °C 10min.

Cycling stage (x35)

95°C 15sec

60 °C 1.0min.

Melt curve

95°C 15sec

60 °C 1.0min

95 °C 15sec

Expected results

Amplification of the wild-type *Opn4* sequence results in a 200bp band with a melting temperature of 82°C. The PCR product resulting from amplification of the *LacZ* gene in the mutant mice has a melting temperature of 85°C and is 300bp in size. The PCR with heterozygous mice carrying both alleles will result in a double peak representing the presence of the wild-type and *LacZ* sequences. In this case the second peak at the higher melting temperature of 85°C is significantly smaller than the wild-type product at the lower melting temperature of 82°C.

Opn1sw Genotyping-

Using the Quantifast SYBR Green PCR kit (Qiagen) under the following conditions:

1. 95°C for 5 min
2. 95°C for 10 sec
3. 60°C for 10 sec
4. 62°C for 20 sec
5. 40 cycles repeat above from step 2
6. 95°C for 15sec
7. 60°C for 60 sec
8. Hold at 4°C

Primers used to confirm replacement of the *Opn1sw* gene by the reporter/selection cassette from http://www.velocigene.com/komp/detail/10640 and listed in Table 2.2. Initially products were checked for correct size on a 2% Agarose gel and later genotyping was based on real-time PCR read-outs for presence or absence of primer products.

Table 2.2 Opn1sw genotyping primers (A) List of primer sequences and **(B)** expected product sizes. WT, Het and KO mice will have a different combination of products based on presence of *Opn1sw* gene and/or ZEN-UB1 selection cassette.

(A)

Primer	Sequence
SU	CACAGAAACCAATACTGACC
SD	AAAGGAAGTGTTACCCATAC
LacInF	GGTAAACTGGCTCGGATTAGGG
LacInR	TTGACTGTAGCGGCTGATGTTG
NeoInR	TACTTTCTCGGCAGGAGCAAGGTG
NeoInf	TTCGGCTATGACTGGGCACAACAG
LacInZRev	GTCTGTCCTAGCTTCCTCACTG
NeoFwd	TCATTCTCAGTATTGTTTTGCC
TUF	GCTGTCACGGATACTTCCTCTTTG
TUR	AGCCCAGGTTGCCTTCAG
TDF	CAGGCTGTCCTTGAACTCAAGAG
TDR	GCTGGACTTATGTGCTGGTACA

(B)

Forward Primer	Reverse Primer	Product Length	WT	het	KO
SU	LacZRev	416bp	-	+	+
TUF	TUR	90bp	+	+	-
TDF	TDR	86bp	+	+	-
NeoFwd	SD	333bp	-	+	+
LacInF	LacInR	210bp	-	+	+
NeoInf	NeoInR	282bp	-	+	+

2.4 Light measurements

Spectral measurements of light sources were made using a radiometrically calibrated spectrophotometer (Ocean Optics, UK). For assessment of light intensities, a Precision Gold N76CC Light meter was used to measure lux for the threshold-entrainment study and then an Illuminance UV recorder (TR-74Ui, T&D Corporation) was acquired, able to measure white light in lux and UV light in mW/cm^2, which was used in all subsequent experiments. Conversion of power measurement to log $photons/cm^2/s$ and vice versa were made using the light rodent toolbox available at http://www.eye.ox.ac.uk/team/principal-investigators/stuart-peirson. All light measurments were made at 'mouse-level' in each apparatus.

2.5 Circadian Activity monitoring for threshold of entrainment

Placed in light-tight ventilated chambers, mice were individually housed in cages fitted with running wheels and the presence of wheel-running activity was automatically recorded in 1-min bins by the ClockLab data acquisition system (Actimetrics, Wilmette, IL, USA). Light was provided by white LEDs (see Figure 2.3 for spectrum) set to 100lux, layers of neutral density (ND) filter were used to decrease light levels by log units to 10 lux, 1lux, 0.1lux, 0.01lux and 0.001lux. After 14 days of initial entrainment, 7 days were spent at each light intensity and stable entrainment assessed. Before moving to a lower light intensity, the light levels were returned to 100lux to ensure that any free-running animals were re-entrained (no animals of any genotyped failed to entrain to the 100lux light level).

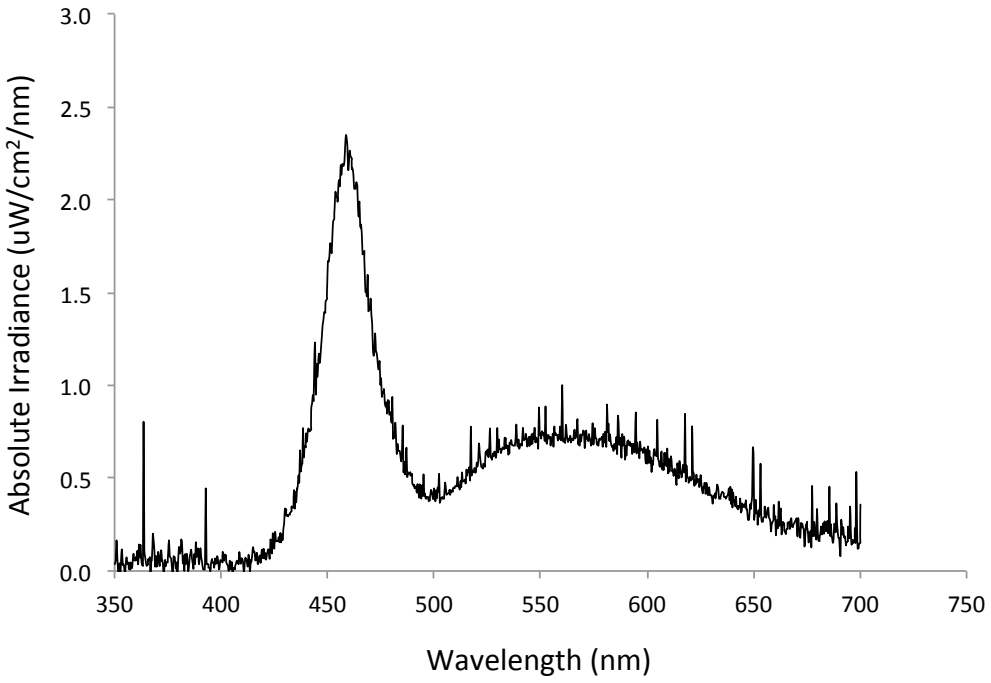

Figure 2.3 Spectrum of White LEDs present in light-tight chambers used for activity monitoring

2.6 Construction of Irradiance Response Curves

Techniques and protocols for measuring circadian phase shifts to discrete light pulses using the phase of onset of circadian wheel running are well established (Albrecht and Foster, 2002). Animals were placed in continuous darkness prior to exposure to a 15 minute phase delaying light pulse of a pre-determined light intensity. The magnitude of the steady-state behavioral phase shift was determined by fitting straight lines to the slopes of activity onsets before and after the light pulse using the ClockLab Software. The time difference between the onset predicted by the 'before' line and that by the 'after' line on the day of the pulse determines the magnitude of the phase shift. Due to the likelihood of transients, the activity onsets on the first three days after the light pulse were excluded from analysis.

For the construction of UV irradiance response curves (IRC), all animals were entrained to 12/12 LD (light/dark) then placed in DD (constant dark) for 2 weeks prior to the initial UV light pulse. Light pulses at 365 nm were given weekly for 15 minutes in a separate pulsing chamber at CT16 using a custom-made light source consisting of 5 UV LEDs (NCCU033, Nichia, Japan) (Figure 2.4 for light spectrum).

Excel (Microsoft) was used to fit a four parameter sigmoid curve to IRCs based upon the method of least squares, as described previously for phase shifting data (Peirson et al., 2005), from which the IC50, or half maximal response, value can be calculated. A sigmoid curve is defined by:

$$\text{Response} = \frac{(Top - Bottom)}{1 + 10^{((EC50 - n) \times k)}}$$

Where 'Top' is the maximum saturating response, 'Bottom' is the baseline response and k is slope (Motulsky and Christopoulos, 2003). Non-linear regression was used to determine the best fit for each phase-shifting data set based on the sum of least squares as stated above. A model was found that minimized the sum of squares (SS) of the regression, which is the sum total of the differences between the phase-shifting data points and model at each irradiance. The difference is squared to make it sign independent. The R^2 value gives a measure of fit for a particular model between 0 and 1 where 1 is a perfect fit. The R^2 value is found by dividing the sum of squares of regression by the total SS (SS_{total}), which is the SS for a model with a straight line through the data mean.

$$R^2 = 1 - \frac{SS_{regression}}{SS_{total}}$$

Thus the $SS_{regression}$ equals zero where there is no difference between the model and data points resulting in R^2 =1. Excel (Microsoft) was used to determine the model where R^2 was as close as possible to 1 for each IRC and IC50 determined from the fit. Approximate parameters were used in each case to avoid the issue of local minimum.

For comparison of UV IRC to IRCs at other wavelengths, wildtype data from Stuart Thompson was used and is shown below for 365, 420, 460, 471, 506, 540, 560 and 580nm (Figure 2.5) (published (van Oosterhout et al., 2012)). These IRCs were used for comparison of UV 365nm and visible 506nm IRCs (see Figure 4.1) as well as for illustration of full wildtype spectral sensitivity (see Figure 4.5). Photopigment templates for comparison of residual sensitivity and figures based off the Govardovskii model (Govardovskii et al., 2000).

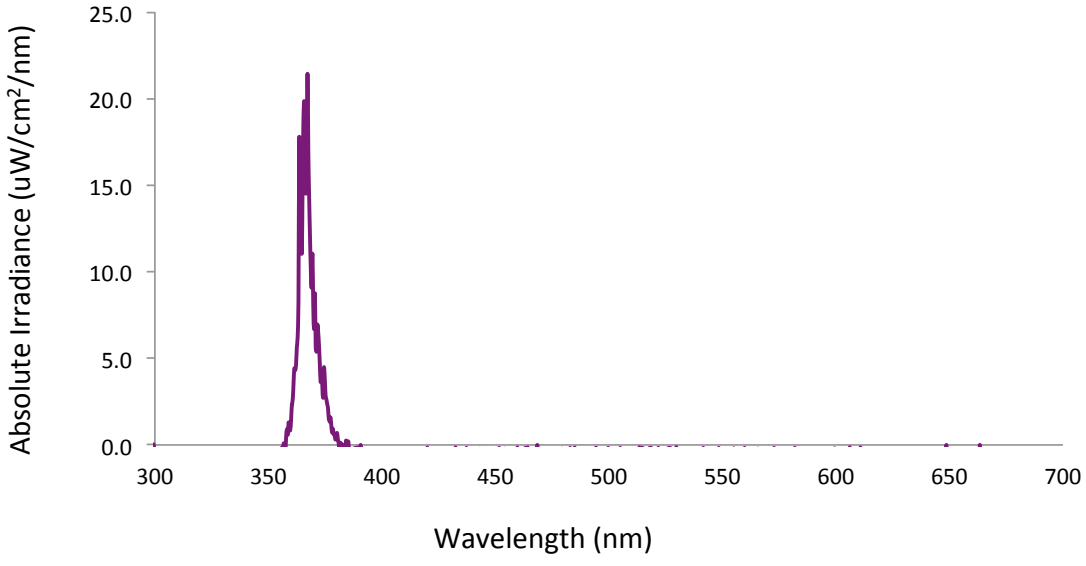

Figure 2.4 Spectrum of UV LEDs (NCCU033, Nichia, Japan) used for all UV light pulses

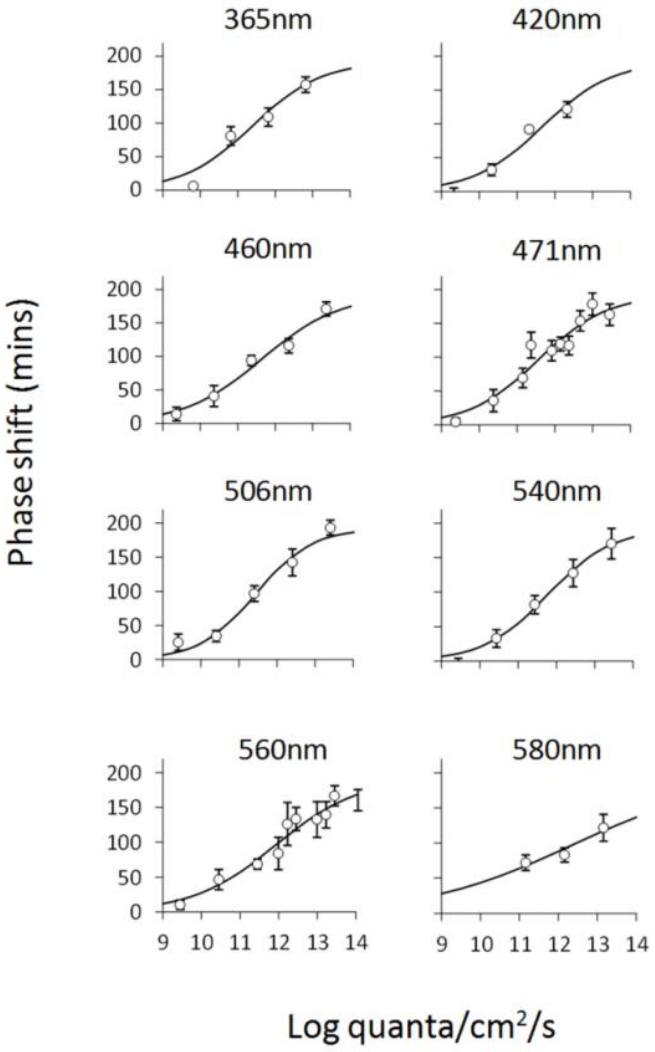

Figure 2.5 Wildtype IRCs Wildtype C3H phase-shifting IRCs for 365, 420, 460, 471, 506, 540, 560 and 580nm monochromatic wavelengths from collaborator Stuart Thompson used in generation of Figures 4.1 and 4.5. Published in (van Oosterhout et al., 2012).

2.7 Immunostaining of retinal flatmounts

Preparation and labelling of retinal sections and retinal flatmounts was performed as described previously by our lab (Hughes et al., 2012c). For labelling of whole retina flatmounts, whole eyes were removed, punctured with a fine gauge needle and placed in 4% paraformaldehyde (PFA) (Thermo Scientific) in Phosphate buffered saline (PBS) at 4^{o}C for 16hr. Retina were then dissected and placed in 30% sucrose for 24h prior to freeze thaw cycles (x2) with liquid Nitrogen. Retina were then further permeabilised in PBS with 1% Triton-X for 30mins, and then blocked in 10% donkey serum for 1hr at room temperature (RT). Primary antibodies were incubated for 24-72h at 4^{o}C, followed by incubation with Alexa (Life Technologies) or Dylight (Jackson Immunoresearch) fluorescent labelled secondary antibodies 1:200 for 2h at RT (Table 2.3). All antibodies were diluted in PBS with 2.5% donkey serum and 1% Triton-X. All wash steps were performed using PBS with 1% Triton-X. For double labelling using *c-fos* and UF006 antibodies, both raised in rabbit, a special staining procedure was performed by Steven Hughes to allow use of both antibodies on the same sections. Antibodies were incubated and labelled sequentially (*c-fos* then UF006) using additional blocking steps with rabbit anti-goat IgG for 2hr at RT and then unconjugated donkey anti-rabbit monovalent Fab fragments (Jackson Immunoresearch) for 2hr at RT to minimize sequestering of the second primary antibody and cross labeling of the second secondary antibody with the first primary antibody. All samples were mounted onto glass slides with Prolong Gold anti-fade media containing DAPI (Life Technologies).

Table 2.3: Antibodies used in ICC for whole mounts and *Opn1sw* sections

Target	Antibody species	Source	Dilution	Secondary antibody
Melanopsin	Rabbit polyclonal	UF006, Advanced Targeting Systems	1:2500	Donkey anti-rabbit Alexa 488 and Alexa 568
MWS opsin	Rabbit polyclonal	RJ492, a kind gift from J. Nathans	1:1000	Donkey anti-rabbit Alexa 568
UVS opsin	Goat polyclonal	Ab code, Santa Cruz	1:1000	Donkey anti-goat Alexa 488 and Alexa 633
c-fos	Rabbit monoclonal	Ab code, Cell signalling	1:200	Donkey anti-rabbit Alexa 568
β-gal	Chicken polyclonal	Abcam AB 9361	1:500	Donkey anti-chicken 488

Image acquisition and analysis

Images were acquired using an Olympus IX71 inverted microscope fitted with a high sensitivity CCD camera (Cascade 512B, Photmetrics) and Metamorph image acquisition software (Molecular Devices). Excitation filters for DAPI, green and red fluorescence were, 350nm, 480nm and 545nm respectively. Emission filters were 460nm, 525nm and 600nm. Where stated multiple images were collected at different focal planes and reconstructed into a single 'in focus' image using an extended focus plugin for ImageJ image analysis software

(Macbiophotonics). High resolution images were collected using an inverted LSM 710 laser scanning confocal microscope (Zeiss) and Zen 2009 image acquisition software (Zeiss). Individual channels were collected sequentially. Laser lines for excitation were 405nm, 488nm, 561nm and 633nm. Emissions were collected between 440-480nm, 505-550nm, 580-625nm and 650-700nm for blue, green, red and far-red fluorescence respectively. For retina images, multiple overlapping image z-stacks (~60-64 z-stacks per retina) were manually collected at x20 magnification using UVS (wildtype), β-gal (*Opn1sw KO*) or melanopsin/marking during dissection (*rd/rd* cl) for orientation. Global enhancement of brightness and contrast levels of all images was performed using Image J software. For M1/M2 *c-fos* positive pRGCs present in whole retina flatmounts, manual counting of samples double labeled with *c-fos* and melanopsin antibodies was performed and melanopsin cells identified by their morphology and projections by Steven Hughes. For c-fos positive cell counts, Image J software was again used, employing a standard level of background subtraction and counting of bright areas from 15-250 pixels inclusive. Manual counting of randomly chosen images from each retinal region was used to confirm accuracy of automated cell counts. The normal distribution of all data was confirmed by the Shapiro-Wilk test using a plug-in for MS Excel (Analyse-it, Analyse-it Software, Ltd).

Light pulse

For c-fos retinal staining, mice were dark adapted for 4h and then exposed to 30-minute light pulses at ZT16 in a separate pulsing cage. Following the cessation of light stimuli mice were kept in the dark for a further 30 minutes before eyes were collected and processed for immuno-staining as described above. Mice receiving sham light pulses were used for

controls and were moved to the pulsing chamber but not exposed to a light stimulus. White light pulses were produced by a white LED light source (Figure 2.3), UV light pulses were produced by 5 UV LED's (NCCU033, Nichia, Japan) (Figure 2.4). Light measurements were always made at mouse-level in pulse set-up.

2.8 Light/ Dark Box

For assessing light aversion, a square light/dark box (28x28 cm) was constructed based on previous studies of this apparatus (Semo et al., 2010) using clear and black opaque Perspex so that the closed opaque side and open clear side were of identical proportions (Figure 2.6). The light source was suspended over the clear half of the arena as was a miniature near infrared (NIR) video camera (Sentient Mini-night vision CCTV camera, Maplin, UK) to record video. White light was provided using a fluorescent stand lamp (See Figure 2.7 for light spectrum) and UV Light using 5 LED set-up described previously (Figure 2.4).

Mice were placed directly into the lighted clear side facing away from the dark half of the box without any acclimatization trial so that a naïve response to the arena was examined in each case and all mice were tested in the light phase of the LD cycle (ZT3-8). So that naïve responses were maintained for both light conditions, different groups of WT and KO animals were used for the white light and UV trials where both groups also contained equal numbers of males and females. The amount of time the mice spent in the lighted side of the area was recorded for a 10-minute trial with the apparatus cleaned fully with ethanol between animals. Video tracking analysis was performed using ANY-maze software (Version 4.5, Stoelting,

US) with tracking beginning from the time where animals first crossed into the dark half to ameliorate two potential confounding factors i) the amount of time animals take to discover the dark half or ii) variability in the freezing behavior all animals exhibited to some extent immediately upon placement into the light.

Figure 2.6 Light/Dark box corner and side view of apparatus (28cm x 28cm)

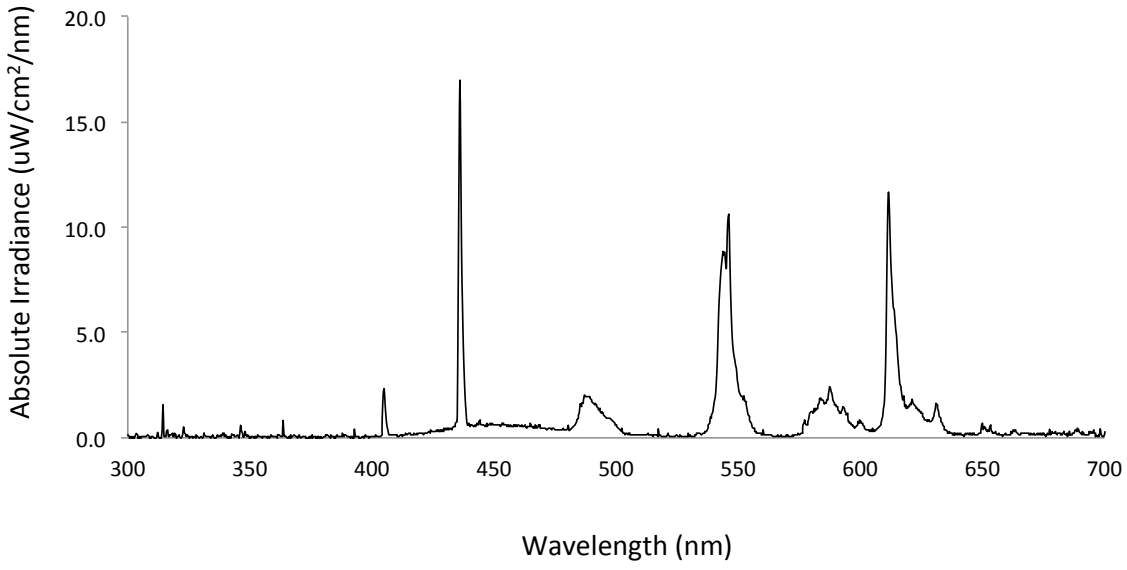

Figure 2.7 Fluorescent light spectrum used for white light in Light/Dark box and OKR

2.9 Optokinetic Drum

An Optokinetic (OKR) drum was constructed by the Oxford University Physics Workshop under our direction with a rotating Perspex drum 29cm in diameter and 56cm tall with a 25cm raised stationary platform at the center where the animal was placed (Figure 2.8). The drum was run off of Stepper Bee (+) software and all animals tested were habituated to the apparatus over several sessions before any recording was done. The mice were placed onto the platform in the center of the drum and given 3 min to acclimatise before a sham run was recorded using a white background. Testing stripe gratings (printed to fit the drum) of 0.1, 0.2, 0.3, 0.4, 0.5 and 0.6 cycles per degree (cpd) were given in a random order. The drum was rotated at a speed of 2 rpm as is standard for testing mice in this apparatus (Douglas et al., 2005), 30s in each direction, repeated twice per trial. Head tracking was recorded using a Logitech webcam under white light trials and then a using a miniature near infrared (NIR) video camera (Sentient Mini-night vision CCTV camera, Maplin, UK) for UV light trials. Videos were counted three times each for the number of head tracking responses per minute and presence or absence of response. A head-tracking response was considered to be a continuous movement of the head of the mouse of the same speed and direction as the drum's rotation. The threshold acuity was considered at least 2 head-tracking episodes per minute to reduce the likelihood of a chance movement at same speed of drum affecting threshold determination. White light was provided using a fluorescent stand lamp (Figure 2.6) and UV Light using 5 LED set-up described previously (Figure 2.4). The light intensity at the platform was also recorded prior to each testing session. After initial white light testing, it was noted that the 0.3 cpd grating had been miss-printed so that the stripe pattern

was different in a region about the level of the animal thus did not maintain a constant cpd. This grating was excluded from analysis and a new corrected 0.3cpd grating was made for analysis of UV *Opn1sw* OKR.

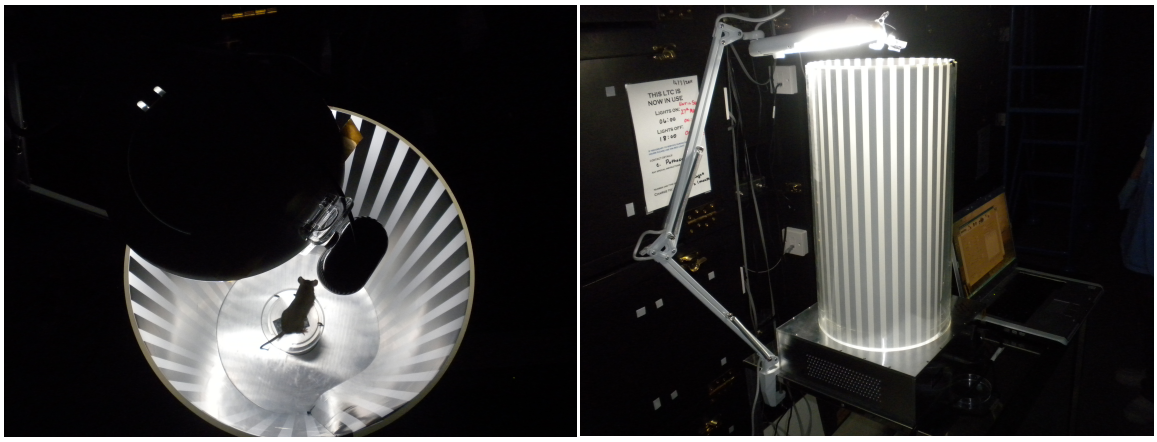

Figure 2.8 Optokinetic Drum Top and side view of OKR drum under white light

2.10 Novel Object Recognition Visual Assay

Arena

A 20 × 20 × 20 cm^3 open top cubic arena made of transparent acrylic was used for the novel-object recognition task. To allow visual discrimination of the four corners, two distinct wallpapers, one with a white five-point star on a black background and the other showing a checkerboard pattern were attached to the outside of two walls (Figure 2.9). Small Velcro sticks (Rip 'n' Grip, Essex, UK) were adhered to the floor and the bottom of all objects, so that objects could be affixed to the floor of the arena during testing. A miniature near infrared (NIR) video camera (Sentient Mini-night vision CCTV camera, Maplin, UK) to

record video was positioned 40 cm above the center of the floor of the arena. White light was provided using White LEDs (Figure 2.3) and UV light using the UV LED set-up (Figure 2.4).

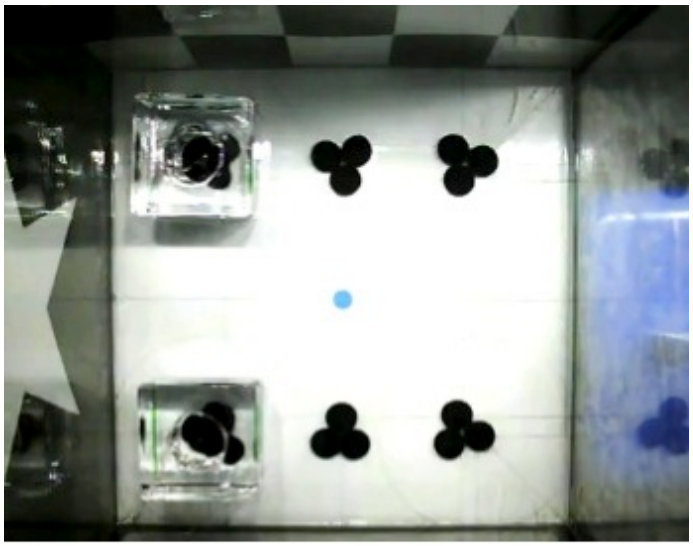

Figure 2.9 Novel Object recognition arena (from above), note checkerboard on top wall and the star on left wall

Objects and Odours

Previous work by group member Eric Tam had examined a large variety of simuli for use in novel-object recognition studies that differed in one or more sensory dimension including ceramic ornaments, light bulbs, and LEGO bricks. For the visual adaptation of this task a glass candle holder (length × width × height: 4.5 cm × 4.5 cm × 2.5 cm) was used with four replicates, so that different replicates of the same object could be presented during the sample and test phases to avoid any chance of odour cues being carried over between the

phases. For the *Opn1sw* line odour recognition experiment, odour cues of natural lemon and vanilla extract were used for the first animal batch while peppermint and banana extracts were used for batch 2. 1 ml of the liquid odour extract was put in clear shot glasses (diameter × height: 2.5 cm × 4.5 cm) and again different replicates of the shot glass were used in the sample and test phases. Both candle holders and shot-glasses were cleaned carefully with ethanol between animals and the arena was cleaned between the sample and test phase as well as between animals.

NOR experimental procedure

The basic structure of the object and odour trials was the same with a 10-minute sample phase, 5 min retention period and a 3 min test phase. In the sample phase of the visuospatial object displacement trial test a mouse was allowed to freely explore for 10 min with two identical replicates of the candleholder object located at the top left and bottom left corners of the arena as shown in Figure 5.10 of Chapter 5. During the delay period, the animal was removed from the arena for 5 min and interior of the arena was cleaned with ethanol. One replicate object was displaced to an adjacent corner (e.g., from the bottom left corner to the bottom right corner), whereas the other replicate remained at the same location (e.g., top left). The replicate that was selected for displacement was counterbalanced within and between all genotype groups. For half of the animals that were given the object displacement trial, the replicate located at the top left corner was displaced to the top right corner; the replicate at the bottom left corner was not displaced. For the remaining animals, the replicate located at the bottom left corner was displaced to the bottom right; the replicate at the top

left corner was not displaced. For the odour trails, the objects in the sample phase were two replicate shot glasses containing 1mL of an identical odour located at opposite corners of the arena. Then for the sample phase, instead of object movement, the shot glass in one corner was presented with a different odour. Different replicates of the shot glass were available, so that a fresh odour sample could be presented at test and the sample phase. Odours were counterbalanced both within and between genotype groups. Diagramic representations of the object and odour trials are presented in Figure 2.10.

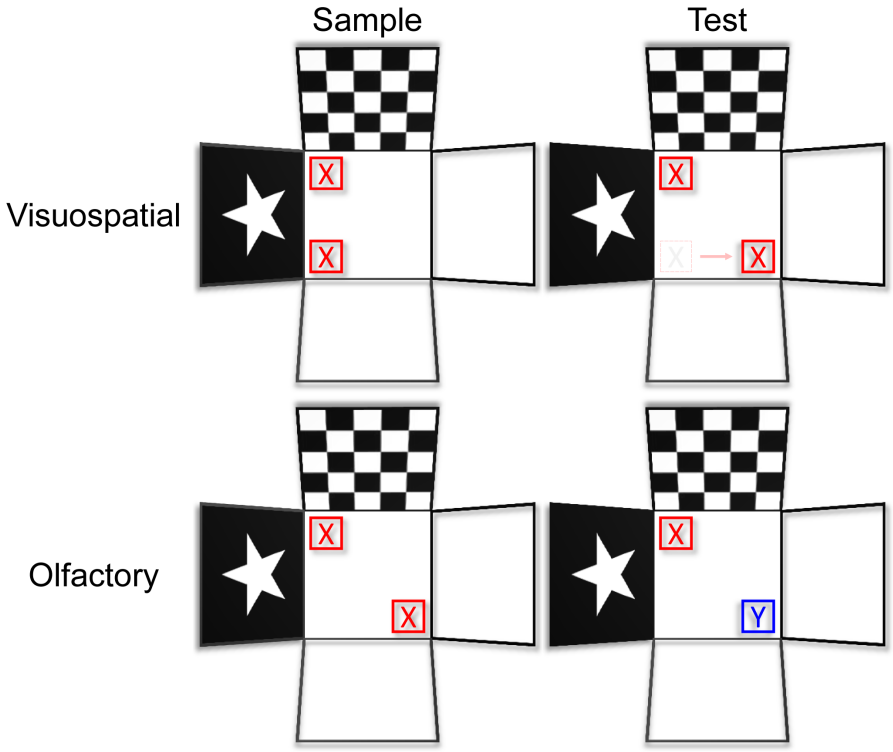

Figure 2.10 Odour and Object Displacement Recognition Trials Locations of objects/ odours in the phase and tests phases, these diagrams are also presented in Chapter 7 as figures 7.6 (object) and 7.9 (odour).

For analysis, videos were recorded during the 10-min sample and 3-min test phases. Automated tracking was subsequently conducted in the ANY-maze software (version 4.5; Stoelting, Wood Dale, Illinois). The tracking protocol used was similar to that in previous studies by members of our group (Tam et al., 2014). For each video file, the floor of the arena was outlined in ANY-maze, and two notional squares were placed at the corners of the arena where the objects were located. The mouse's head was tracked, and its position within the arena was determined on a second-by-second basis. The amount of time the animal's head was within each of the two notional squares was recorded for every minute of the sample and test phases. The recognition performance for each animal was calculated as the ratio of time spent examining the object/ odour representing the familiar (f) versus the new (n) condition so that the ratio= n/(n+f). Ratio greater then 0.5 demonstrated increased interaction with the new condition and the higher above 0.5 the ratio is then the better the recognition performance. A ratio less than 0.5 suggests preference for the familiar stimuli and a ratio of 0.5 suggests no differentiation between the conditions.

Analyses of variance (ANOVAs) were conducted on recognition ratios and the amount of time spent in object exploration was used to compare between genotype groups. Finally, one-sample *t* tests (2-tailed) were conducted to compare mean recognition ratios against chance performance (0.5).

2.11 Assessment of opsin expression in *Opn1sw* KO retina

To examine opsin expression in the *Opn1sw* model, eyes were dissected and immediately placed on dry-ice then stored at -80^{o}C until RNA extraction. For RNA extraction, eyes were manually homogenized in 100µL QIAzol reagent (Qiagen). Homogenized tissue was spun for 10 min at 12,000× g at 2–8 °C, the supernatant transferred into fresh tubes and then kept at RT for 5 min. Next, 0.2 ml chloroform was added the tubes shaken, left to sit for 3 min at RT and then samples were centrifuged at 12,000× g for 15 min at 2–8 °C. The upper aqueous phase was then transferred into a fresh tube, 0.5ml ethanol was added and samples were mixed by shaking. Following 10 min at RT, the RNA was extracted using the RNeasy Mini Kit (Qiagen) protocol and checked for quantity. cDNA was obtained using QuantiTect Reverse Transcription Kit (Qiagen) and used in qRT-PCR with Quantifast SYBR Green PCR kit (Qiagen) under the following conditions:

1. 95°C for 10 min
2. 95°C for15 sec
3. 60°C for 60 sec
4. 76°C for 15 sec
5. 40 cycles repeat above from step 2
6. 95°C for 15 min
7. 60°C for 60 sec
8. Hold at 4°C

Primers used are presented in Table 2.4, Opsin expression levels were normalized to the geometic mean of *Gapdh* (Glyceraldehyde 3-phosphate dehydrogenase), *B2M* (β2 Microglobulin) and *ARP* (acidic ribosomal protein).

Table 2.4: Opsin primers and Housekeeping Genese

Primer Target	Sequence	Tm (^{o}C)	Product Size (bp)
Opn1sw F	TCTTCACAGTCTTCATCGCCAGC	79	134
Opn1sw R	GTTCAAAAGCCAGGAAAGCCAATG		
Opn1mw F	ATGGTGGTGGTGATGGTCTTCG	80	257
Opn1mw R	TGTCTTGGAGGTGCTGGAAAGTTC		
Opn4 F	TCACAGGGATGCTGGGCAATC	82	161
Opn4 R	TTCTTGTAGAGGCTGCTGGCAAAG		
Rho F	TGTTCCTGCTCATCGTGCTGG	83	312
Rho R	GGAAGTTGCTCATCGGCTTGC		
GAPDH F	TGCACCACCAACTGCTTAG	82	176
GAPDH R	GATGCAGGGATGATGTTC		
ARP F	CGACCTGGAAGTCCAACTAC	76	111
ARP R	ATCTGCTGCATCTGCTTG		
B_2-M F	GCTATCCAGAAAACCCCTCAA	78	302
B_2-M R	CATGTCTCGATCCCAGTAGACGGT		

2.12 *Opn1sw* retinal sections staining

Opn1sw KO and WT whole eyes were removed, punctured with a fine gauge needle and placed in 4% paraformaldehyde (PFA) (Thermo Scientific) in PBS at 4^{o}C for 16hr. Retina were then dissected and placed in 30% sucrose for 24hr prior to freezing in Tissue-Tek O.C.T media for cryostat sectioning and mounting on glass slides. Slides were then further permeabilised in PBS with 0.2% Triton-X for 20min, and then blocked in 10% donkey serum, 0.2% Triton-X for 1hr at RT. Primary antibodies were incubated for 2hr at room temperature, followed by 2hr incubation with Alexa (Life Technologies) or Dylight (Jackson Immunoresearch) fluorescent labelled secondary antibodies 1:200 for 2hr at RT (Table 2.3). All antibodies were diluted in PBS with 2.5% donkey serum and 0.2% Triton-X. All wash steps were performed using PBS with 0.2% Triton-X. All samples were mounted onto glass slides with Prolong Gold anti-fade media containing DAPI (Life Technologies) and imaged as described in section 2.7.

2.13 Pupillometry

Mice entrained for 2 weeks under a 12:12 light:dark cycle (100lux white light) and were further dark adapted for 1–2h prior to testing between zeitgeber time (ZT) 14 and 18. A xenon arc lamp (150W) solar simulator, Lot Oriel, UK) with a 480 nm monochromatic filter (Andover, 10nm half-bandwidth) was used to produce a bright light intensity of 14.6 log quanta/cm^2/s (173 μW/cm^2/s). UV Light was produced by UV LEDs. In all cases, light was transmitted to the eye via a liquid light pipe as an irradiant light stimulus using a 2-inch

integrating sphere (Pro-lite Technology, UK). Custom computer software was used to regulate a shutter in the light pathway (LSZ160 shutter, Lot Oriel; custom software supplied by BRSL, Newbury, UK) and control light delivery.

Mice were un-anaesthetized and only temporarily restrained during the recording period. Light stimulus began after 2s of dark-adapted pupil measurement following which the left eye was exposed to the pre-determined wavelength and intensity for 10s. Recording continued for a further 17s for examination of pupil recovery. Images of the pupil were collected with a Prosilica near infrared-sensitive charge couple device video camera (BRSL) at a rate of 10 frames/s. The camera was positioned 90 degree to the contralateral eye, which was itself illuminated by infra-red light emitting diodes (850 nm, 10 nm half-bandwidth). Pupil diameter over the entire 29s protocol (10 images/ sec) was determined using ImageJ image analysis software (http://rsbweb.nih.gov/ij/).

Chapter 3: **Photoreceptor roles in determining the threshold of circadian entrainment**

Introduction

3.1 Aims

The field of mental health is discovering the importance of stable entrainment to neurological function (Ellenbogen, 2005; Hastings and Goedert, 2013) while the function of fundamental physiological processes like metabolism and immune response depend on the precise coordination of the body clock and the external environment (Hastings et al., 2007). For mammals the key external stimulus for entrainment, or zeitgeber, is light which is sensed by the ocular photoreceptors that drive signals down the retinohypothalamic tract (RHT) to adjust the clock as described in 'Clock Adjustment for Entrainment' in Chapter 1. However, there is a threshold of light sensitivity that defines the minimum intensity of light required by an animal to lock onto an external light cycle. While there has been considerable investigation of how discrete amounts of light affect the clock, there has been surprisingly little research examining which ocular photoreceptors are responsible for this threshold of entrainment. Here the background of common experimental methods and genetic models used for assessing entrainment is briefly reviewed as well as the existing evidence for the contributions of specific photoreceptors to mammalian entrainment and entrainment threshold. In this first thesis data chapter, we describe experiments using mouse models lacking one or more of rods, cones and melanopsin to separate individual photoreceptor roles in determining the threshold of entrainment to a 12:12 Light/Dark (LD) cycle of diminishing intensity.

3.2 Assessing entrainment

A common method used to investigate specific elements of the circadian system has been genetic manipulation of animal models to generate mutants lacking key elements of clock or photoreceptor function and assessing the resulting impact in the model animals compared to wildtype under controlled conditions (Jud et al., 2005). For rodent models, activity rhythms have often been assessed by placing running-wheels in cages where wheel rotations give a measure of the activity and rest cycles of the animal (Albrecht and Foster, 2002). The animals can thus be housed under various light environments such as light-dark (LD) cycles varying from the standard 12 hours light, 12 hours dark, which is known as 12:12 LD, to constant light (LL) or constant dark (DD).

The outputs of measured activity locomotor rhythms are often illustrated as actograms where the activity over consecutive days is organized into a vertical stack. For an entrained animal, an activity (*alpha*) and rest (*rho*) phase are determined from the onset and end of the main phase of locomotor activity with the activity occurring during the light phase for diurnal animals or in the dark phase for nocturnal animals like the mouse (Jud et al., 2005). When an external light cycle is present, time over the day is expressed as Zeitgeber time (ZT) so that under a 12:12 LD cycle ZT0 is at lights on and ZT12 at lights off. When an animal is entrained to a light cycle, the time between the start of its activity and, for example, time of lights on will be the same from day to day and this is termed a stable phase angle of entrainment. However, an entrained rhythm does not show the natural internal clock period.

To determine the period or *tau* of an animal, constant dark conditions are used so that there is no external light cue to entrain to. The animal's *alpha* and *rho* will then occur according to the clock time and, as the natural period of most animals is not equal to 24 hours, the activity will begin either slightly earlier or later each day relative to external time depending on if the *tau* is less or greater than 24 hours respectively (Jud et al., 2005). The animal is then said to be free-running and time is expressed as Circadian Time (CT) with CT0 the start of the activity phase for diurnal animals, or the rest phase for nocturnal animals, and CT12 vice versa.

From these wheel-running assessments, a number of different aspects of entrainment can be compared between a wildtype and mutant and/or transgenic animal to determine any changes to circadian function (See Figure 3.1 for example actogram and common terms). The most straightforward is the presence or absence of stable entrainment to a given light cycle and light intensity. The light cycle of an entrained animal can also be advanced or delayed. The mechanism for adjusting the clock limits the maximum magnitude of activity rhythm shift that can occur over a given day (Jagannath et al., 2013) so an animal re-entrains to a large light cycle change over a number of days. As the activity onsets move closer to the light onset defined by the new LD cycle, transient activity rhythms are in evident where the observed rhythm is somewhere between the old cycle and the light input from the new cycle. The number of days an animal takes to re-entrain to a given light cycle shift can be another indicator of clock function. The internal rhythm of an animal will also shift in response to external light input to varying extents over the circadian day. A change in the start of an animal's activity phase following a light pulse during the circadian night is termed a phase

shift (see Figure 3.1). The response to a given light pulse depends on the intensity of light and also on the point in the activity rhythm. Light exposure during the early subjective night will produce a phase delay whereas exposure during the late subjective night will produce a phase advance. By contrast, light exposure during the subjective day will not result in a phase shift (the so-called dead zone) (Jud et al., 2005). A final circadian parameter to note is masking where the overt activity rhythm (or other circadian rhythm) of an animal may not reflect the true internal clock due to an external zeitgeber cue having a strong depressing or enhancing effect. For example, bright light suppresses the activity of nocturnal animals like mice so that an animal may appear entrained to a bright LD cycle due to activity being constrained to the dark period but this is only due to negative masking effects and release of the animal into DD conditions may reveal that the clock is not properly entrained to the point of light on or off. In constant light, the period is lengthened according to the light intensity (called Aschoff's rule) (Aschoff, 1952) but during a prolonged LL light cycle the constant light input to the clock actually desynchronizes SCN neurons and can result in arrhythmic clock output (Ohta et al., 2005).

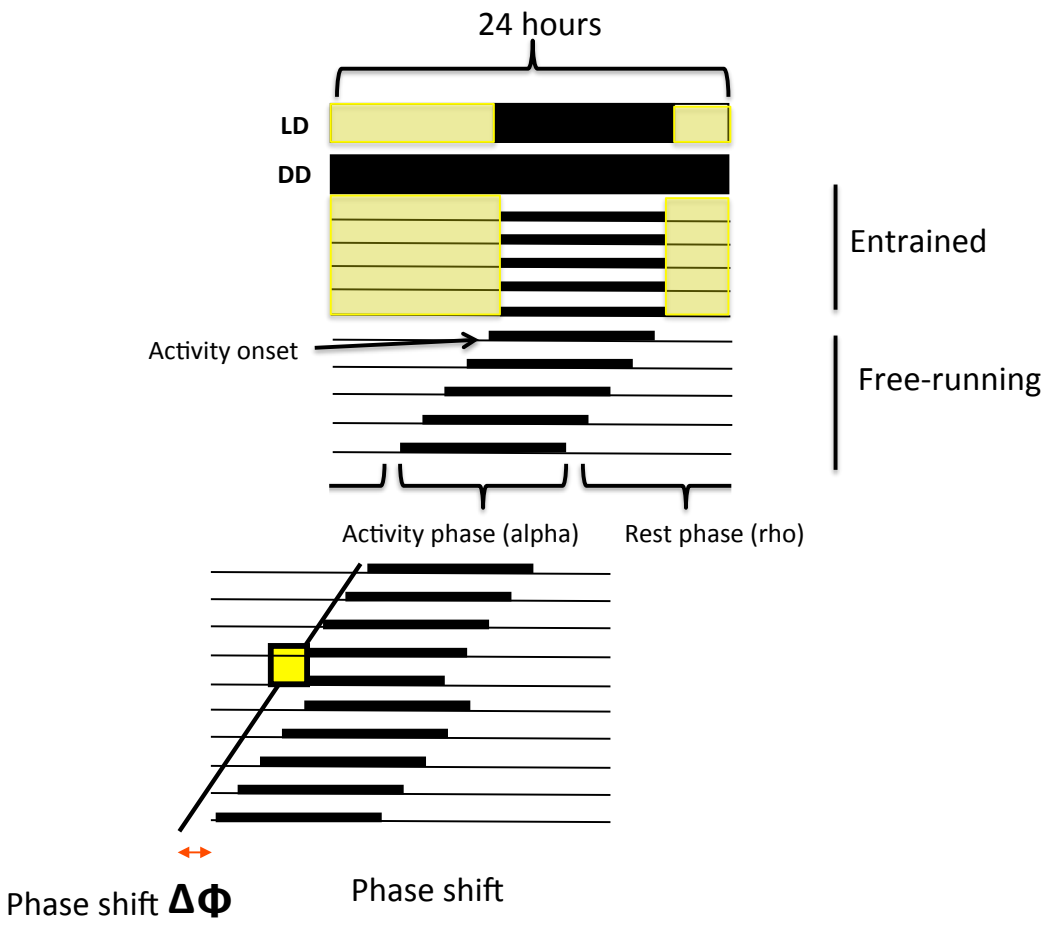

Figure 3.1 Stylized example wheel-running actogram for a mouse This actogram shows a number of the standard features of a wheel-running activity profile from a mouse where the activity phase (alpha) occurs in the dark phase while entrained and the rest (rho) phase in the light. When a light cycle is shifted from a 12/12LD to a constant dark DD condition, the animal's rhythm 'free-runs' with respect to external time based on the length of its internal clock period (tau) as can be seen with the regular movement of the activity onset to the left in the above example as the animal's period is less than 24 hours. When a free-running animal in DD is given a light-pulse (yellow square) the change in its activity onset before and after the pulse can be used as a measure of the sensitivity of the circadian system as the phase shift will be wavelength, irradiance and clock phase dependent.

3.3 Use of transgenic mouse models of photopigment loss: *rd/rd* and *rd/rd* cl mice

The increasing ease of specific genetic manipulations in mouse models has allowed for scientific advances in knowledge across a vast number of areas and made the mouse by far the most common mammalian animal model (Paigen, 1995). For the study of photoreceptor pathways involved in visual and non-visual responses, one of the key issues to overcome is the redundancy present in the visual pathways illustrated by the ability to compensate for the loss of several key genes in the central clock (Bae et al., 2001; DeBruyne et al., 2007; van der Horst et al., 1999; Vitaterna et al., 1999; Zheng et al., 2001) as well as considerable redundancy in outer retinal and melanopsin photoreceptor contributions to circadian responses (Lucas et al., 2012). The genetic basis for one of the most important models of photoreceptor loss initially caused significant problems for the use of the mouse as a model for studying visual responses (Keeler, 1924). Several strains of laboratory mice were found to harbour a mutation in the rod cGMP-phosphodiesterae gene (Bowes et al., 1990) that results in the complete degeneration of rods by two months of age and a secondary loss of cones leaving only a small residual population of cones in the degenerate retina (Carter-Dawson et al., 1978). The *rd* mutation has since made major contributions to visual and circadian studies as well as leading to greater understanding of a number of retinal diseases with the most notable being retinitis pigmentosa (Frasson et al., 1999). However, with studies controlled for genetic background indicating no reduction in the sensitivity of the circadian system in the *rd/rd* mouse (Foster and Helfrich-Forster, 2001), it was unclear if

this reflected the function of a new circadian photopigment or input from residual cones. To resolve this issue, a mouse with a complete loss of rods and cones was generated that contained the r*d* mutation and a *cl* transgene with the A-chain of diphtheria toxin (DT-A) (Soucy et al., 1998) inserted in a locus targeting the MWS opsin expressed in mouse m-cones (Wang et al., 1992). The *rd/rd cl* mouse has been shown by our lab and others to have a complete loss of all rod and cone photoreceptors by 2 months of age (Lucas et al., 1999). The background to the *rd/rd* and the generation of the *rd/rd cl* model can be found in (Foster, 2002).

Despite the great advantages in the use of mouse models, there are aspects that indicate that care must be taken in the interpretation of results. Firstly, differences between strains of research mice can lead to mis-interpretation of the effect of a given mutation. Mutations may also have different effects on different backgrounds like the obese *ob* mutation which causes severe diabetes on the C57BL/KsJ background but not on C57BL/6J background (Coleman and Hummel, 1973). Secondly, genetic changes may also have unforseen secondary effects. For example, many retinal elements are inter-connected and loss of one may have un-anticipated downstream effects. Knockout of the melanopsin gene also results in the loss of circadian control of the cone pathway (Barnard et al., 2006) and rod and cone loss in *Rpe65* $^{-/-}$ mice was found to be accompanied by a loss of pRGCs (Doyle et al., 2006). Thus an observed phenotype in a genetic model may not indicate a direct function of the manipulated gene. Finally, knockouts are often used as ways to assess the function of a given gene by determining the effects of its loss on biological systems, however it is important to remember that a knockout is not necessarily the same as a specific genetic mutation that

inactivates a gene leading to a disease. In the case of *PI3Kγ* the mutation of the active site to inactivate the kinase enzyme has a much less severe effect than that observed in the *PI3Kγ* gene knockout and, similarly, the *ClockΔ19* mutant with a truncation mutation of the *Clock* gene has a much more severe impact on clock function than *Clock* knockout. The latter has been explained to be because the presence of the mutated protein prevents compensation by *Npas2* (DeBruyne et al., 2006, 2007; Pinto and Troy, 2008).

3.4 Evidence for rod and cone, contributions to entrainment responses

It has been established that the outer-retinal photoreceptors are able to input to the circadian system (Lucas et al., 2003; Panda et al., 2002b; Ruby et al., 2002) and that this input is through pRGCs (Güler et al., 2008; Hatori et al., 2008) but determining specific contributions of rods and the different cone opsins to entrainment has been less straightforward.

An assessment of the limits of outer retinal contributions to entrainment responses can be gleaned from melanopsin knockouts where outer retinal photoreceptors are the only light sensitive cells left to input to the SCN. Light-induced negative masking responses in *Opn4* $^{-/-}$ mice are impaired both under bright light and under long light durations (Mrosovsky and Hattar, 2003). The knockout of melanopsin has also been found to result in attenuated phase shifts to 480nm light (Panda et al., 2002b; Ruby et al., 2002). Thus the defects in melanopsin knockouts suggest that situations characterized by long-duration light stimulus and under bright visible wavelengths are where melanopsin primarily drives entrainment responses.

The data from melanopsin knockouts would suggest that one or both of the outer retinal photoreceptors must be able to drive circadian responses at medium to low intensities and many studies utilizing different models to isolate individual photoreceptors have supported a major rod input. *rd/rd* mice with fully degenerate rods and few cones left were found to be unable to entrain below 1lux whereas wildtype mice were able to entrain to less than 0.1 lux (Mrosovsky, 2003). In a transgenic mouse that has the human long-wave cone opsin introduced in place of the MWS cone to spectrally separate cone absorbance away from rods, rods have been found to drive circadian entrainment by phase-shifting and constant light measures even at irradiances where cones provide critical input to PLR and visual responses (Lall et al., 2010).

In a separate study, Altimus et al, used various models with mutations in genes critical to one of rod, cone or melanopsin functions to examine entrainment over intensities from 500lux to 0.1 lux using steps of lowering intensity accompanied by a 6 hour advance in light cycle (Altimus et al., 2010). *Gnat1* $^{-/-}$ mice lacking functional rod transducin showed stable entrainment at 500lux and 10lux but less than half entrained to 1 lux and none entrained to 0.1lux. In *Cnga3* $^{-/-}$*; Opn4* $^{-/-}$ mice missing a cone cyclic nucleotide-gated (CNG) channel and melanopsin, no reliable entrainment was observed to any of the light intensities. Interestingly, loss of CNG should hyperpolarize cones, much as saturating light would, and this appears to block rods from driving entrainment. In mice with both a cone transducin mutation (*Gnat2*$^{cpfl3/cpfl3}$) and *Opn4* $^{-/-}$ status, where cones should be permanently in a depolarized dark state, the mice were able to entrain across the light intensities from 500lux

to 0.1lux just as wildtype mice were. They were also able to entrain to a delayed light onset cycle which was expected to bleach rhodopsin. Melanopsin knockout mice have been found to exhibit attenuated period lengthening under constant light (Mrosovsky and Hattar, 2003; Panda et al., 2002b) and so did *Gnat2*$^{cpfl3/cpfl3}$; *Opn4* $^{-/-}$ mice with only the rod pathway remaining while mice with rod dysfunction (*Gnat1* $^{-/-}$) did not differ from wildtype. This indicates a dominant role for melanopsin in entrainment under these conditions but that rods can partially compensate (Altimus et al., 2010). Finally, to test which signals are transmitted through gap-junctions to cones, mice with diphtheria toxin-ablated cones and melanopsin knocked-out were generated and these were unable to entrain to 500 lux or 10 lux but most were able to entrain to the lower 1 and 0.1 lux intensities (Altimus et al., 2010). To confirm these results with another measure of entrainment, a 15min light pulse of 1000 lux was examined and did not phase shift mice where cones were ablated, or where the cone pathway was constitutively hyperpolarized. However, mice lacking cone transducin and melanopsin (leaving the rod to cone gap junction pathway functional) were able to phase shift indicating that rods signal through cones to drive phase-shifting to even this relatively bright light pulse (Altimus et al., 2010). Furthermore, the surprising versatility of rod contributions to entrainment in these models was not the result of increased sensitivity in the rod-pathway of the mutants as the sensitivity of rod signaling in all three rod-only lines was found to be the same as wildtype in patch clamp recordings (Altimus et al., 2010). Thus, it would appear that rods have a surprisingly prominent role in entrainment and not just at the low scotopic intensities. These results also indicate that rods are able to signal through gap junctions to cones to contribute to entrainment at higher light intensities and that a hyperpolarized cone pathway inhibits the normal rod bipolar to AII amacrine cell pathway that rods utilize under

low light intensities. In terms of real-world application, the results of this study would suggest a model where the input of rods primarily entrains the clock during the low to moderate light period at dawn/dusk, and any moonlight input throughout the night, with melanopsin providing the majority of light input to entrainment in bright daylight (Lall et al., 2010).

This expanded role for rod function would seem to leave little room for cone contributions to entrainment. Supporting this model, both *cl* mice lacking all MWS opsin and much of the UVS opsin and *rd/rd cl* lacking all rods and cones show unattenuated phase shifts to 15min pulses of bright 509nm monochromatic light up to saturating levels (Freedman et al., 1999). In the red-shifted cone model (human long-wavelength cone in place of MWS), irradiance response curves for phase shifts of locomotor activity suggested that the MWS cones are not able to make a significant contribution to this measure of circadian entrainment as the sensitivity threshold was 1000x greater for 644nm light targeted to stimulate the long-wavelength cones relative to the threshold for 500nm light (Lall et al., 2010). However, there is evidence of cone contributions under certain conditions. While the red-shifted cone mouse model indicated that MWS cones could not drive significant phase shifts to 15 minute continuous pulses of light, when that was broken up into 15 discontinuous one minute pulses of long-wavelength light (644nm) with 2 minutes of dark in between, phase shifts of a similar magnitude to those at 500nm light were observed (Lall et al., 2010). In MWS coneless mice ($TR\beta^{-/-}$ mice lacking the thyroid hormone receptor needed for MWS development (Ng et al., 2001)) dim light below 10lux did not result in a stable phase angle of entrainment in the $TR\beta^{-/-}$ and phase shifts were attenuated at 530nm (Dkhissi-Benyahya et

al., 2007). At 480nm, diminished phase-shifting was only observed for very short 1 min light pulses (Dkhissi-Benyahya et al., 2007).

In a follow-up study of the $TR\beta^{-/-}$ model, phase shifts to 1, 5 and 15 minutes of bright 2.8 x 10^{14} photons/cm^2/s light were compared at 365nm, 480nm and 530nm. No difference was found between wildtype and knockout at 360nm for any pulse length but at 480nm, while there was no difference for a 15-minute pulse, the 1 and 5 minute pulses were significantly attenuated in the knockout. At 530nm, the 1 minute pulses could not produce a phase shift in either genotype, only the wildtype mice displayed a significant shift to a 5 minute pulse and knockout phase shift was significantly lower at 15minutes (Dollet et al., 2010). Therefore, based on this model it seems there can be limited cone input to longer-wavelength phase shifts, modeled at 1:1.12 for melanopsin:MWS opsin (Dkhissi-Benyahya et al., 2007) which is somewhat at odds with other cone transgenics (Freedman et al., 1999; Lall et al., 2010). There is agreement though that the cones make their greatest contributions if bright light is presented in short pulses.

Recordings from both SCN neurons and pRGCs have been used to confirm these suggested rod, cone and melanopsin contributions. From these recordings, it was concluded that melanopsin provides a sustained signal but cones can only present a phasic response at light onset (Berson et al., 2002; Brown et al., 2011; Dkhissi-Benyahya et al., 2007; Drouyer et al., 2007; Mure et al., 2007). The sustained responses, containing rod and melanopsin signals are thought to be critical to clock entrainment, with melanopsin making the largest contribution of sustained signals over most light intensities. Phasic cone responses, though initially

strong, decay rapidly and may be encoding contrast information (Brown et al., 2011). This cone-based transient ON and/ or OFF response may be excitatory or inhibitory and is greatly diminished by prior light exposure where the sustained response is not (Drouyer et al., 2007). Indeed, when presented with a more 'real-world' light situation of a steady background light level with brighter steps above, cone-derived signals were greatly reduced (Brown et al., 2011). Recordings from *Opn4* $^{-/-}$ mice under bright white light showed strong phasic responses but a large attenuation of sustained responses (Mure et al., 2007).

The data from these SCN and cell recording studies appears to fit the view that rods and melanopsin drive the sustained responses that result in entrainment over the majority of light conditions. While MWS cones do appear to drive phase shifts in the clock given bright, short stimuli, they do not provide significant input for longer light pulses or given previous light exposure. It has been noted that while light-adaptation limits cone input to the clock, at similar intensities it has a positive influence on cone contributions to vision (Brown et al., 2011), emphasizing the different characteristics of the image and non-image forming pathways. Finally, while it has been assumed that stimulating the UVS cone opsin would result in the same effects as found for MWS, this has not been confirmed.

3.5 Threshold of entrainment and summary of aims

As described above, there has been considerable effort given to investigation towards establishing photoreceptor contributions of rods, MWS cones and pRGCs to photic-entrainment responses under visible wavelengths. Impact on the sensitivity of phase-shifting

responses that shift the activity rhythm of the clock, however, should not be confused with roles at the threshold of entrainment, which is the lowest light intensity that is able to stably entrain the clock to a given light cycle. There has been surprisingly little attention given to the examination of which photoreceptors determine this threshold despite the obvious importance of this knowledge to the field of circadian entrainment. One of the few previous studies comparing entrainment threshold to other measures of circadian system sensitivity in wildtype mice found that it was 1-2 log units lower than the threshold for masking or the pupil constriction response, suggesting a different pathway and/or balance of photoreceptor input (Butler and Silver, 2010). Based on the known characteristics of the mouse photoreceptors and data from mutant mice lacking cone and melanopsin function (Altimus et al., 2010), we would expect the threshold of entrainment to depend largely on rods, as it occurs under dim light intensities, with the loss of cones and melanopsin having no effect but this has not been conclusively established. In this chapter, we aimed to confirm the roles of the mouse photoreceptor classes in this fundamental aspect of entrainment by examining the entrainment of photoreceptor mutants/ transgenics under decreasing levels of white light intensity.

Results

3.6 Loss of rods in *rd/rd* and *rd/rd cl* mice, but not *Opn4*, results in higher threshold of entrainment

In order to examine the contributions of inner and outer retinal photoreceptors to entrainment, the wheel running activity of mice lacking all rods and most cones (*rd/rd*), mice lacking all rods and all cones (*rd/rd cl*) and finally mice lacking melanopsin (*Opn4* $^{-/-}$) was measured under decreasing levels of white light illumination (See white LED spectrum in Methods Chapter 2). Log unit steps of decreasing light intensity steps from 100 lux to 0.01 lux of white light (corresponding to 31.1 μW/cm^2 to 0.0031.1 μW/cm^2 using rodent toolbox available at http://www.eye.ox.ac.uk/team/principal-investigators/stuart-peirson) were made using neutral density filters until free-running behavior was observed. Each week-long step below 100 lux was separated by 7 days back at 100lux to ensure each step began from the same prior illumination state (Figure 3.2). Representative actograms for each genotype are presented in Figure 3.3. *rd/rd* (n=6) were found to have the highest threshold of entrainment, with none of the animals displaying stable entrainment when exposed to 1 lux white light. In contrast, 60% of the *rd/rd cl* mice (n=5) and 83% of the wildtype animals (n=6) entrained to the 1lux step (Figure 3.4A). None of the *rd/rd cl* animals were able to entrain to the 0.1lux step while, in the case of wildtype non-*rd* controls, 50% remained entrained when exposed to 0.1 lux. As one wildtype animal displayed entrainment to 0.01lux, a further step was made from to 0.001 lux to ensure free-running behavior was

observed. The proportion of entrained animals was compared at the first step below the *rd/rd* threshold, 1lux, to examine the difference between *rd/rd* and *rd/rd cl* entrainment. No difference was found between wildtype and *rd/rd cl* entrainment (Fisher's exact test, p=0.55) but the wildtype entrainment did differ significantly from the *rd/rd* (Fisher's exact test, p=0.015). The direct comparison between *rd/rd* and *rd/rd cl* showed a difference that approached statistical significance at the n numbers in this experiment. *Opn4* $^{-/-}$ animals (n=5) and controls (n=5) displayed very similar entrainment thresholds (Figure 3.4B). All of the animals of both genotypes entrained to 1lux, and while one more of the wildtype entrained to 0.1 lux than *Opn4* $^{-/-}$ (60% and 40% entrainment respectively) but there was not a significant difference in proportions. Both genotypes had 1 animal (representing 20% of the group) still displaying entrainment at 0.01 lux and all animals free-ran during 0.001lux.

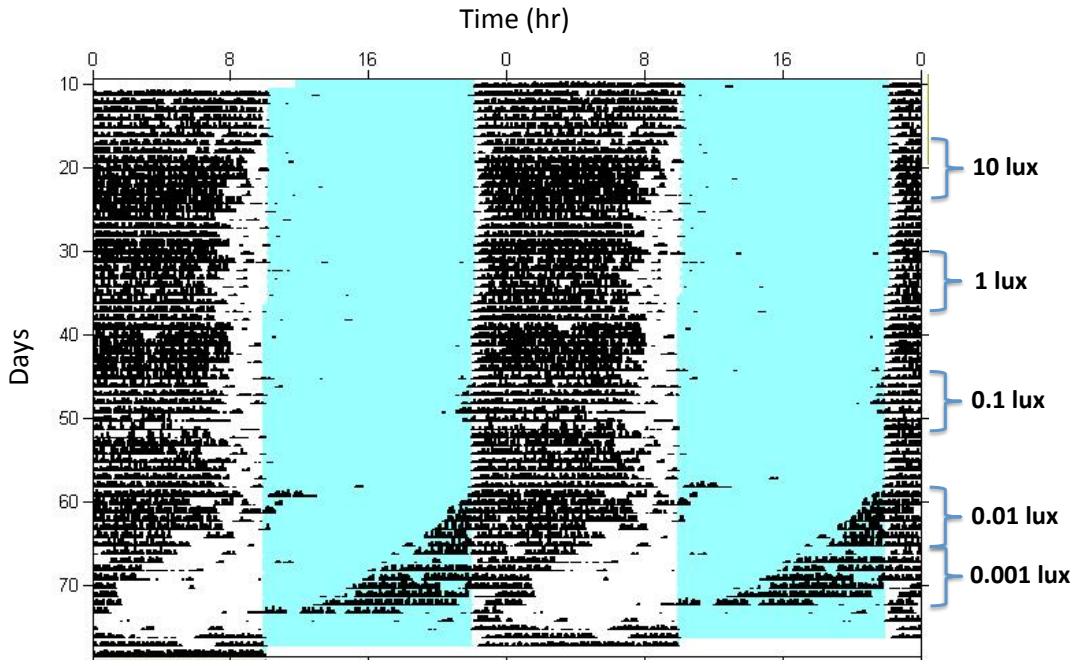

Figure 3.2 Dim-entrainment protocol showing week long light-intensity steps White LED light (see Methods Chapter 2) was set to 100lux and neutral density filter was used to make log-unit steps down to progressively lower intensity to observe the light level at which free-running first appears

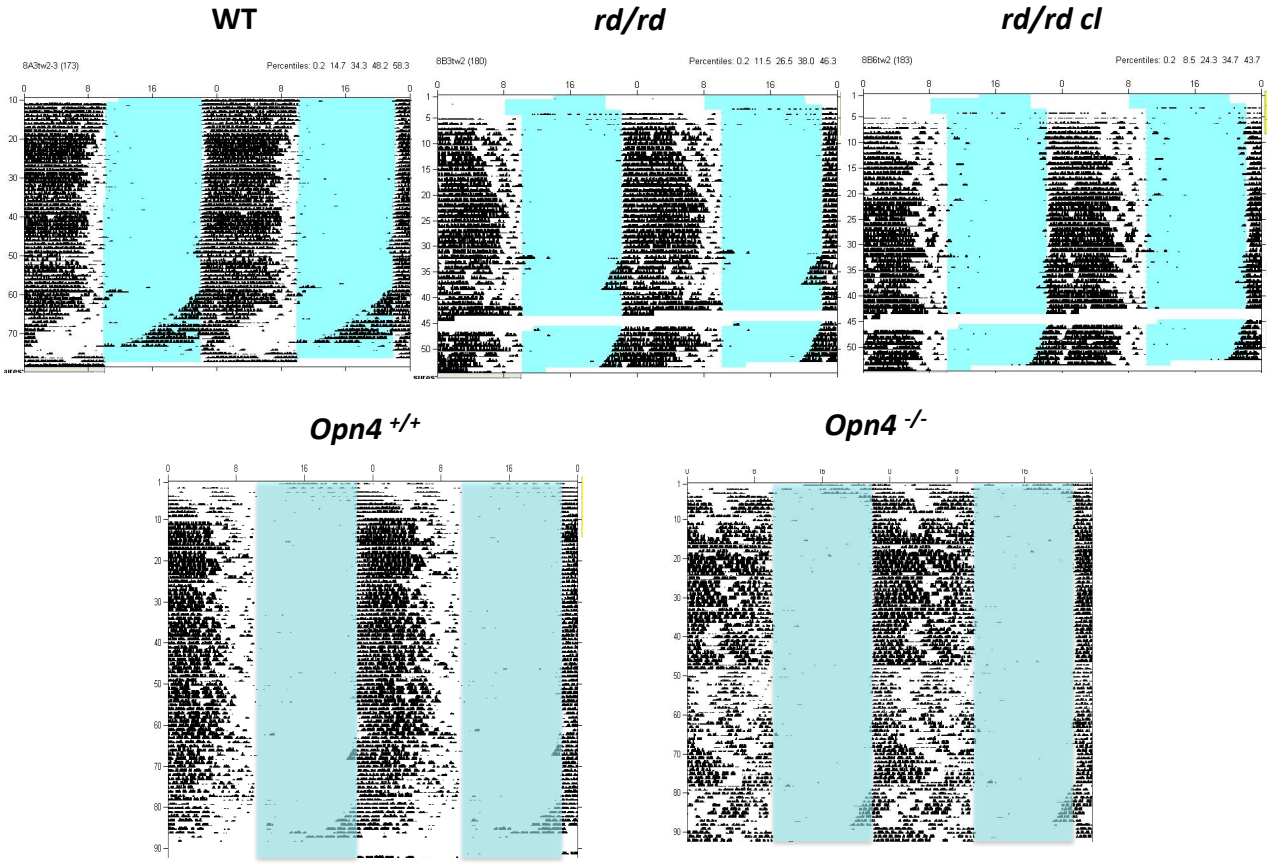

Figure 3.3 Representative dim entrainment actograms of C3H wildtype, *rd/rd*, *rd/rd cl*, *Opn4*$^{+/+}$ *wildtype and Opn4*$^{-/-}$ x-axis time (hr), y-axis days in all actograms.

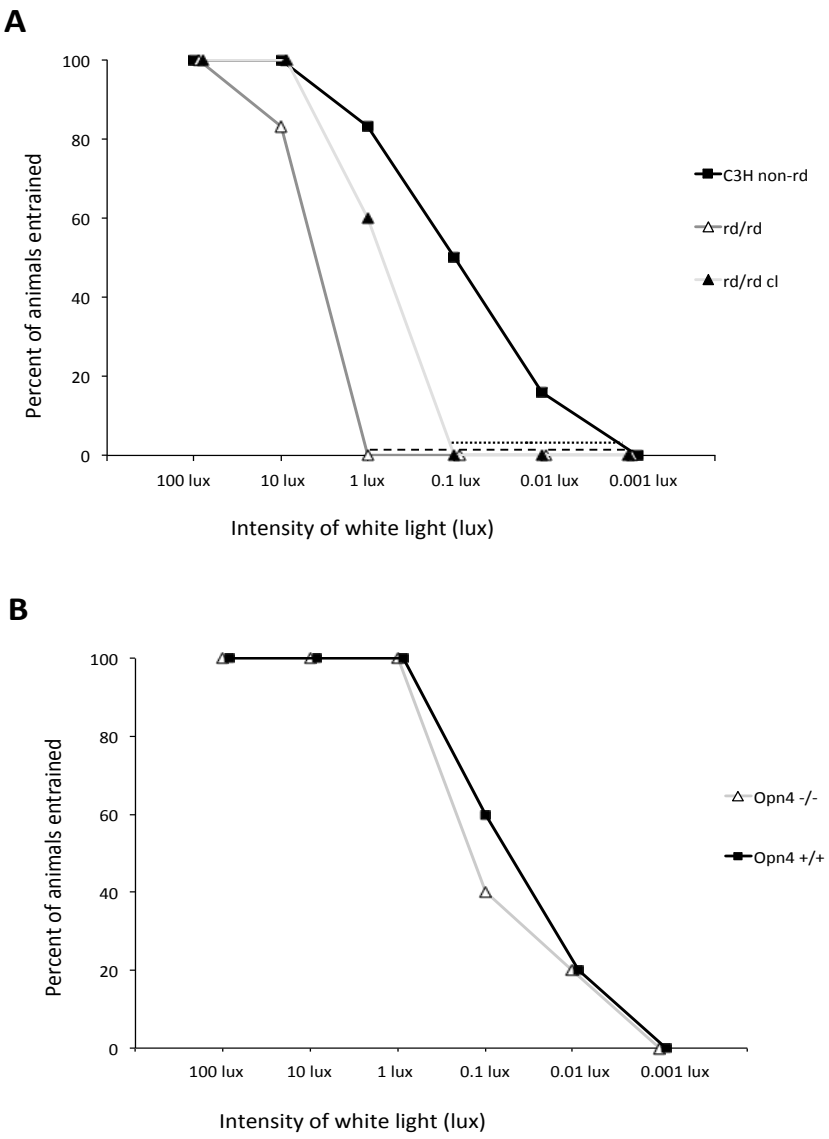

Figure 3.4 Percent of mice entrained to decreasing levels of white light was found to depend critically on rods. The percent of mice entrained to steps of white light is presented for *rd/rd*, *rd/rd cl* and *Opn4*$^{-/-}$ relative to their respective wildtype controls. **(A)** The threshold of entrainment, or the lowest light step at which at least one animal of a particular genotype displayed stable entrainment was found to be 10 lux for *rd/rd* mice (n=6), 1lux for *rd/rd cl* (n=5) and 0.01 lux for C3H non-*rd* wildtype (n=6). A Fisher's exact test of the proportion of mice entrained at 1lux found a significant difference between *rd/rd* and the non-*rd* wildtype (p=0.015) but not between *rd/rd cl* and non-*rd* (p=0.55). Direct comparison between *rd/rd* and *rd/rd cl* found the difference approached significance at n values in this study (p=0.061) **(B)** For *Opn4*$^{-/-}$ (n=5) and *Opn4*$^{+/+}$ controls the

threshold of entrainment was found to be 0.01lux and there was no significant difference in proportions of entrained and free-running at 0.1lux, the only step where the proportions differed between the genotypes.

3.7 Rodless, coneless but not rodless mice display increased error of onset and early onset of activity under dim light

To determine if there were any other differences conferred by the loss of photoreceptors in the *rd/rd*, *rd/rd cl* and *Opn4* $^{-/-}$ mice, the timing of the onset of activity during stable entrainment prior to free-running was examined. The activity onsets of *Opn4* $^{-/-}$ (ZT 22.06 +/- 0.022 Std ER) and *Opn4* $^{+/+}$ wildtype (ZT 22.09 +/- 0.021) were not found to differ significantly (Figure 3.5). Similarly, there was no significant difference between the average ZT of activity onset between *rd/rd* (22.22 +/- 0.020), *rd/rd cl* (22.21 +/- 0.040) and wildtype non-*rd* (22.23 +/- 0.022) (Figure 3.5B). However, it was noted that the standard error in the onset of *rd/rd cl* mice was double that of the other genotypes and the actograms of *rd/rd cl* mice appeared to display increased variation (Figure 3.6).

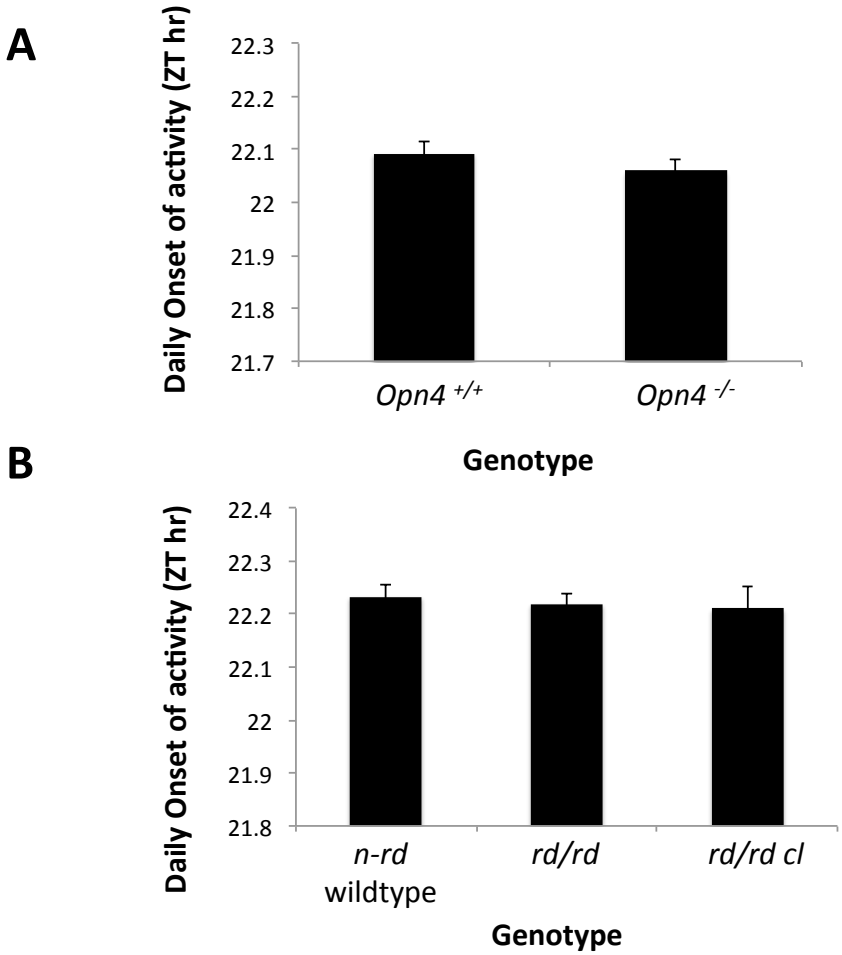

Figure 3.5 No difference in the in activity onset during entrainment between genotypes The onset of activity from ClockLab software (see Methods Chapter 2) was examined for each animal including the daily onsets from all steps at which that animal was entrained. **(A)** No differences were observed between activity onsets in *Opn4* $^{-/-}$ and *Opn4* $^{+/+}$ wildtype (2-tailed Student's t-test, p=0.54). Similarly **(B)** no differences were found between the activity onsets of *rd/rd, rd/rd cl* and non-*rd* wildtype (2-tailed Student's t-test between each genotype, in every case p>0.60). Bars represent mean values +/- SEM.

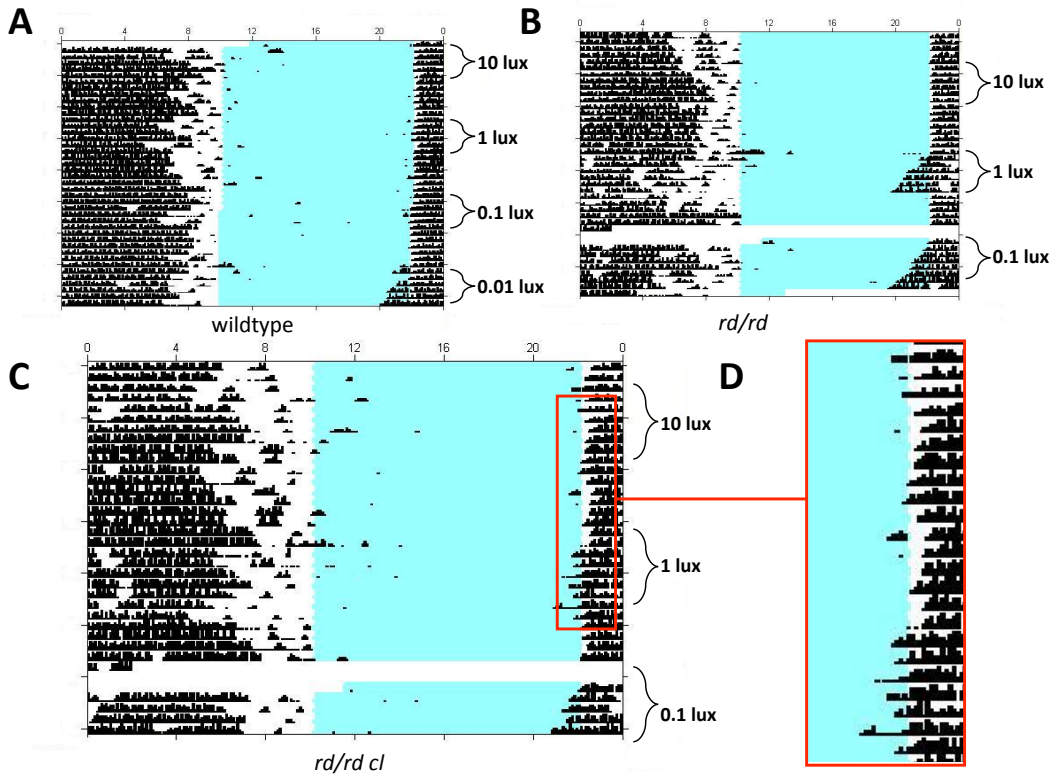

Figure 3.6 Actograms of *rd/rd cl* (C) appeared to show increased onset variation (D) than seen in wildtype (A) or *rd/rd* (B) animals. x-axis time (hr), y-axis days in all actograms.

To determine if this variation was due to an increase in general onset variability or if it only occurred under lower intensity light levels in the *rd/rd cl*, the phase angle difference between lights off and the start of activity for each light intensity where stable entrainment was observed was determined for all strains of mice. In the *Opn4* $^{-/-}$ and wildtype controls, as was expected from the similar average onset timing, both genotypes had similar average phase angles at every light level (Figure 3.7). There was also a trend of increasing phase angles with decreasing illumination as has been found for the C57BL line previously (Ebihara and Tsuji, 1980) but there were no significant differences and interpretation is complicated by

the decreasing number of entrained animals contributing to the average at the lower light levels. The phase angles of entrainment for the rodless, rodless-coneless and control animals were generally near zero at each step but a greatly increased phase angle of entrainment was observed in the *rd/rd cl* at the 1 lux illumination step (0.38hr) and the variability of the phase angles was highest at each step in the *rd/rd cl* (Figure 3.8A). As 1lux light step was the lowest intensity at which the majority of the *rd/rd cl* displayed entrainment, the phase angle of entrainment of each animal at the lowest intensity step at which entrainment was observed (that is the last step where the phase angle remained stable) was compared to the phase angle for that animal in preceding 100lux intermediate step. Averages of these results for each mouse line revealed that the *rd/rd cl* (2-tailed Student's t-test, p= 0.00737) but not the *rd/rd* or non-*rd* wildtype controls displayed significantly advanced activity onset compared to the 100lux step (Figure 3.8B).

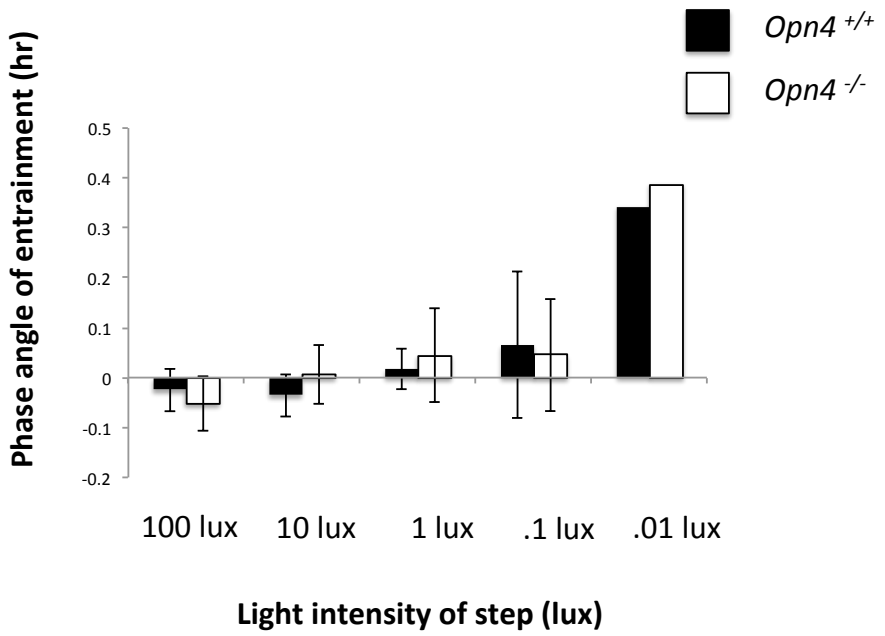

Figure 3.7 Phase angle of entrainment at each light intensity level for *Opn4* $^{-/-}$ and *Opn4* $^{+/+}$ wildtype The phase angle of entrainment at each light irradiance step was determined using ClockLab software (see Methods Chapter 2) and no significant differences was found between steps for *Opn4* $^{-/-}$ and *Opn4* $^{+/+}$ wildtype (Note that increasing SEM at each step is due to decreasing numbers of entrained animals and as only 1 animal of each genotype was entrained at 0.01lux there is no SEM). Bars represent mean values +/- SEM.

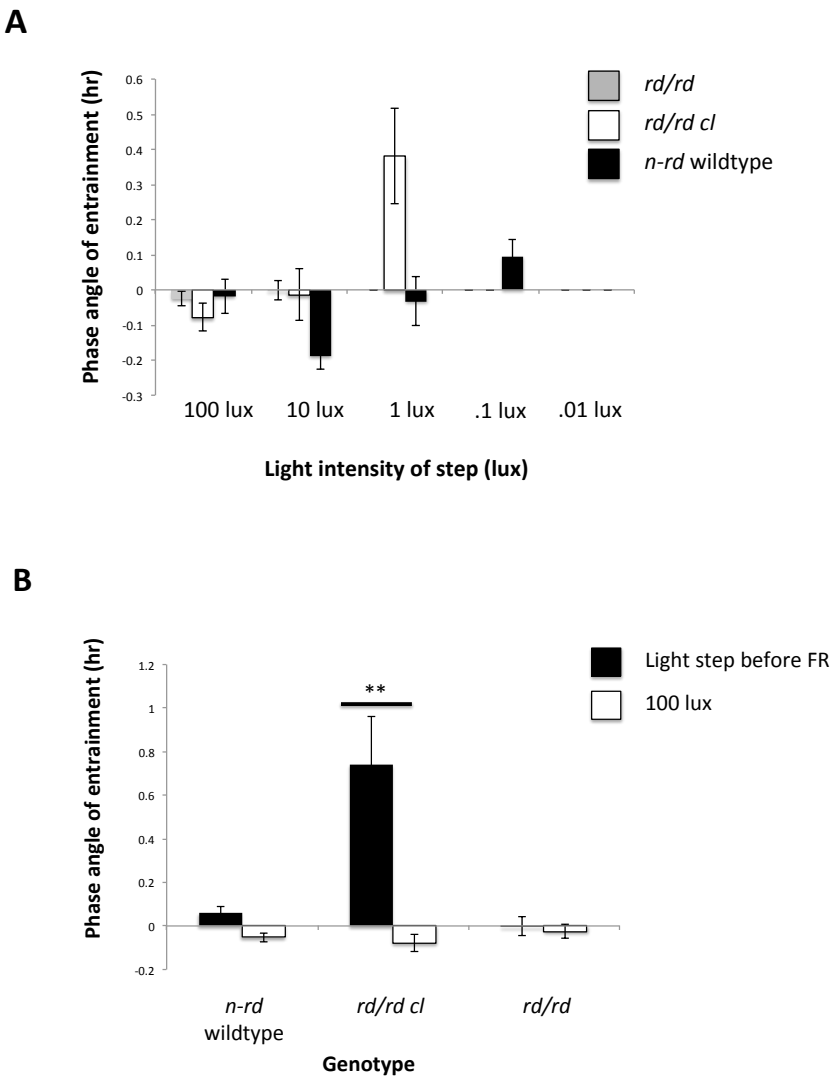

Figure 3.8 Phase angle of entrainment at each light intensity level for *rd/rd, rd/rd cl* and non-*rd* wildtype shows advanced phase angle for *rd/rd cl* under low light (A) The phase angle of entrainment at each light irradiance step was determined using ClockLab software (see Methods Chapter 2) and a large advancement (0.38 of an hour +/- 0.14 SEM) of phase angle in the *rd/rd cl* was observed at 1lux **(B)** Comparing the phase angles at the lowest step where entrainment was observed to the preceeding 100lux step again found only the *rd/rd cl* displayed a significantly advanced phase angle relative to its entrainment to the brighter light (2-tailed Student's t-test, p= 0.00737). *=p<0.05, **=p<0.01, ***=p<0.005. Bars represent mean values +/- SEM.

Finally, as variation of phase angle within each intensity step was observed to be greatest in the *rd/rd cl*, the average error in phase angle difference for each animal at all entrained light intensities was compared and the variability in onset for *rd/rd cl* animals was found to be significantly greater than both the *rd/rd* (2-tailed Student's t-test, $p=0.0025$) and wildtype (2-tailed Student's t-test, $p=0.00084$) while there was no difference between the average error of activity onset of *rd/rd* and wildtype (2-tailed Student's t-test, $p=0.477$) (Figure 3.9A). The same analysis in *Opn4* $^{-/-}$ and wildtype controls confirmed no differences in the onset error ($p=0.356$) (Figure 3.9B).

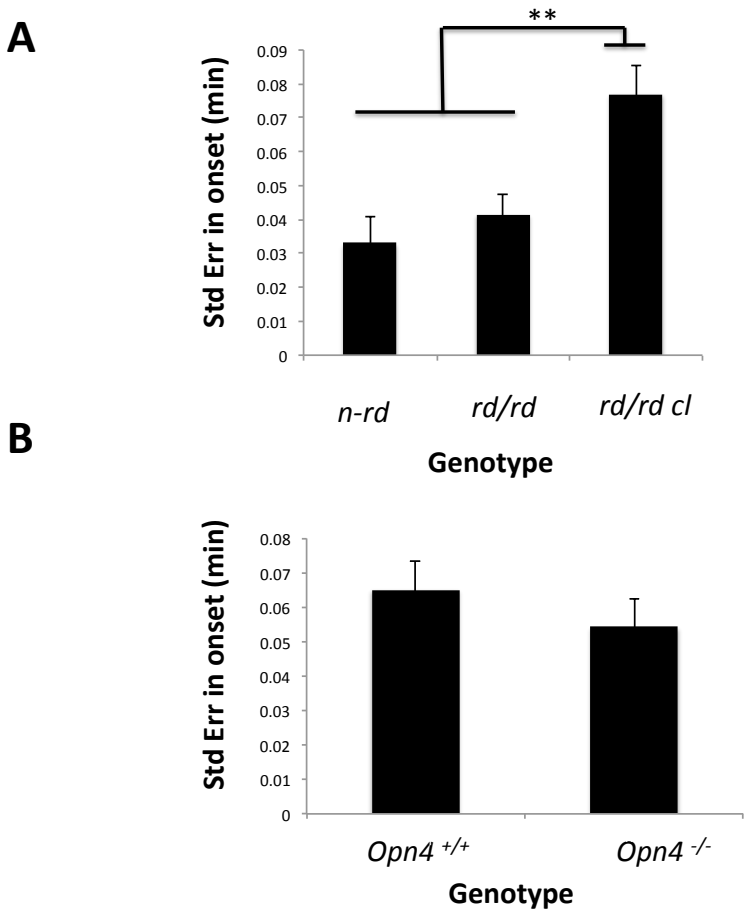

Figure 3.9 Average error in phase angle of entrainment compared between all genotypes The onset of activity from ClockLab software (see Methods Chapter 2) was examined for each animal including the daily onsets from all steps at which that animal was entrained. **(A)** The phase angle variation was significantly greater in *rd/rd cl* relative to both *rd/rd* (2-tailed Student's t-test, p=0.00245) and non-*rd* wildtype (2-tailed Student's t-test, p=0.000835) **(B)** No differences were found between the variation in phase angle of *Opn4* $^{-/-}$ and *Opn4* $^{+/+}$ wildtype (2-tailed Student's t-test, p=0.356). *=p<0.05, **=p<0.01, ***=p<0.005. Bars represent mean values +/- SEM.

Discussion

3.8 Rod input is critical for determination of the threshold of entrainment in mice

From previous studies of photoreceptor roles in the entrainment response, the general view has been that rods and melanopsin contribute to entrainment under normal conditions, with rods being the primary drive at middle to low intensities and melanopsin under brighter light (Altimus et al., 2010; Lall et al., 2010). There is evidence that cones can influence the clock in response to short light pulses but these contributions are diminished by previous light exposure (Brown et al., 2011; Dkhissi-Benyahya et al., 2007; Lall et al., 2010).

The results presented here support the view that rods provide the critical input to entrainment under low intensity stimuli as the loss of rods in the *rd/rd cl* and *rd/rd* resulted in a higher threshold of entrainment in this intensity-step assay while the loss of melanopsin in *Opn4* $^{-/-}$ did not result in any change of sensitivity. This is in agreement with similar entrainment threshold studies in the *rd/rd* that found a higher entrainment threshold in the rodless mice compared to wildtype, with a much lower percentage of *rd/rd* entraining to light levels below 2lux (Mrosovsky, 2003). It is also consistent with a comparison of C3H mice containing the *rd/rd* mutation to wildtype C57BL mice where the *rd/rd* mice were found to be unable to entrain to light levels below 1 lux but some C57BL mice were still able to entrain at 0.01lux (Ebihara and Tsuji, 1980). However, a study using phase-shifting to assess the sensitivity of the *rd/rd* found un-attenuated sensitivity compared to wildtype controls under 515nm light over a range of light intensities from approximately 10 lux to 0.0001 lux

(Foster et al., 1991). These contrasting results may reflect differences in the mode of assessing sensitivity between free-running thresholds and phase-shifting response in the *rd/rd* model but more recent studies examining phase-shifting in different photoreceptor mouse models have confirmed a major role for rods in contributing to this assay of entrainment as well (Altimus et al., 2010; Lall et al., 2010).

3.9 Cone pathway may have inhibitory influence on melanopsin sensitivity in the *rd/rd*

Intriguingly, *rd/rd cl* mice appeared to be more sensitive than *rd/rd* with 60% of *rd/rd cl* but none of the *rd/rd* entraining to 1 lux. As the *rd/rd* and *rd/rd cl* both lack rods but *rd/rd* retain a low number of cones even in the mature retina (see also Chapter 4 Figure 4.4 staining of the *rd/rd* retina), this suggests that the loss of these residual cones is accompanied by higher sensitivity to melanopsin signals, as melanopsin is the only photopigment remaining in *rd/rd cl* mice. Likely the simplest explanation for this change is an inhibitory signal from cones on pRGCs so that the loss of cones results in a disinhibition of pRGCs and a greater melanopsin-based sensitivity. Melanopsin influence on cone signaling has previously been suggested in *Opn4* $^{-/-}$ mice where the absence of melanopsin results in the loss of circadian regulation of sensitivity in the cone signaling pathway (Barnard et al., 2006). Interestingly, studies of the macaque retina have found a subset of pRGCs receive a SWS cone derived OFF-input antagonistic to the standard LWS/ MWS cone-ON inputs (Dacey et al., 2005). The authors suggested that the cone circuitry they observed might have evolved to more precisely set the clock during large abrupt changes in light intensity at dawn and dusk which

is an interesting link to the entrainment stability and phase angle changes we discuss in the next section. There is also evidence from studies of melatonin regulation in humans that cones might inhibit non-image forming responses (Figueiro et al., 2004) but no support for this theory was found in the phase-shifting response of the red-shifted cone model (Lall et al., 2010). It may be that our result is a reflection not of the loss of input from the few cones remaining in the *rd/rd* but instead may be related to an increase in retinal sensitivity to melanopsin signals as the only remaining photoreceptor in the *rd/rd cl* retina. Increased phase-shifting compared to wildtype controls has previously been observed in mice without rods and cones due to specific rod ablation using a rhodopsin targeted diphtheria toxin gene (rdta) and the cl mutation (Freedman et al., 1999) but the rdta model has also been found to display an altered circadian phenotype not seen in the rodless (*rd*) mouse, so these results are likely not comparable (Lupi et al., 1999). That cone input could decrease threshold sensitivity in the *rd/rd* would seem surprising given the scotopic light intensities at the entrainment threshold but it is possible such an influence could exist without cone opsin excitation. Whatever the basis, this data raises the possibility of a cone-signaling pathway exerting a negative influence on aspects of the non-image forming system input through pRGCs.

3.10 Cone loss in the *rd/rd cl* results in a significantly advanced phase angle of entrainment and decreased stability of entrainment

Other potential effects of total cone-loss on entrainment in the *rd/rd cl* mouse were observed in the analysis of onset variability and phase angle changes between light intensities. The

rd/rd cl began running significantly before lights off at the 1 lux light intensity and this low-intensity activity advancement was not seen in either the *rd/rd* or wildtype. The variability in the timing of activity onset from day to day, as determined from the standard error in phase angles at each step, was also found to be greatest in the *rd/rd cl* across all light intensities.

Given that current evidence suggests cones are only be able to contribute to entrainment activity responses such as phase-shifting under conditions of short light exposure (Dkhissi-Benyahya et al., 2007; Dollet et al., 2010; Lall et al., 2010) and recordings from the SCN have found cones are responsible for only phasic responses (Brown et al., 2011) the results here may indicate that the circadian system is able to use these short phasic cone responses to more precisely time activity onset to abrupt light changes. It is thought that rods and melanopsin are primarily responsible for driving entrainment with long sustained responses in the SCN (Altimus et al., 2010; Brown et al., 2011; Lall et al., 2010) but as melanopsin signaling is slower than of cones (Berson et al., 2002), it may not be sufficient to encode abrupt light in the absence of rods in the *rd/rd cl*. Thus the known response characteristics of cones suggest that a contribution to entrainment precision is possible and our data indicates that melanopsin alone is not sufficient for equal entrainment precision. If this is the case then the inputs from the very few remaining cones in the *rd/rd* retina (Carter-Dawson et al., 1978) are sufficient to maintain precise entrainment and do have a functional significance.

Specifically with regards to the advanced phase angle under dim light in the *rd/rd cl*, an advanced phase angle of entrainment was previously observed in *Rpe65* $^{-/-}$ mice which have a complete loss of cone function and severally impaired rod function (Doyle et al., 2006).

This is intriguing as it is again with the total loss of cone function that this advance is observed but it should be noted that, as there is also a reduction in the number of pRGCs in the *Rpe65* $^{-/-}$, it is not an equivalent model to the *rd/rd cl*, and there are likely to be other circadian abnormalities. In the case of the *Rpe65* $^{-/-}$ mice the advance was suggested to be due to enhanced light-dependent positive masking instead of a true phase angle change (Doyle et al., 2006). It could be that this is also the case in the *rd/rd cl* but arguing against this interpretation in both cases is the fact that positive masking has been found to depend on outer retinal photoreceptor function (Mrosovsky and Thompson, 2008) and the loss of positive masking, as well as enhancement of negative masking, has previously been found in both rod ablated mice and *rd/rd* mice (Mrosovsky et al., 1999, 2000). The explanation for this dim-light activity response is therefore unclear.

3.11 Conclusions

The results presented in this chapter confirm our expectation that rod input is the primary factor that determines the threshold of entrainment in wildtype animals under white light. A more surprising result was that we found several indications of cone influence in this assay including potential inhibition of melanopsin sensitivity, helping to determine the precision of entrainment and in an apparent advancement of phase angle under dim light with total rod and cone loss in the *rd/rd cl*. Further evidence of the importance of cones to circadian function may be seen in the blind mole rat where the LWS cone opsin has been retained in subcutaneous eyes and fine-tuned for greater photon capture in an environment where the only known ocular function is circadian entrainment (David-Gray et al., 1999). Thus, in

summary, rods are the key photoreceptor for the threshold of entrainment but it appears that cones may have a broader role in entrainment than previously assumed.

Chapter 4: **Non-image forming responses to UV Light**

Introduction

4.1 Aims

The results presented in Chapter 3 supported a primary role for rods in determining the threshold of entrainment under white light to an external light cycle while cones may have a role in determining the onset of activity. While this is in agreement with the conclusions of previous studies on the various photoreceptor contributions to clock photosensitivity and locomotor activity control (Altimus et al., 2010; Brown et al., 2011; Dkhissi-Benyahya et al., 2007; Dollet et al., 2010; Lall et al., 2010), phase-shifting responses have been found to 357nm UV light that are equal or greater than those to 515nm light and remained un-attenuated in *rd/rd* mice (Provencio and Foster, 1995). As UV light used in these experiments is far from the peak sensitivity of rods or melanopsin photopigments, it is unclear if the established roles of rod, cone and melanopsin in phase-shifting could explain these findings or if a different photoreceptor balance might drive entrainment responses to UV. In this introduction we review the evidence for ultraviolet sensitivity in rodents. The aim of this chapter is to examine the contributions of the various photoreceptors to ultraviolet circadian sensitivity in the mouse using phase-shifting and immunohistochemistry.

4.2 Evidence for UV non-image forming sensitivity in rodents

As discussed in the general introduction Chapter 1, ultraviolet sensitivity is widespread in rodents, and is found in rats (McGuire et al., 1973), hamsters (von Schantz et al., 1997), mice, gophers and gerbils (Jacobs et al., 1991). Much of the investigation on this sensitivity to date has focused on the potential roles for ultraviolet vision in rodents in territorial control or color vision (Chávez et al., 2003; Desjardins et al., 1973; Jacobs et al., 2002, 1991). However, many of the rodent species in which this UV sensitivity has been demonstrated are nocturnal. Although ultraviolet light is present during the day and at dawn/ dusk, there is little ultraviolet light available for vision over the majority of the time that nocturnal rodents like rats are foraging and active (Jacobs et al., 2001). Indeed, in mice, ERG recordings suggest that the sensitivity to the UVS cone input exceeds that of the MWS by factors from 3 to 9 times (Jacobs and Williams, 2007; Jacobs et al., 1991; Lyubarsky et al., 1999, 2004), perhaps linked to the UVS opsin expression being three times that of the MWS in the mouse (Applebury et al., 2000). Behavioral visual discrimination measurements, however, indicate a much lower UV sensitivity than the ERG (Jacobs and Williams, 2007). This difference may be due to the co-expression of MWS and UVS in the majority of mouse cones which are M cones in terms of ganglion cell connections, and thus perhaps display muted UV signals at the level of visual processing (Jacobs and Williams, 2007). Overall, the ecology and visual system of mice and other rodents do not seem to have evolved to make use of UV vision in such a way as to explain why rodents have regained a high degree of UV sensitivity, and a UVS opsin where most mammals have lost it.

Inputs to the non-image forming system provide another possible explanation for the apparent importance of UV sensitivity in this group. There is significant evidence for UV sensitivity in a wide range of rodent NIF behaviors from entrainment and phase-shifting (Amir and Robinson, 1995; Dollet et al., 2010; Hut et al., 2000; Provencio and Foster, 1995; von Schantz et al., 1997; Sharma et al., 1998, 2000) to melatonin suppression (Benshoff et al., 1987; Brainard et al., 1994; Podolin et al., 1987), PLR (Yao et al., 2006) and body temperature rhythms (Amir and Robinson, 1995; McGuire et al., 1973). The natural environmental niche of rodents would also seem to lend itself to a non-image forming role because, while rodents are nocturnal, they are also active around dawn/ dusk. It has been demonstrated that, although UV intensity is highest at noon, it is relatively highly enriched at both dawn and twilight, with a much higher ratio of 360:520nm light (Hut et al., 2000). If the NIF sensitivity in rodents was the primary driver behind the evolutionary pressure leading to the UV sensitivity in these species, then this might also explain the strong dorsal/ ventral gradient of UVS opsin expression in the mouse retina. The lower retina would be better suited to capture UV light from above for input to circadian brightness detection, while it is a seemingly poor arrangement for use of UVS opsin primarily in vision on the ground (Gouras and Ekesten, 2004).

However, it should be noted that, although UV has been shown to influence all of these NIF functions, differing sensitivities relative to visible wavelengths may indicate differing mechanisms of input and photoreceptor involvement. For instance, while phase-shifting and PLR sensitivities to UV have been found to be equal or greater than those to visible wavelengths (Provencio and Foster, 1995; von Schantz et al., 1997; Yao et al., 2006),

melatonin suppression required 10 times the light intensity at 360nm as compared to 500nm in hamsters (Podolin et al., 1987) and body temperature rhythms were similarly less influenced by ultraviolet wavelengths in rats (McGuire et al., 1973).

While the focus on the basis of UV visual sensitivity has naturally been on the UVS cone, since cones are well established in the visual pathways, the role of the UVS cone in the NIF system is less clear. There is debate about the extent of cone contributions to NIF functions. It may be the β-band, the secondary shorter-wavelength absorption peak that all photopigments possess, that allows non-cone photopigments to drive circadian sensitivity at wavelengths far below their major α-band absorption peak (Hut et al., 2000). The case of Syrian golden hamster would seem to support this view as, despite the lack of a UVS cone photopigment (Calderone and Jacobs, 1999), this species has been found to display large phase-shifting responses to bright (2.3×10^{15} quanta s^{-1} m^{-2}) ultraviolet light (von Schantz et al., 1997). However, these responses were found to be similar in magnitude to 515nm pulses of the same intensity. Von Schantz et al. noted that this was hard to explain simply given β-band involvement as the β-band response in the UV should be much lower than the α-band sensitivity for the same photopigment. An alternative explanation is that the bright light pulses administered in the study were saturating.

Summary of Aims

In this chapter, we aimed to determine if cones play a major role in phase-shifting responses to UV light using models of rod and cone loss. We also contrasted retinal responses to UV

and white light to determine how photoreceptor gradients drive c-fos induction across the retina, and particularly in pRGCs, to gain further insight into how the photoreceptors combine under different wavelengths.

Results

4.3 Phase shift responses in wildtype mice show equal sensitivity at 506nm and 365nm

Wildtype phase shift data from Stuart Thompson (Methods Chapter Figure 2.5) was analyzed to compare circadian sensitivity at 506nm, close to the peak sensitivity of rods/ MWS cones and melanopsin, to that in the UV at 365nm. Irradiance response curves (IRCs) were compared using a modified F-test as described previously (Peirson et al., 2005) and no difference (F2,48=0.41, P=0.668) was found between sensitivity profiles at these two wavelengths indicating high circadian sensitivity in the UV (Figure 4.1).

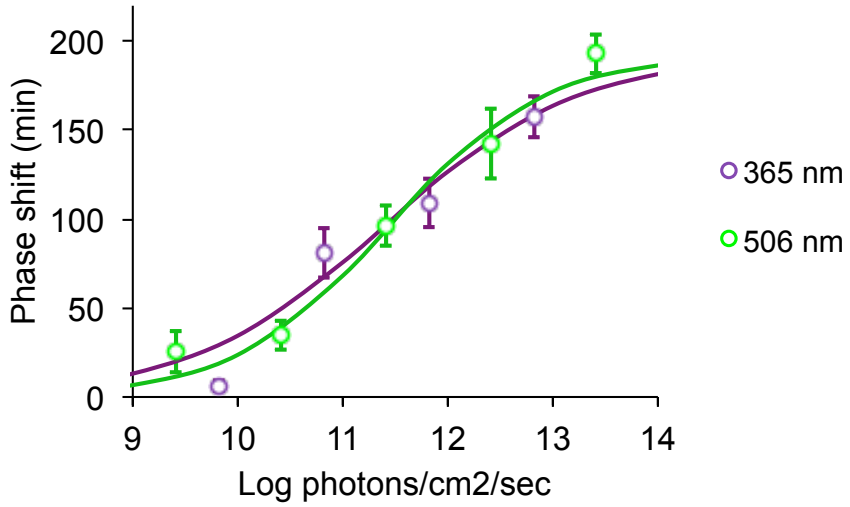

Figure 4.1 Comparison of wildtype sensitivity to 365nm and 506nm monochromatic light. Comparison of IRCs for C3H wildtype phase-shifting responses to 365nm light was not significantly different from responses at maximal sensitivity (506nm IRC) ($F_{2,48}$=0.41, P=0.668). The IRCs were fit according to method of least

squares (See Methods Chapter 2) and tested using a modified F-test as described previously (Motulsky and Christopoulos, 2003).

4.4 Loss of phase-shifting sensitivity to UV light is associated with complete loss of cones in the rodless/coneless mouse (*rd/rd cl*)

To investigate which photoreceptor is responsible for this significant ultraviolet sensitivity, we conducted a series of phase-shifting experiments in *rd/rd* and *rd/rd cl* retinal mutants/ transgenic models to generate irradiance response curves to 365nm UV light (See UV LED spectrum in methods) between 10.6 and 13.6 log photons/ cm^2/ s (or 0.02 and 21.7 $\mu W/cm^2$). Comparison of the irradiance response curves revealed that *rd/rd* mice lacking rods and with only few remaining cones did not differ in sensitivity from wildtype controls, but the *rd/rd cl* showed a marked attenuation in response to UV light (Figure 4.2). The IC50s for each genotype (half-sensitivity based on IRC fitting to individual animals, in all cases $R^2>0.89$) confirmed a significant decrease of sensitivity in the *rd/rd cl* compared to wildtype (~1.5 log units, 2-tailed Student's t-test $p = 1.8x10^{-5}$) (Figure 4.3). It was also noted that, while there was no significant differences between IC50 sensitivity of the *rd/rd* and wildtype, both of the degenerate models had significantly lower phase-shifting at the lowest irradiance examined (2-tailed Student's t-test, p=0.03).

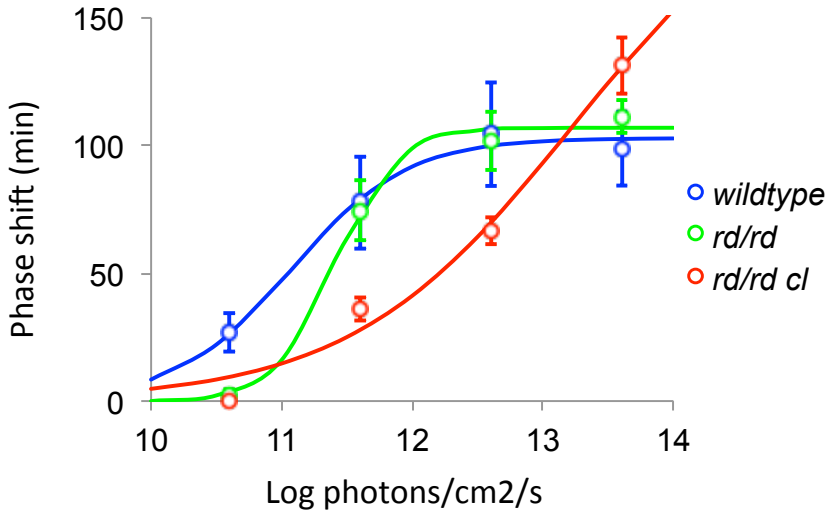

Figure 4.2 UV Phase-Shifting Irradiance Response Curves in *rd/rd*, *rd/rd* cl and wildtype mice Irradiance response curves (IRCs) for phase-shifting responses ± SEM of wild-type C3H, *rd/rd*, and *rd/rd* cl mice to UV light (15 min pulse at CT16, 365 nm UV LEDs).

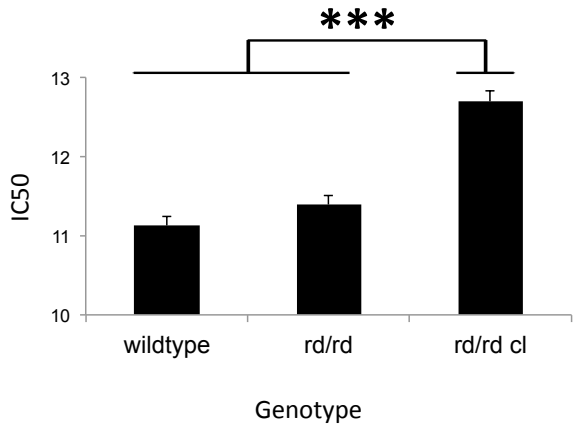

Figure 4.3 UV Phase-shifting IC50s for rd/rd and rd/rd cl sensitivity to UV light was assessed by IRC IC50 based on individual IRC fitting using Excel (Microsoft) to fit a four parameter sigmoid curve based upon the method of least squares (See Methods Chapter 2). Mice lacking rods and retaining a reduced population of cones (*rd/rd)* n=5 show no reduction in UV sensitivity compared to wildtype controls n=5. By contrast, mice lacking all rods and all cones (*rd/rd cl*) n=5 show a significant attenuation of UV sensitivity, with an IC50 1.57 log units higher than controls (p=1.80E-05). All comparisons used Student's 2-tailed t-test, *=p<0.05, **=p<0.01, ***=p<0.005. Bars represent mean values +/- SEM.

Given the significant difference in sensitivity between the two mutant/transgenic models, with *rd/rd* sensitivity appearing similar to wildtype and *rd/rd cl* significantly reduced, retinal samples were taken from our *rd/rd* retinas at the ~ 80 days of age used in our experiments (Figure 4.4) and over 200 days of age (Figure 4.5) to confirm the status of cone opsins in retina considered fully degenerate in this line. The analysis of these samples revealed a complete absence of rod outer segments. In contrast, in all of the retinas examined from these highly aged mice, a small number of cones expressing UVS and MWS remain with some cones retaining outer-segments even in retinas at approximately 230 days old. In the flat mounted retina, it is clear that the UVS cone loss due to degeneration is much greater in the central retina. Along with the normal dorsal-ventral gradient of UVS expression across the mouse retina, this means that by far the greatest number of residual cones are present in the most ventral part of the *rd/rd* retina (bottom right corner of Figure 4.4B). By comparison, *rd/rd cl* retina of a similar age were not found to have any remaining UVS or MWS expression (images not shown).

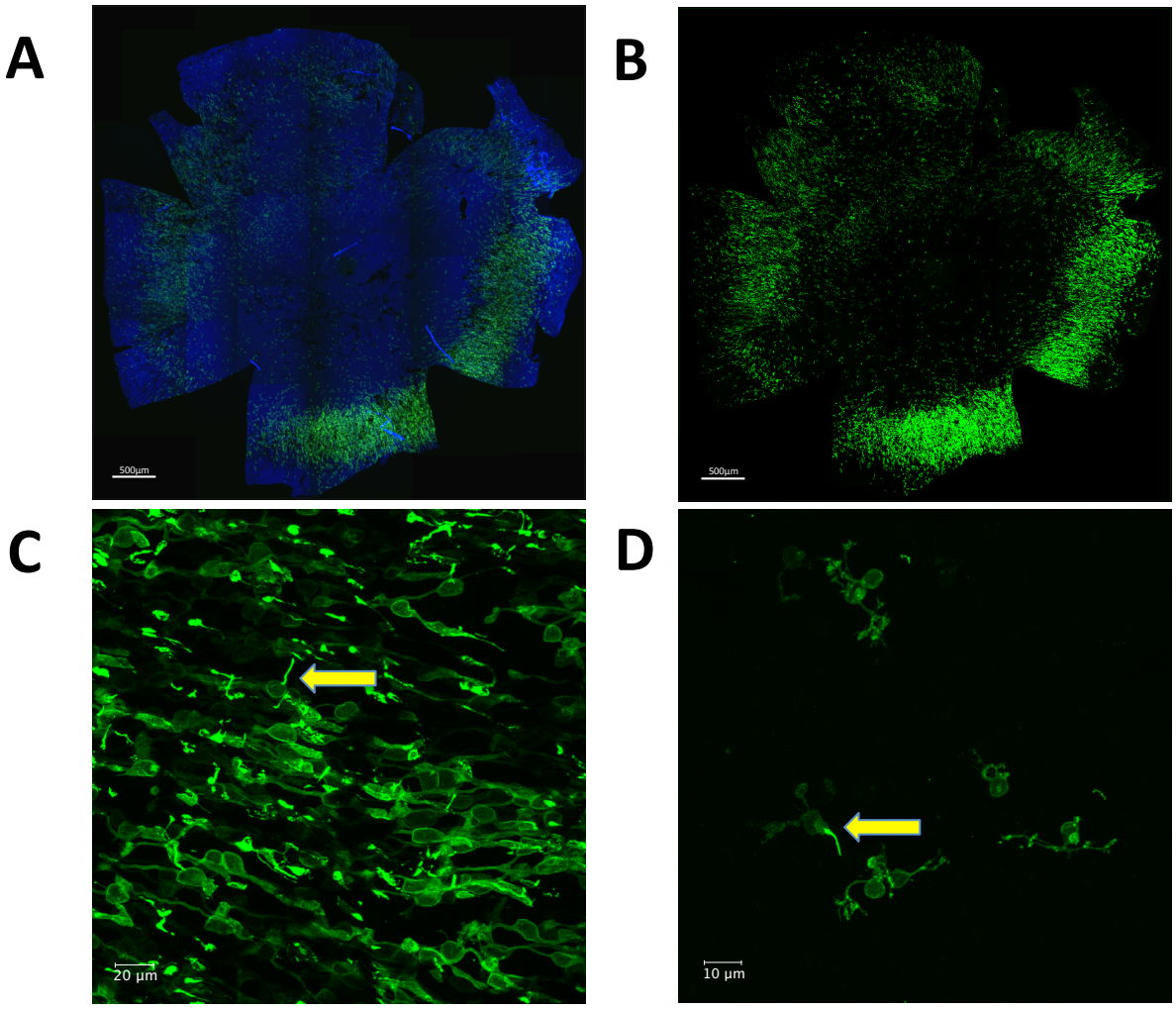

Figure 4.4 UVS opsin expression in aged *rd/rd* retina Whole mounted retina from rodless *rd/rd* mice between 75-95 days of age were examined for presence of UVS opsin. Flat mounted retina showed high level of UVS (green) loss in the central retina but significant numbers of UVS expressing cones present in peripheral retina (shown with DAPI in **(A)**, and with increased brightness in **(B))**. Closer examination showed UVS expression in cone outer-segments (indicated by arrows) both in peripheral, **(C),** and central, **(D)**, retinal areas. Scale bars are 500µm in A and B.

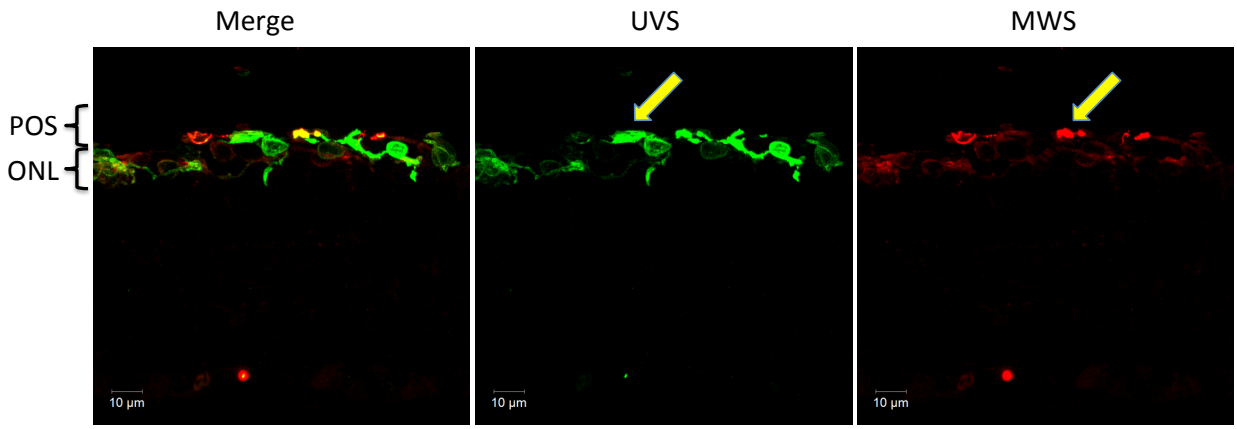

Figure 4.5 UVS opsin expression in outer segments of highly aged *rd/rd* retina Sections from ~230day old *rd/rd* retina stained for MWS (red) and UVS (green). The images above show both UVS and MWS staining in cone cells bodies in the outer nuclear layer (ONL) and in outer segments (POS), although in the apparent complete absence of supporting rod outer-segments these were lying horizontal on external limiting membrane as indicated by the yellow arrows above.

To highlight the difference in sensitivity between wildtype and *rd/rd cl* mice, wildtype IRC data from Stuart Thompson and previously published *rd/rd cl* data from our group (Hattar et al., 2003), were plotted along with our data at 365nm against absorption templates for the photoreceptors remaining in the respective transgenic retinas. Thus wildtype (Figure 4.6A, full IRCs in methods Figure 2.5) and *rd/rd cl* mice (Figure 4.6B, IRCs from 4.2 and (Hattar et al., 2003)) are compared across 8 wavelengths. It is clear that, in the UV range where the *rd/rd cl* has substantially lower sensitivity, melanopsin is unable to compensate for the absence of outer retina photoreceptor input as it does for longer wavelengths.

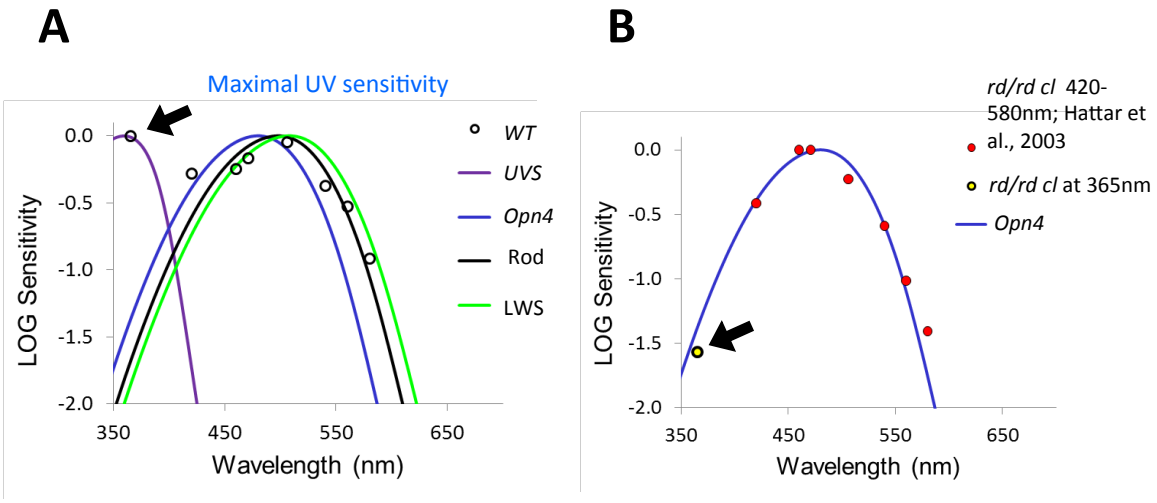

Figure 4.6 Action spectrum for circadian phase-shifting in wildtype and *rd/rd cl* mice. (A) Full irradiance response curves were constructed by Stuart Thompson for eight monochromatic wavelengths (365, 420, 460, 471, 506, 540, 560 and 580nm; see Methods 2.5) in wildtype C3H mice. Action spectrum data are plotted here against the known photopigments of the mouse retina (UVS cone λ_{max}=360nm, Opn4 λ_{max}=480, Rod λ_{max} =498nm, LWS cone λ_{max} =508nm) with standard absorption templates based on the Govardovskii model (Govardovskii et al., 2000). **(B)** Action spectrum for circadian phase-shifting in *rd/rd cl* mice. The irradiance response curve from Figure 4.2 was used to determine the sensitivity at 365nm. For comparison, we have used our previously published data for 420, 460, 471, 506, 540, 560 and 580nm by Hattar et al., 2003 (Hattar et al., 2003). Action spectrum data are plotted against the known absorption spectrum for the *Opn4* photopigment (λ_{max}=480), the only photopigment remaining in the *rd/rd cl* retina.

While *rd/rd cl* mice displayed a significant reduction in UV sensitivity, they displayed phase-shifting responses similar to wildtype at the brightest UV irradiances. This was expected to arise from absorption of the short wavelength limb of melanopsin as that is the only photopigment remaining in the *rd/rd cl* retina. If both α and β absorption peaks contributed to melanopsin's absorption of UV, we would predict a residual sensitivity

relative to the wildtype of 25%, as compared to 4% if only the α-band contributes to absorption (See Table 4.1 for photoreceptor absorptions at 365nm). The measured response of 3% is plotted against the α and β absorption peaks for melanopsin (Figure 4.7).

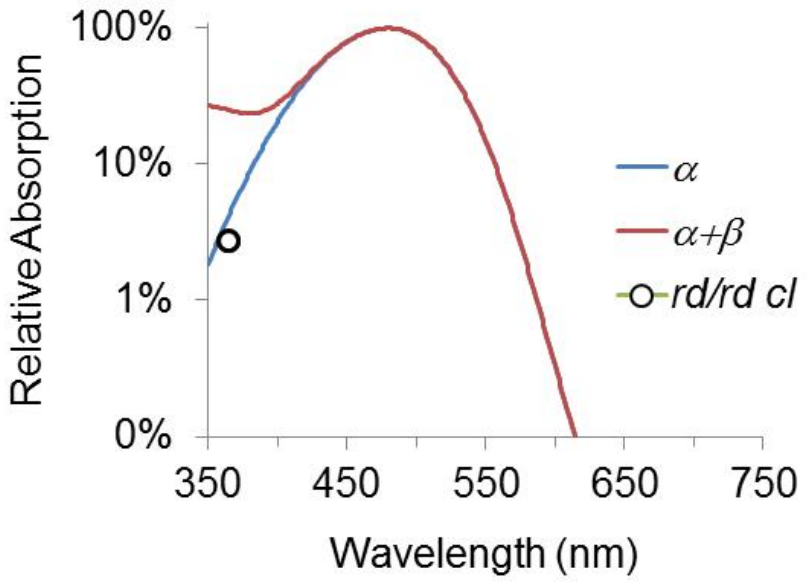

Figure 4.7 Residual absorption in *rd/rd cl* shows no evidence of β-band involvement in phase-shifting The full absorbance spectrum of any opsin/vitamin A visual pigment consists of an alpha-band in the visual range (e.g. the alpha band λmax for melanopsin is at 480nm) and a smaller amplitude and significantly shorter wavelength absorbance beta-band (e.g. the beta band λmax for melanopsin is at 345nm). Normally only the alpha-band is shown. Both the alpha- and beta-bands are shown here. Absorption by the beta-band has been proposed as one mechanism whereby a photopigment with an alpha-band in the visual range might still show relatively high sensitivity to UV light (Hut et al., 2000; von Schantz et al., 1997). However, the strong match between the alpha-band absorbance for melanopsin at 365nm and UV sensitivity of *rd/rd cl* at 365nm (3% of wildtype sensitivity) provides no evidence for beta-band involvement.

Table 4.1 Absorptions of mouse photopigments at 365nm Based off the standard Govardovskii model for photopigment absorption (Govardovskii et al., 2000), the residual sensitivity of the mouse photopigments at 365nm is shown relative to maximal absorption at their respective λ-max. As shown here, Rhodopsin, MWS opsin and melanopsin all absorb at low levels at 365nm (the wavelength of UV light produced by UV LEDs used in this thesis, see Methods Chapter 2) and so, given a sufficiently bright UV stimulus, would potentially be able to contribute to UV sensitivity.

Photopigment	λ-max	Relative absorption at 365nm
MWS opsin	508nm	1%
UVS opsin	360nm	98%
Melanopsin	480nm	4%
Rhodopsin	498nm	2%

4.5 UV light but not white light pulses produces a dorsal-ventral retinal c-fos gradient in wildtype retina

Although phase-shifting responses suggested cones as being primarily responsible for the UV circadian sensitivity in mice, it did not separate the cone classes. To further investigate the photoreceptor classes, we used the inherent opsin gradients in the mouse retina. Double labeling with melanopsin and UVS opsin antibodies demonstrated the opposing gradients of these two photopigments in the mouse retina (Figure 4.8). Melanopsin is most highly expressed in the upper (dorsal) retina, where the highest density of M1 and M2 pRGCs are found (Hughes et al., 2013), while the greatest expression of UVS is in the lower (ventral) retina, resulting in significantly varying ratios of melanopsin:UVS across the retina. Due to

antibody species limitations, separate staining was necessary to highlight the UVS: MWS retinal distribution (Figure 4.9A and B). This also highlights how large the dorsal ventral UVS gradient is, with a severe drop of UVS expression in the mid-dorsal retina (Figure 4.9A). The MWS gradient is less significant but, like that of melanopsin, opposes the UVS gradient with maximal expression in the dorsal retina (Figure 4.9B).

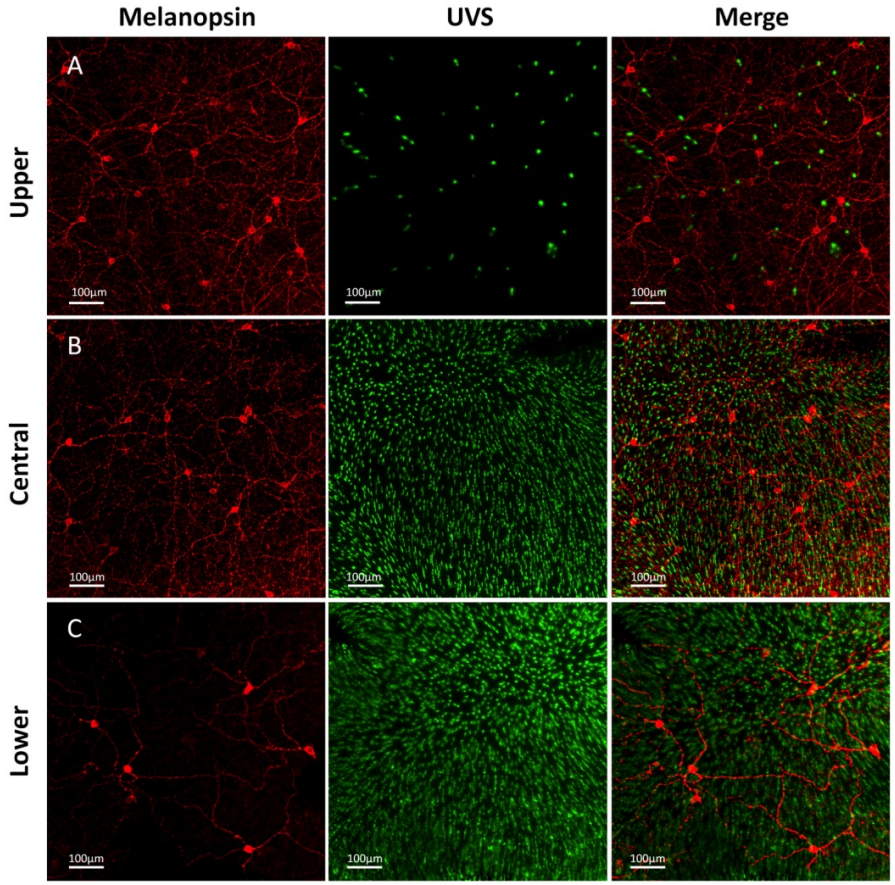

Figure 4.8 Melanopsin and UVS gradients in the wildtype mouse Whole-mount retinal images showing expression of melanopsin (red) and UVS (green) in the upper, central and lower retina of wildtype C3H mice illustrating opposing gradients: dorsal-ventral for UVS and ventral-dorsal for melanopsin. Scale bar=100µm.

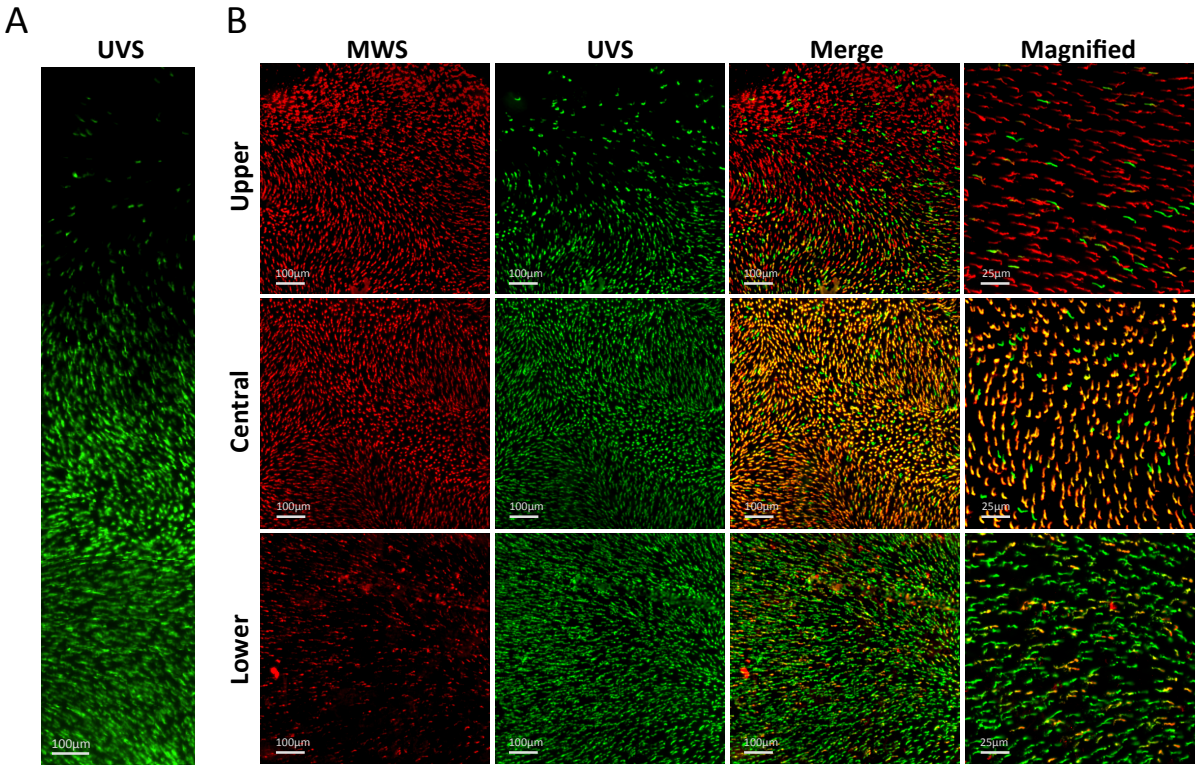

Figure 4.9 Opposing gradients of cone opsins in the wildtype mouse (A) Whole mount retinal images courtesy of Dr Steven Hughes to show gradient of UVS across the retina from ventral (bottom) to dorsal (top) with dramatic cut-off in the mid-dorsal retina **(B)** Double labeled images of MWS (red) and UVS (green) opsin antibodies in the upper, central and lower retina. The majority of cones in the mouse retina are m-cones and express both UVS and MWS cone opsins (95% of all cones) with dorsal m-cones expressing mainly MWS and ventral m-cones mainly UVS. This range of co-expression can be seen in change from red through orange to green seen in merged panels above. Only a minority of cones express the UVS opsin alone and are identifiable as the green cones in the merged images of the central and upper retina as they lack any red MWS labeling. Scale bars= 100µm is all images but magnified column where scale bars= 25µm.

To utilize these gradients to gain information regarding retinal UV responses, retinas of mice exposed to pulses of UV (monochromatic 365nm) or white light (containing no significant irradiance below ~425nm, see Methods for spectral data) were stained for c-fos to determine the difference in the pattern of c-fos under these different wavelengths. After pulses of UV light, the pattern of c-fos positive cells displayed a dorsal-ventral gradient like that of UVS opsin (Figure 4.10B) while a largely even gradient was observed following white light pulses (Figure 4.10C). No specific c-fos staining was observed in the retina of a mouse exposed to a sham light pulse (Figure 4.10A). To determine if this gradient represented a significant difference in activation of the melanopsin-containing pRGCs, the wildtype retina flat-mounts were co-labeled for melanopsin and c-fos by Dr. Steven Hughes and the percentage of c-fos positive, melanopsin positive cells in the dorsal and ventral retina were determined (Figure 4.10D). Light pulses and tissue collection was performed by Thomas Watson, co-labeling procedure with melanopsin and c-fos antibodies by Dr. Steven Hughes and both parties were involved in the imaging and retinal counts. Retina that had been pulsed with white light displayed a ventral-dorsal expression gradient trend (dorsal 87.9% +/- 1.9% SEM, ventral 77.0 +/- 3.9% SEM, 2-tailed Student's t-test $p=0.07$) while a significant dorsal-ventral gradient was found for UV pulsed retina (dorsal 54.3% +/- 4.0% SEM, ventral 72.7 +/- 3.7% SEM, 2-tailed Student's t-test $p=0.01$). These results are consistent with melanopsin/MWS driven input to these pRGC under bright white light and UVS input under UV light based on the opposing gradients seen in Figure 4.9.

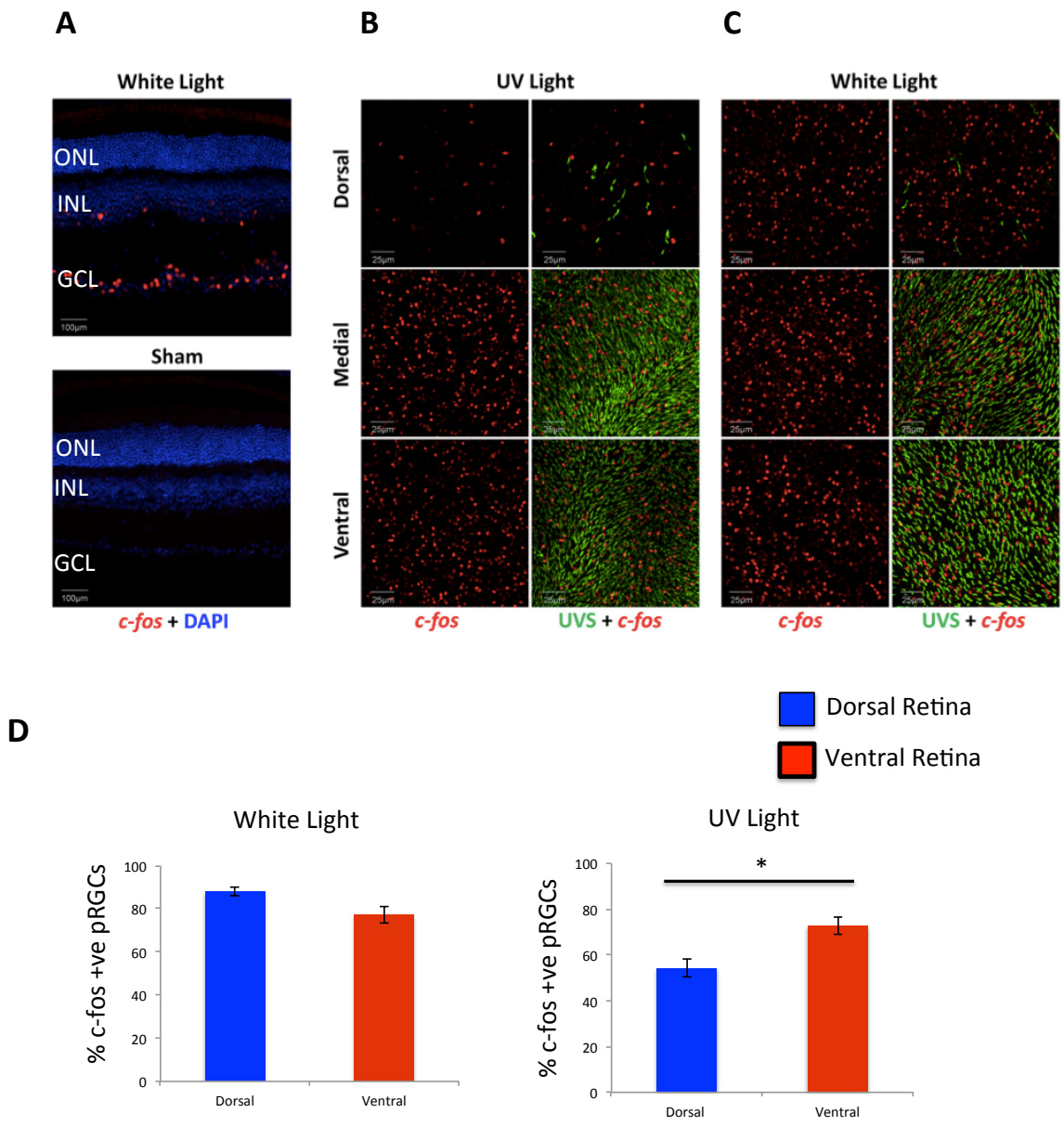

Figure 4.10 Retinal c-fos induction following UV and white light pulses in wildtype mice. (A) No significant c-fos expression was seen in the retinal sections of C3H wildtype mice following a sham light pulse involving movement of the mice but no light exposure while 100lux white light was found to induce c-fos expression mainly in the Ganglion cell layer (GCL) and to a lesser extent in the Inner-nucleur layer (INL) **(B)** Following a 30 minute UV light pulse at Z16 of 12.6 log photons/ cm^2/ s (2.2 µW/cm^2), immunostaining of retinal whole mounts co-labeled for c-fos (red) and UVS (green) revealed c-fos expression in the wildtype retina followed a dorsal-ventral expression gradient mirroring the UVS gradient. A severe reduction in c-fos and UVS expression was observed the mid dorsal retina with limited expression present in the upper dorsal

retina. **(C)** Following a bright 500lux white light pulse (approximately 14.7 log photons/ cm^2/ s, 155.4 $\mu W/cm^2$), high levels of c-fos expression were found across the retina and did not show an obvious gradient in response. **(D)** Whole-mounted wildtype retina (n=3) that had been pulsed with white or UV light as in (B) and (C) were co-labeled with c-fos and melanopsin antibodies by Steven Hughes using extra steps outlined in methods for these antibodies both raised in rabbit and manual counts on 8-10 retinal regional sections ($25mm^2$) were performed in retina for melanopsin positive, c-fos positive cells. Gradients in the percentage of c-fos (+), melanopsin (+) pRGCs were observed in different directions to white (dorsal 87.9% +/- 1.9% SEM, ventral 77.0 +/- 3.9% SEM, 2-tailed Student's t-test p=0.07) and UV (dorsal 54.3% +/- 4.0% SEM, ventral 72.7 +/- 3.7% SEM, 2-tailed Student's t-test p=0.01) but was only significant for the dorsal-ventral gradient under UV light. Retinal orientation was performed using UVS gradient. *=p<0.05, **=p<0.01, ***=p<0.005. Bars represent mean values +/- SEM. Scale bars=25µm whole-mount images, scale bars=100µm in sections.

4.6 M1 and M2 gradients to UV light are lost in the *rd/rd cl*

To examine the spectral tuning of specific pRGC subtypes, we pulsed retina of *rd/rd cl* mice using the same conditions (30 minute pulse, 500lux white light pulse, ~14.7 log photons/ cm^2/ s, 155.4 $\mu W/cm^2$; UV light (12.6 log photons/ cm^2/ s, 2.2 $\mu W/cm^2$) and co-labeled with melanopsin and c-fos antibodies (Figure 4.11A). These retinas were imaged and, along with the wildtype retina from 4.10D, the number of c-fos positive and negative M1 and M2 cells (melanopsin positive) was determined with pRGC subtype identified based on levels of melanopsin expression and the location of their dendrites in the OFF (M1) or ON layers (M2) of the IPL. The percentage of c-fos positive M1 and M2 cells in the dorsal and ventral retina were compared for each light condition (Figure 4.11B). As before, light pulses and tissue collection was performed by Thomas Watson, co-labeling procedure with melanopsin and c-fos antibodies and idenfication of M1 verus M2 cells by Dr. Steven Hughes with both

parties were involved in the retina imaging and data analysis.

Near-saturating M1 responses were found for both wildtype (dorsal retina, 96.7% ± 1.4% SEM and ventral retina, 92.8% ± 3.7% SEM, 2-tailed Student's t-test, p = 0.31) and *rd/rd cl* (dorsal, 81.5% ± 1.0% SEM and ventral, 86.8% ± 1.7% SEM, 2-tailed Student's t-test, p = 0.54) under white light but no significant dorsal-ventral gradients were found. In contrast, UV light induced a significant dorsal-ventral gradient in c-fos positive M1 cells in the wildtype (dorsal, 56.0% ± SEM 5.4% and ventral, 71.9% ± 6.8% SEM, 2-tailed Student's t-test, p = 0.03) while again no gradient was found in the *rd/rd cl*. Interestingly, a significantly higher percentage of M1 c-fos induction was found in the dorsal retina of *rd/rd cl* mice compared to wildtype mice under UV light (WT versus *rd/rd cl* 2-tailed Student's t-test, Dorsal retina comparison p = 0.03, Ventral retina p = 0.21).

For M2 pRGCs, significant retinal gradients were found for both white and UV light conditions but while white light induced a ventral-dorsal gradient (Dorsal retina, 84.4% ± 1.7% SEM and Ventral, 56.9% ± 6.5% SEM, 2-tailed Student's t-test, p = 0.0032), UV light induced a dorsal-ventral gradient as was observed in M1 cells (Dorsal, 50.8% ± 8.4% SEM and ventral, 75.0% ± 9.3% SEM, 2-tailed Student's t-test, p = 0.038). Again neither white nor UV light resulted in gradients in c-fos positive M2 cells in the *rd/rd cl*.

These responses are consistent with UVS opsin driving responses in both M1 and M2 cells under UV light along with MWS expression in m-cones driving M2 responses under white light. The greater percentage of c-fos positive M1 cells in the *rd/rd cl* dorsal retina compared to the wildtype may indicate a level of inhibition.

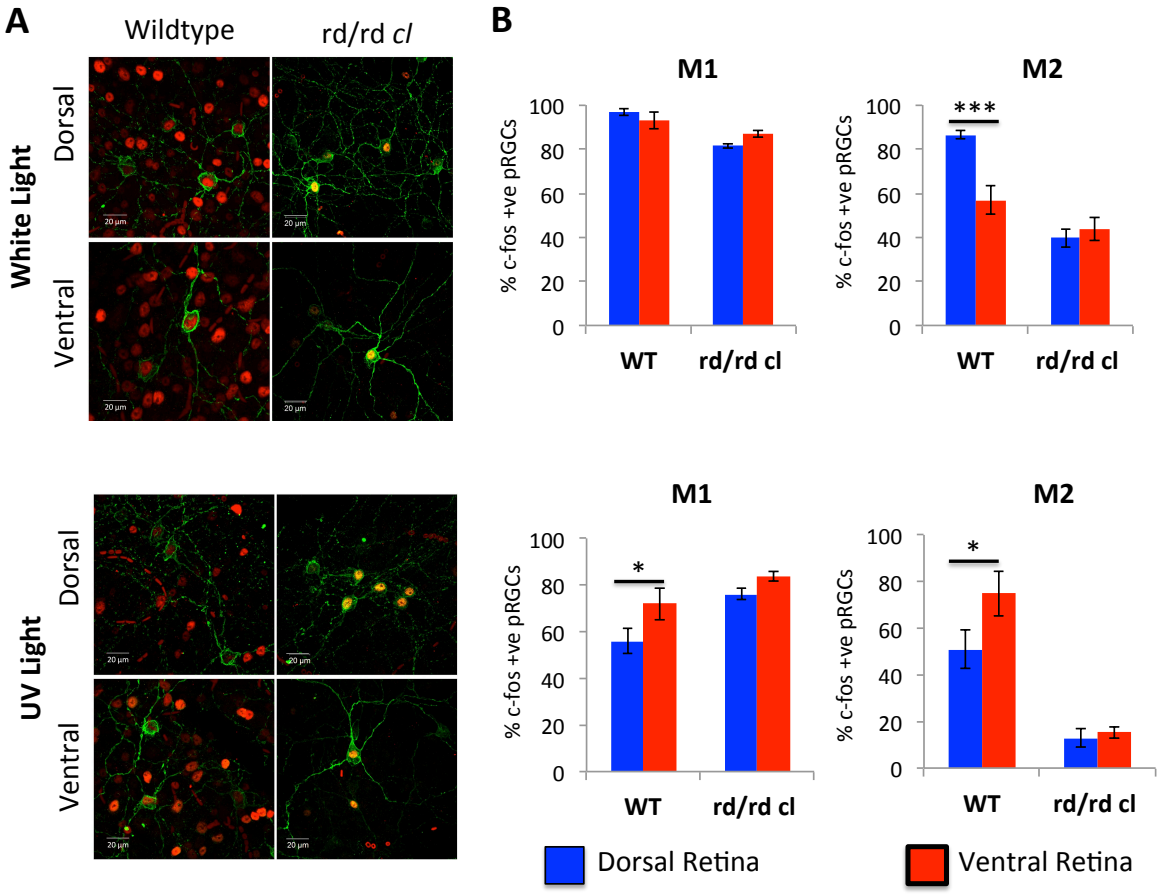

Figure 4.11 Percentage of c-fos positive M1 and M2 pRGCs in the wildtype and *rd/rd cl* retina following UV and white light exposure (A) Whole-retina flatmounts from wildtype and *rd/rd cl* mice pulsed with 30 minutes of white (500lux white light pulse, ~14.7 log photons/ cm^2/ s, 155.4 µW/cm^2) or UV light (12.6 log photons/ cm^2/ s, 2.2 µW/cm^2) at Z16 and collected 30 minutes after the pulse were co-labeled with melanopsin (green), c-fos (red) antibodies as detailed in Methods Chapter 2. The orientation of the retina was typically determined by staining of UVS cone opsin (wildtype), or through melanopsin gradient and/or marking the orientation of retina during dissection (*rd/rd cl*). **(B)** The number of c-fos positive M1 and M2 pRGCs was determined by manual counting of images from non-overlapping regions, typically n=8-12 0.25mm^2 regions, from n=3-4 retina per group with pRGC subtype based on levels of melanopsin expression and the location of their dendrites in the OFF (M1) or ON layers (M2) of the IPL. Significant dorsal- ventral gradients in the

percentage of c-fos positive pRGC subtypes were observed for both M1 and M2 cells in the wildtype under UV light (M1: dorsal, 56.0% ± SEM 5.4% and ventral, 71.9% ± 6.8% SEM, n = 3 retina, 2-tailed Student's t-test, p = 0.03; M2 Dorsal, 50.8% ± 8.4% SEM and ventral, 75.0% ± 9.3% SEM, n = 3 retina, 2-tailed Student's t-test, p = 0.038). White light also induced a significant ventral-dorsal gradients in M2 cells in the wildtype (Dorsal retina, 84.4% ± 1.7% SEM and Ventral, 56.9% ± 6.5% SEM, n = 3 retina, 2-tailed Student's t-test, p = 0.0032). Neither white nor UV light resulted in gradients in c-fos positive M1 or M2 in the *rd/rd cl* but it was observed that UV light resulted in a significantly higher percentage of M1 c-fos induction in the dorsal retina of *rd/rd cl* mice compared to wildtype (WT versus *rd/rd cl* 2-tailed Student's t-test, Dorsal retina comparison p = 0.03, Ventral retina p = 0.21). Note: pRGC subtype quantification and co-labeling procedure of c-fos and melanopsin antibodies, both raised in rabbit was done by Dr. Steven Hughes who separately assessed response in *Opn4* $^{-/-}$ and an Opn4.Cre line containing an EYFP reporter to examine M4 and M5 responses as these subtypes do not show appreciable staining with the melanopsin antibody. This data is published along with the *Opn4* $^{-/-}$, EYFP data in (Hughes et al., 2013). *=p<0.05, **=p<0.01, ***=p<0.005. Bars represent mean values +/- SEM. Scale bars in all images=20μm.

4.7 Phase-shifting responses to UV light in cone-deficient *cl* mouse lacking MWS cones do not significantly differ from wildtype

The pattern of c-fos activation following UV light pulses indicated UVS cones as being primarily responsible for UV responses. To test the importance of cones to UV sensitivity in a further animal model, a 'coneless' mouse containing only the *cl* transgene was bred from our *rd/rd cl* mice to compare these responses to those of the *rd/rd* and *rd/rd cl*. The retinas of these mice were found to have normal rod outer segments and very reduced numbers of cones. Indeed, MWS cones were almost completely absent with only a few observed across the entire retina (Figure 4.12). UVS cone numbers were severely reduced across the retina

with almost no UVS cones in the upper dorsal retina and highly reduced expression across the central and lower retina (Figure 4.12). Retinal sections revealed that the remaining UVS expression was in the outer segments of cones and the general histology of the *cl* retina remained intact (Figure 4.13). While this model retained a small number of UVS cones, the lack of MWS cones allowed an opportunity to examine any involvement from MWS photopigments in the observed UV circadian sensitivity. The phase-shifting of the *cl* model was examined under a series of UV light pulses to generate an irradiance response curve (IRC) as was done for the *rd/rd* and *rd/rd cl*. The IRC was fitted in the same manner as the other models (Figure 4.14) and IC50s compared (Figure 4.15). The average IC50 for the *cl* was slightly higher at 11.99 log photons/ cm^2/ s versus 11.24 for the wildtype and 11.34 for the *rd/rd* but all three models were much lower than the *rd/rd cl* at 13.32 log photons/ cm^2/ s. Based on the IC50 data, the UV sensitivity of the *cl* was found to not differ significantly from wildtype (2-tailed Student's t-test, p=0.158) or *rd/rd* (2-tailed Student's t-test, p=0.171) but was significantly more sensitive than the *rd/rd cl* (2-tailed Student's t-test, p=0.0334). At the lowest irradiance, the *cl* matched wildtype values and was higher than both *rd/rd* and *rd/rd cl*. Together, these results support the UVS opsin as being responsible for the significant UV phase-shifting sensitivity in the mouse.

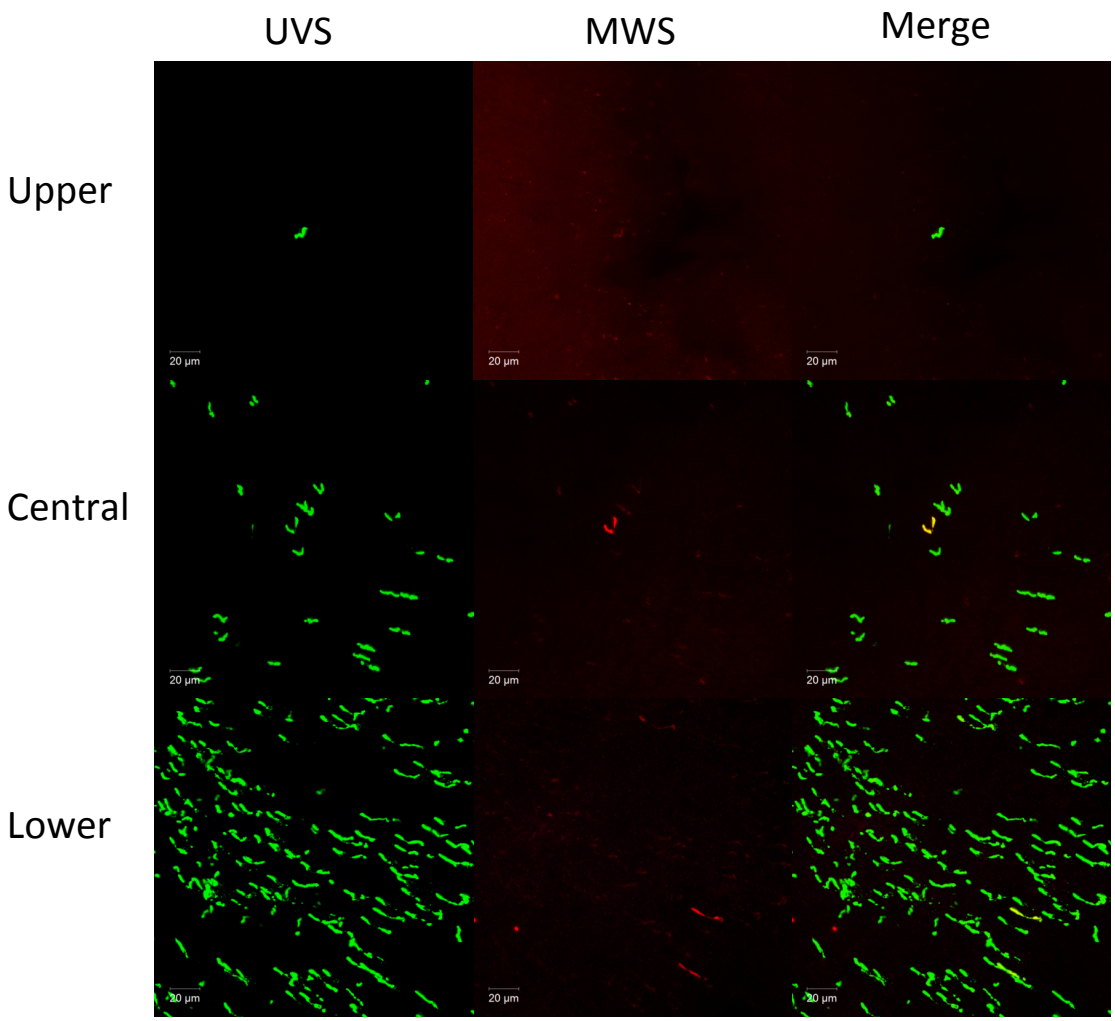

Figure 4.12 Cone survival in the *cl* mouse Double labeling of whole-mounted *cl* retina (~80 days old) with UVS (green) and MWS (red) antibodies found highly reduced levels of UVS across the normal expression gradient but with a significant number of cones remaining in the ventral retina. MWS expression was almost completely absent with very few cones showing co-expression (orange) of MWS and UVS. Scale bars=20µm.

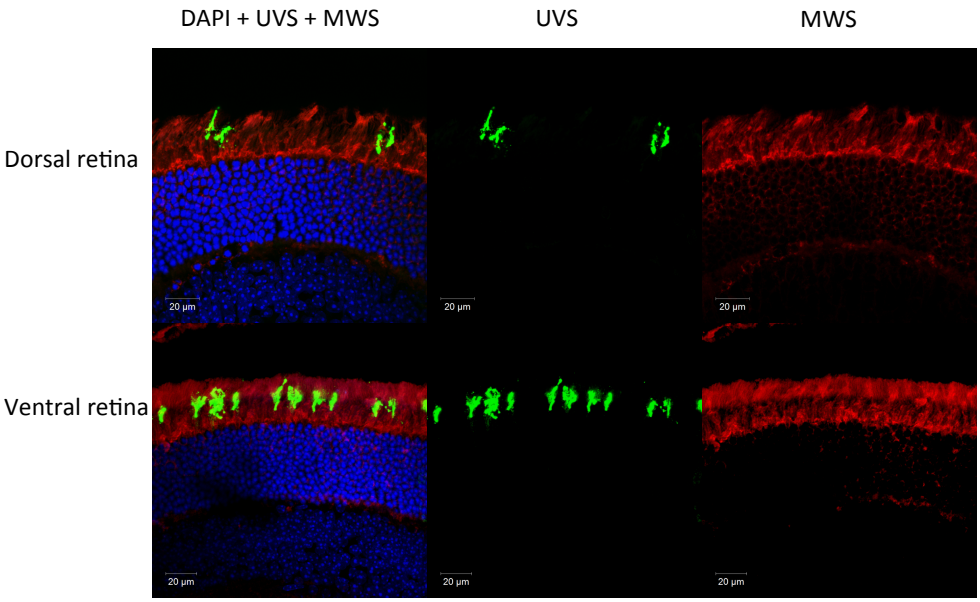

Figure 4.13 Retinal sections of *cl* Immunostained sections from the dorsal and ventral retina of ~80 days old *cl* mice double labeled with UVS (green) and MWS (red) antibodies found UVS expression in outer-segments of cones in both the upper and lower retina. No cones were observed in these sections with MWS expression. Blue nuclear staining is DAPI, scale bars=20µm.

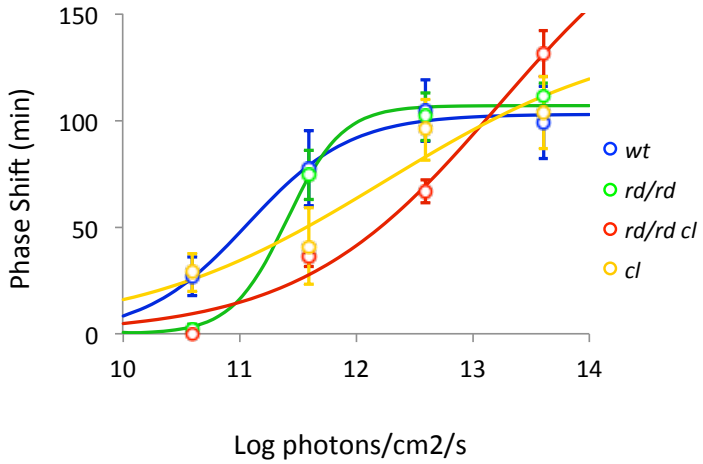

Figure 4.14 Phase-shifting IRC of *cl* mice Irradiance response curve of coneless (*cl*) mice (n=5) to 365nm UV light (15 min light pulses, 365nm UV LEDs) plotted along with *rd/rd* and *rd/rd cl* data from Figure 4.2.

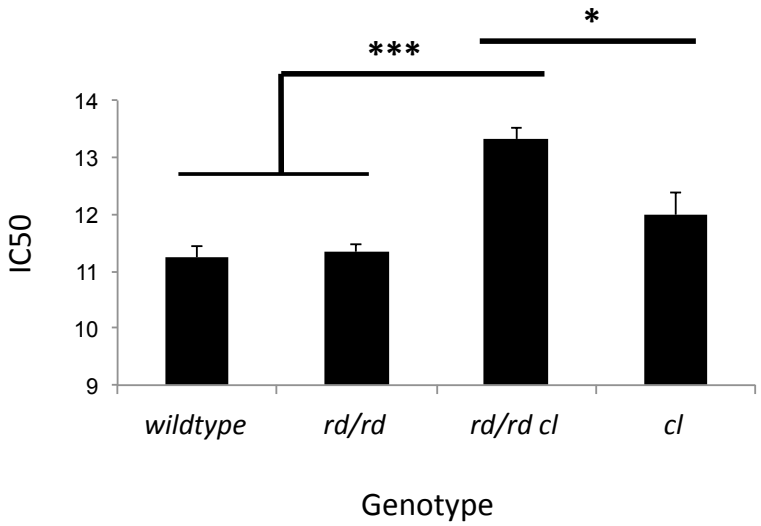

Figure 4.15 Phase-shifting IC50 comparison in *cl*, *rd/rd*, *rd/rd cl* and wildtype. Sensitivity to UV light was assessed by IRC IC50 fit as previously described to individual animal IRCs (see Methods Chapter 2) and compared between wildtype, *rd/rd*, *rd/rd cl* and *cl*. No significant difference in IC50 was found between wildtype (p=0.158) or *rd/rd* (p=0.171) and the *cl* but the coneless IC50 was significantly lower than the *rd/rd cl* (p=0.0334), indicating significantly greater UV sensitivity. All comparisons using 2-tailed Student's t-test, *=p<0.05, **=p<0.01, ***=p<0.005. Bars represent mean values +/- SEM.

4.8 Triple knockout mice do not display any phase-shifting responses to UV light

As confirmation that the observed phase-shifting to UV light was due to the known photoreceptor classes and not an aspect of the pulsing methodology, we obtained triple knockout mice (TKO) containing *Gnat1* $^{-/-}$, *Cnga3* $^{-/-}$ and *Opn4* $^{-/-}$ knockout mutations known to affect functions of rod (Miyamoto et al., 2010), cone (Xu et al., 2012) and melanopsin photopigments respectively. Given the bright UV pulses (13.6 log photons/ cm^2/ s) the TKO

mice did not display a significant phase shift response (average 1.80 min +/- 2.01) (Figure 4.16). It should be noted that light aversion responses have been found in these triple knockouts previously (Semo et al., 2010) perhaps due to partial compensation for the loss of *Gnat1* but these responses are not strong and did not result in a phase-shifting response in this experiment despite the bright stimuli.

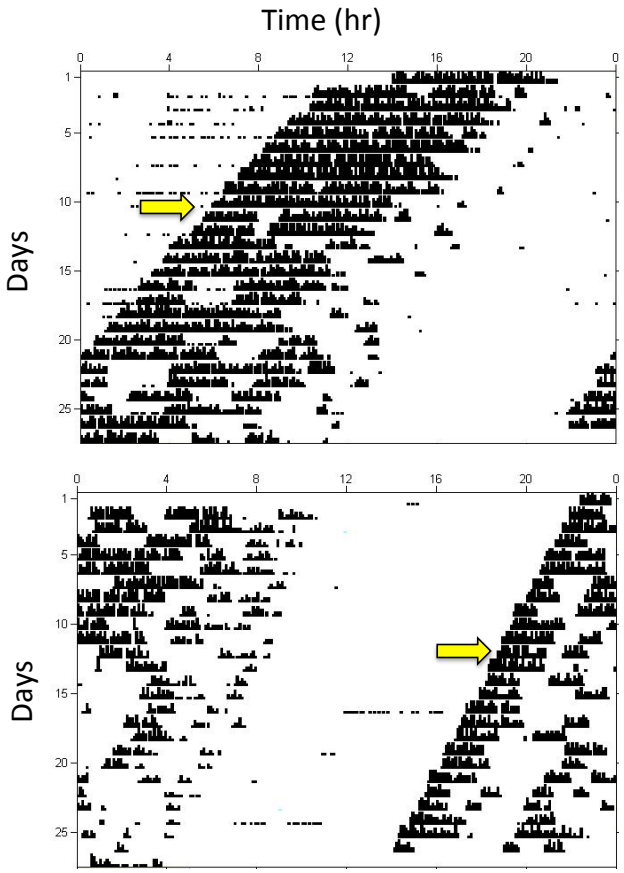

Figure 4.16 Lack of phase-shifting in the Triple-Knockout Bright UV light pulses of 15 minutes, 13.6 log photons/ cm^2/ s failed to produce any significant phase-shifting in (n=5) triple-knockout (*Gnat1* $^{-/-}$, *Cnga3* $^{-/-}$ and *Opn4* $^{-/-}$) mice. Two representative actograms are shown from triple knockout mice where light pulses given at CT16 on the days indicated by arrows produced no observable phase delays (average based on onsets before and after pulse, 1.80 min +/-2.01 SEM).

Discussion

4.8 Mice display phase-shifting responses to ultraviolet light which are comparable to visible light

It is clear that, in many rodent species, UV light influences a number of NIF functions including circadian entrainment, temperature, PLR and melatonin to differing degrees of sensitivity (Amir and Robinson, 1995; Benshoff et al., 1987; Brainard et al., 1994; Dollet et al., 2010; Hut et al., 2000; McGuire et al., 1973; Podolin et al., 1987; Provencio and Foster, 1995; von Schantz et al., 1997; Sharma et al., 1998; Yao et al., 2006). Work in our group in collaboration with colleagues from the University of Leiden has sought to more closely examine the effect of UV light on phase-shifting in mice. The key objective was to see if the behavioral outputs have the same characteristics as visible light responses. In particular, members of our group generated a full phase response curve to UV light pulses (12.9 log photons/ cm^2/ s, 45min) that displayed greatest phase delays early in the subjective night (~CT13.5-16.5), smaller phase advances late in the subjective night (~CT 19.5-22.5) and no responses during the subjective day (CT0-12) (van Oosterhout et al., 2012). These response patterns matched those found for wildtype mouse responses to white light (Pittendrigh and Daan, 1976; vanderLeest et al., 2009). Similarly, the magnitude of phase shifts in response to changing UV light pulse duration also followed the pattern found for white light (Nelson and Takahashi, 1999; Pittendrigh and Daan, 1976). Finally, previous studies have found phase shifts to visible and UV wavelengths to be of a similar magnitude but in each case this was

only investigated at a single irradiance (Dollet et al., 2010; Provencio and Foster, 1995). To more closely examine the relative sensitivities, we compared full irradiance response curves of C57 wildtype mice to pulses of 365nm and 506nm light. Surprisingly, there was no significant difference between the irradiance response curves to UV and visible light close to the peak absorptions of rods, melanopsin and MWS cones, as it might be expected that the circadian system would be tuned to wavelengths most important for clock adjustment. These wavelengths have been thought to be those in the visible spectrum to input to rods and melanopsin as discussed in Chapter 3. Our results confirm that UV input to clock phase-shifting responses is comparable to that of the visual range and suggests there must be a significant biological role for UV input.

4.9 Phase-shifting sensitivity to ultraviolet light is cone dependent

That UV input to circadian responses in the mouse is so strong, despite the limited sensitivity of rods and melanopsin in the UV, suggests that another photoreceptor may be responsible for primary input to the SCN at these wavelengths. Our data showed that mice lacking all rods do not differ in UV IC50 sensitivity from wildtype animals. This suggests that rods do not play a major role in responses to these wavelengths. With the further loss of cones in the *rd/rd cl*, the resulting ~37 fold drop in sensitivity indicates that cones are responsible. The residual sensitivity in the *rd/rd cl* was found to precisely match that which would be expected given α-band absorption of melanopsin at 365nm. So while melanopsin is able to provide some sensitivity to UV, this is very limited due to the wavelengths being so far removed from the maximal absorption peak. The β-band does not seem to be able to

drive behavioral responses which resolves this question posed by previous studies (Hut et al., 2000; Jacobs et al., 2001; von Schantz et al., 1997). The lack of any significant phase-shifting response to bright UV in TKO animals demonstrates the observed effects are entirely due to known photoreceptors' input to the clock, rather than handling effects or extra-retinal photosensitivity.

That the *rd/rd* sensitivity did not differ from wildtype is even more surprising given that the *rd/rd* mutation results in gradual cone degeneration (Carter-Dawson et al., 1978) leaving only a small population in the fully degenerate retina of the adult mice used in our study (Foster et al., 1991). Yet this small number of cones is apparently sufficient to drive a full response. Phase-shifting responses to UV light equal to those of wildtype have previously been seen in the *rd/rd* (Provencio and Foster, 1995) and our results in the coneless (*cl*) model support this result, as the small population of UVS cones remaining in these mice was also able to drive a UV response that was not significantly different from wildtype. The number of cone perikarya remaining in the peripheral retina of the 4 month old *rd/rd* (where the ventral retina will contain predominantly UVS opsin) is 14% (Carter-Dawson et al., 1978) while the *cl* retina contains less than 5% of the normal number of UVS cones (Freedman et al., 1999). Our own immunohistochemical examination generally supported these previous observations as both models retained UVS staining (in some cases it appeared 80 day old *rd/rd* had more expression than the *cl*, perhaps explaining what the *cl* had slightly lower sensitivity). We also found that our *rd/rd* mice retained UVS cones even when highly aged (~230 days). Some of these UVS cones appeared to retain outer-segments which differed from original observations of this model (Carter-Dawson et al., 1978). The pattern of cone

degeneration in the flat mounted *rd/rd* retinae we examined was strikingly high in the central retina with much greater numbers of cones, and particularly cones retaining outer-segments, remaining in the peripheral retina. If only sections of the central retina were sampled in a particular study then there would be the appearance of a much higher level of cone loss than has actually occurred, which may have contributed to an assumption by some authors that the *rd/rd* is a close match for the *rd/rd cl*. The cones observed in our study were abnormal in appearance and lying horizontal in the absence of the rod outer segments to provide structure but our results strongly suggest that these cones are still able to provide functional circadian input at 80 days of age. Even though small numbers of cones remain in both models, pRGCs projecting to the SCN are known to form a dendritic net across the retina, each contacting many bipolar and amacrine cells, and thus each cell receives input from many rods and cones (Belenky et al., 2003; Sekaran et al., 2003; Tu et al., 2005). This net may be key to explaining our results as it would allow pRGCs to gather the responses from remaining UVS cones in these models and apparently generate a sufficiently strong signal for a normal response over these UV light intensities. Interestingly, we also observed over the course of our experiments that there is variation in the speed of cone degeneration in the *rd/rd* so that some animals at 80 days of age appear to have greater numbers of cones remaining than others. As this has not been noted in other *rd/rd* studies it could be unique to our line but, if it is a general feature of *rd/rd* that has not been recorded previously, it may provide an explanation for the variation in the observed cone responses of different *rd/rd* mice.

Despite the focus on cones, our results have also highlighted a role of rod input at low light intensities. This has previously been shown for visual wavelengths (Altimus et al., 2010;

Lall et al., 2010) but the significant difference between the wildtype and cl, both of which have rods, as compared to the *rd/rd* and *rd/rd* cl, lacking rods, at the lowest UV irradiance indicates that this rod role at low irradiances appears to be maintained at UV wavelengths. Rods do have a minimal residual sensitivity at 365nm, which can be estimated at around 2% of maximal using the standard photopigment absorption template. An alternative explanation might be that the cone response at these intensities requires interaction with the rod pathway. Rods have been found to require the gap-junction connections to cones that drive entrainment at higher white light levels (Altimus et al., 2010) and, in a recent study using mice, dim flash sensitivity in patch recordings of cones was found with a shift towards what was called a 'rod-like phenotype' highly variable among the cone population. This appeared to depend on gap junction connections to rods (Asteriti et al., 2014). Gap junctions at the synaptic pedicles of cones contact adjacent photoreceptors and allow signal transmission between the photoreceptor classes (O'Brien et al., 2012). This coupling is known to allow rod signals to enter the cone pathway (Soucy et al., 1998) but this new evidence suggests that this connection may also allow rod influence to modulate cone signals. The degree of coupling may be both circadian and light-dependent regulated by phosphorylation of gap junction protein connexin36 by kinases such as calmodulin-dependent protein kinase II (Asteriti et al., 2014). How this connection might work to increase the sensitivity range of cones is not clear but could explain our results if the sensitivity range of cones is increased in the presence of rods. Further experiments are needed to determine if this low intensity response is dependent on cones as none of our models eliminated the cone response while retaining the rod.

4.10 Retinal responses to ultraviolet light follow the UVS expression gradient

Behavioral experiments seeking to untangle the various photoreceptor contributions to NIF responses are significantly complicated by the overlapping absorbance of the rod, cone and melanopsin photopigments. While UV responses are better suited in this regard being further away from the absorbance maxima of most of the mouse photopigments, there is still residual sensitivity of these opsins in the UV and photoreceptor degeneration and knockout models are not conclusive proof of what the relative photoreceptor contributions are under natural conditions in the wildtype system. Thus, to examine responses to UV light using a different approach, we examined retinal expression of the immediate-early gene c-fos. In the SCN, c-fos is strongly linked to light induced phase-shifting responses as the expression of c-fos mRNA and the protein FOS follows the phase response curve, only occurring when light input phase shifts the clock (Colwell and Foster, 1992; Kornhauser et al., 1990; Morin and Allen, 2006; Rea, 1992; Rusak et al., 1990). Inhibition of c-fos expression also inhibits light responses (Abe et al., 1991; Colwell et al., 1991; Vindlacheruvu et al., 1992; Wollnik et al., 1995). Key to our experiments, retinal *c-fos* expression following light exposure occurs in both the GCL and INL (Chambille et al., 1993; Dkhissi-Benyahya et al., 2000; Earnest et al., 1990; Huerta et al., 1997, 1999; Koistinaho and Sagar, 1995; Lupi et al., 1999; Sagar and Sharp, 1990) and further studies have shown expression in RGCs is the result of photoreceptor activation (Hannibal et al., 2001; Pickard et al., 2009; Semo et al., 2003).

Thus c-fos is a well-established marker for light activation of RGCs and, given the differing photopigment expression gradients in the mouse retina, this can be used to gain information concerning which photoreceptors are driving light responses to particular irradiances or wavelengths of light. Rod distribution across the retina is relatively even when, as our staining demonstrates, UVS and MWS opsins have opposing expression gradients (Haverkamp et al., 2005; Hughes et al., 2013; Szél et al., 1993). We found that UV light pulses in wildtype mice induced a dorsal-ventral gradient of c-fos expression while white light, that contained almost no wavelengths below ~425nm, did not induce an obvious gradient. That the gradient of c-fos positive cells follows the UVS gradient in response to UV light, and not the opposing MWS or melanopsin gradients, points to the UVS cone population as the critical photopigment of UV detection in the mouse retina.

To quantify these differences and see if the observed c-fos positive cell gradient is indicative of gradients in pRGC response, the retina of wildtype and *rd/rd cl* mice were stained for both melanopsin and c-fos following UV and white light exposure. As melanopsin staining in the retina allows the quantification of M1 and M2 type pRGCs, with the melanopsin expression in other subtypes too low for visualization, these subtypes are expected to be included in the counts of c-fos positive, melanopsin positive cells. We found a significant dorsal-ventral gradient in c-fos positive pRGCs following UV light that was mirrored by significant dorsal-ventral gradients in the percentage of c-fos positive cells for both M1 and M2 subtypes. While white light did not induce a significant gradient in overall c-fos positive cells, there was a trend of higher dorsal responses and, when the M1 and M2 subtypes were separated with help of Dr. Steven Hughes, a highly significant ventral dorsal gradient was found for

M2 pRGCs but not M1s. No significant gradients in c-fos positive M1 or M2 pRGCs were found in *rd/rd cl* under UV or white light pulses. Further analysis of this data by Steven Hughes examined *Opn4* $^{-/-}$ mice and an *Opn4.Cre* line containing an EYFP reporter to examine M4 and M5 responses. This work indicated greater spectral tuning of M2-M5 pRGC subtypes by the opposing cone opsin gradients in m-cones. These subtypes may be more susceptible to cone influence due to their lower endogenous sensitivity with lower levels of melanopsin expression (Hughes et al., 2013) and, given pRGC subtypes project differentially to NIF brain regions (Baver et al., 2008), the differences in spectral tuning has implications for the spectra sensitivity of NIF behaviors. Intriguingly, the separate analysis of M1 and M2 responses also suggested an inhibitory input from outer retinal photoreceptors to M1 type pRGCs following UV light exposure as a greater number of M1 cells were found to be c-fos positive in *rd/rd cl* dorsal retina than in wildtype retina which is un-expected given the loss of UVS cone input (Hughes et al., 2013). This is an interesting result considering the entrainment data presented in Chapter 3 also suggested an inhibitory influence of cones on melanopsin. Further discussion of the theory of cone inhibition can be found in the final discussion in Chapter 9.

4.11 Conclusions

The phase-shifting results from the *rd/rd* and *rd/rd cl* models support cones as the major photoreceptors involved in driving UV photic-entrainment responses. The strong responses of the *cl* mice, lacking MWS cones, as well as the strong dorsal-ventral gradient of c-fos pRGC activation by UV light in wildtype mice, support the hypothesis that UV light

responses in mice are due to UVS cone input. While it may not seem surprising that the ultraviolet sensitive photopigment would be responsible for UV sensitivity, the short transient responses of cones have been considered restricted as drivers of specific NIF functions. These results suggest responses to UV light pulses of a duration at which cones have been shown to play limited role under visible light (Altimus et al., 2010) are driven by UVS photopigments rather than rods or melanopsin. This supports a distinct role for UVS cones in circadian responses. However, final confirmation of UVS cone contributions to NIF responses requires a more specific model of UVS cone loss.

Chapter 5: **Optokinetic responses and novel object recognition as tests of visual function**

Introduction

5.1 Aims

Phase-shifting responses to UV light suggest a key role for UVS cones in entrainment, supporting the hypothesis that input to the NIF system reflects an important contribution of UV sensitivity in mice. This may explain the particular emphasis on short-wavelength sensitivity in this species. However, the presence of a UVS photopigment in rodents was first discovered in visual experiments (Jacobs et al., 1991). Therefore, to determine the role of UVS cones in image-forming vision, an optokinetic drum system was developed to assess the visual acuity in mice. In addition, a modified version of the novel object recognition (NOR) test was also investigated as a further test of cortex-dependent vision. This chapter will review the study of the visual pathways of mice and the most common methods used to assess mouse vision. Our aim was to confirm the function of our OKR drum, to examine the relative contributions of rods and cones to the optokinetic reflex using retinal photoreceptor mutants/transgenics, and to develop a test of cortical visual function for further UV visual testing in an *Opn1sw* mutant line.

5.2 The mouse visual system as a model for mammalian vision

Despite the importance of mouse models in the study of cellular and physiological elements of the visual pathway, behavioral studies of vision have generally preferred other animal

models as the mouse was considered to be a poor correlate to primate (including human) visual systems (Prusky and Douglas, 2008). However, as the ability to generate mouse models with specific genetic manipulations becomes more refined it has become clear that, if the limits of possible comparison are understood, the mouse can play a vital role in understanding mammalian vision and human visual diseases (Baker, 2013). Thus, significant recent research has focused on developing effective tests of mouse vision to screen new mutant models and to determine how the mouse visual system compares to our own.

Brain pathways and visual areas

In the mouse, as in other mammals, vision begins with light information being transmitted through the retina to the retinal ganglion cells. Almost all of the mouse ganglion cells have projections along the retinogeniculate path to the dorsal LGN (dLGN) (Hofbauer and Dräger, 1985), which has been shown to contain significant elements homologous with the dLGN of primates (Huberman and Niell, 2011). Signals are then passed from the dLGN to the primary visual cortex (V1) (Figure 5.1 shows primary visual pathway in mice). Examination of higher visual processing in the visual cortex has suggested that mice again share many key visual properties with other mammals, just at a size-restricted lower spatial resolution (Glickfeld et al., 2014; Huberman and Niell, 2011). For instance, mice have been found to maintain a functional segregation of information passing from the V1 to downstream target areas (Andermann et al., 2011; Marshel et al., 2011) and the normal elements of cortical visual processing across the V1 involved in spatial summation, directional sensitivity, contrast gain control and contrast-invariant tuning (Niell and Stryker,

2008). There are obvious differences in the complexities of organization and resolution between the mouse visual system and that of other mammalian models such as primates due to size differences in brain areas. For example, fewer visual cortex neurons are present per area of the visual field in the mouse (Sirotin and Das, 2010). That said, the eventual use of integrated visual information to drive responsive motor outputs is through the same structures as in the primate including the superior colliculus (SC), motor cortex and amygdala (Glickfeld et al., 2014).

There are also suggestions that the division of processing between the cortex and other visual areas might differ between the mouse and mammals like cats and primates. Apart from the primary visual pathway to the cortex, like those of most mammals mouse RGCs also project directly to visual areas in the midbrain pretectal area, involved in the reflex control of the pupil adjustment to light, and the SC, which controls movements of the eyes and head needed to maintain visual orientation (Hofbauer and Dräger, 1985; Provencio et al., 1998b). While in primates, only about a tenth of RGCs have been found to project to the SC (Rodieck and Watanabe, 1993), almost all mouse RGCs have projections to the SC (Hofbauer and Dräger, 1985). Again studies have found the basic receptive field organization of the SC to be similar to other mammals. However, single-unit extracellular recordings suggested that some of the basic functions of the SC, such as orientation selectivity, were independent of input from the visual cortex in the mouse indicating that the SC may be able to process directional information from RGCs themselves (Wang et al., 2010). This is supported by the previous discovery that mice with visual cortex lesions were still able to complete some basic directional tasks (Prusky and Douglas, 2004). Whether this

means that the SC of mice has retained functions found in non-mammalian vertebrates where the SC/ optic tectum is the main visual processing area or that the role of the SC in other mammals has been underestimated will be an intriguing area for further study (Lovejoy and Krauzlis, 2010).

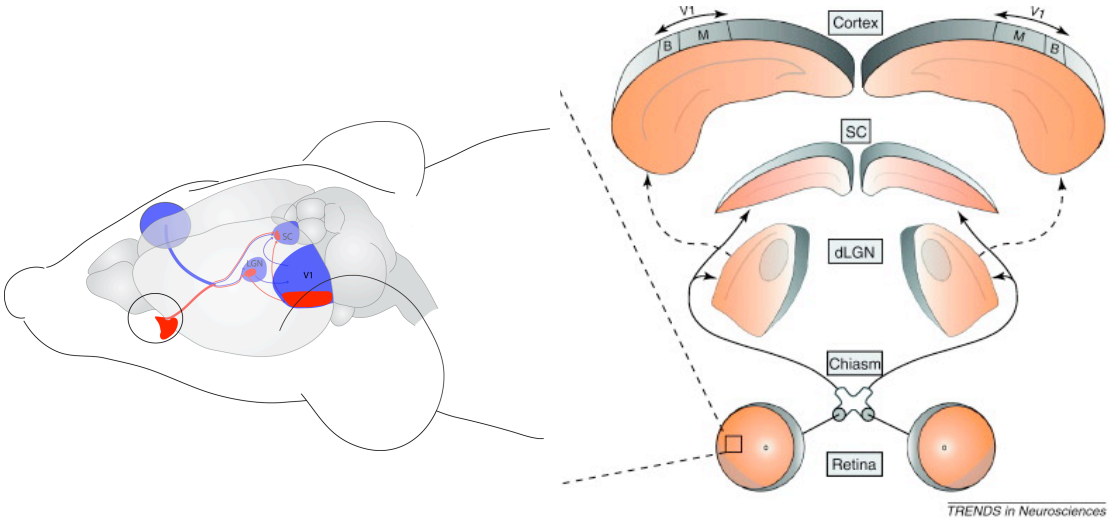

Figure 5.1 Representation of the major visual pathways in the mouse The majority of mouse RGCs project both down the retinogeniculate pathway to the LGN (where signals are relayed to the primary visual cortex V1) and to the SC. Mouse head representation from (Wilks et al., 2013), visual pathway diagram adapted from (Huberman and Niell, 2011).

Functional abilities of mouse vision limited by structure

In terms of the function of mouse vision, despite having similar photoreceptor densities as primates like the macaque (Jeon et al., 1998; Packer et al., 1989) and peak RGC densities similar to carnivores like the cat (Stone, 1978), mouse vision has very poor spatial acuity, more than 50 times worse than in humans (Prusky and Douglas, 2008). Mice have a rod

dominated retina with 97% of photoreceptors being rods (Jeon et al., 1998) and also lack the foveal region of primates which, at only 1% of the retinal area, contains 99% of all cones and is vital for high contrast and acuity vision (Perry and Cowey, 1985). In fact, the average cone density of the mouse is similar to that of the human eye only 3 mm away from the fovea region (Jeon et al., 1998). Other structural differences include the higher number of RGC classes in mice compared to primates (Field and Chichilnisky, 2007; Völgyi et al., 2009) and the laterally placed eyes in the mouse which lead to large disparities in the contralateral and ipsilateral retinofugal pathways and evidently to binocular vision (Dräger and Olsen, 1980).

However, the lack of acuity does not mean that mouse vision is functionally useless. As mentioned above, the mouse retina is comparable to the peripheral primate retina in terms of photoreceptor ratio and density (Huberman and Niell, 2011) and there is behavioral evidence that mice are indeed able to use cone visual sensitivity at a level similar to that in the human retinal periphery (Naarendorp et al., 2010). As such, acuity over the short distances in which most locomotion and interaction decisions would occur may be more than adequate for the mouse's requirements (Prusky and Douglas, 2008). From a processing standpoint, there is evidence that a significant limitation to the mouse visual system's capacity to incorporate more information is its photoreceptor compliment. Mice have dichromatic vision but, when a third cone photopigment was introduced using a relatively simple manipulation, the result was trichromatic vision, demonstrating that the basic circuits for this more advanced visual discrimination are present in the mouse and this ability is only hindered by the normal opsin complement (Jacobs et al., 2007).

In summary research has shown that the organization and many of the key properties of vision in primates and other more visually dependent mammals are present in the mouse visual system. This supports the use of the mouse as an experimental model to provide relevant insight into human visual processing. Also, the level of sophistication in the mouse visual system is sufficient to allow vision to be of significant use to the mouse, despite a general perception of mice as nocturnal creatures that are virtually blind (Prusky and Douglas, 2008).

5.3 Behavioral visual assessments

Any study of the mouse visual system is dependent upon appropriate assays to measure visual performance. There are several different ways to assess visual performance in mice and other animals. One method involves the assessment of the electrical activity of photoreceptors or visual pathways in the brain. Electroretinography (ERG) assesses field potential on the surface of the eye, which changes as light excites photoreceptors. As ERG is non-invasive, it can be widely applied as a diagnostic tool in determining retinal function of human patients as well as for live experimental animals (Cameron et al., 2008). As described in Cameron et al's review, the approach of modifying the light stimuli and testing under dark and light conditions can be used to isolate rod and cone ERG responses. Electrical potentials resulting from visual stimulation can also be examined in the brain through visual evoked potentials (VEP). The VEP is recorded using electrodes placed on the skin over the visual cortex and is another valuable diagnostic tool used to determine the function of visual

pathways from the retina (Pinto and Enroth-Cugell, 2000). As both ERGs and VEPs show circadian variation, they can also be used to examine daily changes in the visual system (Cameron et al., 2008; Stolz et al., 1987). However, while ERG and VEP are both useful methods of assessing the basis of visual signals and visual system function, there are limits to what can be learned about the visual system solely through the use of electrical signals. Furthermore, these methods often involve the use of anesthetized animals, which may influence system sensitivity. Because the core function of vision is in functional visual performance to inform behavioral decisions, behavioral visual assays are able to assess vision at a different level from the ERG and VEP.

For complete assessment of visual function, assays that involve visual processing and integration may offer different insights than those examining electrical potentials. However, these tests are complicated by the challenge of training mice to perform more complex visual tasks (Whishaw, 1995). Some of the most common trained behavioral tasks include the adapted forced-choice discrimination task, which has been instrumental in studies of mouse ultraviolet sensitivity and color vision (Jacobs, 1983; Jacobs et al., 1991, 1999, 2001, 2007) and the Morris water maze (Morris et al., 1982), a spatial memory and navigation task that has been adapted for visual acuity (Robinson et al., 2001, 2004). Based on these original assays, adaptations and novel tests continue to be developed to investigate visual thresholds and behavior in the mouse. An adapted swimming forced-choice Visual Water Task has been shown to involve cortical function (Prusky and Douglas, 2004), while a recent novel method trained mice to halt wheel running for a water reward when given a visual stimulus

and thus is able to assess visual function and thresholds in naturally behaving mice (Naarendorp et al., 2010).

As motivation is a major issue in training mice to the visual tasks, the examination of reflexive visual behaviors is another common way to assess mouse visual function with no training requirement. Two examples of ocular reflexes that have been utilized in assays are the pupil reflex, which examines the non-image forming visual system being driven by rods, cones and pRGCs, and the optokinetic stabilizing reflex, which involves rapid movement of the eye or head in response to a moving stimulus (Pinto and Enroth-Cugell, 2000).

We aim to assess ultraviolet vision in a mouse model lacking UVS opsin in later chapters and thus, as potential visual testing methods, we consider the optokinetic reflex and examine the basis for a modification of an object recognition task to examine cortex-dependent vision.

The Optokinetic Reflex

The optokinetic reflex/response (OKR) is a stabilization reflex that involves a series of rapid tracking movements (saccades) and slower movements that follow moving stimuli to keep an image stabilized on the retina. In mice, this results in head movements to track the direction and velocity of a stimulus (See Figure 5.2) and the use of an apparatus with varying grating frequencies can be used to assess the function of the visual system (Cowey and Franzini, 1979).

Figure 5.2 The Optokinetic reflexive response in mice A rotating grating stimulus (A) in a mechanical or virtual (projected) drum will cause a mouse (B) to reflexively follow the speed and direction of rotation using rapid tracking movements with its head. From (Prusky et al., 2004). In (A), we see the projected stimulus circle. The cycles per degree of the stimulus is the portion of the light/dark cycle pattern present in each degree of this circle centered on the animal and is thus a measure of grating frequency that can be maintained between studies using different drum sizes.

The neural pathway mediating the OKR involves the pretectal nucleus of the optic tract (NOT) and the terminal nuclei of the accessory optic tract in the midbrain (Simpson, 1984). Indeed, the horizontal and vertical components of the optokinetic response have been associated with different nuclei in the accessory optic system in birds (Burns and Wallman, 1981; Montgomery et al., 1982). There is also significant evidence that the superior colliculus, which is a target of projections from the NOT, plays a central role in supporting optokinetic tracking while the OKR has not been found to depend on input from the visual cortex (Biral et al., 1982; Douglas et al., 2005; Hobbelen and Collewijn, 1971). Visual acuity

thresholds as determined from cortex dependent tasks (eg Visual Water Task) have also been found to be slightly higher than those based on optomotor responses (Prusky and Douglas, 2004). However, while the reflex itself may be subcortical, it seems the cortex is able to influence and modulate the OKR as monocular deprivation by eye covering was found to result in an enhanced OKR visual acuity threshold (Prusky et al., 2006). Exposure to optomotor testing during early postnatal development has also been found to improve thresholds, demonstrating cortex-dependent regulated plasticity of this visual response (Prusky et al., 2008).

The standard OKR apparatus is a rotating drum placed around an animal where the tracking responses are recorded as the stripe frequency of gratings is modified. The spatial frequency grating of the stimulus is commonly expressed as cycles per degree (cpd) as this describes the portion of the alternating stripe pattern (cycle) that is present in each degree of the circle centered on the test subject (see Figure 5.2) and thus can be adjusted to a given drum size to keep measures of visual acuity meaningful between different test apparatus. There are several variations of the OKR assay, firstly in what part of the animal is assessed as different studies of mouse OKR have used the tracking movements of the eye (Faulstich et al., 2006), head (Abdeljalil et al., 2005) and whole body (Schmucker et al., 2005). Determination of the tracking movements may be automated or manual and a virtual system has been developed that allows improved control of variables such as animal movement in relation to the stripe gratings, as well as allowing more precise control of the grating cpd and variation of contrast (Prusky et al., 2004).

As a method of genetic research, it is now possible to generate mice with unknown mutations using techniques such as N-ethyl-N-nitrosourea (ENU) mutagenesis then select those with specific phenotypes of interest before determining the gene responsible (Acevedo-Arozena et al., 2008). Such methods have the potential to give new insights into the mechanisms of known pathways and into the basis of human diseases but require effective and fast screening methods to identify the desired phenotypes. With the ability to rapidly determine visual threshold, the OKR system has been identified as a method well suited to screen for visual mutations (Abdeljalil et al., 2005; Prusky et al., 2004). Indeed, OKR is able to assess each eye independently simply by changing the rotation direction as clockwise rotation, from left to right, relies on left eye response while counter clockwise rotation tests the right eye (Douglas et al., 2005). Such screening may not be able to assess the cortical aspects of vision but it is a reliable method of determining photoreceptor degeneration as animals with outer retinal degeneration are unable to head track in response to any grating frequency (Thaung et al., 2002).

With the increased application of this assay, there has been interest in which photoreceptors contribute to the OKR. Studies on mice lacking rod and/ or cone function have found somewhat contradictory results. One study used mice lacking rods (*Rho*$^{-/-}$ and *Cngb1*$^{-/-}$ models), cone (*Cnga3*$^{-/-}$) or both found that the loss of rods resulted in mice only displaying tracking responses to large gratings (up to 0.1 cpd) under the brightest illuminance levels (30cd/m2 or about 400lux), and loss of rods and cones resulted in total absence of tracking responses (Schmucker et al., 2005). However, they also observed mice lacking cone response due to the cyclic nucleotide-gated (CNG) cation channel knockout displayed

responses similar to the wildtype. These results suggested that the OKR is primarily driven by rods and that the rod response is not saturated even under illuminance entering the phototopic range. However, another study using different rod (*Gnat1* $^{-/-}$) and cone (*Gnat2*^{cpfl3}) mutant models found loss of cones resulted in photopic tracking deficits while the mice lacking rods could not track at scotopic intensities (Umino et al., 2008). Whether these inconsistencies represent differences in methodology or in these specific mutants is not clear.

Novel Object Recognition Test of visual stimuli

Novel object recognition tasks are a well-established behavioral method of assessing aspects of memory performance in rodents (Bevins and Besheer, 2006; Ennaceur and Delacour, 1988). These tests rely on a natural tendency to explore novel stimuli as an animal is allowed to freely explore two identical objects for a given period then, after a delay during which one object is replaced with a different one, the animal is again allowed to freely interact with both the familiar and the novel object for a set interval. If the recognition memory performance has been successful, the animal will spend a greater proportion of its time exploring the novel object, demonstrating recognition of the familiar object (Ennaceur, 2010). This is considered a particularly useful assay of cognitive recognition memory performance as the exploratory behavior is a natural spontaneous one and requires only a small amount of time for habituation and training (Silvers et al., 2007).

Performance in the NOR task has been found to be impaired by lesions of both the hippocampus and cortex, specifically being tied to the entorhinal and perirhinal cortex regions in the medial temporal lobe with roles in many aspects of memory and visual perception (Aggleton et al., 2010; Albasser et al., 2009, 2011; Buckmaster et al., 2004; Clark et al., 2000; Hammond et al., 2004). The NOR task can be modified to test a wide range of specific memory types (Taglialatela et al., 2009) and also tuned to test recognition memory in a specific sensory mode by restricting the classically complex stimuli to target only one of the olfactory, somatosensory or visual systems (Albasser et al., 2011; Winters and Reid, 2010). The potential for visual and non-visual cue use has been illustrated through use of a transparent barrier between the mouse and objects to prevent object contact (Whitt and Robinson, 2013; Winters and Reid, 2010). Recognition performance was maintained above chance even with this barrier in place but, without the barrier in place, successful recognition has also been obtained when the task was run in complete darkness (Albasser et al., 2011; Winters and Reid, 2010). Thus a modified NOR task restricted to visual stimuli could represent a novel method of behavioral screening for more complex visual system function in mutant mice but requires further validation of photoreceptor involvement.

5.3 Chapter aims summary

In this chapter we characterize OKR responses in retinal degeneration and melanopsin knockout models to examine the relative contributions of rods, cones and melanopsin pRGCs, given the previous contrasting conclusions regarding the role of cones in this visual assay. We also examine OKR responses under UV light and characterize a novel visual

modification of the novel-object recognition (NOR) task to evaluate use of these visual assays in the assessment of a UVS opsin knockout model.

Results

5.4 Wildtype OKR threshold and sensitivity

Wildtype C3H mice were tested on our OKR drum system at 200 lux (59.4μW/cm^2) to confirm its function using stripe gratings with a range in cpd from 0.1 to 0.6. The threshold acuity (2 or more head tracking responses per minute, see Methods: Chapter 2 for testing procedure and definitions) of head-tracking response was 0.5 cpd with the maximal responses per minute occurring at 0.2 cpd (Figure 5.3). None of the animals displayed head tracking response to a sham completely white background (0 cpd). One wildtype animal was discovered during initial pupillometry testing of our UVS opsin *Opn1sw* KO (data discussed in Chapter 6) that appeared to have corneal damage in its right eye (Figure 5.4). This animal was tested on the OKR drum to confirm its ability to assess individual eye responses and over 8 trials at 200lux and 0.2 cpd, chosen as the grating which produced maximal responses in our wildtype tests, head-tracking was only observed during clockwise rotation corresponding to the left eye responses (Figure 5.4).

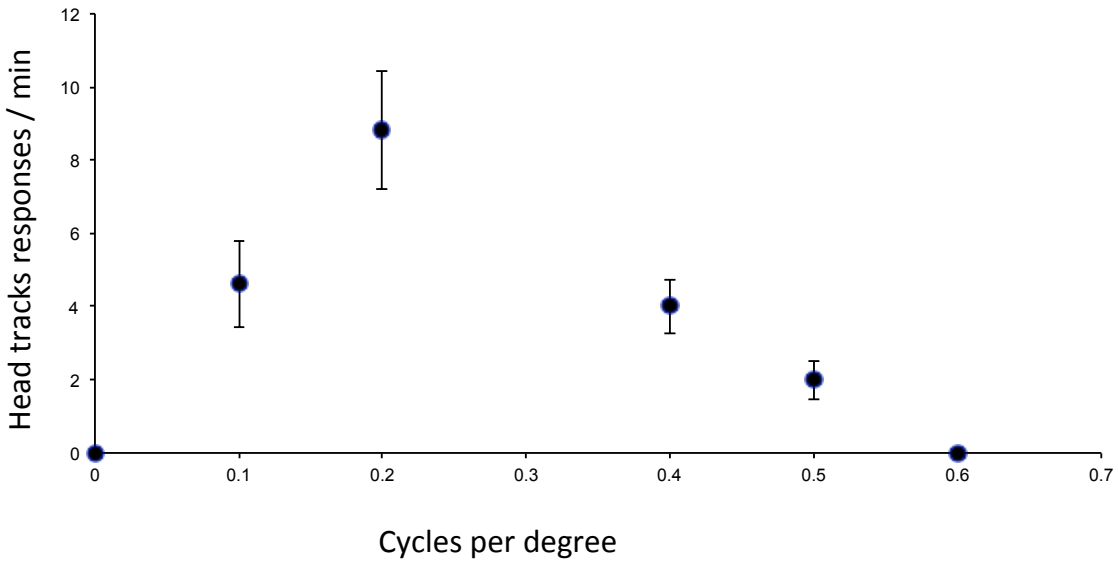

Figure 5.3 Optokinetic responses in wildtype C3H mice The optokinetic reflex (OKR) of wildtype C3H mice (n=6) was measured in our mechanical drum under 200lux (59.4μW/cm^2)white light over spatial gratings from 0.1 to 0.6 cycles per-degree (cpd). Threshold of acuity was defined as the smallest cpd stripe grating at which an average equal or greater than 2 responses per minute was observed. Acuity threshold for the C3H was found to be 0.5cpd and maximal responses of 8.8 head tracking responses/ minute was found at 0.2cpd. A sham trial (shown here as 0 cpd) used a completely blank white sheet in the drum. No head-tracking was observed to sham stimulus.

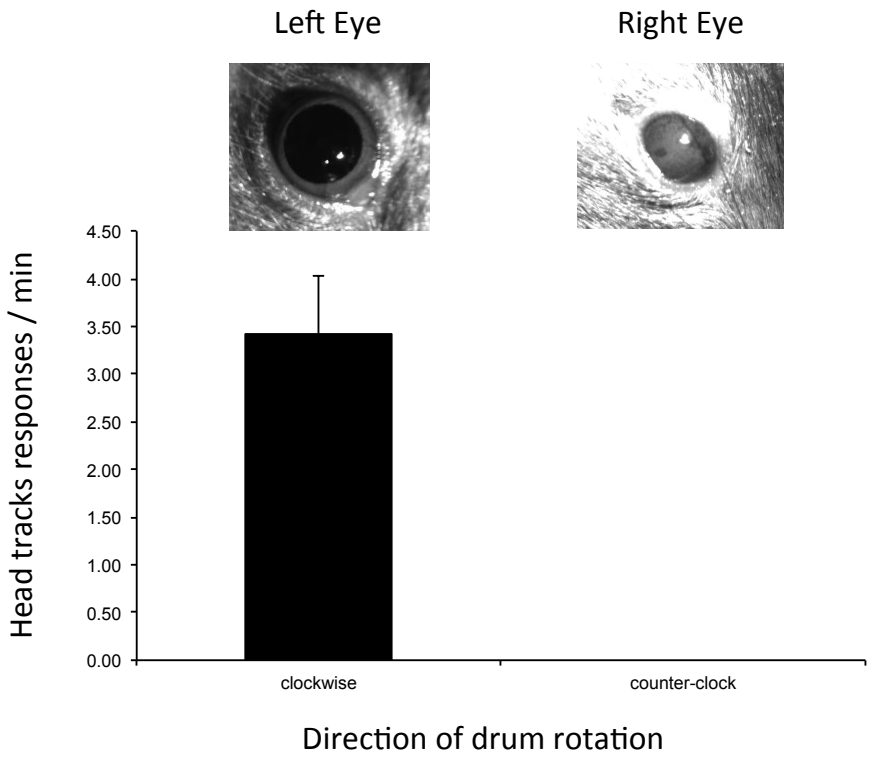

Figure 5.4 Evidence of independent eye OKR assessment in cornea-damaged mouse A wildtype mouse with apparent severe corneal damage to its right eye was found during pupillometry and tested to examine the ability of our drum to differentiate left and right eye tracking. Images of the left and right eye showing abnormal cornea in right eye are shown. Over 8 two-minute trials, the mouse displayed an average of 3.4 head-tracks per minute when the drum rotated clockwise but no head-tracking during counter-clockwise rotation. This response is consistent with the ability of OKR drums to assess independent eye acuity (Douglas et al., 2005).

5.5 Photoreceptor contribution to OKR using *rd/rd*, *rd/rd cl, cl* and *Opn4* -/- models

The OKR response of mouse models of retinal degeneration and photoreceptor loss were examined in *rd/rd cl* mice lacking all rods and cones, *rd/rd* mice with no rods and limited

cones, *cl* mice with rods and a small number of UVS cones and finally *Opn4* $^{-/-}$ mice lacking melanopsin in pRGCs.

For the rod and cone models, responses were tested at both at moderate (~100lux, 29.72μW/cm^2) and bright (~600 lux, 178.2μW/cm^2) white light intensities. Neither of the models with the rod degeneration *rd* mutation displayed head tracking responses at any cpd grating under the low or high light stimulus while C3H wildtype thresholds were ~0.5cpd under both moderate and bright light (Figure 5.5). The spatial grating of maximum sensitivity, as determined by average responses per minute, was unchanged for the wildtype though there was a slight trend for lower responses under the bright condition (Figure 5.6). Cone deficient *cl* mice had identical threshold to the non-*rd* wildtype under the moderate light but the acuity threshold was reduced to ~0.4 cpd under bright light (Figure 5.5). As suggested from the threshold reduction, there was an overall trend of decreased sensitivity to all stripe gratings under bright light in the *cl* and a significant decrease in responses/ min at the 0.5 cpd grating under bright light (2-tailed Student's t-test, p=0.0054) (Figure 5.7).

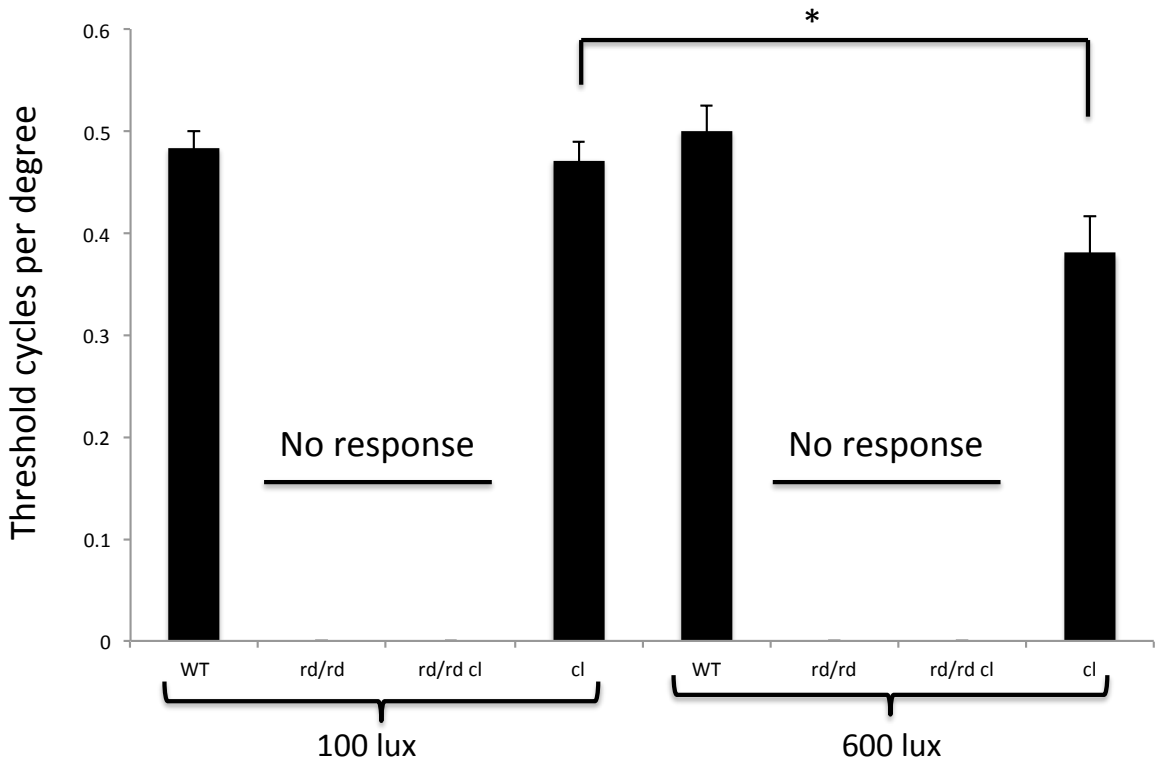

Figure 5.5 Acuity thresholds for models of rod and cone loss under moderate and bright light OKR responses of wildtype, *rd/rd*, *rd/rd cl* and *cl* mice, all n=6, were examined under moderate (~100lux, 29.72μW/cm^2) and bright (~600lux, 178.2μW/cm^2) white light. Every animal had two trials at each light intensity and one trial for a cl-animal under bright light was excluded, as it appeared distressed when placed into the apparatus and did not track at any cpd. The average threshold calculated from individual animal thresholds (lowest cpd at which 2 or greater head-tracking movement were observed/ minute) are represented in the graph along with +/- SEM. No head tracking was observed for *rd/rd* or *rd/rd cl* animals at either light intensity. Wildtype head tracking showed no significant change between the light intensities but *cl* threshold was significantly reduced (2-tailed Student's t-test, $p=0.037$) under bright light. *=$p<0.05$, **=$p<0.01$, ***=$p<0.005$. Bars represent mean values +/- SEM.

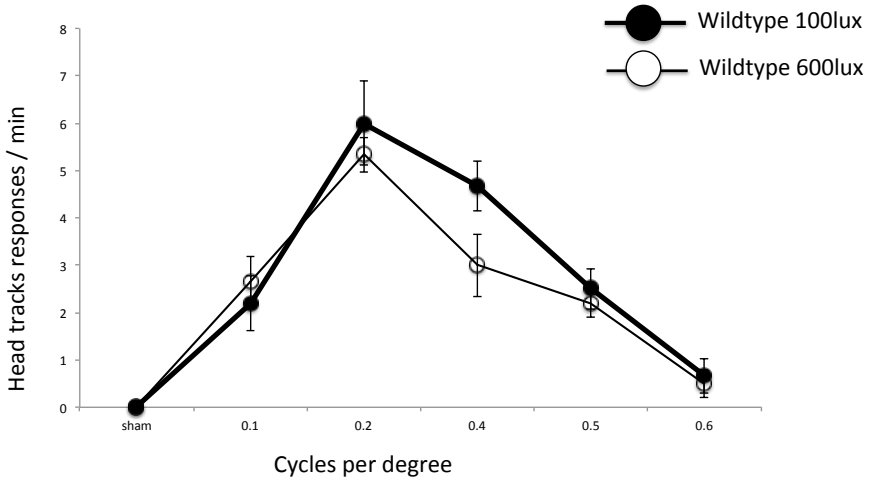

Figure 5.6 OKR responses of wildtype mice under different intensities of white light The OKR responses of wildtype mice (n=6) under ~100lux and ~600lux was unchanged in terms of both cpd of maximal sensitivity (0.2cpd) and threshold (0.5cpd). No significant differences were found for comparisons between light conditions at any spatial gratings.

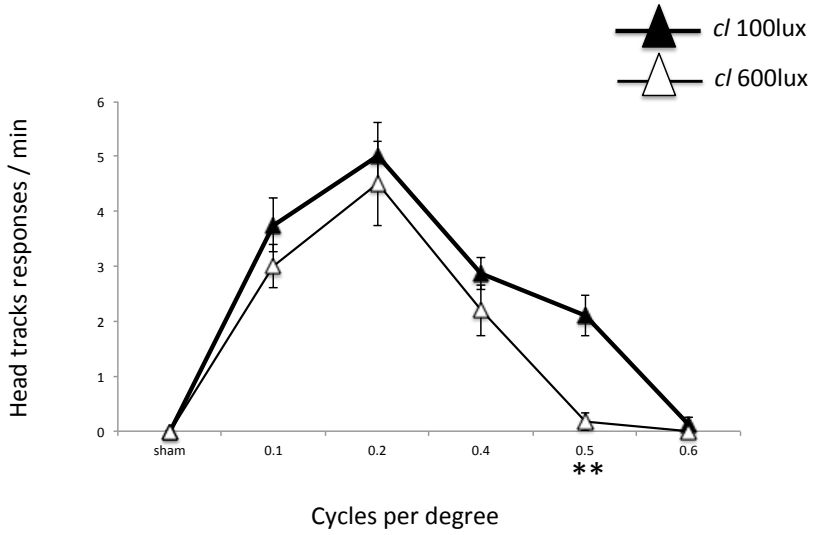

Figure 5.7 OKR responses of *cl* mice under different intensities of white light The OKR responses of *cl* mice (n=6) under ~100lux and ~600lux was unchanged in terms of cpd of maximal sensitivity (0.2cpd) but a reduction in threshold was observed under the brighter light with a significant difference in responses to the 0.5cpd spatial grating (2-tailed Student's t-test, p=0.0054). **=p<0.01

Along with the wildtype C3H mice presented in Figure 5.3, C57BL/6 *Opn4*$^{+/+}$ wildtype mice were also tested along with *Opn4* $^{-/-}$ to look for a melanopsin contribution under 200 lux (59.4μW/cm^2) white light and there was no significant difference between knockout and wildtype animals at any grating cpd (Figure 5.8). The acuity threshold of both genotypes was found to be 0.5cpd. A few animals of both genotype displayed limited responses at 0.6 cpd but the average was less than 2 responses/ min, which was our defined criteria for a positive result at any spatial frenquency. Interestingly, although threshold acuities were the same, we observed maximum response frequencies per minute to be slightly higher (around 2-3 head-tracks per minute) in these mice on the C57BL/6 background than was observed for any of the C3H background mice including the *rd/rd*, *rd/rd cl* and *cl*.

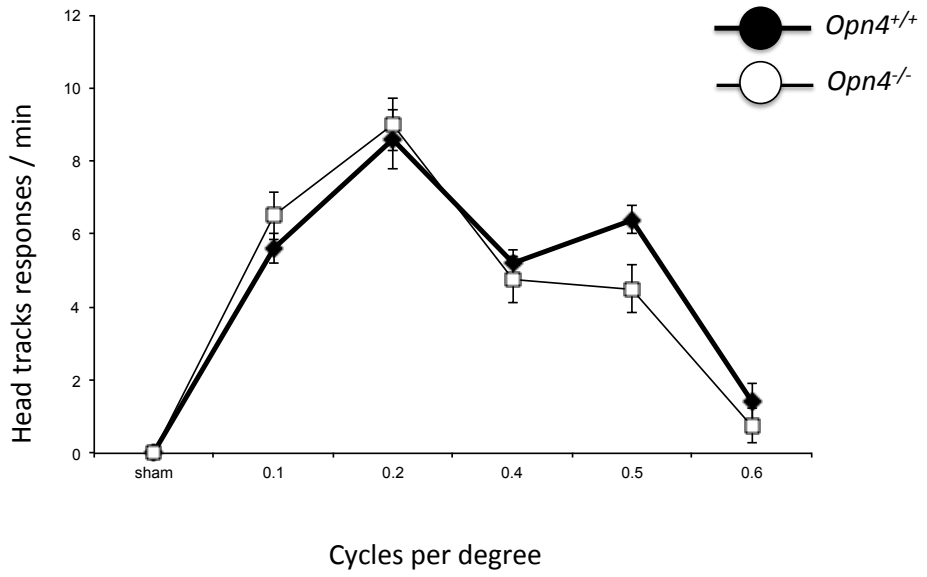

Figure 5.8 OKR responses of Opn4 $^{-/-}$ indicate no role for melanopsin Visual acuity performance of *Opn4* $^{-/-}$ (n=6) and wildtype C57BL/6 mice (n=5) was assessed along with the wildtype C3H mice presented in Figure 5.3 under 200lux white light between 0.1 and 0.6cpd. No difference was found in either threshold (0.5 cpd) or spatial grating of maximal responses (0.2cpd).

5.6 Coneless but not *rd/rd* or *rd/rd cl* show visual tracking under ultraviolet light

As we could not find any previous study of OKR under UV light, wildtype non-*rd*, *rd/rd*, *rd/rd cl* and *cl* mice were tested under 250 lux white (74.3 μW/cm^2) and bright UV light (13.6 log photons/ cm^2/ s, 21.7 μW/cm^2) at the maximally responsive 0.2 cpd stripe grating to assess UV responses in this visual assay. None of the *rd/rd* or *rd/rd cl* mice displayed head tracking responses (data not shown). Non-*rd* wildtype mice responded at similar levels to white and UV light, as did the *cl* mice (Figure 5.9). Neither displayed any head tracking under a dark 'lights off' conditions tested at 0.2 cpd. This confirms that the observed head tracking responses were due to the UV light stimulus rather than any background illumination or infra-red light from the camera.

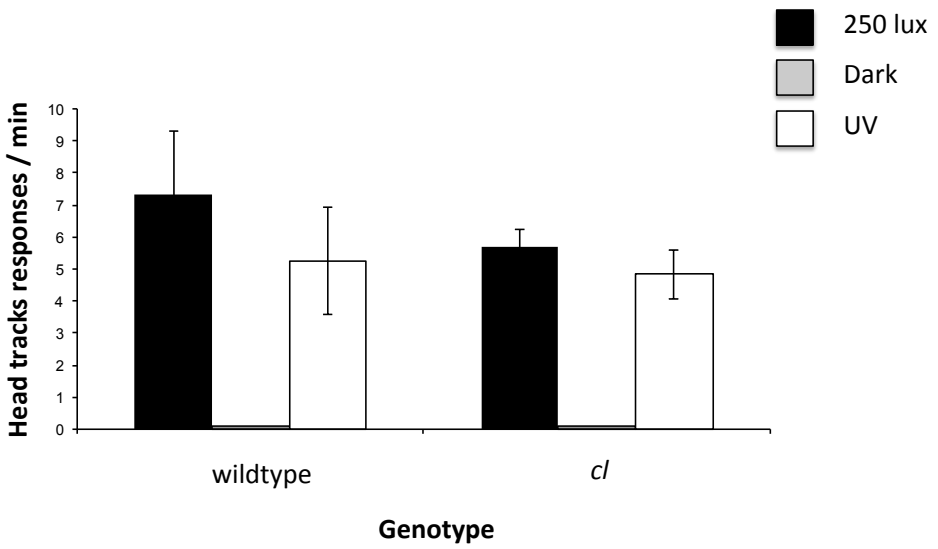

Figure 5.9 Head tracking to ultraviolet light in both *cl* and wildtype mice OKR was assessed at 0.2cpd under 250 lux white (~14.3 log photons/ cm^2/ s, 74.3µW/cm^2) and bright UV light (13.6 log photons/ cm^2/ s, 21.7 µW/cm^2) in *cl* (n=4) and C3H wildtype mice (n=6). Head tracking responses at similar frequencies to white light were observed for UV light in both genotypes at 0.2cpd. A dark control with no illumination was used to assess if background room illumination or other influences such as infra-red light from near infrared (NIR) video camera was sufficient to allow head-tracking. There were no significant differences in responses either between white and UV light or between genotypes. No responses were observed under the dark condition at 0.2cpd, the grating to which wildtype mice have displayed the greatest frequency of response. Bars represent mean values +/- SEM.

5.7 Novel object recognition is able to assess outer retinal degeneration

A visuospatial adaptation of the one-trial spontaneous novel object recognition (NOR) task was assessed using 9 retinal degenerate *rd/rd cl* and 8 wildtype C3H non-*rd* control mice. The experiment used an arena where star and checked patterns on two of the walls allowed visual discrimination of the four corners of the cube as distinct areas. A mouse was placed in

the arena with identical objects in two of the four corners and allowed to freely explore for a 10-minute sample phase (See Figure 5.10 for pictures of the test arena during the sample and test phases). After a 5-minute delay, the mouse was placed back into the arena where one of the objects had been moved to an adjacent corner and its movements recorded during a 3-minute test phase (Figure 5.10). This video was then analyzed and the recognition performance for each animal was calculated as the ratio of time spent with the object in the familiar (f) versus the new (n) location given by the ratio: n/(n+f). If this ratio was greater than 0.5 then the animal had demonstrated increased interaction with the new object and the higher above 0.5 the stronger the visuospatial recognition performance. As the objects were identical with regards to tactile and olfactory stimuli (being carefully cleaned between sample and test phases), the visual cues on the walls of the arena were the only ones available to the animal to distinguish the object as being in a new location and therefore to result in increased interaction. As long as the animals are forced to rely on the visual cues, recognition of the movement of one of the identical objects was hypothesized to be possible only for the wildtype animals as the *rd/rd cl* mice, lacking the classical visual photoreceptors, should be unable to use the visual stimuli.

Different batches of animals were used in 2 trials under 200lux (62.2 $\mu W/cm^2$) white light and the mean time spent with the moved or stationary object during the test phase was averaged for each animal. The wildtype C3H non-*rd* spent significantly more time exploring the object in the new context during the test phase, resulting in a recognition ratio of 0.7804 with a SEM +/- 0.053 that was significantly above chance (2-tailed 1-sample, p=0.010) while the *rd/rd cl* did not perform differently from the chance level of 0.5 (2-tailed 1-sample

t-test, p=0.086) with a recognition ratio of 0.4306, SEM +/- 0.063 (Figure 5.11). A significant difference in performance was found between genotypes (genotype by batch ANOVA, $F_{1,15}$, p=0.002)

Sample Phase

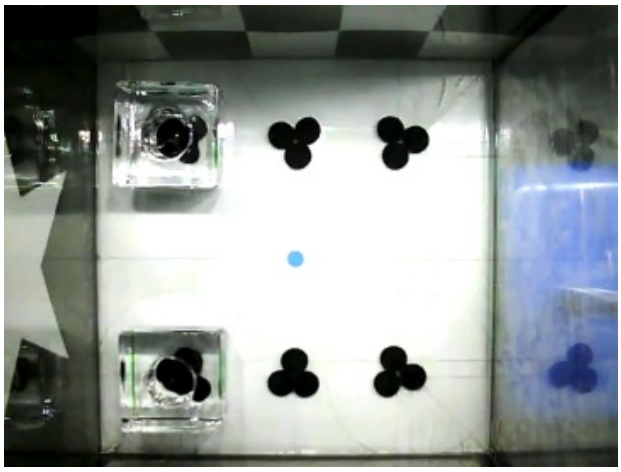

Test Phase

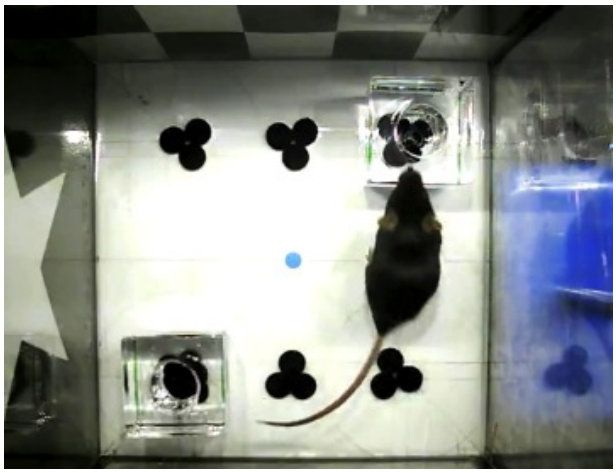

Figure 5.10 NOR test arena showing position of object replicates in sample and test phases during the visuospatial task

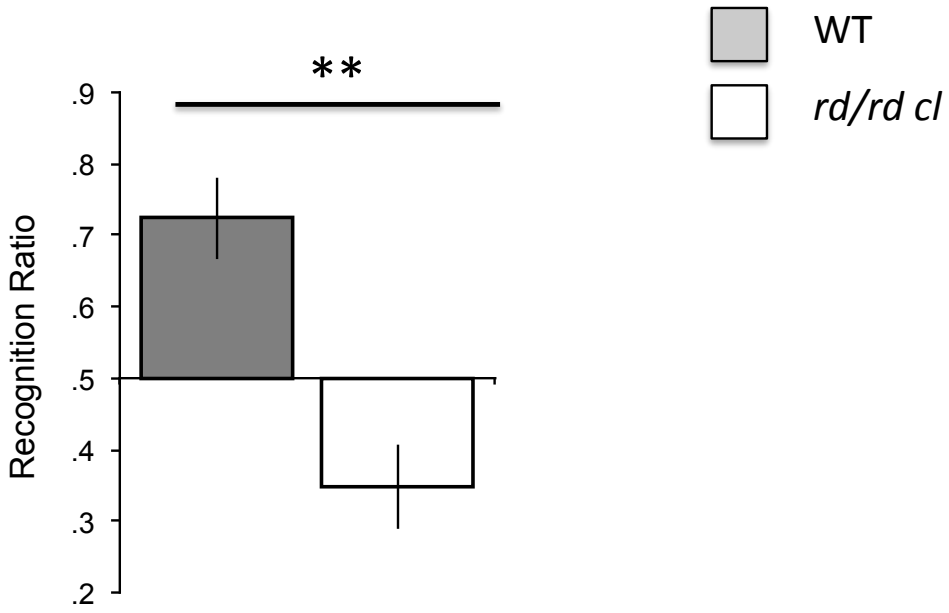

Figure 5.11 Visuospatial Object Recognition trial with *rd/rd cl* and wildtype mice Recognition performance of wildtype non-*rd* (n=9 in batches 1 and 2) and *rd/rd cl* (n=8 in batches 1 and 2) mice was examined in a visuospatial adaptation of the novel object recognition task. WT animals were found to perform significantly above chance level of 0.5 (2-tailed 1-sample t-test p=0.010) while the *rd/rd cl* did not (2-tailed Students's t-test, p=0.086). ANOVA analysis found a significant difference between genotypes performance (genotype by batch ANOVA $F_{1,15}$, p=0.002). *=p<0.05, **=p<0.01, ***=p<0.005. Bars represent mean values +/- SEM.

There was no difference in the overall amount of exploratory behavior between the genotypes during the sample or test phase thus the observed effect was not due to increased sampling behavior in the wildtype mice (Table 5.1).

Table 5.1 Analysis of overall exploratory behavior during sample and test phases for *rd/rd* cl and Wildtype non-*rd* controls in visuospatial NOR task

Mean total object exploration (and standard error of mean) during sample phases

Genotype Comparison	**White Light**
	Visuospatial
WT	241.99 s (25.67 s)
rd/rd cl	223.06 s (20.73 s)
p=	0.074

Mean total object exploration (and standard error of mean) during test phases

Genotype Comparison	**White Light**
	Visuospatial
WT	11.90 s (1.62 s)
rd/rd cl	15.99 s (1.65 s)
p=	0.358

Discussion

5.8 The OKR drum assay produces threshold values consistent with previous studies

The OKR drum used in these studies was found to produce results consistent with published data, but we also found limitations of a simple drum set-up. The threshold of acuity measured for wildtype mice using our system was about 0.5 cpd for both C3H and C57BL/6 strains, which is slightly higher than the 0.3-0.4 found by Schmucker et al. (2005), who used an automated whole body analysis of C57BL/6 in a mechanical rotating drum, as well as the ~0.4cpd found by both Prusky et al. (2004) and Pinto et al. (2007) for C57BL/6 mice using a virtual drum system (Pinto et al., 2007; Prusky et al., 2004; Schmucker et al., 2005). The response sensitivity (as determine by responses/ min) peaked at a spatial frequency of 0.2 cpd then decreased toward the threshold acuity which closely matches the 0.1-0.2 cpd peak found previously (Schmucker et al., 2005).

The reason for the slightly higher acuity threshold found using our OKR set-up is likely due to the ability of mice to freely roam the central platform of our rotating drum during experiments. We did not use any method of restraint for the mouse, relying on the height of the central platform to keep the animal in place. This was intended to make the procedure less stressful for the animal and avoid any filtering effect on the spectrum of light (of concern for the later UV experiments) that would be caused by a clear perspex cylinder such

as was used to restrain mice in other OKR systems. However, as the grating cpd is set to the center of the drum, movement of the mouse to the edge of the platform would increase its viewing angle. This would have the effect of reducing the spatial frequency, resulting in tracking to a slightly higher cpd then the true threshold. This effect was previously found for a small drum set-up where the mouse could move on a central platform (Schmucker et al., 2005). Differences in measured acuity are also tied to the light level in a given experiment as acuity has been found to increase with irradiance (Schmucker et al., 2005; Umino et al., 2008) and acuity values of up to ~0.6 cpd have been found under very bright irradiance (Umino et al., 2008). Despite this slightly higher spatial threshold, our mechanical drum and method of manual assessment of video recordings allowed for consistent repeatable threshold assessment.

5.9 The mechanical drum OKR assay appears to be primarily rod-driven

Given the previous conflicting conclusions concerning the relative contributions of rods and cones to OKR, we examined the responses of retinally degenerate mice lacking all rods and cones (*rd/rd cl*) and those with only a small population of cones remaining (*rd/rd*). We also examined responses of *cl* mice with rods but lacking virtually all MWS cones. There is agreement in the existing literature that rods drive responses at low light levels while there is inconsistency concerning the importance of cones (Altimus et al., 2010; Schmucker et al., 2005; Umino et al., 2008). Given that our interest is particularly in using the OKR to examine UV vision and UVS cones, we examined the responses of our mice at ~100 lux and ~600 lux, in the photopic range where any cone response should be evident.

Interestingly, our results indicated that rods were the primary photoreceptor responsible for the OKR response in photopic irradiances. Neither of our retinally degenerate mice, *rd/rd cl* and *rd/rd,* displayed head tracking responses to any spatial frequency. Previous studies have found *rd/rd* mice lack any OKR in a similar drum assay to ours (Thaung et al., 2002) and our result indicates that, although the remaining cones in the *rd/rd* were able to drive phase-shifting response to UV light, they were not sufficient to drive OKR. The response of the *cl* is more interesting as we found only a very modest change in threshold between the light intensities and overall performance similar to wildtype despite almost complete loss of MWS cones, the cone type most sensitive to white light stimulus. This supported the results of Schmucker et al. (2005) that rods are responsible for driving the OKR response even into photopic intensities above 400lux (Schmucker et al., 2005). Rods have been found to signal through the cone-pathway at mesopic light intensities (Sharpe and Stockman, 1999; Smith et al., 1986) and it may be rods are able to continue to signal through cones to contribute to brighter conditions than was considered possible for the primary rod pathway. It has been suggested that the reason cones seem unable to play a major role in OKR in mice is that as they represent less than 3% of the total photoreceptors in the mouse retina (Jeon et al., 1998) and are not organized into a fovea or other concentrated central area (*area centralis*) seen in other mammalian species. It was therefore concluded that the cones were not present in a sufficient density in the mouse to be useful in spatial vision (Schaeffel, 2008).

However, it is also worth noting that the study by Schmucker et al. (2005) and our results which concluded that cones make very limited contribution to OKR, both used a mechanical

drum while two studies with a virtual OKR set-up have found significant OKR deficits in cone mutants under photopic light conditions (Altimus et al., 2010; Umino et al., 2008). It is therefore possible that the fine control of spatial frequencies and contrast provided by the virtual set-up are necessary to detect cone responses and/ or that computer screens used for the virtual drum provide a better stimulus display for cones responses compared to the grating prints used in mechanical drums.

Under bright ultraviolet light, again neither of the retinal degeneration models (*rd/rd* and *rd/rd cl*) showed any tracking responses when tested with the spatial frequency we found elicited the greatest responses in wildtype mice. However, both wildtype and *cl* mice with rods and a number of residual UVS cones demonstrated UV responses comparable to white light tracking at 250 lux. The observation that head tracking is similar between the UV and white light condition is interesting considering there is a clear difference in irradiance between the white light (74.3 $\mu W/cm^2$) and UV light (21.7 $\mu W/cm^2$), though care must be taken in comparing mono-chromatic to white light stimuli. Indeed, rather than the OKR sensitivity to these two types and levels of light happening to be equal, the similar result likely reflects a limiting factor on response rates inherent our assay, perhaps due to the tendency of mice to explore the platform instead of watching the gratings, which prevents finer resolution. This may explain why we did not observe an increase in performance with increasing irradiance as has been observed in other studies (Schmucker et al., 2005) or it may simply be that the range of our white light intensities was not sufficient to observe such a change. Thus, while our OKR drum is able to determine the presence or absence of acuity for a given cpd, it is likely not the best method to assess finer points of spatial response rates.

5.10 The Novel Object Recognition Test represents an effective test of visual stimuli

To test the visual-dependence of the recognition responses in our adaptation of the NOR task we examined the responses of visually blind mice with total outer-retinal degeneration and our results suggest that this assay represents an effective test of image-forming pathways in mice. Visuospatial recognition performance by wildtype but not retinal degenerate *rd/rd cl* mice was not due to differences in exploratory behavior or stimulus sampling as time spent interacting with objects was comparable between the genotypes. Further experiments by Eric Tam in our lab demonstrated that *rd/rd cl* were able to demonstrate successful recognition performance comparable to wildtype when the stimuli could be distinguished by tactile or odour cues, giving further support that the visuospatial adaptation of this test assesses image forming system function (Tam et al., 2014, manuscript in preparation). As reported in this manuscript, visuospatial recognition performance was also found to be unaffected by melanopsin knockout.

5.11 Conclusions

The OKR assay was found to give consistent threshold responses for wildtype mice that are comparable to previous OKR acuity studies while responses to UV light indicate that this test can be used to examine responses in a UVS opsin mutant. The visual adaptation of the NOR task was also found to depend on outer-retinal function and represents a novel method

of assessing more integrated vision-dependent behavior in mice. This technique is also used to assess the UVS opsin knockout model characterized in Chapter 6.

Chapter 6: **Characterisation of a novel UV cone knockout**

Introduction

6.1 Aims

UVS opsin expression in mouse cones allows for a high degree of UV sensitivity and has been shown to contribute to vision (Jacobs et al., 1991). Previous studies and data presented in this thesis (Chapter 4) suggest UVS cones also make an important contribution to circadian responses to UV light. To further the investigation into the role of UV sensitivity in both image and non-image forming visual pathways in the mouse, we recovered a novel *Opn1sw* (UVS) complete gene knockout (KO) mouse model from an ES cell line. In this chapter we aim to confirm the loss of UVS expression in this *Opn1sw* complete gene KO and characterize the normal function of the non-image forming system to white light.

6.2 Data from previous *Opn1sw* targeted mutants

A significant challenge in determining the specific contributions of photoreceptors is separating the absorption spectra of individual photopigments. In the mouse, overlapping absorption specta of melanopsin, rod and MWS cone opsins mean that even monochromatic light pulses will not target individual photoreceptor responses. Recent advances in genetic manipulation techniques have allowed both for targeted knock-in models and knock-out models of different opsins, as demonstrated by Smallwoood et al. (2003) who replaced the mouse 'green' cone opsin with the human long-wavelength 'red' cone opsin (Smallwood et

al., 2003). With maximal sensitivity at longer wavelengths, this construct separated the cone responses and allowed for more detailed analysis of cone contribution to visual systems and behaviors (Allen et al., 2011; Jacobs et al., 2007).

The mouse also contains a UVS opsin maximally sensitive to 360nm UV wavelengths (Jacobs et al., 1991) and, although its absorbance is farther from the other mouse photopigments, questions remain about which of the UV sensitive behaviors are driven by the UVS cone, as opposed to the extension of the sensitivity of rod or melanopsin photopigments into the UV. A UVS (or S-opsin) knockout would provide significant insight. There are two previous studies involving models of S-opsin knockout/ disruption, with one of these being published as this thesis was being written.

The model of Daniele et al. (2011) inserted a neomycin resistance gene between exons 3 and 4 of the mouse *Opn1sw* gene to disrupt transcription of the S-opsin (see Figure 6.1 for illustration of the *Opn1sw* gene in this model). This resulted in a severe reduction in *Opn1sw* transcription and western blotting could not detect any OPN1SW protein (Daniele et al., 2011). In this study it was noted that, based on the analysis of tissue from mice 1.5 to 8 months of age, the hypomorphic UVS S-opsin allele resulted in elevated MWS m-opsin protein levels by an average of 1.6 fold, though there was no observed change in *Opn1mw* mRNA. This increase appeared to be especially pronounced in the ventral retina, given observed light-evoked changes in membrane current following light flashes. There was no change in the expression of rhodopsin however, indicating that there was not a global increase in opsins levels in the *Opn1sw*$^{Neo/Neo}$ animals. The kinetics of individual cone light

responses were found to be normal as was cone density across the *Opn1sw*$^{Neo/Neo}$ retina. However, while cones in the dorsal and middle retina exhibited normal morphology, cones in the ventral retina were often found to have abnormal outer-segments. Outer-segments in these ventral cones were less substantial with mis-aligned discs and sometimes outer-segments were found to completely absent in the far-ventral retina. Inner segments, cell bodies and axons were normal across the retina.

Recently, a second mouse model of *Opn1sw* knockout was published by Greenwald et al. (2014) in which complete deletion of exons 2, 3 and 4 of the *Opn1sw* gene was combined with targeted replacement of *Opn1mw* gene with a human long-wavelength opsin (Greenwald et al., 2014) (see Figure 6.1 for illustration of the *Opn1sw* gene in this model). Immunohistochemical analysis of retinal sections indicated a complete loss of s-opsin expression in the *Opn1sw* knockout mice. ERG responses of 3-month-old animals given light targeted to stimulate the s-opsin were absent in the *Opn1sw* knockout. It was also noted that light targeted to m-opsin showed increased sensitivity at lower light levels in the knockout animals while responses at higher light intensities were similar to wildtype. ERGs collected over 16 months also indicated a much greater age-dependent decrease in m-opsin sensitivity associated with the *Opn1sw* knockout. Interestingly, this effect was rescued in animals in which the *Opn1sw* knockout was combined with the replacement of the m-opsin with the human LWS opsin. qRT-PCR of ventral retinal tissue from 12 month old mice found 44% lower m-opsin expression in the UVS knockouts and staining sections from 16 month old mice found a reduction of m-opsin in both *Opn1sw* knockout lines, particularly in the ventral retina. Again the LWS opsin knock-in appeared to rescue the m-opsin loss to an

extent. Counts of outer segments in the retinas of the 16-month-old mice found that, while there were no differences in dorsal retina counts, there were major reductions in the number of cone outer-segments in the ventral retina of both strains of *Opn1sw* knockout mice (with and without LWS opsin replacement).

Summary Aims

Here we characterize the opsin expression and white light NIF responses of a novel *Opn1sw* KO model containing a complete knockout of the coding region of the *Opn1sw* gene and relate our results to previous *Opn1sw* models. With this model we intend to examine the visual system UV sensitivity in mice so identifying any unexpected effects of the *Opn1sw* mutation is vital for correct interpretation of results in further experiments.

Results

6.3 Generation of *Opn1sw* knockout

A transgenic *Opn1sw* gene knockout was generated using ES cell material from the Knockout Mouse Project (KOMP) with help from Dr. Ben Davies and The Wellcome Trust Center for Human Genetics (University of Oxford) who generated chimeric animals that contained a targeted deletion of all coding material of the mouse *Opn1sw* gene on Chromosome 6 (exons 1-5) achieved through homologous recombination with a target vector (See Methods Chapter 2 for a full description of construct and deleted sequence). Mice were healthy with no overt phenotype and were maintained as het/het breeding pairs so *Opn1sw* wildtype (WT) used were littermate controls. Figure 6.1 shows a representation of the deletion in the *Opn1sw* gene of this model compared to the previous *Opn1sw* models discussed in the introduction.

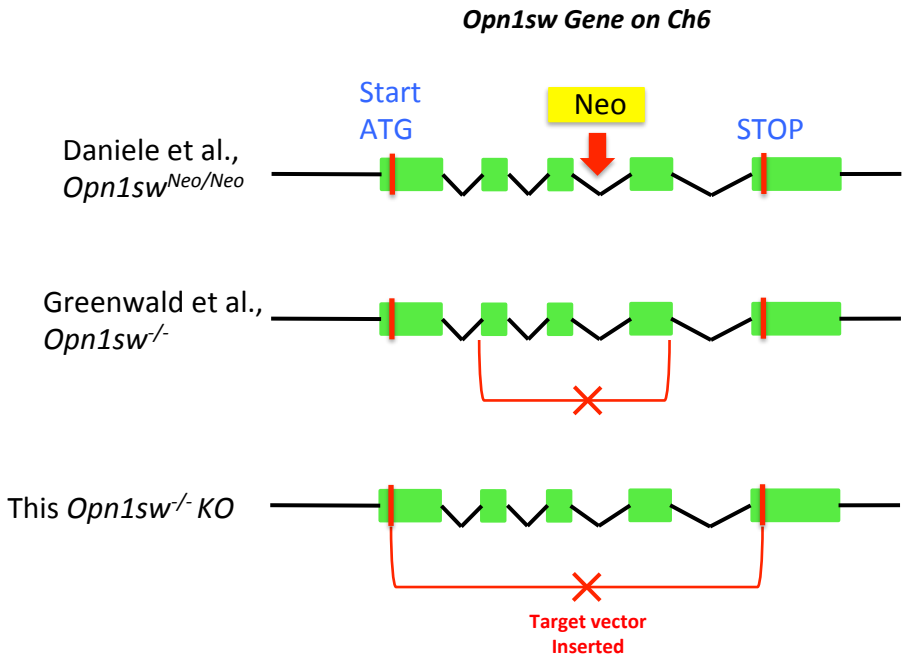

Figure 6.1 Schematic of the mouse *Opn1sw* gene on chromosome 6 consisting of 5 exons. The deletion in our *Opn1sw* KO model is compared to the changes to the *Opn1sw* gene in the previous models of (Daniele et al., 2011) and (Greenwald et al., 2014) discussed in the introduction to this chapter.

6.4 PCR quantification of opsin expression in *Opn1sw* KO

To determine the change in opsin gene transcription in the KO, heterozygous (het) and WT, quantitative real-time PCR (qRT-PCR) was performed on total RNA extracted from manually homogenized whole-eyes. At the time of collection, the ages of the mice were all between 6 and 10 months of age and eyes were collected between ZT3 and 5. For comparison, mean ages for each genotype were KO, 8.2 months, WT, 7.5 months and het, 7.3 months with Student's t-tests finding no difference in mean ages (2-tailed Student's t-test comparisons, in all cases $p>0.6$). The messenger RNA levels were compared for all opsins in the mouse retina including *Rho* (Rhodopsin), *Opn1mw* or M-opsin (MWS cone opsin),

Opn1sw or S-opsin (UVS cone opsin) and *Opn4* (melanopsin). Expression levels were normalized to the geometric mean expression of three housekeeping genes: *Gapdh* (Glyceraldehyde 3-phosphate dehydrogenase), *B2M* (β_2 Microglobulin) and *ARP* (acidic ribosomal protein). Comparison of normalized expression revealed UVS opsin mRNA was reduced over 8000 fold in the KO eye representing a highly significant reduction (2-tailed Student's t-test p= 0.000542) (Figure 6.2). In the het eyes, UVS expression levels were significantly reduced (2-tailed Student's t-test p= 0.030) to around half of wildtype expression. There were no significant differences in the expression of *Rho*, MWS or *Opn4* between the genotypes, although there was a noted reduction in KO MWS opsin (2-tailed Student's t-test p= 0.169) to 69.1% +/- 12.4% of wildtype expression.

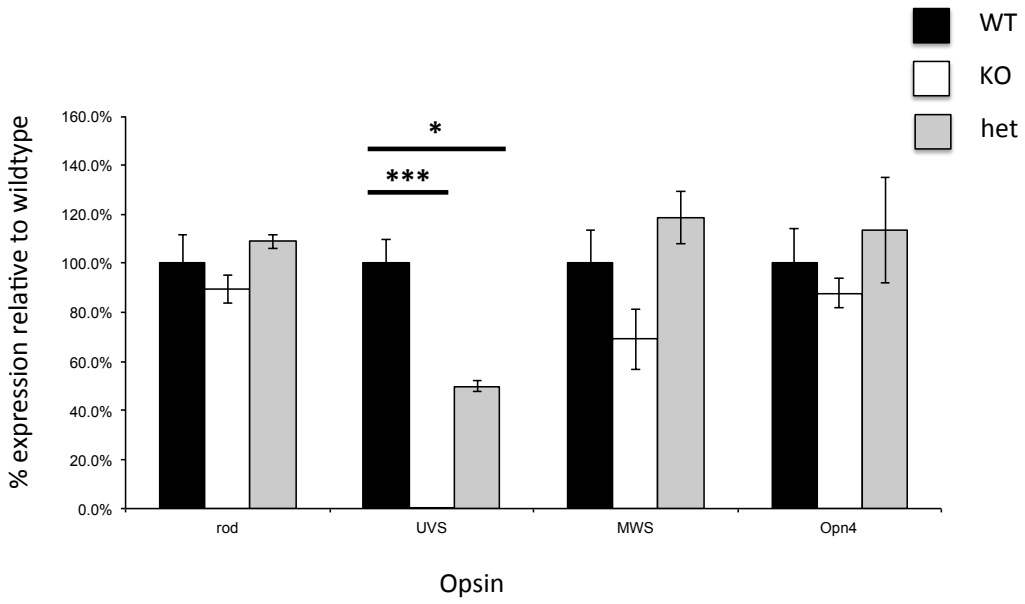

Figure 6.2 Real-Time PCR quantification of opsin levels in Opn1sw transgenic mice RNA was extracted from whole eyes of *Opn1sw* KO, WT and het animals between 6 and 10 months of age. Opsin expression of Rhodospin, Melanopsin, MWS and UVS was compared against the geometric mean of 3 housekeeping genes (*Gapdh*, *B2M* and *ARP*). Relative to WT, there was a significant reduction in mRNA of UVS to 0.012% (2-

tailed Student's t-test p= 0.000542) and 49.9% in the het (2-tailed Student's t-test p= 0.030). Note that UVS expression is plotted in the above for each genotype but is too low to appear on the given scale in the KO. Full primer sequences in Methods Chapter 2, n=3 for each genotype. *=p<0.05, **=p<0.01, ***=p<0.005. Bars represent mean values +/- SEM.

6.5 UVS staining is absent in the retina of *Opn1sw* KO mice

We examined retinal sections from ~5-6-month-old wildtype and *Opn1sw* KO mice to confirm loss of UVS opsin protein from the *Opn1sw* KO and look for any other retinal effects of the deletion. Figure 6.3 shows mid-retinal sections stained with nuclear DAPI stain as well as antibodies against both UVS and MWS cone opsins. We found that, while retinal histology appeared normal (all retinal layers observed, no obvious disruptions or differences in KO compared to WT sections), no UVS staining was observed in any of the KO sections while MWS staining was normal. Quantification of specific cell-type densities was not preformed and, particularly in the case of cone photoreceptors as will be mentioned later in this chapter, this is an area for future work with this model. Whole-mount retinas stained for UVS opsin found a strong dorsal-ventral expression gradient in both *Opn1sw* wildtype and het animals while a complete lack of UVS opsin was again observed across the retina of KO mice (Figure 6.4). Finally, to confirm that normal cone morphology was maintained in knockout mice we stained retinal sections for β-galactosidase (β-gal), which is the protein product of the *Lac-Z* reporter gene in the target construct that replaced the *Opn1sw* gene. β-gal expression followed the dorsal-ventral gradient expected for UVS opsin (see whole mount images in Chapter 8) and was also used to confirm that s-cones in the dorsal retina are still present despite the loss of UVS opsin and do not contain compensatory MWS

expression (Figure 6.5). Figure 6.6 shows β-gal staining throughout cones of the mid-ventral retina of the *Opn1sw* KO and the cone structure appears intact.

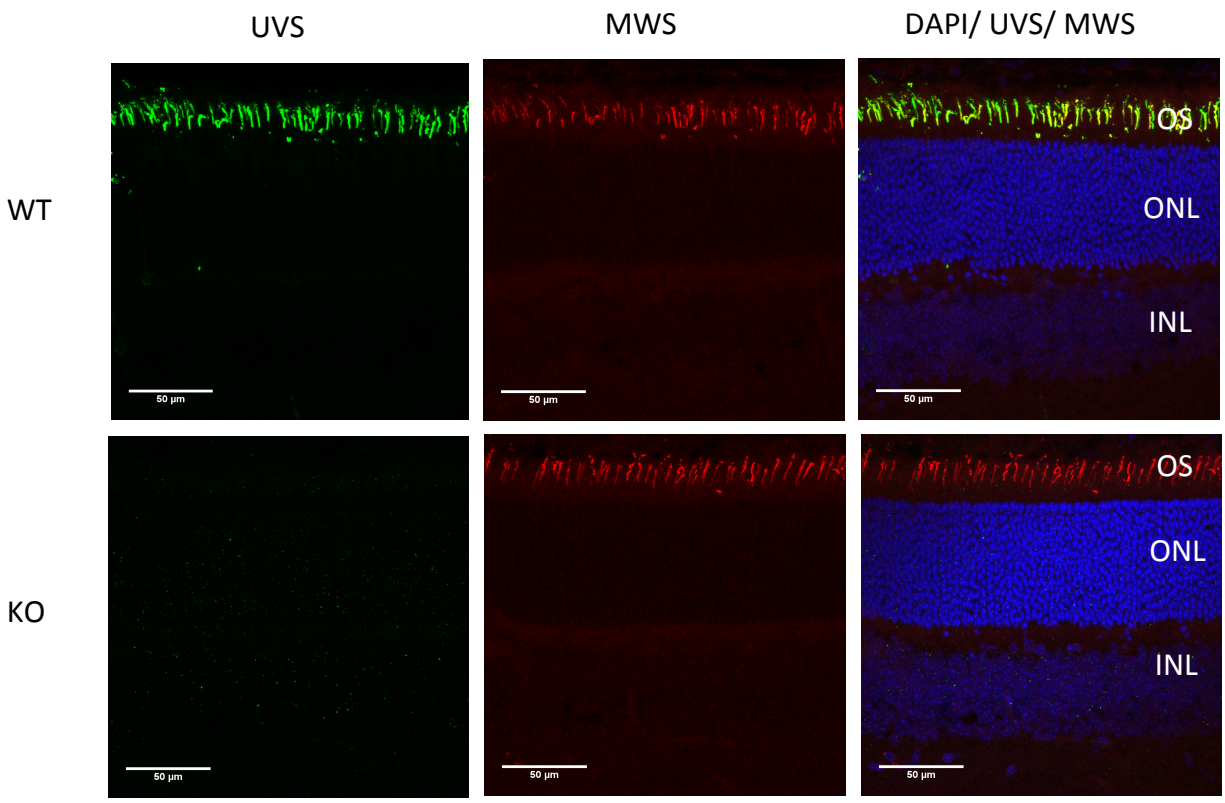

Figure 6.3 Immunostaining of *Opn1sw* KO and WT retinal sections *Opn1sw* KO and WT retinas were sectioned and stained with UVS (green) and MWS (red) antibodies to examine expression in ~6-month old animals. OS-outer segments, ONL-outer nuclear layer, INL-inner nuclear layer. Blue nuclear stain is DAPI. Scale bars=50µm.

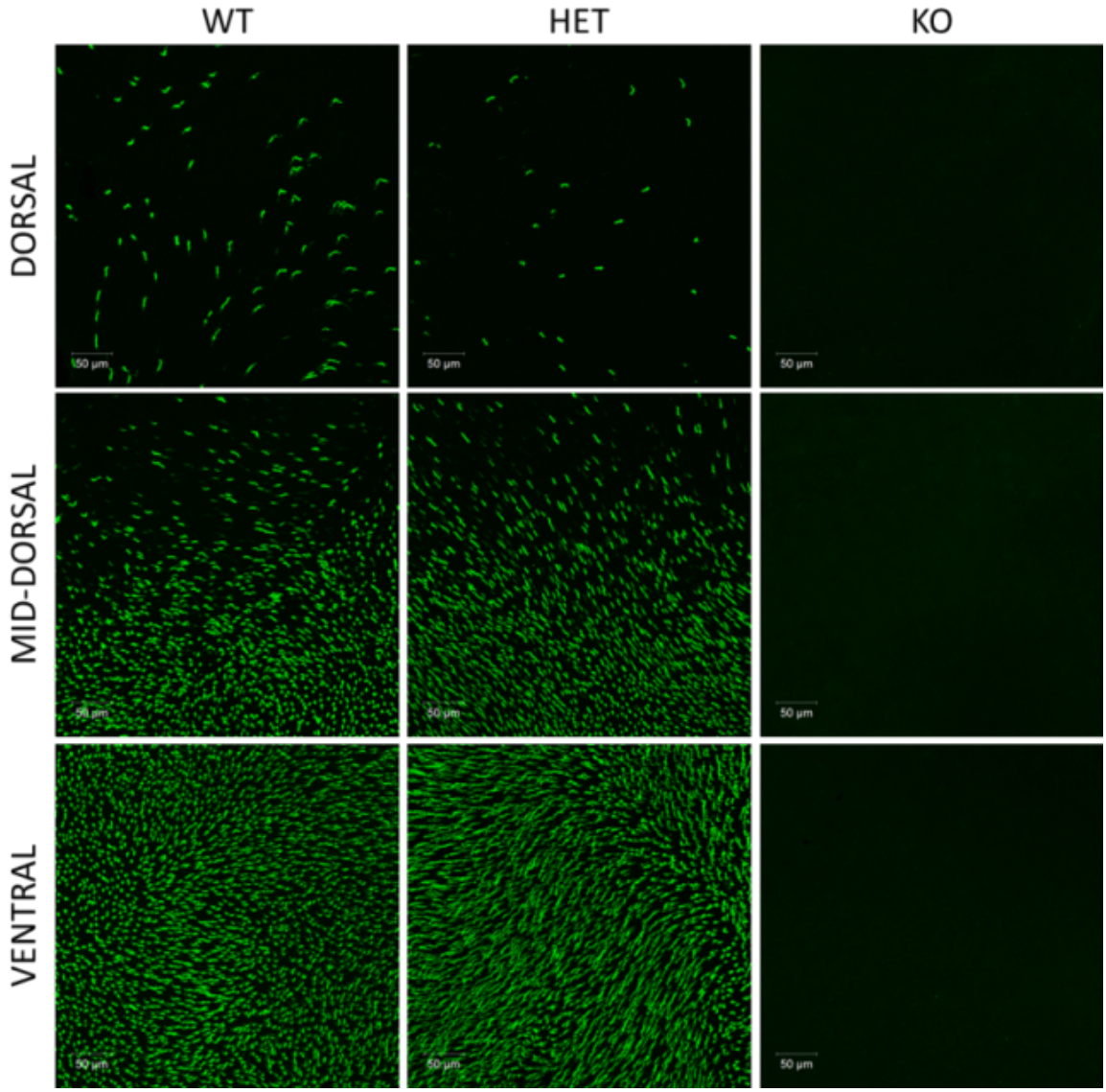

Figure 6.4 Opsin expression in *Opn1sw* KO whole-mounted retinas Retinal whole-mounts from *Opn1sw* KO, WT and heterozygous animals were stained for UVS opsin (green). While the gradient in het animals closely resembled the expected dorsal-ventral gradient seen in the WT (Szél et al., 1996), no UVS opsin was detected in the KO retina. Scale bars=50µm.

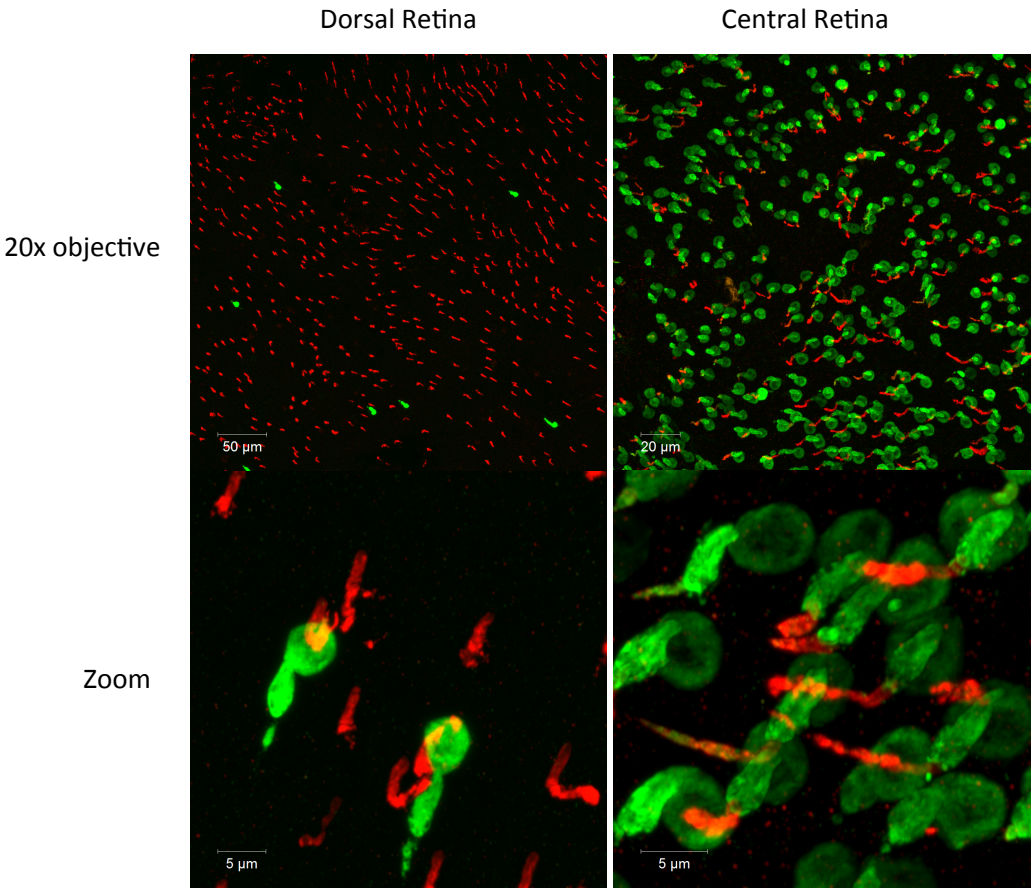

Figure 6.5 β-gal and MWS expression in retina of *Opn1sw* KO confirms S-cones still present Retina of *Opn1sw* KO stained for MWS (red) and β-gal (green) (LacZ reporter in target cassette inserted in place of the *Opn1sw* gene, see Methods Chapter 2 for full details). Dorsal retina sections show expected high level of MWS staining in outer-segments of m-cones with only a few isolated cones expressing β-gal. Magnified image of dorsal retina shows that the β-gal-expressing cones are s-cones that have no MWS expression in outer segments. No m-cones co-expressing β-gal and MWS opsin were observed in the dorsal retina. In the central retina, β-gal expression is seen throughout m-cones, as indicated by MWS expression in outer-segments of β-gal-expressing cones. Retina were collected from ~5 month old KO mice. Scale bar top left image=50µm, top right =20µm, bottom row images scale bars=5µm.

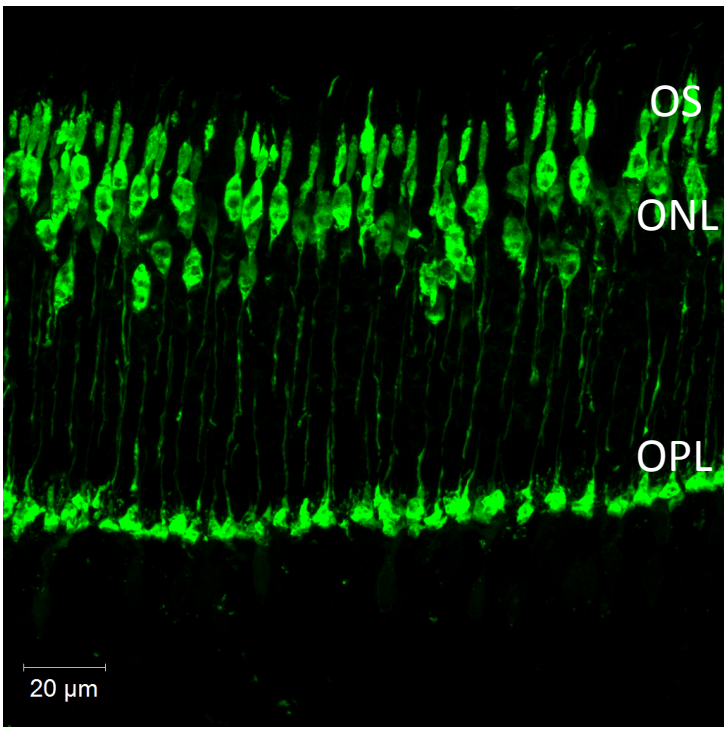

Figure 6.6 Cone morphology in ventral cones of *Opn1sw* KO Expression of β-gal is due to *LacZ* reporter in target cassette inserted in place of the *Opn1sw* gene (See Methods Chapter 2 for full details) and β-gal staining (green) is found throughout UVS expressing cones as seen here in middle of the ventral retina. Retinal position was determined using β-gal gradient, which follows UVS gradient as shown in Chapter 8, and the presence of the optic nerve in sections through the eye. In these cones that normally express a majority of UVS opsin, structure appears intact, including outer-segments, despite lack of UVS. Sections were from the retina of a ~5 month old KO animal. Scale bar=20µm.

6.6 Non-image forming screen of *Opn1sw* animals under visible light

Given that the qRT-PCR and immunohistochemical analysis indicated no significant abnormalities other than the absence of UVS opsin in the *Opn1sw* KO mice, we expected basic visual and non-visual system functions of the KO would be indistinguishable from WT under white light as these functions rely on input from a combination of rhodopsin,

melanopsin and MWS opsin with little input expected from the UVS opsin. Two functional tests were conducted: circadian screen and pupillometry.

Circadian Screen

To test entrainment clock function, we completed an entrainment screen that compared wheel-running behavior of the *Opn1sw* KO and WT and tested a number of key circadian parameters under 100lux (31.1 μW/cm^2, 13.9 log photons/cm^2/s) white light. Figure 6.7 gives an example of a double-plotted actogram outlining the light schedule used in the circadian screen. No difference was found between *Opn1sw* WT and KO mice in any of the tested parameters as outlined in Table 6.1. To highlight some of the most important comparisons, average free-running period length (Tau) shown in Figure 6.8 was 23.55 hr in the KO and 23.57hr in the WT (2-tailed Student's t-test p=0.861). Days taken to re-entrain to a six-hour phase advance (Figure 6.9) and length of phase shift to a one-hour light pulse at CT16-CT17 (Figure 6.10) were also not found to differ with p-values of 0.183 and 0.634 respectively.

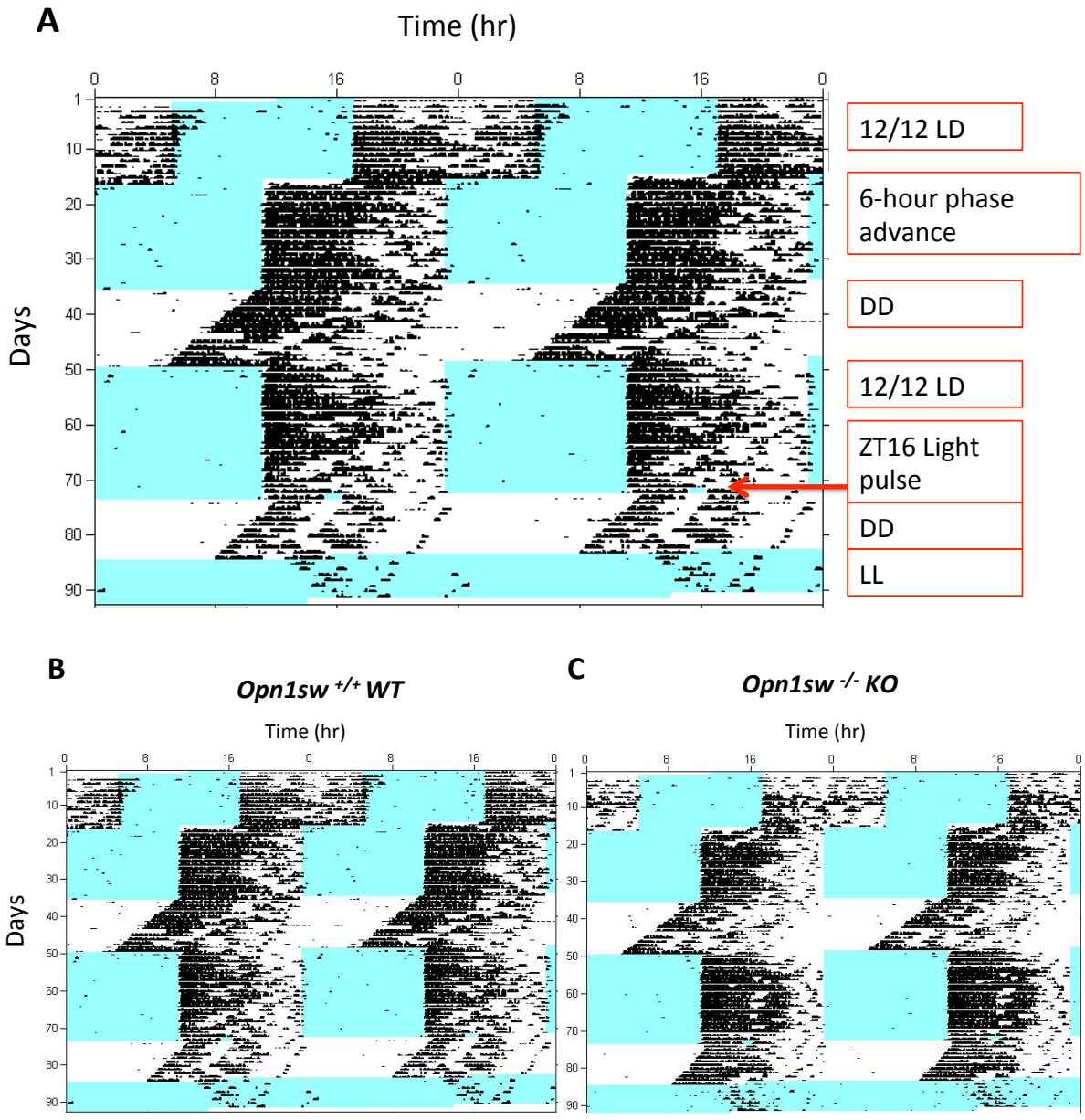

Figure 6.7 Circadian screening protocol (A) Double-plotted actogram showing circadian screening protocol to examine key measures of locomotor clock function under 100lux white light. Un-labeled representative actograms are shown for **(B)** *Opn1sw* $^{+/+}$ WT and **(C)** *Opn1sw* $^{-/-}$ KO.

.

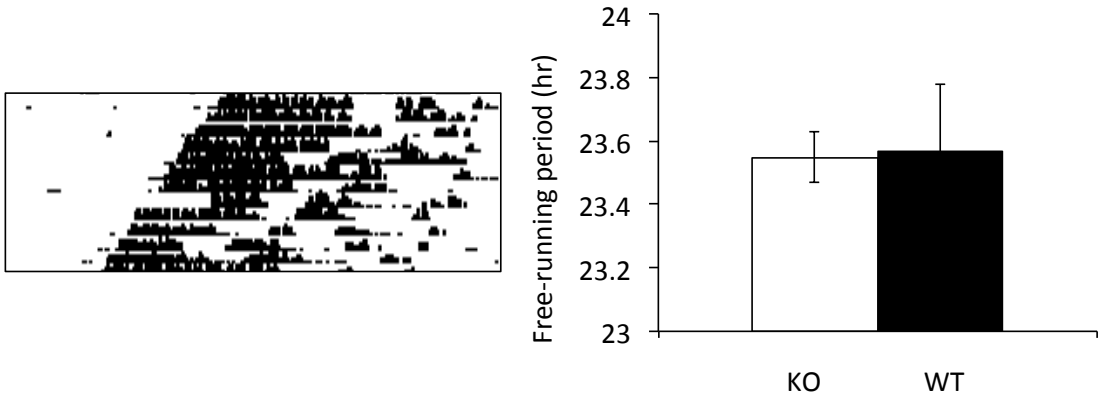

Figure 6.8 Free-running period length (tau) in *Opn1sw* KO and WT animals Free-running period was determined from the first DD portion of the circadian screen (left above shows example of protocol taken from *Opn1sw* WT actogram). There was no difference in free-running period length between *Opn1sw* KO and WT mice (2-tailed Student's t-test p=0.861), n=6 for both genotypes. Bars represent mean values +/- SEM.

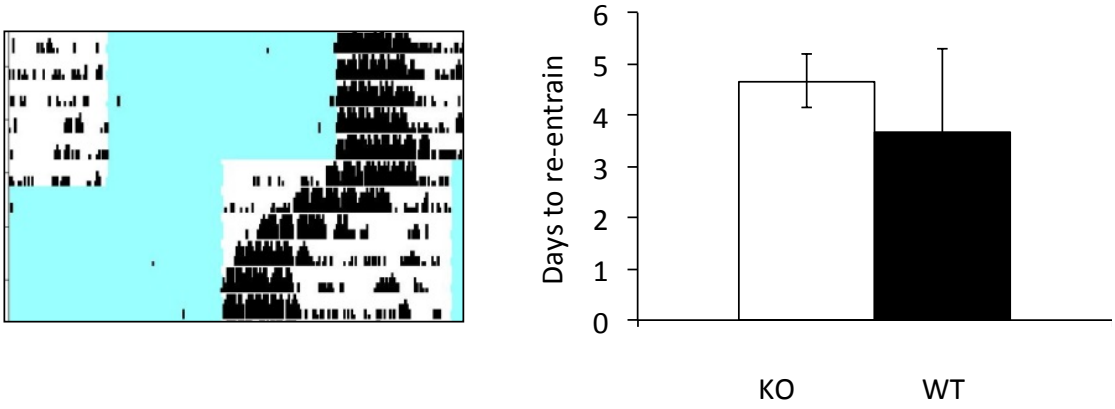

Figure 6.9 Re-entrainment to phase advance in *Opn1sw* KO and WT animals There was no difference in days taken by *Opn1sw* KO and WT mice to re-re-entrain following a 6-hr phase advance (left above shows example of protocol taken from *Opn1sw* WT actogram) in a 100lux white light 12/12 LD cycle (2-tailed Student's t-test p=0.183), n=6 for both genotypes. Bars represent mean values +/- SEM.

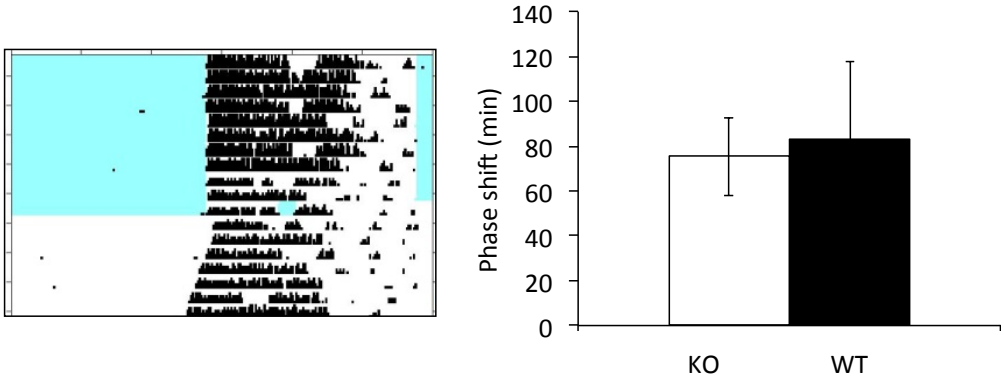

Figure 6.10 White light phase-shifting in *Opn1sw* KO and WT animals There was no difference in the magnitude of phase shifts to a 1hr 100lux white light pulses delivered between ZT16-17 (left above shows example of protocol taken from *Opn1sw* WT actogram) in *Opn1sw* KO and WT mice (2-tailed Student's t-test p=0.634), n=6 for both genotypes. Bars represent mean values +/- SEM.

Table 6.1 *Opn1sw* circadian screen summary Circadian measures assessed are listed along with p-values (n=6 for both genotypes)

Light schedule	Capacity under investigation	Specific circadian parameter analysed	Result (2 tailed T-Test p value)
12/12 LD	Accuracy of entrainment	Onset Error to lights-on	No difference (p=0.431)
	Activity characteristics	Average bout length	No difference (p=0.187)
		Total activity	No difference (p=0.187)
		Light phase activity	No difference (p=0.341)
		Dark Phase activity	No difference (p=0.180)
		Length of active phase (alpha)	No difference (p=0.714)
6hr phase advance	Speed of re-entrainment	Days to activity starting at new light-on	No difference (p=0.183)
DD	Free-running period length	Free-running Tau	No difference (p=0.861)
Phase shifting light pulse	Size of phase delay	Size of phase delay	No difference (p=0.634)
LL	Period lengthening	Tau under LL	No difference (p=0.397)

Pupillometry

To examine another assay of non-image forming system function, we performed pupillometry under bright 480nm light in *Opn1sw* KO and WT. This was again expected to show no difference given the light was far from the maximum sensitivity of UVS opsin and indeed the pupil light response (PLR) profiles of the two genotypes did not show any differences in response (Figure 6.11) and maximal constriction was found to be similar (2-tailed Student's t-test, p=0.213). Constriction to ~10% of dark adapted value is consistent with previous values found for bight 480nm stimulus in wildtype animals and greater than that seen in *rd/rd cl* animals suggesting some MWS cone involvement in this response (Hughes et al., 2012c).

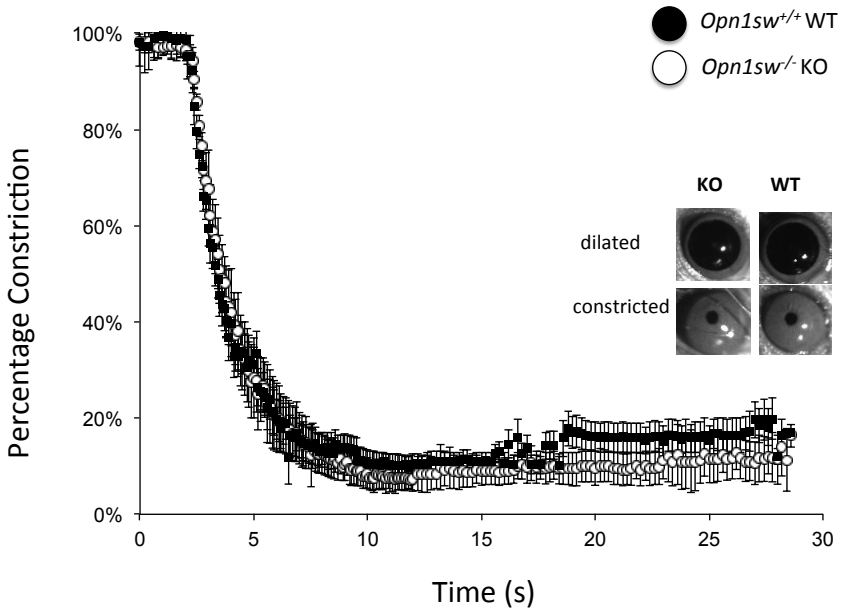

Figure 6.11 480nm pupillometry in *Opn1sw* KO and WT The PLR to bright 480nm light (~14.3 log photons/ cm^2/s, 82µW/cm^2) was examined in *Opn1sw* WT (n=5, was n=6 but one animal found to have cataract/ eye defect and used for OKN in Chapter 5) and KO (n=6). No difference was observed in the constriction profiles or in maximum constriction values (2-tailed Student's t-test, p=0.213).

Discussion

6.7 Complete loss of UVS opsin in novel *Opn1sw* KO

Given the difficulties involved in separating the specific contribution of photopigments to visual functions in the wildtype mouse, we aimed to generate a mouse lacking UVS opsin in order to examine effects on ultraviolet visual responses. Our *Opn1sw* KO mouse was found to have an approximately 8000-fold reduction in UVS transcript levels while the levels of rhodopsin and melanopsin were unaffected and no UVS protein was observed in the KO retinal sections or whole-mount staining. These results support the conclusion that the deletion has successfully targeted the UVS opsin. In the wildtype littermates of the knockout mice, the UVS expression gradient in whole-mount retinas exhibited the expected dorsal-ventral pattern (Applebury et al., 2000; Szél et al., 1992, 1996). In both genotypes, the general retina structure and morphology appeared normal.

6.8 Absence of UVS opsin results in slightly lower MWS expression but not broader M-opsin protein effects

While at the time we generated our *Opn1sw* knockout there were no other studies of complete gene s-opsin knockouts as the Daniele el al. (2011) knock-down model uses a neomycin insert, the recently published study by Greenwald et al. (2014) involves a deletion method similar to that reported here and thus offers an opportunity for closer comparison

with our model. Both studies reported a complete loss of UVS protein and both noted effects of the UVS loss on the M- or MWS opsin in the knockout retinas but specifics of this effect appeared to be distinct. The Daniele et al *Opn1sw*$^{neo/neo}$ model was found to have increased MWS expression and increased sensitivity to middle wavelengths in the ventral retina (Daniele et al., 2011). By contrast, Greenwald et al. reported a significant reduction both in MWS expression and sensitivity to ERG stimulus (Greenwald et al., 2014). This differences could be tied to differences in the method of *Opn1sw* gene disruption by neomycin insert versus the deletion of several exons but an alternative explanation for the disparity can be found in the ages of the mice. Greenwald found the loss of m-opsin ERG sensitivity was age-dependent and determined m-opsin levels from the retina of mice at or above 12 months of age while Daniele et al. only used mice between 1.5 and 8 months of age for their study. Considered with the age of test animals, these results suggest that s-opsin loss initially causes an increase in M-opsin expression in young animals but that this drops off in older animals so that expression and sensitivity is lower than wildtype controls. Both studies also reported effects on cone-outer segments in the ventral retina, where UVS expression would normally be highest. Although cone densities were normal across the retina, abnormal out-segments were observed in ventral cones in both models and, in mice 16 months of age, significant numbers of ventral cones were observed have completely lost their outer-segments in the Greenwald et al. model (Greenwald et al., 2014).

As another point of comparison, a mouse model of disrupted MWS opsin function through knockout of thyroid hormone receptor *TRβ*$^{-/-}$ was found to have a total absence of MWS opsin and up-regulation of both UVS and melanopsin but not rhodopsin (Dkhissi-Benyahya

et al., 2007). They do not state of ages of mice from which RNA is collected, however, so it is not clear how this result compares to the opsin changes seen in the *Opn1sw* models.

In our *Opn1sw* KO model, we observed a trend towards reduction of MWS transcript in the RT-PCR of knockout retinas from 6-10 month old animals but levels of MWS expression did not appear to differ from wildtype in retinal sections. Indeed, Greenwald et al. included mid-retinal/ near ventral sections, very near the region that was stained in Figure 6.3, and showed a significant reduction in the number of m-opsin expressing outer segments and those remaining displayed more variation in structure than the wildtype (Greenwald et al., 2014). One explanation is that this difference is due to the age of animal tissue used for the sections, given the data from both previous models. However, Greenwald et al. do not state the age of the retina used for sectioning so a direct comparison of age-matched sections is not possible. Our β-gal staining showed both s-cones in the dorsal retina and m-cones in the ventral retina retained outer-segments and appeared to have normal morphology. Again, this was done using retinas of *Opn1sw* KO animals around 5-6 months of age. Given the recent results of Greenwald et al in their study, it would be interesting to use β-gal to model ventral m-cone and dorsal s-cone structure in progressively aged KO animals as well as whole mount MWS staining in those animals in a future investigation.

6.9 Implication from *Opn1sw* KO models of minimum opsin threshold for outer-segment function

The observations of the retinal effects of UVS opsin loss have interesting implications for both the mechanisms of opsin regulation in the mouse retina and on the importance of the opsin protein for normal-cone health. Firstly, despite the abnormal and eventual loss of ventral cone outer-segments following the loss of the UVS opsin, no effect on the rod photoreceptors or any of the other retinal layers was observed in our model nor in either of the two previous *Opn1sw* gene disruptions even out to 16 months of age (Daniele et al., 2011; Greenwald et al., 2014). This contrasts with the observed effects of loss of rod outer-segments in the rhodopsin knockout. In the $Rho^{-/-}$ animal, loss of opsin leads to degeneration and outer-segment loss as seen in older UVS opsin knockouts. However, the effect is more immediate with no rod outer-segments observed after birth despite normal numbers of rod cell nuclei (Jaissle et al., 2001). The loss of rod outer-segments also leads to significant cone degeneration so that no cone outer-segments remain by 1.5 months of age (Toda et al., 1999) and in 3 month-old animals, in addition to the loss of the photoreceptor layer, the ONL of the retina displayed greatly reduced thickness (Jaissle et al., 2001). The explanation for why the loss of rod opsin results in faster outer-segment degeneration may be related both to MWS opsin partly compensating for UVS loss in mid-retinal cones as discussed below, and to structural differences between the outer-segments of rods and cones. In rods, the photopigment-containing discs (or lamellae) are bound within the plasma membrane, stacked within the thin outer-segments, while those of cones are not membrane bound in the generally much shorter cone outer-segments (Forrester et al., 2002b). Thus the rod lamellae

are more integral to outer segment structure. The wider retinal effect of rod loss is indicative of the greater relative importance of rods to mouse retinal structure. As cones make up only 3% of mouse photoreceptors (Jeon et al., 1998), the stability of the outer-segment layer is largely due to the support of rod-outer segments. Loss of rod-outer-segments in the rhodopsin knockout results in significant structural changes to the retina and its interaction with both the RPE and outer limiting membrane (Yu et al., 2004). As close association with the RPE is necessary for the RPE-visual cycle that replenishes photopigments of both rod and cone photoreceptors, it is not surprising that the observed loss of cone function should follow this changes (Travis et al., 2007).

The effects on ventral cone outer-segments in the UVS opsin disrupted models also indicate the importance of opsin expression to the maintenance of the outer-segments. The observation that the outer-segment effects were only seen in those cones which would have little or no MWS expression in the wildtype points to a minimum threshold level of opsin being required for outer-segment viability. Daniele et al suggest that the increased level of OPN1MW they observed, despite finding no changes to *Opn1mw* gene transcription levels, is due to the competition of cone opsin transcripts for translation in wildtype animals (Daniele et al., 2011). The impact of the loss of UVS opsin on the system equilibrium follows La Chatelier's principle and allows a greater proportion of the MWS mRNA to be turned into protein. From modeling the observed M-opsin increase against the loss of cone-outer segments, they determined that a minimum of 20% of normal opsin level was required for outer-segment maintenance. As the level is lower than this in ventral cones that normal express almost entirely UVS, these cones would show progressive outer-segment

abnormality and then loss in the knockout (Daniele et al., 2011). The presence of a required threshold opsin level for outer-segments has previously been found for rods (Sakurai et al., 2007; Shi et al., 2007).

6.10 Further investigation of opsin regulation in *Opn1sw* model

Our main aim for generation of the *Opn1sw* KO in this study was to investigate UVS cone contributions to image and non-image forming system functions. However, it is clear that with β-gal expression in the KO occurring throughout all cones that would normally express UVS, this model provides an excellent opportunity to further investigate the age-related cone changes recently described by Greenwald et al. in their model of *Opn1sw* KO (Greenwald et al., 2014). We did not examine aged animals here but, if similar outer-segment loss did occur in our model, the presence of β-gal would allow modeling of cone-anatomy changes over time where we might expect increasing abnormality in ventral cones relative to dorsal cones. Indeed, detailed co-labeling of β-gal and MWS, similar to that in Figure 6.5, would allow specific examination of s-cones in the dorsal and central retina which could be extremely interesting in a number of different aspects as little is known about the less common cone class in the mouse. This is despite the discovery of sustained s-cone mediated responses in the PON suggesting fundamental difference in signaling between s- and m-cones (Allen et al., 2011).

6.11 Conclusions

Our characterization of a novel *Opn1sw* knockout model demonstrated a complete loss of UVS opsin in the knockout retina while the retina structure and other opsin levels were not different from wildtype in the ages of animal used in this study. It is possible that our model would show loss of MWS opsin in aged animals as was observed by Greenwald et al in their *Opn1sw* knockout. Animals around or under 8 months of age were used for all experiments in this study and significant changes were only observed after this age in the previous studies. Furthermore, our data indicates both opsin levels and general cone morphology, even in the ventral retina of *Opn1sw* KO mice, are not significantly different from wildtype at the ages examined in this study. White light control tests were included for each behavioral assay and these would have revealed any m-cone dysfunction discrepancies between the knockout and wildtype control animals. As anticipated, our UVS model demonstrated normal non-image forming responses to white light and is well suited for investigation of the role of UVS opsin in mediating UV sensitivity of image and non-image forming visual systems.

Chapter 7: **Image-forming responses in *Opn1sw* KO**

Introduction

7.1 Aims

The presence of high levels of UVS opsin and the unique profile of cone opsin expression in the mouse retina remains to be fully explained in terms of its significance for visual function. Having characterized our novel UVS knockout in the previous chapter, we have laid the necessary foundation to use this model to examine UV visual sensitivity in various visual assays. Here we have aimed to assess the impact of the loss of UVS opsin dependent sensitivity in the UV on a range of image forming visual responses from basic light preference to cortex-dependent tasks.

7.2 ERG versus behavioral assessments of UV vision in mouse

The presence of a UVS photopigment in the mouse is well established but the assessments of the degree of UV visual sensitivity in mice have been limited. This is no doubt related to the fact that only relatively recently has the mouse been widely used as an experimental model for visual research (as discussed in Chapter 5), but with the increased use of mice in studies of the mammalian visual system and ocular diseases it is important to understand the full extent of its visual capabilities.

The initial indication of the UVS opsin and UV visual sensitivity in mice was derived from ERG recordings that found a second sensitivity maxima, in addition to the one at 510nm, at

370nm in the UV. Even more surprising was that this UV peak was higher than that in the visible light range (Jacobs et al., 1991). Mice are known to have three times more UVS expression than MWS (Applebury et al., 2000) and the translation into such high retinal UV sensitivity led to speculation concerning why UV vision might be so important for mice in their natural habitats (Chávez et al., 2003; Desjardins et al., 1973; Jacobs et al., 2002). However, while more recent ERG recordings confirmed the higher UV peak by this measure, a behavioral assay of vision found the UV visual sensitivity peak was significantly smaller than that in visible wavelengths (Jacobs et al., 2004). The assay used was the three-alternative, forced-choice discrimination task, a modification of a common forced-choice reinforcement assay (Prusky and Douglas, 2008), where mice are trained to indicate which of three identical test panels is lit by a particular test light to receive a food reward. Through changing the lit panel location and characteristics of test stimulus over hundreds of trials, a measure of visual detection threshold can be obtained. The difference between the field potential on the eye surface measured by ERG and the integrated use of visual sensitivity examined by behavioral assessments was discussed in Chapter 5. Interestingly, the relationship between ERG and behavioral measurements found in mice contrasts with data from other mammals, including the closely related rat, where ERG has been found to under-estimate short-wavelength sensitivity compared to increment-threshold measurements (Jacobs et al., 2001; Sperling and Mills, 1991). One possible explanation for this difference is linked to the co-expression and wiring of the mouse cones. Only 3-5% of mouse cones have been identified as true s-cones expressing only UVS and contacted by a dedicated blue cone bipolar cell (Haverkamp et al., 2005). It has been suggested that the rest of mouse cones are m-cones in which a developmental switch that is observed to turn off early UVS

expression in favor of MWS in rat m-cones has been lost (Jacobs et al., 2004; Neitz and Neitz, 2001). In this case then the majority of mouse cones possess m-cone connections and the opposing influence with respect to the spectral response of ganglion cells and their connections in the visual system might result in some cancellation of the UVS signal from the m-cones and explain the lower behavioral measurements (Jacobs and Williams, 2007; Jacobs et al., 2004). Thus, while there is no doubt that a particularly high retinal UV sensitivity is reflected in ERG measurements, to date visual behavior experiments have not found that the processing of UVS signals in the mouse allows for especially great visual sensitivity.

It could also be that the behavioral assay used to assess UV vision in the mouse (three-alternative, forced-choice discrimination task (Jacobs and Williams, 2007; Jacobs et al., 1991, 2004)) did not capture the full extent of its sensitivity or that the high level of UV sensitivity is adapted to perform non-visual functions where different retinal circuitry exists. We examine UV vision using OKN and a visuospatial task in this chapter and examine the UVS contribution to the NIF system in the next chapter.

7.3 Mouse Colour vision and UVS opsin

Another way of looking at the utility of ultraviolet sensitivity in the mouse, beyond the direct quantification of sensitivity in various assays, is in terms of visual capabilities that are gained through the presence of a second cone opsin in the retina. Perhaps the most obvious potential advantage is the capacity for colour vision that would allow greater visual detail

and discrimination. Using stimuli where spectral differences were the only cues, mice could be trained to discriminate successfully between visual displays suggesting that wildtype mice have the capacity for limited color vision (Jacobs et al., 2004). However, significant performance in this assay required 6,000-10,000 training trials for each animal and simply identifying the capability for discrimination does not mean that it is at a physiologically significant level and sufficient to be useful in a natural environment or reflective of how the mouse naturally uses its visual system. Indeed, co-expression of two opsins in the same cone photoreceptor is a poor mechanism for a widespread comparison of spectral signals from different cones to distinguish color and the UVS expression gradient is heavily biased towards the ventral, sky-facing retina instead of the mid or upper retina that would be directly useful for visual tasks in front of the mouse (Applebury et al., 2000; Röhlich et al., 1994; Szél et al., 1992). As regional sensitivity measurements across the mouse retina have found that retinal responses follow that expected from the UVS gradient, with the greatest UV sensitivity in the ventral retina (Calderone and Jacobs, 1995), it does not seem that the cone-opsins in the mouse are arranged for color-discrimination visual ability. This leads again to the debate as to the functional role of UV visual signals in mice that conferred selective advantage to the dorsal-ventral expression gradient and high level of UVS opsin.

Summary of aims

In this chapter, we use three visually dependent assays, a light/dark box, the OKR and a visuospatial variant of the NOR task to examine the effects of UV sensitivity and UVS opsin loss on aspects of visual system response. In the light/dark box we expected a similar level

of white light aversion response in the *Opn1sw* KO but that under UV light the *Opn1sw* KO would display a reduced response to the UV light. We also investigated if UVS expressing cones played roles in the OKR response and visuospatial object recognition performance under UV light. ERG was not assessed here as we aimed to obtain behavioral measures of the use of UV light in the mouse visual system to expand on the results of the three-alternative forced-choice assay, the only previous assay of this type to find evidence in support of UV vision in mice.

Results

7.4 Wildtype mice spend more time under UV than *Opn1sw* KO in Light-Dark box

As one of the most basic light responses, preference for avoidance of light stimulus was examined in a light/dark box where animals could choose to spend time in an open lighted half of clear Perspex area or in an equally sized area of opaque black Perspex (Figure 7.1). Time spent in the dark versus the light half of the light-dark box arena was analyzed over a 10-minute trial in *Opn1sw* KO and wildtype control mice. Analysis for each animal began at the time of the first dark entry or crossing from lighted half into the dark to avoid variation due to the observed freezing response of animals when first introduced to the open lighted half of the arena. All animals were tested in the naïve state, having never been exposed to the light-dark environment before so prior experience in the arena could not influence behavior.

Figure 7.1 Light-Dark Box apparatus Side and corner views of light/dark box used for test of light avoidance behavior to white and UV light in the *Opn1sw* transgenic model

Both genotypes demonstrated significant aversion to the open half of the light-dark box under 500 lux (14.6 log photons/cm^2/s, 148.5 μW/cm^2) white light, with significantly more than 50% of the trial spent in the dark half of the arena for both *Opn1sw* KO and wildtype animals (Figure 7.2). But there was no difference between the genotypes in this dark half preference (2-tailed Student's t-test, p=0.21).

The test for aversion was repeated under 10μW/cm^2 or approximately 13.3 log photons/cm^2/sec (10.86 μW/cm^2) UV light. In this case a difference was observed between the genotypes with wildtype animals spending a significantly smaller percentage of time than the *Opn1sw* KOs in the dark half of the light-dark box (2-tailed Student's t-test p=0.036) (Figure 7.2). Compared to the non-preference level of 50%, the *Opn1sw* KO animals again were found to spend a significantly greater portion of time in the dark half (1-sample t-test compared to no-preference 50%, t(6), p=0.011), while wildtype animals were not (1-sample t-test compared to no-preference 50%, t(5) p=0.21). Further analysis compared the aversion between the light conditions within each genotype and the wildtype mice were found to have spent significantly more time in the dark half under white light when compared to UV conditions (78.0% +/-5.49% SEM in white versus 55.8% +/-3.71% SEM in UV, 2-tailed Student's t-test p=0.0067). While the *Opn1sw* KO animals also spent a greater percentage of time in the dark area for the white light condition than they did for UV (87.3% +/- 4.46% compared to 76.8% +/- 7.42%) this difference was not significant (2-Tailed Student's t-test p=0.27).

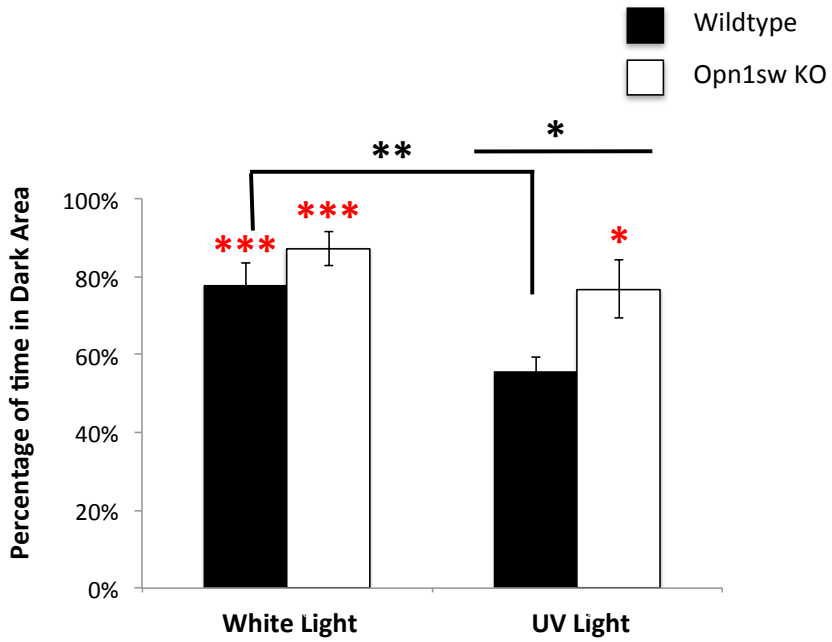

Figure 7.2 Light aversion behavior in *Opn1sw* KO and WT under white and UV light The amount of time spent in the dark half of a light-dark apparatus was analyzed in *Opn1sw* KO and WT under 500lux (14.6 log photons/cm^2/s, 148.5 µW/cm^2) white light and 13.3 log photons/cm^2/sec (10.86 µW/cm^2) UV light. 1-sample t-tests comparing the percentage of time in the dark half to the no-preference level of 50% found both *Opn1sw* KO ($p=0.0004$) and WT ($p=0.0034$) spent a significantly greater proportion of time in the dark half under white light but only the *Opn1sw* KO maintained a significant preference for the dark half under UV light ($p=0.011$ for KO and $p=0.179$ for wildtype). Comparing between the light conditions, wildtype mice were found to spend a significantly smaller percentage of time in the dark half of the box under UV light than they did under white light (2-Tailed Student's t-test $p=0.0067$) but, while the KO did spend less time in the dark half this difference was not significant (2-Tailed Student's t-test $p=0.27$). Finally, only for UV (2-tailed Student's t-test $p=0.036$) but not white (2-tailed Student's t-test $p=0.221$) was there a difference between the genotypes. Different batches of mice were used in white and UV light tests, for white light, n=6 for WT and n=6 KO, for UV light n=6 WT and n=7 KO. *=$p<0.05$, **=$p<0.01$, *** =$p<0.005$, *=2-tailed t-test comparison between genotypes or light conditions, *=1-sample t-test comparing to no-preference level of 50%. Bars represent mean +/- SEM.

7.5 Optokinetic responses of *Opn1sw* KO match wildtype responses under white and UV light

The optokinetic reflex responses of wildtype and *Opn1sw* KO animals were tested using a mechanical OKR drum (Methods Chapter 2 for testing procedure) under 200 lux white light to confirm the normal performance of the KO under visible-wavelengths. KO responses closely matched those of littermate wildtype controls at all spatial gratings (Figure 7.3). Acuity threshold (defined as the lowest cpd grating where an average of 2 or more head-tracking responses were observed) was 0.5 cpd and maximal sensitivity was found at 0.2-0.3 cpd. No responses were observed in the control condition with 0.2cpd but lights off (dark).

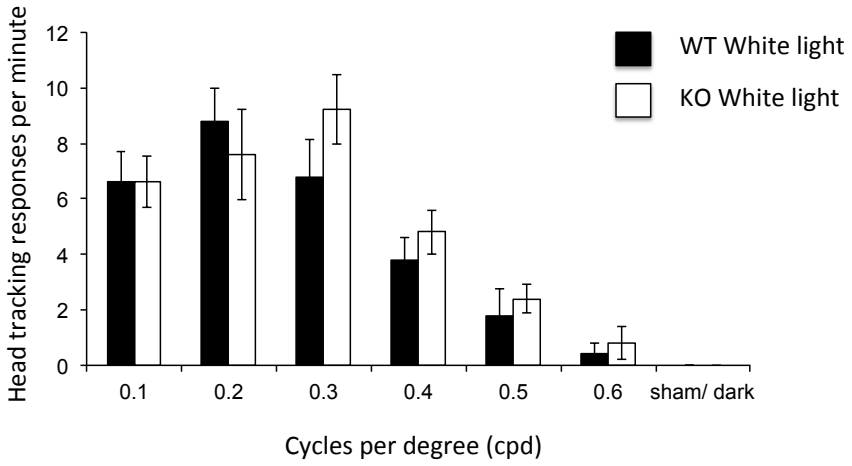

Figure 7.3 OKR assessment of *Opn1sw* KO and WT under white light OKR responses of *Opn1sw* KO (n=8) and WT (n=8) mice, were examined under 200lux (14.2 log photons/cm^2/s, 59.42 µW/cm^2) white light. The threshold acuity (lowest cpd at which 2 or greater head-tracking movement were observed/ minute) was 0.5cpd for both KO and WT animals while maximum sensitivity was between 0.2 and 0.3 cpd for both genotypes. Dark control was run with lights-off and 0.2cpd grating. Bars represent mean values +/- SEM.

OKR responses were tested under dim (11.6 log photons/ cm^2/ sec, 0.2 µW/cm^2) and bright (13.9 log photons/ cm^2/ sec, 40 µW/cm^2) UV light conditions. Responses did not differ between the genotypes at any cpd in the dim (Figure 7.4A) or bright (Figure 7.4B) UV conditions. However, there was an effect of light intensity on the performance of both genotypes. The number of responses per minute was significantly higher under bright UV for every spatial grating (Figure 7.5) and acuity threshold dropped from ~0.5 cpd to 0.3 cpd for both genotypes.

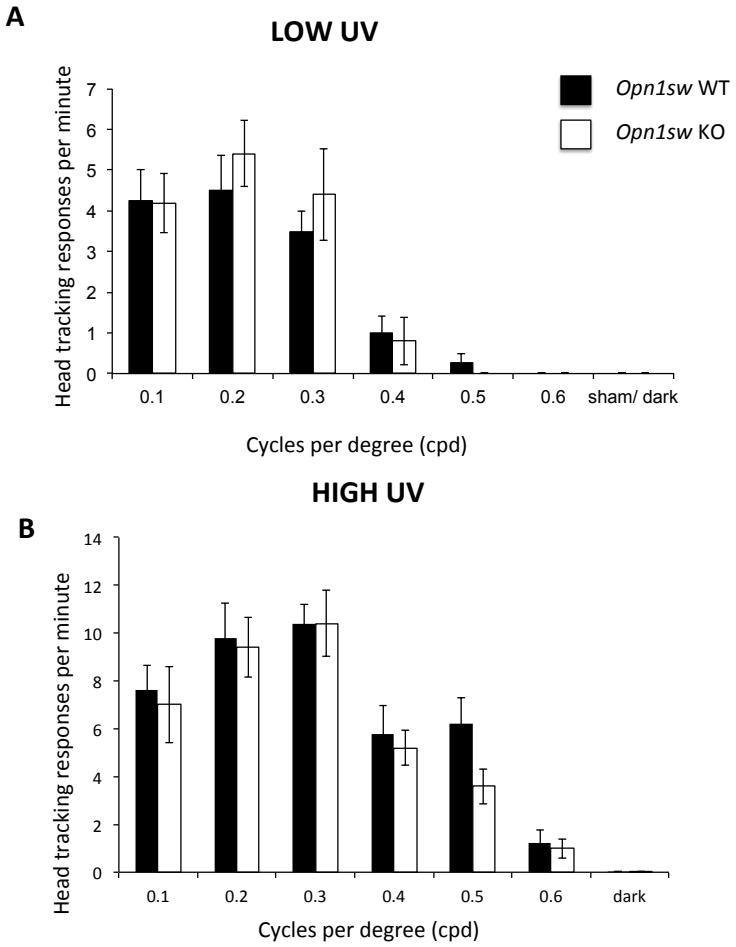

Figure 7.4 OKR assessment of *Opn1sw* KO and WT under UV light OKR responses of *Opn1sw* KO (n=8) and WT (n=8) mice, were examined under (A) dim (11.6 log photons/ cm^2/ sec, 0.2 µW/cm^2) and (B) bright (13.9 log photons/ cm^2/ sec, 40 µW/cm^2) UV light conditions. No significant differences were found between

the genotypes at any cpd (2-tailed student t-tests in each case p>0.05). The threshold acuity (lowest cpd at which 2 or greater head-tracking movements were observed/ minute) was 0.5cpd for both *Opn1sw* KO and WT animals under the bright UV condition but dropped to 0.3 cpd in dim UV (significant drop in thresholds for both genotypes, p<0.005). Maximum sensitivity was 0.2-0.3 cpd under bright UV and under dim UV similar levels of responses were seen for 0.1, 0.2 and 0.3 cpd gratings. Bars represent mean values +/- SEM.

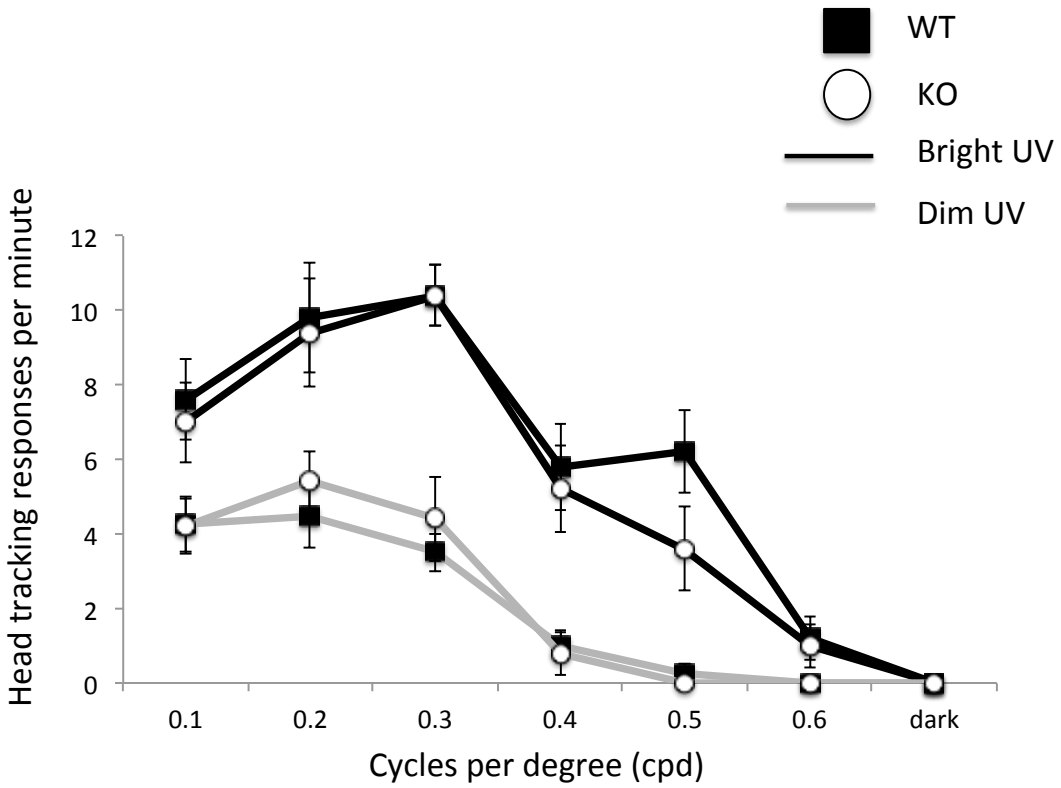

Figure 7.5 Response frequency is intensity dependent under UV light. Data from Figure 7.4 A and B is replotted together to illustrate the changes in the frequency of head-tracking responses/minute between the dim and bright UV condition. Responses were higher under bright UV light at every cpd irrespective of genotype (2-tailed Student's t-tests for each cpd found p<0.05).

7.6 Visuospatial recognition performance is impaired in *Opn1sw* KO animal under UV light

The visuospatial adaptation of the novel object recognition (NOR) task described in Chapter 5 was used to test for visual performance differences between *Opn1sw* KO and WT animals under white and UV light. Animals were given a 10-minute sample phase to interact with two identical objects in an arena where the walls could be distinguished by visual patterns. Following a 5 minute delay, the animals were again introduced to the arena for a 3 minute test phase where one of the identical objects had been moved to an adjacent corner (Figure 7.6). As objects were chosen such that they did not differ with respect to tactile or olfactory stimuli, recognition of the novel object location requires the use of visual stimuli on the wall of the arena to recognize that one object is in a new location. Recognition ratio above 0.5 indicates success in the task and the more the ratio is above 0.5 the stronger the performance (ratio of time with object in familiar (f) versus the new (n) location given by n/(n+f)).

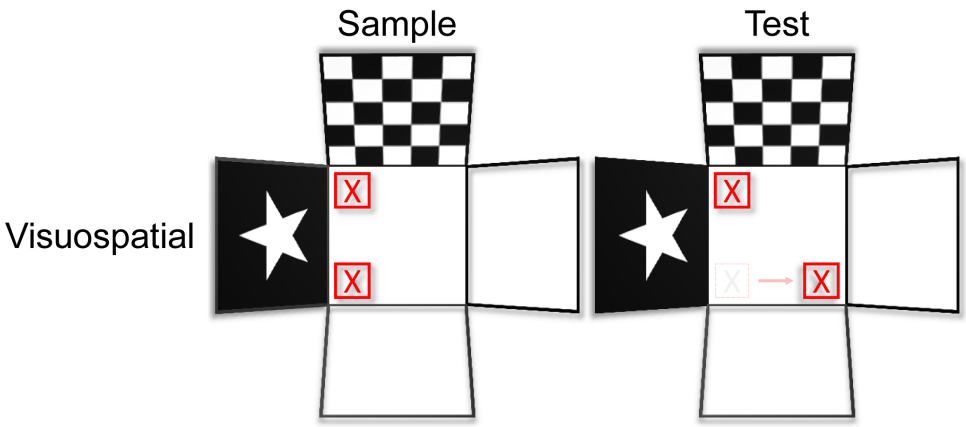

Figure 7.6 Representation of Visuospatial Object Recognition Task showing object movement between sample and test phases.

To confirm the expected normal visual performance under visible wavelengths of the KO animals lacking UVS opsin, we tested *Opn1sw* KO and wildtype mice under 100 lux white light. A significant recognition performance was observed for both WT (2-tailed 1-sample t-test p=0.007) and KO (2-tailed 1-sample t-test p=0.002) (Figure 7.7). There was no difference between the WT and KO performance, (ANOVA, p=0.945). There was also no difference found between genotypes in general exploratory activity during sample or test phases (Table 7.1).

An identical testing set-up was used to examine recognition performance under low (11.6 log photons/cm^2/s, 0.22 μW/cm^2) and high (13.6 log photons/ cm^2/s, 22 μW/cm^2) UV light. Visuospatial recognition performance was examined both separately and by combining the performance across both UV light intensities. Under low light, neither *Opn1sw* KO (2-tailed 1-sample t-test p=0.759) or WT (2-tailed 1-sample t-test p=0.158) performed above the chance level of 0.5 although the WT performance of 0.606 was higher than the KO ratio of 0.525 (Figure 7.8A). Under bright UV, both groups were able to perform above chance (WT, p<0.0005; KO p=0.002) again with WTs outperforming KO with ratios of 0.756 and 0.662 respectively (Figure 7.8B). When the data for UV light was combined, overall *Opn1sw* WT displayed significantly higher visuospatial recognition under UV light with a genotype by batch ANOVA finding a significant difference in recognition ratio p=0.033 (Figure 7.8C). The overall performance of both genotypes was also above chance when the combined data was analyzed (WT p<0.0005; KO, p=0.0013) and there was no genotype difference in total exploration time during sample or test phase (Table 7.1).

The recognition ratios of wildtype *Opn1sw* control animals were higher for the visuospatial task under white light (0.828) than under bright UV (0.756) but this difference was not significant.

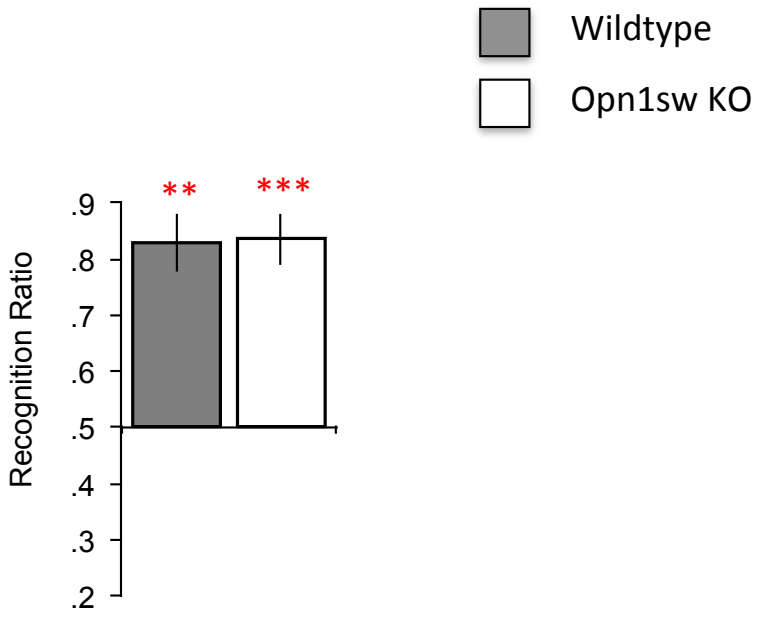

Figure 7.7 White light visuospatial Object Recognition trial with *Opn1sw* KO and wildtype mice

Recognition performance of KO (n=7) and WT(n=6) *Opn1sw* mice was examined in a visuospatial adaptation of the novel object recognition task under 100lux white light (13.94 log photons/cm^2/s, 31.1 µW/cm^2). WT animals were found to perform significantly above chance level of 0.5 (2-tailed 1-sample t-test p=0.007) as were KO (2-tailed Student's t-test p=0.002). ANOVA analysis found no difference between genotypes performance ($F_{1,11}$, p=0.945). *= significantly above chance, *=p<0.05, **=p<0.01, *** =p<0.005. Bars represent mean values +/- SEM.

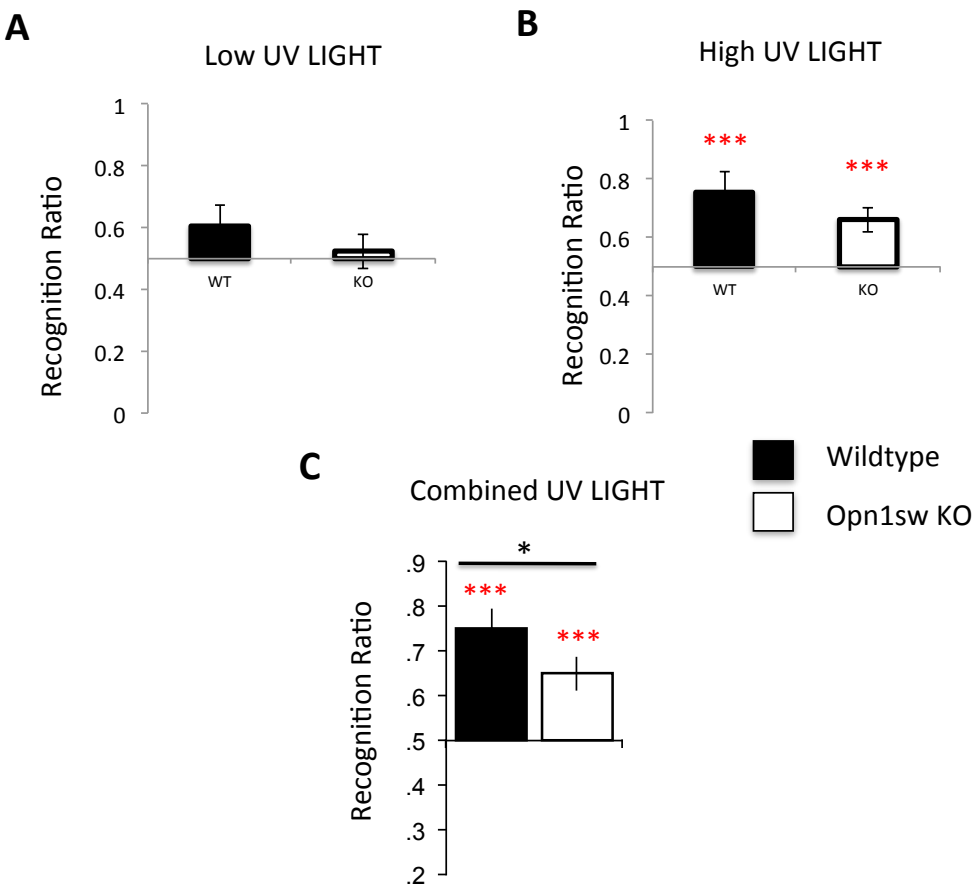

Figure 7.8 UV light visuospatial Object Recognition trial with *Opn1sw* KO and wildtype mice

Recognition performance of *Opn1sw* mice was examined in a visuospatial adaptation of the novel object recognition task under low (11.6 log photons/cm^2/s, 0.22 µW/cm^2) and high (13.6 log photons/ cm^2/sec, 22 µW/cm^2) UV light intensities. **(A)** Under dim light trial in KO (n=7) and WT (n=7), neither genotype performed above chance recognition level, KO (2-tailed 1-sample t-test p=0.759) or WT (2-tailed 1-sample t-test p=.158). **(B)** Under the bright UV light both animals from the dim light batch and a further batch were tested creating overall group sizes as follows; KO n=14 and WT n=13. Both WT and KO animals were found to perform significantly above chance level of 0.5 (WT, p<0.0005; KO p=0.002). **(C)** Combined UV light data for non-overlapping animals (WT n=12, KO n=13) found overall both genotypes performed above the chance recognition level of 0.5 (WT p<0.0005; KO, p=0.0013) while ANOVA analysis showed WT animals performed significantly better than KO (F1,23, p=.033). *=p<0.05, **=p<0.01, *** =p<0.005; *= significant genotype difference, *= significantly above chance. Bars represent mean values +/- SEM.

Table 7.1 Overall activity/ explorations for *Opn1sw* animals in Visuospatial and Olfactory recognition tests (all tests 2-tailed Student's t-test)

Mean total object exploration (and standard error of mean) during sample phases

Genotype Comparison	UV Light		White Light
	Visuospatial	*Olfactory*	*Visuospatial*
WT	160.17 s (17.39 s)	151.16 s (15.21 s)	141.17 s (23.65 s)
Opn1 sw	152.07 s (10.36 s)	129.60 s (15.80 s)	138.96 s (16.03 s)
	p=0.72	p=0.22	p=0.74

Mean total object exploration (and standard error of mean) during test phases

Genotype Comparison	UV Light		White Light
	Visuospatial	*Olfactory*	*Visuospatial*
WT	23.02 s (2.40 s)	17.38 s (2.05 s)	13.50 s (2.19 s)
Opn1 sw	17.21 s (1.90 s)	17.63 s (1.23 s)	12.71 s (2.95 s)
	p=0.078	p=0.85	p=0.36

7.7 Olfactory recognition performance shows genotype difference under UV light

Given the observed genotype effect on visual performance under UV light, we examined whether differential sensitivity to UV light would affect recognition performance of other sensory modalities like olfactory responses if these were performed under bright UV light (13.6 log photons/ cm^2/sec, 22 $\mu W/cm^2$). We hypothesized that *Opn1sw* KO animals, having

decreased visual sensitivity to UV light, might rely more heavily on other sensory cues like scent and so display higher olfactory recognition relative to wildtype where the visual stimulus did not change. For this experiment, the times of sample and test phases remained the same but instead of moving a visually identical object with respect to the arena visual cues, the objects remained in the same place but the scent of one object was changed (Figure 7.9).

We found that the recognition ratio for *Opn1sw* KO was significantly higher than that for WT animals (by batch ANOVA p=0.048), however neither of the groups displayed a recognition ratio significantly different from the chance level of 0.5 (2-tailed 1-sample t-test, WT p=0.184; KO p=0.203) (Figure 7.10). There was no difference in general activity or exploratory time between the genotypes (Table 7.1).

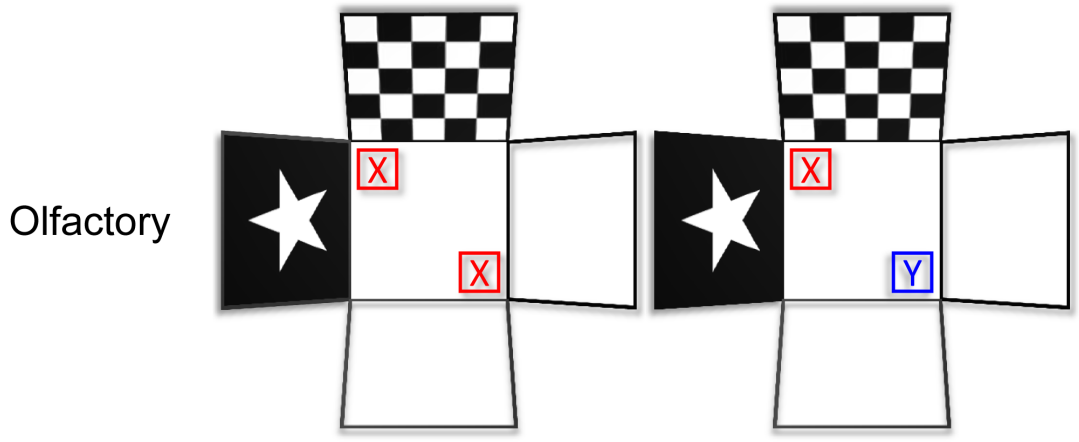

Figure 7.9 Representation of Olfactory recognition task showing object movement between sample and test phases

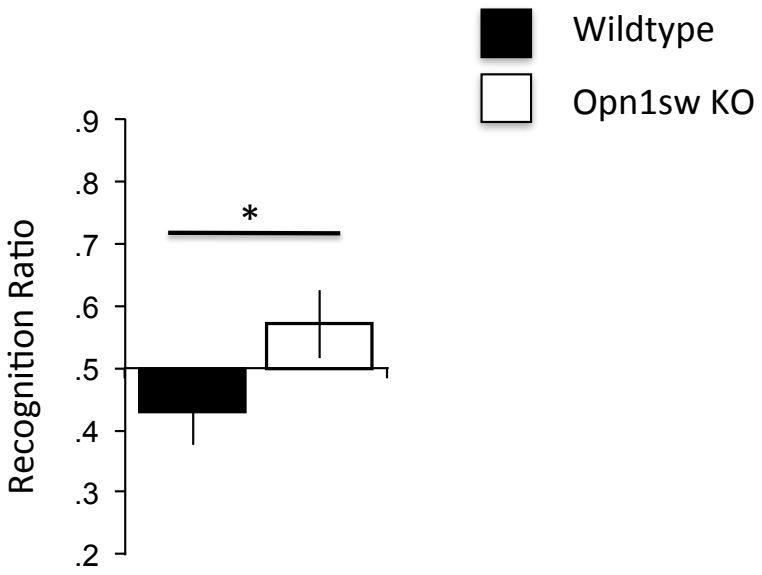

Figure 7.10 Olfactory recognition performance in *Opn1sw* KO and wildtype mice under UV light

Olfactory recognition performance of KO (n=14) and WT (n=13) *Opn1sw* mice was examined under (13.6 log photons/ cm^2/s, 22 µW/cm^2) UV light. Neither group displayed recognition significantly different from the chance level of 0.5 (2-tailed 1-sample t-test, WT p=0.184; KO p=0.203) but the KO performance was significantly higher than the WT (by batch ANOVA p=0.048). *=p<0.05, **=p<0.01, *** =p<0.005; *= significant genotype difference, *= significantly above chance. Bars represent mean values +/- SEM.

Discussion

7.8 Wildtype mice show preference for UV light

One of the most basic light responses is the natural aversion behavioral response to acute visible light found in nocturnal rodents such as rats (Crozier and Pincus, 1927) and mice (Crawley and Goodwin, 1980; René Misslin, 1989). This response can be assessed through the use of a light-dark box consisting of dark and lighted chambers that the animals are able to cross between to show a preference or aversion to the light condition. As the behavior is also related to the level of anxiety of an animal, this test has been widely used in anti-anxiety or anxiolytic drug development (Bourin and Hascoët, 2003).

The photoreceptor basis for the light response has been found to depend on both the outer retinal rods and cones as well as melanopsin containing pRGCs. In light/dark box tests, studies had found differing results to the question of whether *rd/rd* mice retain (Mrosovsky and Hampton, 1997) or lack (Lin et al., 2008) a residual light aversion response. The difference could be due to testing methodology or due to variation in the incomplete cone degeneration we saw in *rd/rd* retinas (Chapter 4). In recent evaluations using *rd/rd cl* mice as a more complete model of retinal degeneration to compare to a triple knockout (TKO) mouse with mutations affecting all the photoreceptors classes in the mouse retina, it was found that while rods and cones are responsible for the majority of the aversion response, melanopsin is also able to contribute a clear light preference over a 22 hour time-period (Semo et al., 2010).

The light-aversion response represents one of the most basic visual responses to light as albino mice with visual deficits that are unable to display any head-tracking OKR response under scotopic or photopic conditions were found to display a clear preference for the dark in a light/ dark box test (Abdeljalil et al., 2005). Similarly, the triple-knockout mouse with disruption of melanospin and rod/cone function (*Gnat1* $^{-/-}$, *Cnga3* $^{-/-}$ and *Opn4* $^{-/-}$) has not been found to display PLR, entrainment, masking (Hattar et al., 2003) or phase-shifting (Chapter 4, this study) responses but did display a light aversion response in a light/dark box test using retinal signals (Semo et al., 2010), perhaps due to compensation for part of the rod mutation. Thus, this test provides a basic level on which to examine the contributions of the UVS cone to UV sensitivity.

The results we observed under white light showed a strong preference for the dark half of the light/ dark box arena in both the wildtype control and UVS KO animals. This is consistent with the expected aversion response being maintained in the *Opn1sw* KO as would be anticipated given the limited UVS absorption under visible wavelengths.

Interestingly, under UV light, the *Opn1sw* KO again spent more time in the dark half of the arena while the wildtype animals no longer demonstrated the preference for the dark half that they showed under white light. This result was unexpected and the opposite trend to our prediction that the loss of UV sensitivity in the *Opn1sw* KO would result in a reduction in the light aversion response. Our prediction was based on the assumption that UV light would result in an aversion response like that seen to visible wavelengths. While the UV light level used was certainly bright enough to generate responses from a combination of the rods,

melanopsin and MWS cones remaining in the *Opn1sw* KO (see residual photopigment responses to UV light in Chapter 4 Table 4.1), we expected that the loss of the sensitivity provided by the unique UV sensitivity of UVS cones would result in the *Opn1sw* KO showing a lower level of aversion than the wildtype. The *Opn1sw* KO animals did spend a smaller percentage of time in the dark portion of the arena during the UV light trial but this trend was not significant and the wildtype animals showed a much greater drop in the time spent in the dark half of the arena.

The results we observed in wildtype mice suggest that UV light does not cause aversion like visible wavelengths. This result is not without precedent as a previous study of mole-rats, which also retain a UVS cone opsin, found they avoided blue but not UV light in a comparison of monochromatic stimuli (Kott et al., 2010). Several species of bird have also been found to prefer UV lit areas (Ross et al., 2013).

It could be that there is a significant innate preference for the dark half of our arena and also a preference for UV visual environments in the mouse. This would explain why the *Opn1sw* KO, unable to 'see' the UV light to the same degree at the wildtype, spent more time in the dark-half under UV light. However, as we were focused on the *Opn1sw* KO and wildtype aversion comparison under UV light, all of our animals were placed in one or other light group during the experiment with white light regarded as the control given the expected aversion response. We did not compare *Opn1sw* KO and wildtype preference for one or other side of the light-dark box in 'dark' conditions without a light stimulus. In hindsight this experimental design could have been improved as the light/dark box is also an established

test of anxiety and there could be confounding factors between the genotypes other than the presence or absence of UVS opsin that caused the observed effect.

7.9 OKR response to UV light is not dependent on UVS cones

We had previously examined the responses of *rd/rd*, *rd/rd cl*, *Opn4* $^{-/-}$ and *cl* models using our OKR drum and found that white light responses were primarily driven by rods even under light levels where cones would be expected to make a significant contribution to vision. A preliminary test of UV responses at spatial grating of maximal sensitivity found that both wildtype and *cl* mice (which lack MWS cones but retain a population of UVS cones and rods) displayed strong head tracking while neither *rd/rd* or *rd/rd cl* showed any response (Chapter 5, Figure 5.7). This experiment did not preclude the possibility of UVS cones contributing to OKR and this was investigated here using the *Opn1sw* model. The finding that there was no difference between the wildtype and *Opn1sw* KO responses, even under the high UV condition, again suggests that the OKR response here was primarily rod-driven, supporting the conclusions in Chapter 5.

However, one aspect of these results that we did not find in the examination of white light responses in Chapter 5 was intensity dependent changes in acuity. These have previously been reported both where photopic conditions resulted in higher response rates than scotopic (Abdeljalil et al., 2005) and in a study where a step-wise decrease in light irradiance was mirrored by a decrease in relative responses (Schmucker et al., 2005). We found acuity threshold and response rates were decreased at the lower intensity of UV light for both the

wildtype and KO genotypes. The 0.5 cpd threshold acuity value at the brighter UV light level as well as the 0.2-0.3 cpd spatial grating level of maximal response rate both matched what we had found under white light conditions (Chapter 5 Figure 5.1) which demonstrates that UV light can be used by the mouse to similar levels of acuity as white light so long as the UV light is sufficiently bright. Given that our results indicate rod absorption is key to the OKR assay, we would predict that bright light would be required to generate equivalent responses to white light given the low level of rhodopsin sensitivity in the UV (see Chapter 4, Table 4.1).

7.10 UV light sensitivity through UVS cones is used for cortical visual tasks

Our results indicate that UV sensitivity through UVS cones allow mice a greater visuospatial recognition performance as evidenced by the fact that wildtype mice outperformed KO mice under UV but not white light in the object-recognition task. Significant levels of performance under UV light were reached for the high but not low UV light level and while the performance of the *Opn1sw* KO and wildtype did not differ under 100 lux (13.94 log photons/cm^2/s, 31.1 μW/cm^2) white light, the performance of both genotypes under this white light condition was higher than even bright UV light performance. It should be noted that this is a comparison of monochromatic light to white light and 100 lux white light represents a slightly higher total irradiance than the bright UV (13.9 versus 13.6 log photons/cm^2/s), but, similar to the results of the forced-choice discrimination behavioral test (Jacobs et al., 2004), we did not see any evidence for the significant enhancement of UV

sensitivity over visible wavelengths in the mouse visual system suggested by ERG results (Jacobs et al., 1991, 2004). As cortex involvement has been implicated in rodents for both the NOR (see Chapter 5 introduction of NOR assay) and the forced-choice discrimination task (Petruno et al., 2013) they represent assessment of integrated use of visual sensitivity for learning and behavioral environmental interaction that differs from the information derived from photoreceptor function measured by ERG. These results support the suggestion that the organization and pattern of opsin co-expression may reduce the signal from UVS opsin to the image-forming system in the mouse (Jacobs and Williams, 2007; Jacobs et al., 2004).

It is also clear that, while recognition performance in the NOR visual task under UV light was reduced in the KO model lacking UVS opsin, successful recognition was still found in the KO under bright UV. Though it is possible that tactile or other non-visual cues could have resulted in successful recognition, as we found retinally degenerate *rd/rd cl* mice were unable to perform this assay (Chapter 5 Figure 5.9), it was concluded that successful performance is dependent on the use of visual context cues. Thus the limited sensitivity of rod and MWS cone photopigments in the UV may be sufficient to allow visual performance in this assay given bright UV light (again see Chapter 4, Table 4.1 for residual photopigment sensitivities at 365nm). This performance could also be due to UV-induced visible fluorescence of the test objects or arena where the high levels of UV light are absorbed and result in fluorescence in the visible wavelengths that could then excite non-UVS photopigments and thus allow for visual recognition. This is another reminder that while we are investigating the UVS opsin as the primary UV-sensitive photopigment in the mouse,

other photopigments may mediate UV sensitivity in animals when UV is at sufficiently high levels of irradiance.

7.11 Difference in olfactory recognition between genotypes but it is unclear if this reflects true variation in sensory integration

Finally, we examined whether the deficit in UV light sensitivity due to the loss of UVS cones would cause other changes to sensory performance. Given a background UV illumination we thought that *Opn1sw* KO animals, having decreased visual sensitivity to UV light, might rely more on other sensory input and so display higher olfactory recognition relative to wildtype when the scent but not visual stimuli was changed. While we did find the *Opn1sw* KO significantly outperformed the wildtype, this analysis is complicated by the fact that neither genotype performed at a level significantly different from chance. In addition, the wildtype animals showed a slight, though non-significant, preference for the familiar scent even though two trials were conducted with different combinations of scent stimuli and all experiments were counterbalanced with respect to stimulus presentation. Thus it is not clear from this data whether the visual deficit influenced performance in a different sensory modality but this would be an interesting area for further investigation with regards to sensory integration in mice.

7.12 Conclusions

We examined the mouse visual sensitivity to UV light in a UVS opsin knockout using three different visual assays, a light/dark box test of aversion, an OKR drum and a visuospatial adaptation of the NOR task. Our results suggest that UV light does not necessarily cause the light-avoidance response seen to visible light in the mouse but the basis for the observed difference between *Opn1sw* KO and wildtype remains unclear. We also found that the OKR response to UV light is not dependent on UVS cones. However, we found that loss of UVS opsin does impair visuospatial object-recognition performance under UV. The demonstration of visual deficit in this spontaneous visual task has further importance as it is only the second behavioral test, following a number of studies involving the 3-alternative forced-choice discrimination task by Jacobs et al., to show UV visual performance in the mouse. As the forced-choice discrimination test requires training over hundreds of trials, this adaptation of the NOR task provides a valuable new assay to test visual sensitivity in mice.

Chapter 8: **Non-image forming responses in *Opn1sw* KO**

Introduction

8.1 Aims

In Chapter 4, we investigated the circadian sensitivity to UV light present in the mouse and our results suggested that UVS cones played a major role in mediating this sensitivity. In this chapter, we aimed to utilize our *Opn1sw* KO model, specifically lacking UVS cone opsin, to examine circadian activity regulation under UV light to confirm the central role of UVS cones suggested by our previous work. We also aimed to determine if a role for UVS cones in the non-image forming system was restricted to entrainment or if there was also an impact on pupillary light responses. Finally, to follow up on the study of the c-fos induction in pRGCs presented in Chapter 4, we examined c-fos expression in the retina following UV light exposure to determine how this was affected by the presence and absence of the UVS opsin. Comparing non-image forming roles for UV sensitivity to the image-forming data presented in the previous chapter should provide an indication of the role UV light plays in mouse physiology.

8.2 Evidence suggests varying balances of rod, cone and melanopsin contributions to different non-image forming system outputs

In the investigation of photoreceptor roles in mediating UV sensitivity, it is important to realize that the contributions of the photoreceptor classes are not uniform across the NIF system. Even within the same wavelength range, there is abundant evidence that the relative

contributions of rods, cones and melanopsin under visible light is dependent on which aspect of the non-image forming visual system is being examined. Thus, comparison of UV light responses to those under visible light should be restricted to the same NIF behavior. Here we summarize the current evidence for photoreceptor contributions to major parts of the NIF system and compare the established roles for rods, cones and pRGCs.

The Pupil Light Reflex

Pupil constriction and dilation are controlled by contraction of the ring of iris sphincter muscle fibers around the pupil margin and the dilator muscle fibers spreading from the pupil aperture respectively. The sphincter muscle, and thus constriction, is controlled by the parasympathetic nervous system while dilation is controlled by the sympathetic system. In the pupillary light reflex (PLR), light detection in the retina results in signals down RGC axons terminating in the olivary pretectal nuclei (PON) which itself innervates the Edinger-Westphal nucleus (EWN) of the third cranial nerve (Grozdanic et al., 2003; Klooster et al., 1995). Oculomotor nerves from the EWN are sent to the ciliary ganglion and from there parasympathetic postganglionic axons project to the sphincter muscle (Klooster et al., 1993). In the dark, RGC projections pass signals to hypothalamic neurons projecting to the spinal cord (segments T1-T3). Sympathetic neurons from there project to the superior cervical ganglion which in turn signals down the ciliary nerve to the iris dilator which contracts to result in pupil dilation (Barlow and Root, 1949).

The PLR is dependent on light detection by the retina by some combination of rod, cone and melanopsin as mice with disruptions to all three photoreceptor classes showed no constriction response (Hattar et al., 2003). Under low light intensity or short light durations, PLR appears normal in mice lacking melanopsin but bright light intensities and longer light exposure show significant deficits including attenuated maximal constriction (Lucas et al., 2003). Meanwhile, *rd/rd cl* have greatly reduced sensitivity under low light but are still capable of maximal constriction at high light intensities (Lucas et al., 2003), with peak sensitivity at 479nm consistent with melanopsin responses (Lucas et al., 2001). Another study of *Opn4* $^{-/-}$ melanopsin knockout mice found they were unable to sustain constriction under bright light, losing constriction after only 20 seconds, and responses were also reduced following bright light exposure (Zhu et al., 2007). These results suggest that melanopsin is critical for responses during high intensity light, especially under conditions of long-term exposure.

Detailed studies in human patients and further mouse models have supported and expanded on these conclusions. Lall et al. (2010) recorded pupil reflex responses in *Opn1mw*^{R} mice where the human long-wave opsin replaced the *Opn1mw* gene and thus red-shifted the MWS cone population to distance its absorption from that of melanopsin (Smallwood et al., 2003). Comparisons of the *Opn1mw*^{R} and wildtype mice revealed cones and melanopsin combine to drive constriction over a wide range of irradiance from about 10^{8} to 10^{15} photons/cm^{2}/s (Lall et al., 2010), presumably with rods primarily driving responses to lower irradiances although exact estimates of thresholds differ (Yao et al., 2006). The red shifted cones were found to make major input up to about 10^{11} photons/cm^{2}/s, above which melanopsin makes a major

impact due to its resistance to bleaching (Zhu et al., 2007). Similar to kinetics observed in human studies (Gooley et al., 2012), cones were found to be critical in driving initial constriction with the contribution from melanopsin apparent only after a delay of around 0.8s (Lall et al., 2010). Studies of blind human patients lacking rods and cones have found similar contributions with melanopsin driving constriction in these individuals (Zaidi et al., 2007) and patients unable to track short-intermittent light stimuli at 480nm, even when it was relatively bright (13 log photons/cm^2/s), due to melanopsin's slower response kinetics (Gooley et al., 2012).

Aside from the evidence from pupillometry, Allen et al. (2011) recorded light responses in the PON of *Opn4* $^{-/-}$ mice and the *Opn1mw*^{R} red-shifted cone model. They found that long-wavelength stimulation targeted to the red-shifted cones could support phasic responses to abrupt light intensity changes but not sustained responses to continuous light (Allen et al., 2011). However, comparing *Opn4*$^{-/-}$ and *rd/rd cl* mice, melanopsin and rods did not account for all of the tonic activation recorded in the PON. This result was surprising given the evidence of only phasic responses from red-shifted MWS cones as it indicated that at least some cones were able to support sustained responses. In further testing in *Opn4* $^{-/-}$ they found that 460nm light over 13 log photons/cm^2/s (corresponding to 10 log photons/cm^2/s corrected for UVS absorbance) resulted in tonic responses with a distinct OFF-inhibition that must originate from the relatively rare UVS-only s-cone population (Haverkamp et al., 2005) as the only other known distinct cone population in the mouse retina (Allen et al., 2011). Their general conclusion was that, while the PON relied heavily on melanopsin to encode absolute irradiance, s-cones could respond to significantly slower changes in light than the

UVS/MWS co-expressing cone population and that the s-cones support tonic response in the PON, thought previously to be a property only of the melanopsin expressing pRGCs and rods (Allen et al., 2011).

Masking

Light exposure can result in acute effects on locomotor activity that may either suppress activity (negative masking) or enhance activity (positive masking) (Mrosovsky, 1999). Whether light causes positive or negative masking effects is phase (Pendergast and Yamazaki, 2011) and irradiance dependent. In wildtype mice negative masking occurs under high irradiance, whereas positive masking occurs under low irradiance. The range of white light irradiance which effectively, defined as between 90-10% activity suppression, induces negative masking in mice was found to be around 1 log unit from 16.5–3.4 $\mu W/cm^2$ (Thompson et al., 2008). Photoreceptor input to masking has been shown to depend on a balance of rod, cone and melanopsin input. Negative masking in *Opn4* $^{-/-}$ mice is lost given long-durations of light exposure, indicating an important role for melanopsin in maintaining masking effects (Mrosovsky and Hattar, 2003). Negative masking has also been found to be equivalent under exposure to 500nm and 365nm light, providing some evidence for both MWS and SWS contributions (Thompson et al., 2008). Finally, positive masking was absent in *rd/rd cl* mice and the range of white light intensity that induced negative masking of between a 90 and 10% activity reduction increased to over 2 log units (121.9–0.56 $\mu W/cm^2$) suggesting that rods and cones are responsible for controlling the balance of negative and positive masking effects over a range of irradiances (Thompson et al., 2008).

Entrainment/ phase-shifting

The evidence for photoreceptor contributions to entrainment responses is discussed in detail in the introduction to Chapter 3 in this thesis. To briefly summarize the existing conclusions, from behavioral studies of mouse models with various photoreceptor mutations and SCN recordings it seems that rods and melanopsin are the dominant photoreceptors in the sustained responses that drive entrainment (Altimus et al., 2010; Brown et al., 2011; Lall et al., 2010). Melanopsin has a central role under long-durations of bright light while rods have been found to be able to drive entrainment through cones even into the lower photopic range (Altimus et al., 2010; Freedman et al., 1999; Panda et al., 2003). Although there is contradictory data, evidence thus far has generally suggested that cones support mainly phasic responses in the SCN under visible light (Brown et al., 2011) and although they support phase shifts to short pulses of bright light (Dkhissi-Benyahya et al., 2007), given longer light pulses or previous light exposure, MWS cones are not able to make a significant contribution to phase-shifting responses (Lall et al., 2010).

Sleep Regulation

The role of the non-image forming system in sleep appears to be through at least two pathways. Entrainment of the circadian clock, relying on rods, melanopsin and to some extent cones as mentioned above, helps to time the sleep/wake cycle (Saper et al., 2005) but there are also phase-dependent acute effects of light exposure on sleep and wakefulness.

Acute light exposure leads to increased alertness in diurnal species including humans (Lockley et al., 2006) but induces sleep in nocturnal rodents (Borbély, 1976). Regulation of the timing of sleep has been shown to be a property of the non-image forming system as melanopsin aDTA mice with targeted ablation of melanopsin pRGCs have intact vision and free-running circadian rhythms but no entrainment of sleep rhythm or impact of acute light on sleep (Altimus et al., 2008).

The induction of sleep bouts due to light exposure during the dark period in wildtype mice was shown to be almost entirely melanopsin-dependent for 1hr pulses of white light, not relying on significant outer retinal input, and involves activation of known sleep areas such as the ventrolateral preoptic nuclei (VLPO) and superior colliculus (Lupi et al., 2008; Tsai et al., 2009). In a study using longer periods of light (3hrs), rods and cones were found to play a role in sleep maintenance over the longer light pulse but again melanopsin was dominant in the initial sleep induction immediately following the start of the light exposure (Altimus et al., 2008). As to how melanopsin might support a response independent of outer retinal input, there is evidence from SCN recordings that a population of pRGCs projecting to the hypothalamus do not receive any rod or cone input as they responded only to melanopsin activity (Brown et al., 2011). Brown et al. also found a minority of SCN neurons lacked a melanopsin-derived signal so, while a majority of pRGCs certainly receive outer retinal signaling, this is not an absolute rule.

Apart from the acute regulation of sleep, the accumulation of 'sleep drive', as assessed by EEG delta power, during wakefulness was significantly reduced in *Opn4* $^{-/-}$ mice suggesting

there is also an important role for melanopsin in the homeostatic regulation of sleep (Tsai et al., 2009).

Melatonin Induction

Melatonin is a hormone synthesized and released by the pineal gland of many mammals and provides a physiological signal of darkness widely used as a phase marker of the circadian system in human studies (Sack et al., 1998). Its release is under control of the sympathetic nervous system and synthesis is regulated both by the central clock (Shanahan and Czeisler, 1991) and acute light exposure with bright light inhibiting its production in humans (Lewy et al., 1980). The daily rhythm of melatonin is tightly linked to the circadian clock and regular melatonin administration is able to entrain free-running rats (Redman et al., 1983). Melatonin has also been found to have some sleep-promoting influence as release in the biological night helps facilitate sleep and administration of exogenous melatonin to humans has phase-dependent sleep inducing effects (Hughes and Badia, 1997; Rajaratnam et al., 2004; Wyatt et al., 2006). One of the initial pieces of evidence supporting the presence of a further class of photoreceptor to the rods and cones was that *rd/rd cl* mice, lacking both classical photoreceptors, showed normal melatonin suppression by light (Lucas et al., 1999). However, evidence from the study of human melatonin suppression under different wavelengths of light suggests that regulation is not solely dependent on melanopsin (Revell and Skene, 2007). In a later human study, long-duration exposure to bright light at 460nm and 555nm indicated that cones are initially able to suppress pineal melatonin release to the same extent as melanopsin. However the 555nm response decays quickly under continuous

illumination and melanopsin serves as the critical photopigment under bright-sustained light (Gooley et al., 2010). The study of melatonin in mice is complicated by the fact that not all strains of laboratory mice (eg C67Bl/6) secrete melatonin (Ebihara et al., 1986) which indicates that its presence is not critical for the control of sleep and wakefulness in all mammals.

Summary of trends and aims

In summary, for PLR and melatonin induction, rods contribute under dim light with cones supporting across moderate to bright light and melanopsin is critical for sustaining responses under bright light. Negative masking is similar, occurring under bright light, and as such dependent on a balance of cones and melanopsin. By contrast, evidence suggests positive masking is entirely dependent on rod and cone input. Entrainment and sleep behaviors seem slightly more complicated; as discussed above, rods play a wider role in entrainment responses into moderate light intensities with melanopsin supporting bright light entrainment and only a limited role is found for cones under natural light conditions. Acute sleep regulation is largely melanopsin-dependent with evidence also suggesting an important role for melanopsin in the accumulation of sleep drive during waking.

It should not be surprising that studies have found slightly different balances in photoreceptor contributions to the various NIF outputs as a study of photic thresholds of entrainment, masking and PLR, found that the threshold for circadian entrainment was between 1-2 log units lower than the light intensity required to elicit a masking or PLR

response and that the spectral sensitivities also differed (Butler and Silver, 2010). This result supports the idea that different mechanisms are responsible for these NIF behaviors as does indications of different balances of rod and cone input to M1 and M2 pRGC subtypes (Schmidt and Kofuji, 2010) given these subtypes project differentially to the SCN and PON (Baver et al., 2008). Butler and Silver also found that spectral sensitivity at the entrainment threshold pointed to rods as the primary photoreceptor in determining the threshold intensity. This is consistent with our examination of threshold of entrainment in Chapter 3 that also found rods to be the dominant photoreceptor.

In this chapter we examine the impact of UVS cone loss on UV sensitivity of the PLR and phase-shifting light responses in the context of expected cone-contributions to these NIF functions. We also examine retinal c-fos induction to determine if there is a loss of response gradient in the *Opn1sw* KO as would be predicted by the wildtype c-fos results in Chapter 4.

Results

8.3 UV phase-shifting sensitivity in *Opn1sw* KO mice

To examine the impact of UVS cone loss on phase-shifting responses to UV light we generated irradiance response curves (IRCs) to UV light pulses as was done with retinal degeneration models in Chapter 4. *Opn1sw* wildtype controls and knockout animals were given 15 minute pulses of 365nm light at CT16 over a range of 5 light intensities and the light induced phase delay was determined for each animal (Figure 8.1). The responses of the *Opn1sw* KO indicated a significant attenuation of UV sensitivity associated with the absence of the UVS opsin (Figure 8.2). When the average IC50 for each genotype was determined (half-sensitivity based on IRC fitting to individual animals, in all cases R^2>0.82), the IC50 for the Opn1sw KO was significantly lower than the wildtype (2-tailed Student's t-test, p = 6.2 x10^{-6}) representing a drop of ~15 fold in the KO (Figure 8.3). Residual sensitivity of 6.8% in the *Opn1sw* KO, as determined from IC50 comparison to wildtype, is close to the combined residual sensitivity expected from melanopsin and rhodopsin α-band absorbance at 365nm (4% and 2% respectively, see Chapter 4, Table 4.1).

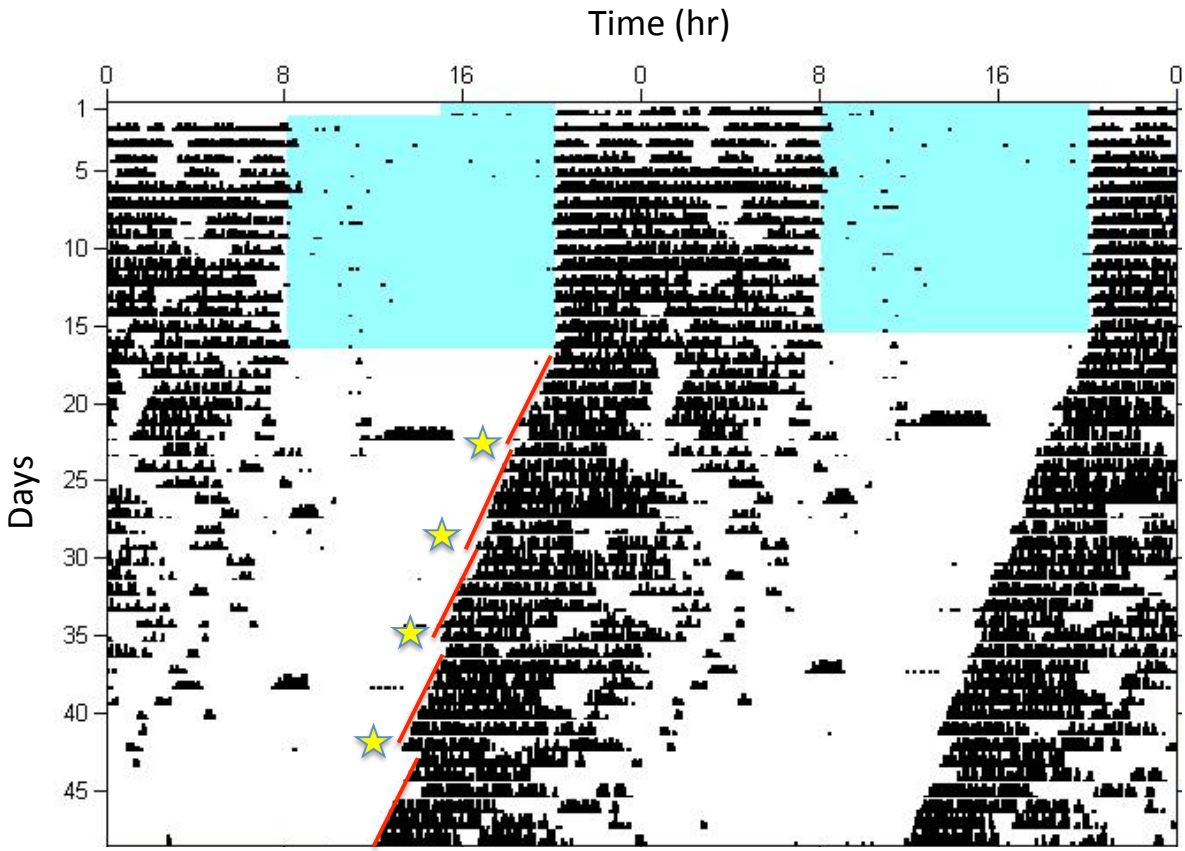

Figure 8.1 Generation of irradiance response curve Free running animals in DD are exposed to light pulses (indicated by yellow stars) of increasing intensity. Using ClockLab software, lines fit to activity onset pre and post light pulse (lines in red, these are examples to illustrate fit and not onset fits done using ClockLab for analysis) indicate the change in onset due to the light exposure and allows comparison of the effect of light on the activity rhythm set by the SCN based central clock.

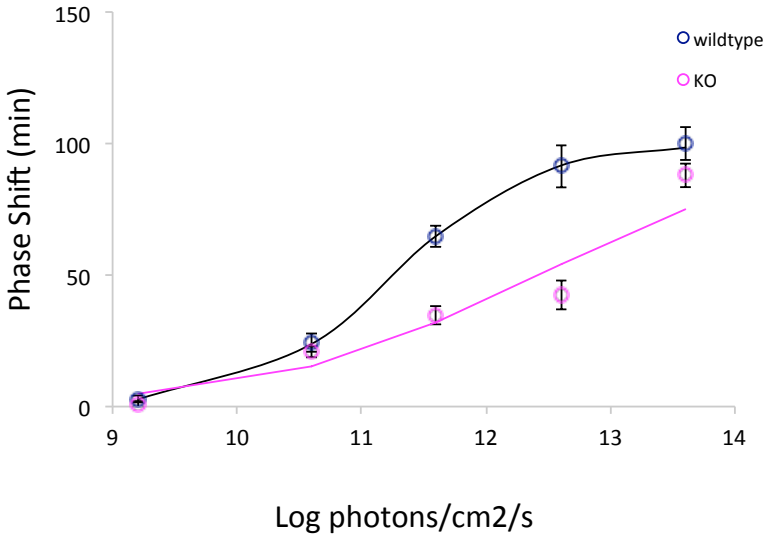

Figure 8.2 UV Phase-shifting Irradaince Response Curves in *Opn1sw* KO and WT mice Irradiance response curves (IRCs) for phase-shifting responses ± SEM of wild-type (n=6) and *Opn1sw* KO (n=6) mice to UV light (15 min pulse at CT16, 365 nm UV LEDs). Details of methods provided in Methods Chapter 2.

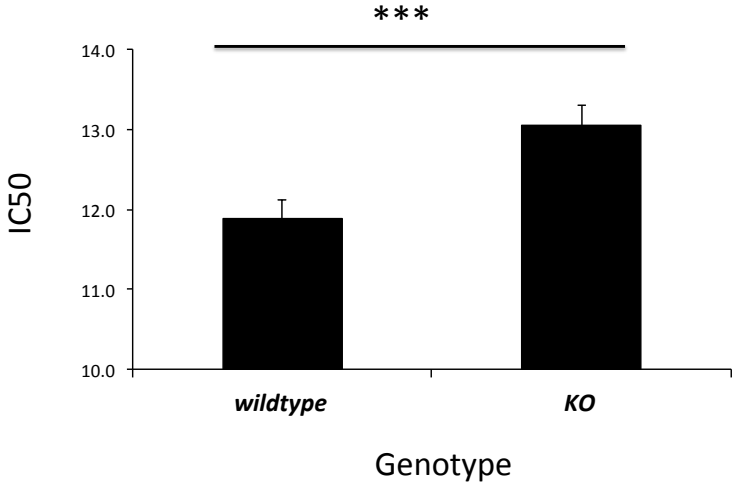

Figure 8.3 UV Phase-shifting IC50s for *rd/rd* and *rd/rd cl* Sensitivity to UV light was assessed by IRC IC50 based on individual IRC fitting using Excel (Microsoft) to fit a four parameter sigmoid curve using the method of least squares, in all cases R^2>0.82 (See Methods Chapter 2). *Opn1sw* KO mice lacking UVS opsin show a significant attenuation of UV sensitivity compared to wildtype (2-tailed Student's t-test, p=6.2 x10^{-6}). *=p<0.05, **=p<0.01, ***=p<0.005. Bars represent mean values +/- SEM.

As seen in Figure 8.2, the range of intensity for the light pulses was between 9.2 and 13.6 log photons/ cm^2/ s, over a log unit lower minimum than was used for the *rd/rd* and *rd/rd cl* IRC. Both the KO and wildtype displayed a significant phase shift to the 10.6 log photons/ cm^2/ s light intensity and the magnitude of the phase-shift was not different between the genotypes (2-tailed Student's t-test p=0.46). This result could be due to an amount of phase delay generated from our method of light pulsing as, if this was the case, then there would be a residual phase shift no matter how low the light pulse intensity that would be expected to be independent of genotype. To resolve this question, we performed a further light pulse at a lower light level. As neither genotype displayed a significant phase-shifting response at 9.2 log photons/ cm^2/ s, this suggests that the responses at 10.6 log photons/ cm^2/ s did represent phase-shifting responses to only the light pulse and further that this responses was not dependent on UVS cone opsin.

8.4 Intensity dependent impairment of pupil constriction under UV light in *Opn1sw* KO

In Chapter 6 we found no difference in the pupil response of *Opn1sw* KO and wildtype to 480nm light. We investigated if there were any differences in pupil constriction responses to UV light at a low (0.5 $\mu W/cm^2$ or ~11.9 log photons/cm^2/s), medium (6 $\mu W/cm^2$ or ~13.0 log photons/cm^2/s) and high (35 $\mu W/cm^2$ or ~13.8 log photons/cm^2/s) intensity UV light. Constriction and recovery curves appeared most different under low UV (Figure 8.4A) with the pupil constriction occurring at a similar rate initially but then leveling off quickly to a

lower maximal constriction in the KO before recovering after the light pulse at a similar rate to the wildtype through to the end of the 30-second recording. Under the medium light condition, the KO again appeared to constrict to a lesser extent than the wildtype but the difference was much smaller (Figure 8.4B). The pupil response to high intensity UV light showed very similar constriction for KO and wildtype animals (Figure 8.4C). When maximal constriction was examined at the timepoint just before the light turned off (12s), a significantly higher constriction was found for the wildtype animals for low UV (2-tailed Student's t-test p=0.0066) while no difference was found between the genotypes for the medium (2-tailed Student's t-test p=0.49) or high (2-tailed Student's t-test p=0.98) UV conditions (Figure 8.5). The pupil constriction increased for both genotypes from the low to medium to high light intensities with the KO increasing from 41.8% to 19.1% from low to high UV intensities (percentage indicating % pupil area relative to full dilation before light-on) and the WT from 26.2% to 19.2%. The constriction data for high and low UV one second each side of the point of light exposure start was examined to look for differences in response latencies but no significant differences in the time of initial constriction were noted (Figure 8.6).

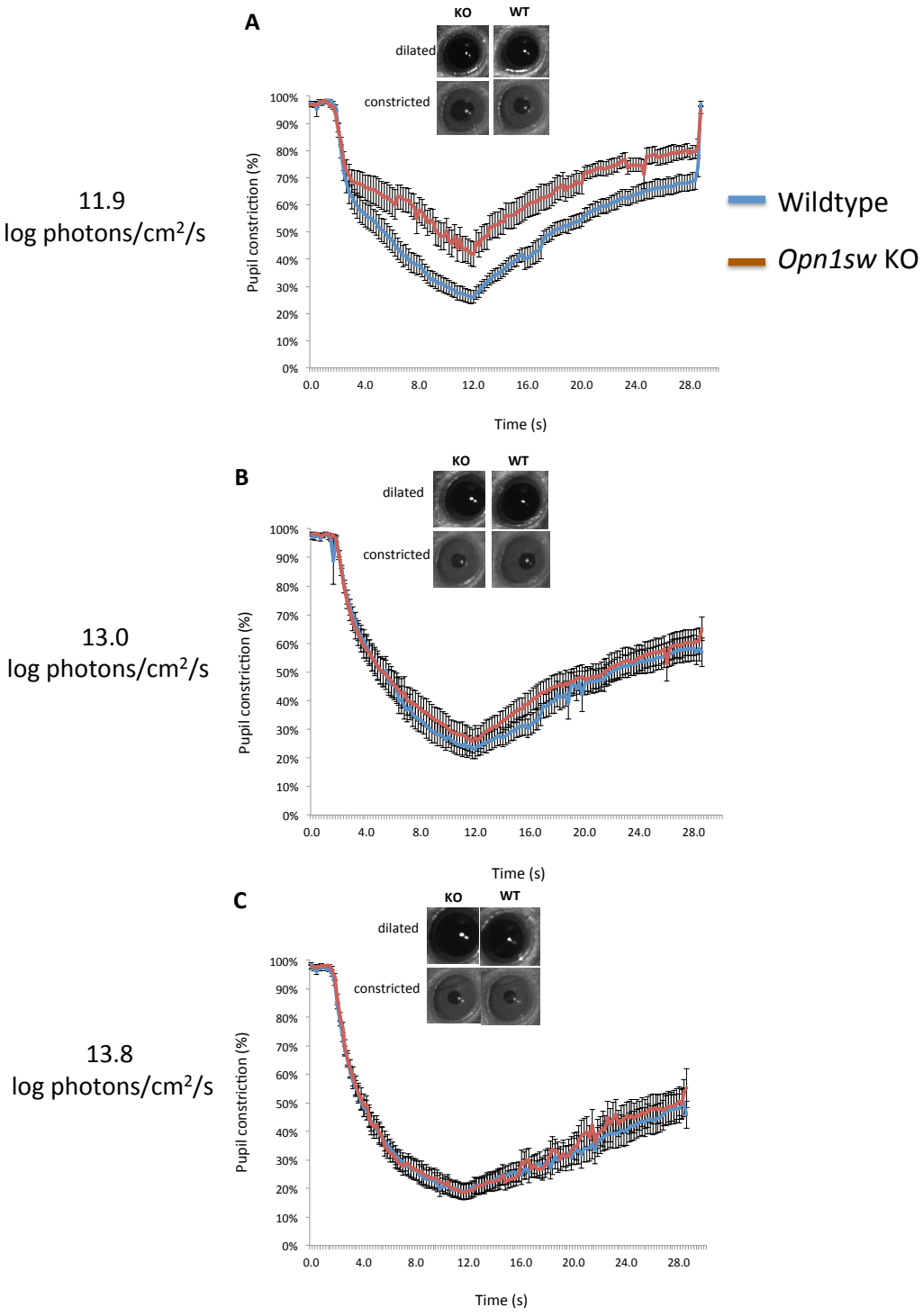

Figure 8.4 Pupillary constriction in response to increasing intensities of UV light in the *Opn1sw* KO PLR was examined in 2 batches of *Opn1sw* KO (n=6) and wildtype (n=6) at three different intensities of UV light: **(A)** low (0.5 µW/cm^2 or ~11.9 log photons/cm^2/s), **(B)** medium (6 µW/cm^2 or ~13.0 log photons/cm^2/s) and **(C)** high (35 µW/cm^2 or ~13.8 log photons/cm^2/s).

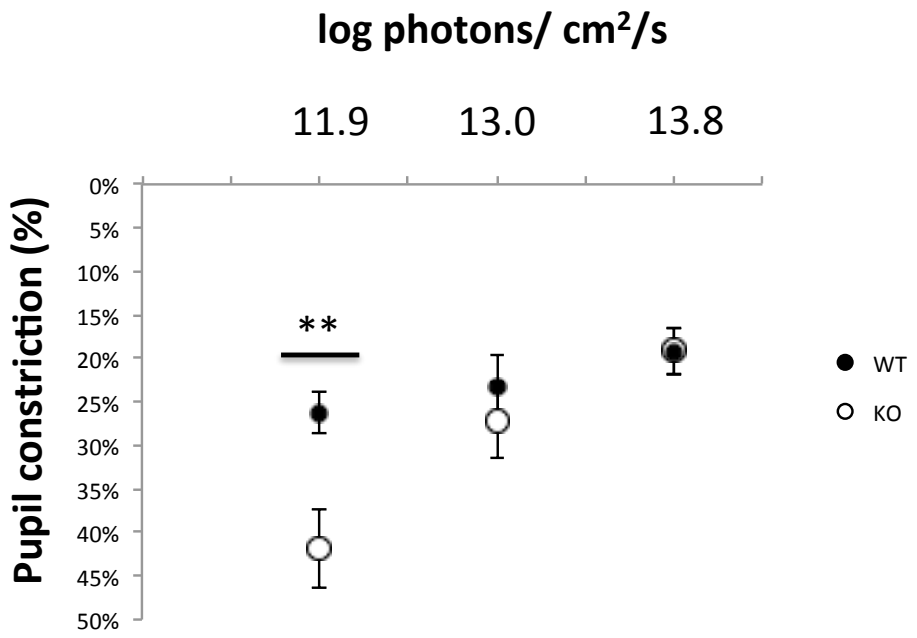

Figure 8.5 Irradiance dependent differences in maximum pupil constriction in *Opn1sw* KO Comparison of maximum pupil constriction at the end of the 10sec light exposure (12 sec on constriction profiles in Figure 8.4) relative to dilated dark state pre-light found difference between mean constriction at this point increased with decreasing irradiance with a significant difference at the lowest UV light intensity (2-tailed Student's t-test $p=0.0066$). **= $p<0.01$

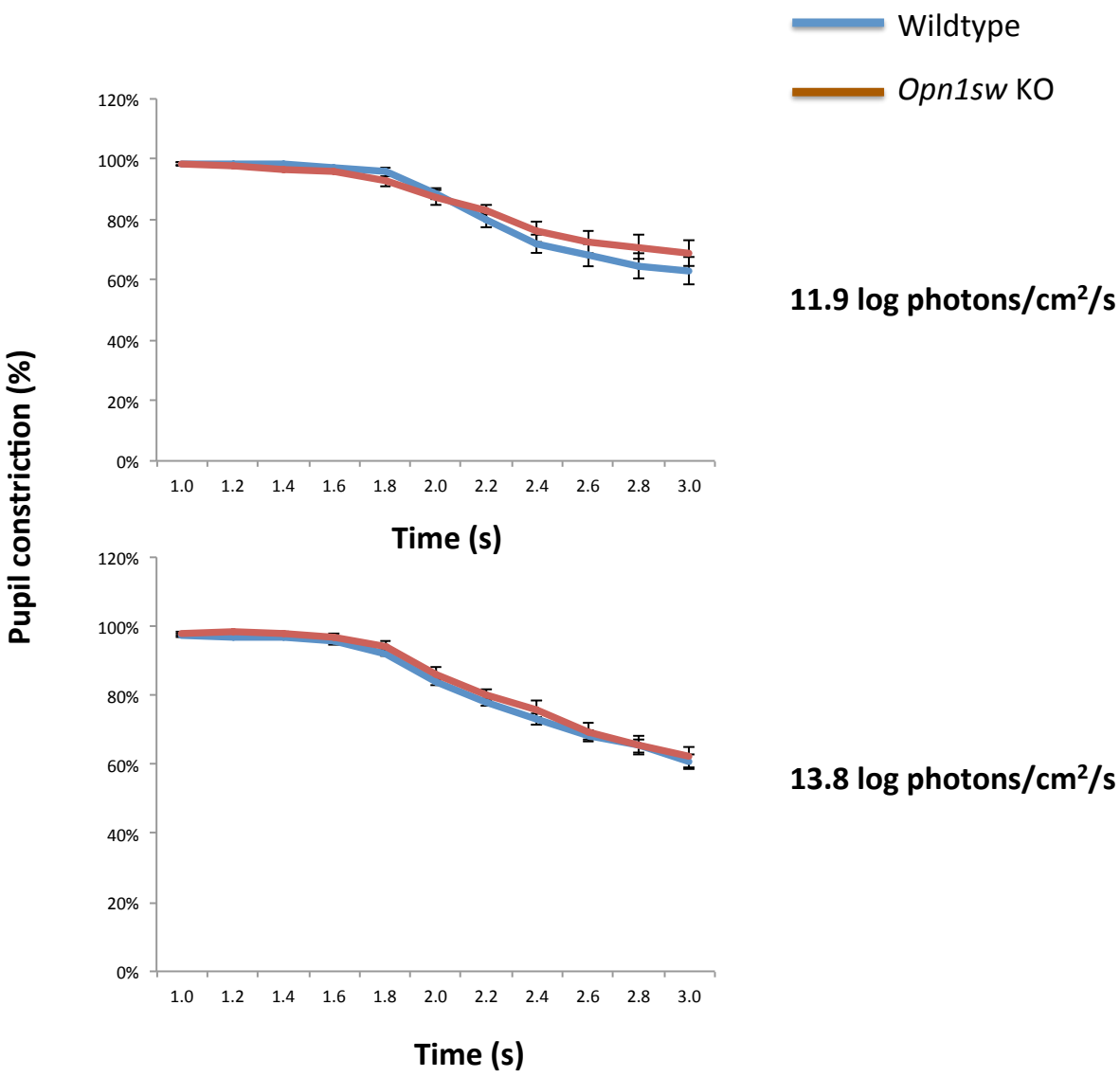

Figure 8.6 No difference in initial constriction kinetics between *Opn1sw* KO and WT Closer examination of the first second of light exposure found no obvious differences in initial constriction profiles of KO and WT animals (connected scatter-plots shown above) under the low or high UV irradiance condition from Figure 8.4.

8.5 Retinal c-fos expression follows UVS opsin gradient under UV light in wildtype but not *Opn1sw* KO

We previously observed that UV, but not white light, pulses induced a dorsal- ventral expression gradient of the immediate-early gene c-fos in the wildtype mouse retina that mirrored the gradient of the UVS cone opsin expression (Chapter 4 Figure 4.10). We expected that we would see a similar result in the wildtype, but not *Opn1sw* KO animals due to the absence of UVS opsin. Without UVS, the pattern of c-fos expression in the KO retina must be due to absorption by some combination of rhodopsin, MWS cone opsin and melanopsin. Indeed, we observed that, following white light pulses, the c-fos expression was largely even across the retinas of both wildtype and KO animals (Figure 8.7A) while following UV light pulses, only the retina of wildtype mice showed a strong gradient of c-fos as would be expected from UVS opsin being the major contributor to c-fos activation in the RGCs (Figure 8.7B).

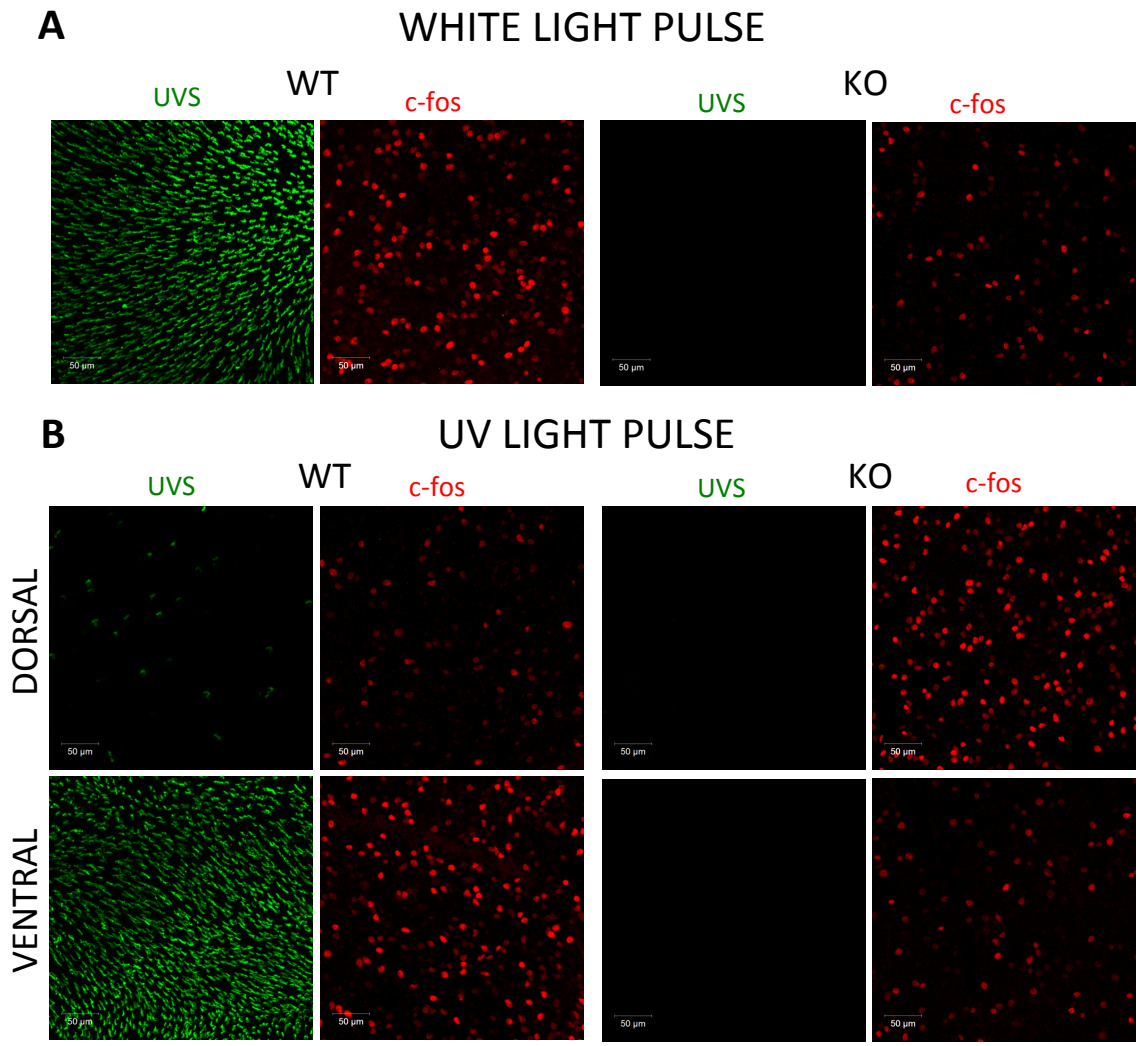

Figure 8.7 c-fos induction in *Opn1sw* following UV light shows no gradient Whole-mounted *Opn1sw* KO and WT retina were stained with UVS (green) and c-fos (red) antibodies following **(A)** a 30-minute bright 500lux white light pulse (approximately 14.7 log photons/ cm^2/ s) and **(B)** a 30 minute UV light pulse at Z16 of 12.6 log photons/ cm^2/ s. After the white light pulse, high levels of c-fos expression were found across the retina of both genotypes and did not show a significant gradient in response. Contrastingly, UV light resulted in a clear dorsal-ventral gradient of c-fos induction in the WT but not KO retina. Scale bars=50µm.

8.6 Dorsal ventral gradient of c-fos positive cells in wildtype retina following different intensity UV light pulses

To quantify the effects of UV and white light pulses on the number and distribution of c-fos positive (+) cells in *Opn1sw* KO and wildtype mice we performed counts on the retinas of mice pulsed with one of two light intensities. Retina from three different mice for each genotype were collected following pulses of high UV (5.0 μW/cm^2, ~13 log photons/ cm^2/s), low UV (0.05 μW/cm^2, ~11 log photons/ cm^2/s), high white (100 lux, ~31 μW/cm^2, ~14 log photons/ cm^2/s) or low white light (1 lux, ~0.31 μW/cm^2, ~12 log photons/ cm^2/s) at CT16. The values of UV light intensity were chosen based on our phase-shifting IRC to UV light to be at points of high and lower circadian response (Figure 8.2) while the white light values were chosen using literature white light wildtype mouse IRCs to be at roughly similar points of the white light phase-shifting curve (Foster et al., 1991; Sharma et al., 1999). For each retina collected, 3 confocal Z-stack images were taken of non-overlapping areas in each of the dorsal and ventral retina with the retinal location identified by the UVS gradient in the case of *Opn1sw* wildtype or the equivalent β-gal staining in the case of the *Opn1sw* KO (Figure 8.8). We were unable to successfully co-label retina with c-fos and melanopsin antibodies. Both antibodies were raised in rabbit and the alternative antibodies we tested did not result in comparable staining. In Chapter 4, a blocking process developed by Dr. Steven Hughes did allow co-labelling to specifically count c-fos positive pRGC but this was not successful with the *Opn1sw* retina thus only general c-fos positive cells were analysed. Two layers of c-fos positive cells were observed in each retina and these were combined in the Z-stacks for total retinal c-fos expression. Automated counts of c-fos positive cells in each

image were found using ImageJ software and verified by manual counts of randomly chosen areas. Coloured pixel area data was also collected for each image and trends in this data matched those found in cell counts (data not shown).

There were significant differences in the average number of c-fos (+) cells in the dorsal compared to ventral retina for *Opn1sw* wildtype mice for both high (2-tailed Student's t-test p=0.0099) and low (2-tailed Student's t-test p=0.00046) UV light conditions but not for high (2-tailed Student's t-test p=0.085) or low (2-tailed Student's t-test p=0.31) UV in the *Opn1sw* KO (Figure 8.9). Under white light, dorsal and ventral retina counts were similar in both wildtype and KO for both light intensities (Figure 8.10). Total numbers of c-fos positive cells were higher for both light intensities under white light compared to the UV intensities with high intensity white light counts much higher. In both genotypes, there was an obvious trend of high intensity pulses resulting in higher total c-fos positive cell counts than the low intensity pulses, although this trend was only near significance in all cases other than between white light in the wildtype (2-tailed Student's t-test p=0.048).

Comparing counts in the upper or lower retina between KO and wildtype within the same light type and intensity found no differences under white light but under low UV light, ventral counts were significantly higher (2-tailed Student's t-test p=0.023) and dorsal counts significantly lower (2-tailed Student's t-test p=0.024) in the wildtype compared to the KO. Under the high UV condition, ventral counts were very similar (2-tailed Student's t-test p=0.99) but again dorsal counts were lower in the wildtype although this trend was not significant (2-tailed Student's t-test p=0.099).

Across all genotypes and conditions there was a general trend of higher ventral counts than compared to the dorsal counts, ignoring the large significant difference for wildtype following UV exposure already mentioned. This trend was non-significant except for a weak significance for the KO under low white light (2-tailed Student's t-test p=0.44). As it is such a general trend across the data set, this is very likely due to the light used to pulse the mice being situated above the cages. From above, more of the light would be expected to hit the bottom of the mouse retina than the top resulting in the observed consistent small difference in activated cells irrespective of genotype or light type.

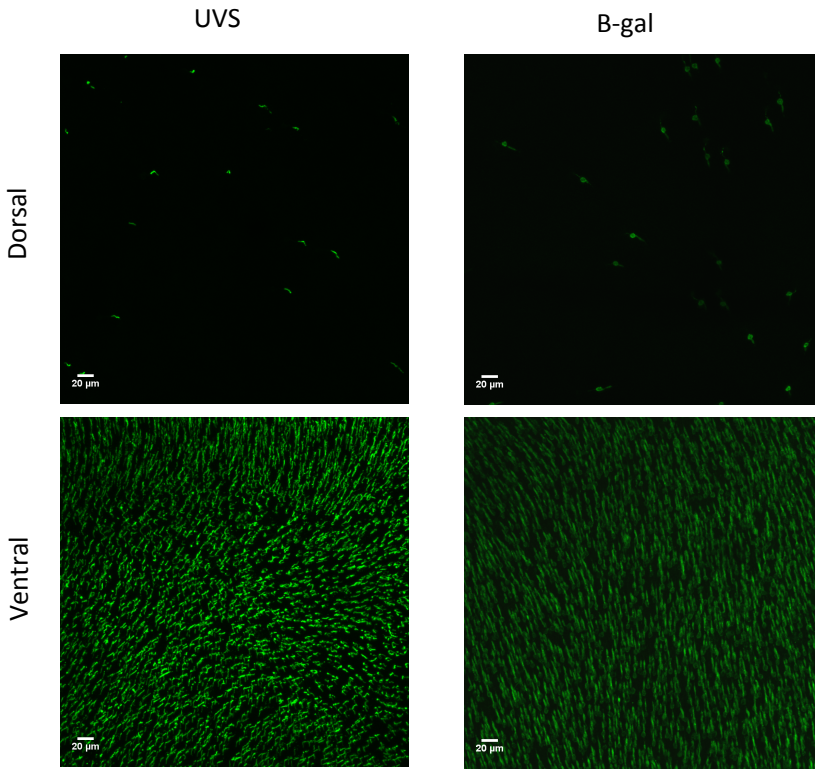

Figure 8.8 β-gal expression in UVS-expressing cones of the *Opn1sw* KO β-gal expression due to the LacZ reporter in the target vector inserted in place of the *Opn1sw* gene allows determination of retinal position in KO retina against the dorsal-ventral gradient as the UVS gradient allows in the WT. Scale bars=20µm.

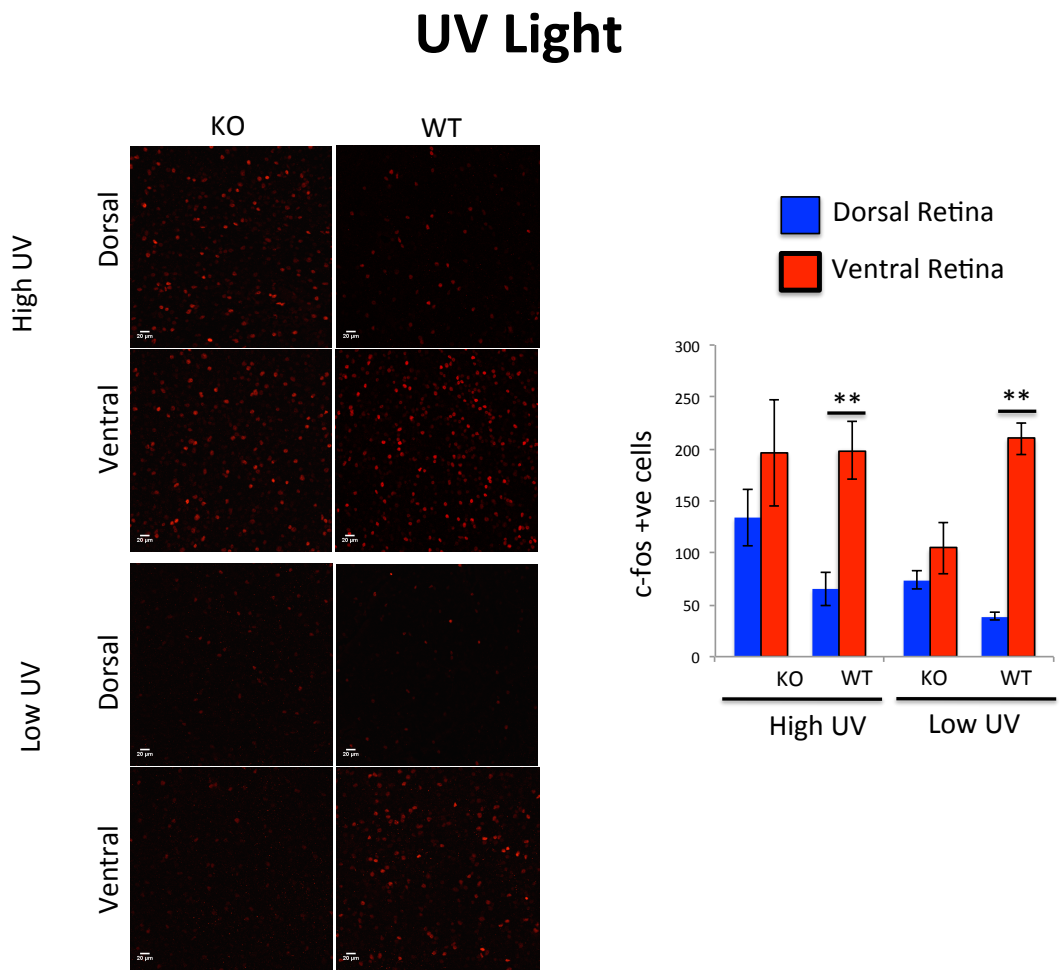

Figure 8.9 Patterns of c-fos induction differ between Opn1sw KO and WT animals following low and high irradiance light pulses of UV light *Opn1sw* KO and WT animals were exposed to 30-minute light pulses of higher irradiance UV light (5.0 μW/cm^2, ~13 log photons/ cm^2/s) or lower irradiance UV light (0.05 μW/cm^2, ~11 log photons/ cm^2/s) at CT16. Retina's were collected 30-mintues following the end of light pulse, whole-mounted and stained with UVS (green, WT) or β-gal (green, KO) and c-fos (red, both genotypes). n=3 for both genotypes at each light intensity and 3 images where taken of both upper and lower retina for cell counting in every retina. UV light induced significant greater c-fos induction in the ventral retina of WT mice under both high (2-tailed Student's t-test p=0.0099) and low (2-tailed Student's t-test p=0.00046) irradiance. No significant difference was found for KO retina. Comparing between light irradiances, ventral counts were significantly higher (2-tailed Student's t-test p=0.023) and dorsal counts significantly lower (2-tailed Student's t-test p=0.024) in the wildtype compared to the KO under low UV. Under the high UV condition, ventral counts were very similar (2-tailed Student's t-test p=0.99) but again dorsal counts were lower in the wildtype

although this trend was not significant (2-tailed Student's t-test p=0.099). *=p<0.05, **=p<0.01, ***= p<0.005. Bars represent mean values +/- SEM. Scale bar=20µm for all images.

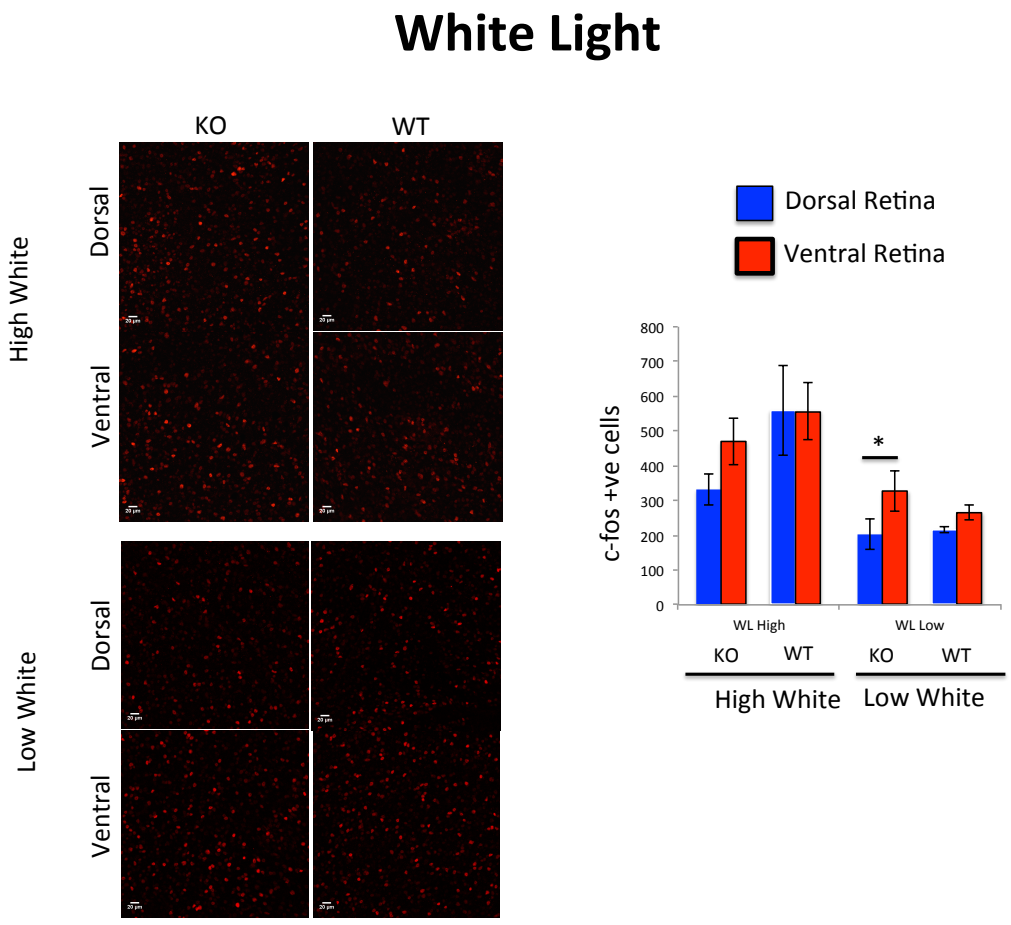

Figure 8.10 Similar patterns of c-fos induction in retina of *Opn1sw* KO and WT animals following low and high irradiance light pulses of white light *Opn1sw* KO and WT animals were exposed to 30-minute light pulses of higher irradiance white light (100 lux, ~31 µW/cm^2, ~14 log photons/ cm^2/s) or lower irradiance white light (1 lux, ~0.31 µW/cm^2, ~12 log photons/ cm^2/s) at CT16. Retinae were collected 30-mintues following the end of light pulse, whole-mounted and stained with UVS (green, WT) or β-gal (green, KO) and c-fos (red, both genotypes). n=3 for both genotypes at each light intensity and 3 images where taken of both upper and lower retina for cell counting in every retina. The only significant difference in c-fos positive cell counts was found between dorsal and ventral retinal counts in KO mice under low white light (2-tailed Student's t-test p=0.044). *=p<0.05, **=p<0.01, ***= p<0.005. Bars represent mean values +/- SEM. Scale bar=20µm for all images

Discussion

8.7 UVS cones are critical for phase-shifting responses to UV Light in mice

The significant difference in phase-shifting sensitivity to UV light between the *Opn1sw* KO lacking UVS opsin expression and wildtype littermate controls confirms a central role for UVS cones in driving this NIF response. This is an intriguing result given that there is significant evidence that MWS cones do not make a large contribution to phase-shifting.

Mice with the *cl* mutation lose almost all MWS opsin as well as much of the UVS as seen in our staining of the *cl* (Chapter 4, Figure 4.11). However, 15 minute light pulses of 509nm light in the *cl*, the same duration of light pulse used to examine UV phase-shifting here, were found not to differ from wildtype mice up to response-saturating light intensities (Freedman et al., 1999). More recently, in the red-shifted mouse model with human LWS opsin in place of the mouse MWS, significant phase shifts to 15-minutes of 650nm light targeted to the shifted cone opsin were only generated for intensities greater than 13 log photons/cm^2/s (Lall et al., 2010). Compared to responses to light pulses at 500nm, this represented a 1000 fold drop in sensitivity suggesting very little role for cones in this response and examination of a cone-only *Gnat1*$^{-/-}$ *Opn4*$^{-/-}$ mouse model confirmed that cones could not reliably drive stable activity entrainment responses even to very bright irradiances (Lall et al., 2010). However, when a 15-minute pulse was presented as fifteen 1 minute pulses with 2 minutes of dark separating each, the phase-shifting response to long-wavelength light was greatly enhanced

suggesting that it is the length of continuous light that prevents cone responses from resulting in significant responses under most intensities (Lall et al., 2010). Somewhat contradictory evidence was found in a MWS coneless mouse model, in addition to being slower to adjust to light-cycle delays, phase shifts were attenuated under bright 530nm light though very little difference was found at 480nm (Dkhissi-Benyahya et al., 2007). A follow-up study in the same model again found phase-shifting deficits to short pulses of very bright light (2.8×10^{14} photons/cm^2/s) (Dollet et al., 2010). The results of this model are therefore in somewhat contradiction to those of the red-shifted cone model which may be model dependent as effects on the other opsins were reported in the *TRβ*$^{-/-}$ MWS-model (Dkhissi-Benyahya et al., 2007). However, even in the MWS coneless model, the differences in light pulses to 530nm were relatively minor and, when modeled, indicated a relative contribution ratio of melanopsin: MWS of 1:1.12 at longer wavelengths in wildtype mice (Dkhissi-Benyahya et al., 2007). Therefore, the bulk of evidence supports the idea the MWS cones make fairly limited photoentrainment except for short-duration pulses. Providing a good explanation for these results, recordings in the SCN have found prior light exposure greatly diminishes cone responses (Brown et al., 2011; Drouyer et al., 2007), thus it is likely that longer duration light pulses would similarly limit cone contribution but short pulses with darkness in-between would allow cones to recover to make contributions at each intermittent pulse.

It had been assumed, given the co-expression of cone opsins in the mouse, that UVS opsin would follow a similar pattern to MWS in terms of entrainment contribution. Our data, however, suggests that UVS cones are the primary factor in driving phase shifts to 15-minute

pulses of UV light. It is not immediately clear how UVS opsin could drive phase shifts in the co-expressing cones to a much greater extent than MWS in the same cones. One explanation is related to expression levels as it is established that UVS expression is higher than MWS in the mouse (Applebury et al., 2000; Szél et al., 1996) and it could be that this high opsin level results in greater relative SCN signals from UVS than MWS. The role of UVS indicated by our data is much greater than the about 3x greater expression levels seen in the retina or the nearer to 4x higher sensitivity measured at the cornea (Lyubarsky et al., 1999) which argues against this explanation. Another possibility is that the phase-shifting response is due to the UVS-only s-cones which make up around 4% of total cones (thus ~8000 across retina (Lyubarsky et al., 2008)) and connect to a dedicated bipolar cell (Haverkamp et al., 2005). These cones thus represent a separate cone pathway to the larger cone population expressing UVS and MWS to varying extents across the retina. There is evidence that s-cones drive tonic responses to light in the PON different from the normal phasic cone responses (Allen et al., 2011). Sustained responses of melanopsin in the SCN are thought to be indicative of its ability to support entrainment (Brown et al., 2011) and, if s-cones were also able to drive more sustained responses in the SCN as well as the PON, would be well suited to support entrainment in a way that the phasic responses of the majority of cones could not. A potential objection to the s-cone theory for the basis of UVS phase-shifting is the rarity of the s-cones in the mouse as they are such a small proportion of cones which themselves are only ~3% of the total retinal photoreceptors (Jeon et al., 1998). However, it is clear from our study of *rd/rd* and *cl* phase shifting that large populations of cones are not required to drive robust responses and a study of *Opn4*$^{aDTA/+}$ mice found that only a small population of functional pRGCs is sufficient to drive full pupil constriction (Güler et al., 2008). A more

significant issue is that it is not confirmed if the s-cone/ blue-cone bipolar cell pathway drives significant sustained responses in the SCN (Brown et al., 2011). It may also be that UVS cones form specialized connections with different sub-populations of pRGCs, as there is evidence of differential input of photoreceptor classes to specific types of pRGC (Schmidt and Kofuji, 2010), or that UVS opsin input results in different pRGC signals to the SCN than those from MWS opsin. Our UVS knockout certainly affects s-cones in addition to the co-expressing m-cone population but without more evidence of pRGC input or SCN signaling it is not possible to determine if s-cones are indeed responsible for the very high UVS contribution we observed.

8.8 Rods may support UV phase-shifting a low light intensities

Our data also indicated that, while UVS absorption is responsible for the majority of phase-shifting sensitivity at 365nm, the 10.6 log photons/cm^2/s light intensity did not result in significantly different phase shifts between *Opn1sw* wildtype and KO mice. We previously observed that both *rd/rd* and *rd/rd cl* mice lacked phase-shifting responses at the 10.6 log photons/cm^2/s although wildtype mice could respond (Chapter 4 Figure 4.2). This was despite there being no significant difference between *rd/rd* and wildtype IC50s fit to UV phase-shifting IRCs. This suggested that, while rods were not the dominant photoreceptor in UV phase-shifting sensitivity, the presence of rods was the important factor in phase-shifting to low intensity UV light. This conclusion would also explain why the loss of UVS did not result in lower responses to the 10.6 log photons/cm^2/s light intensity in this experiment as the rhodopsin levels and rod structure in the Opn1sw KO are unaffected (Chapter 6, Figure

6.1). Even though this explanation fits the data from both sets of mouse models, as mentioned in the Chapter 3 discussion of the *rd/rd cl* and *rd/rd*, the residual sensitivity of rods at 365nm is only about 2% based on the standard photopigment absorption template so even the ~20min phase shifts observed in the wildtype and KO at the 10.6 log photons/cm^2/s here are quite large if only this low residual sensitivity is responsible.

8.9 UVS cones extend cone contribution to PLR into UV

While the major role of UVS cones in supporting phase-shifting response is fairly surprising, the role of UVS cones in supporting PLR indicated here is consistent which the general view of cone contributions to PLR. We found a significant difference between KO and wildtype under moderate UV light of about 12 log photons/ cm^2/s at the position of the mouse's eye, the lowest irradiance that we could examine with the UV LEDs in our pupillometry set-up, but this difference in maximal constriction disappeared as the intensity was increased towards very bright 13.7 log photons/ cm^2/s. Bright white light produces maximal constriction in the *rd/rd cl* lacking rods and cones (Lucas et al., 2003) and melanopsin and MWS cones have been shown to combine to support pupil responses over a wide range of intensities, with melanopsin important in brighter light (Lall et al., 2010). Given the established co-expression of UVS and MWS in the majority of mouse cones (Applebury et al., 2000), UVS would be expected to be drive similar contributions to those found for cones in the visible wavelengths. In a previous study, the point where melanopsin was found to begin to dominate over cone contribution was around 11 log photons/cm^2/s (Zhu et al., 2007) but this was in the visible wavelengths where melanopsin sensitivity is much higher than at

365nm light used here. It is therefore not surprising that melanopsin could not fully compensate for UVS cone loss at 12 log photons/ cm^2/s of UV light but, as the intensity was increased to very bright levels, the residual sensitivity of melanopsin was sufficient to drive similar responses in both wildtype and KO animals. Our results differ from a previous study that reported the magnitude of PLR to UV light matched that of green light and was not dependent on cone loss (Yao et al., 2006). However, there are several issues with this study including that the model of cone loss (*cpfl 1*) has also been reported to also contain very abnormal retinal morphology from early in developmental (Chang et al., 2009) and that their results appear to discount any role for melanopsin in the PLR which is in disagreement with the vast majority of other literature.

We were not able to observe any differences in response kinetics with our pupillometry set up. Given the loss of UVS cones, it might be expected that the KO mice relying only on residual melanopsin absorption rather than a cone response for constriction would begin to respond slightly slower following the start of light exposure as the melanopsin response is thought to be significantly slower than that of cones (Berson et al., 2002). Differences in initial PLR kinetics between cone and melanopsin responses have been observed previously for both human and mice (Gooley et al., 2012; Lall et al., 2010). However, given the PLR response latency of melanopsin in the mouse has been estimated at less than a second (Lucas et al., 2001), it is possible that the resolution of our experiment was not sufficient to pick up this difference. It is also possible the MWS cone opsin, which is expected to be present and functional in the UVS KO and also has very low residual sensitivity at 365nm, is able to contribute the faster cone response kinetics in the KO.

8.10 UVS cones drive retinal c-fos induction to UV light in the mouse

In Chapter 4, we described that white light pulses in the wildtype mouse produced an even gradient of c-fos expression but UV light exposure resulted in a strong dorsal-ventral gradient of c-fos positive cells that followed the UVS opsin expression. To confirm the association between UVS opsin and the observed expression gradient, we performed light pulses in the *Opn1sw* KO. Supporting the previous results, UV light resulted in a fairly even distribution of c-fos in the KO retina while UV light in littermate wildtype controls again showed a dorsal-ventral gradient. Quantifying the number of c-fos positive cells, the wildtype retinas had significantly more c-fos positive cells in the ventral relative to dorsal retina following both high and low intensity UV pulses, while counts across the knockout retina did not find significant regional differences.

Interestingly, comparing the dorsal retinal counts of c-fos positive cells in wildtype and KO animals under both high and low UV light revealed a trend of lower dorsal counts in the wildtype compared to the KO. The higher ventral counts in the wildtype under low UV is unsurprising given the presence of UVS opsin in these animals resulting in increased sensitivity but why the presence of UVS opsin might result in lower dorsal counts under UV light in the wildtype is less clear. The lower dorsal count trend was not observed under either of the white light conditions suggesting it is a UV specific response tied to the UVS opsin. A negative inhibition by cones was suggested in human melatonin regulation (Figueiro et al., 2004), by our examination of dim entrainment threshold and in our analysis of c-fos positive

M1 and M2 cells where a greater percentage of dorsal retina M1 pRGCs responded in the *rd/rd cl* relative to the wildtype under UV light (see Chapter 4). However, examination of the phase-shifting response in the red-shifted MWS cone model did not find any indication of m-cone related inhibition (Lall et al., 2010). As with the M1 pRGC data in Chapter 4, the change in dorsal c-fos positive cell counts between KO and wildtype under UV light could again be explained by a level of UVS cone inhibitory signalling. In the dorsal retina of KO mice, the lack of UVS means that c-fos activation in response to UV light must be due to residual MWS, rod and melanopsin absorbance and it is more likely due to melanopsin or rods given the even gradient seen across the retina. In wildtype animals, the level of UVS expression in the dorsal m-cones is very low and s-cones expressing only UVS are rare (Applebury et al., 2000; Haverkamp et al., 2005; Szél et al., 1996). This balance means, as opposed to the ventral region, the dorsal retina of wildtype mice have a much greater proportion of c-fos activation due to residual melanopsin and rod sensitivity in the UV light condition, as occurs in the KO. If UVS activation, perhaps in s-cones, inhibits one of the other photopigment pathways then this would offer a reasonable explanation as to why the dorsal retina of the wildtype has fewer c-fos positive cells than the KO. This inhibition would be insignificant in the ventral wildtype retina due to the positive contribution of very high UVS expression in m-cones. That this response consistent with the observed response in M1 pRGCs (Chapter 4 Figure 4.11), both in terms of the trend being in the dorsal retina and only under UV light, is strong evidence this is not an artefact of the *Opn1sw* KO model and indeed tied to the loss of the UVS cone opsin. A model of cone inhibition based on the evidence in this thesis is presented in Chapter 9.

We observed two layers of c-fos positive cells in the retina (also seen in sham pulses in wildtype, Figure 4.10A) which is consistent with previous reports of light-induced c-fos expression in amacrine and RGCs in the INL and GCL respectively (Hannibal et al., 2001). c-fos expression in the SCN has been strongly linked to circadian phase-shifting sensitivity and occurs in locations linked to the projections of the retino-hypothalamic tract (RHT) (Colwell and Foster, 1992; Kornhauser et al., 1990; Morin and Allen, 2006; Rea, 1992; Rusak et al., 1990). In the retina, c-fos expression has been found at dawn and following light stimulation in the dark (Yoshida et al., 1993). Light stimulation was found to activate both PACAP and non-PACAP containing RGCs in the mouse retina, though expression in the PACAP-containing RGCs persisted longer in the light (Hannibal et al., 2001). As the PACAP-containing RGC population was later identified as the melanopsin-expressing RGCs (Hannibal et al., 2004) c-fos induction is a strong marker of light activation leading to non-image forming sensitivity. It should be noted, however, as we were not able to successfully co-label retina with c-fos and melanopsin as was done with wildtype and *rd/rd cl* in Chapter 4, pRGCs will make up only a fraction of the c-fos positive cells we counted in our analysis. Thus there may be differences in patterns and trends in response of pRGCs that were missed in this study. However, as the pRGC trends in Chapter 4 mirrored the observed gross retinal c-fos gradient, the c-fos counts here are likely to be consistent with the trends of pRGCs.

8.11 Conclusions

We found that UVS opsin is the critical photopigment in the UV sensitivity of the mouse phase-shifting response, able to drive responses to a much greater extent than the established

model for MWS contributions under visible light. In contrast, the contribution of UVS opsin to the PLR under UV light is consistent with known MWS contributions. Finally, we determined UVS opsin is the dominant photopigment responsible for c-fos activation under UV light in the wildtype retina. These results all indicate a broad and important role for UVS opsin in NIF UV sensitivity in the mouse but while this UVS contribution is likely to come from m-cones for the PLR, phase-shifting responses may involve an s-cone input.

Chapter 9: **Discussion and Conclusions**

9.1 The basis of non-image forming UV sensitivity in mice

The influence of UV light on the circadian system of rodents has been the subject of considerable investigation and contradictory results. NIF UV sensitivity has an influence on a range of behaviors including regulation of the reproductive system, phase-shifting, melatonin suppression and body temperature rhythms in rats, hamsters and in mice (Brainard et al., 1986, 1994; McGuire et al., 1973; Provencio and Foster, 1995; von Schantz et al., 1997) while retinal sensitivity in the UV has been identified in further rodent species including gerbils and gophers (Jacobs et al., 1991). These results were of particular interest to investigators as UV sensitivity was long thought to be absent in mammals (Goldsmith, 1994; Jacobs, 1992). Furthermore, the UV responses found in these species of rodents were of similar or even greater magnitude relative to responses under visible wavelengths (Jacobs et al., 1991; Provencio and Foster, 1995; von Schantz et al., 1997). This widespread sensitivity was thought to potentially indicate unique and important roles for UV light in the natural environment of rodent species (Chávez et al., 2003) and perhaps a common mechanism of retinal UV input. An obvious candidate was the UVS cone class, found to be present along with the known MWS opsin in the eyes of many rodents including rats (Szél and Röhlich, 1992) and mice (Szél et al., 1992) with absorbance maxima around 360nm (Deegan and Jacobs, 1993; Yokoyama et al., 1998). However, while the UVS opsin was the candidate for the NIF UV behavioral sensitivity of rats and mice, the Syrian Golden Hamster was also found to show significant UV phase-shifting responses despite the fact that this species lacks a UVS cone opsin (von Schantz et al., 1997). The finding of photic-entrainment responses of equal magnitude to 357nm and 515nm light in the Syrian hamster

introduced considerable doubt as to whether the UVS cone was responsible for UV phase-shifting or indeed any of the other UV NIF behavioral responses in rodents. An alternative mechanism was then proposed by which one of the photopigments known to drive NIF function, such as rhodopsin or melanopsin, might provide UV sensitivity through absorption of the secondary β-band peak. The β-band is known to extend into the short-wavelength range as part of the absorption spectrum of vertebrate photopigments but had not been shown to drive behavioral responses (Hut et al., 2000; von Schantz et al., 1997).

Here we resolve the question concerning the basis of UV NIF phase-shifting sensitivity in mice through examination of phase-shifting responses of mice with varying degrees of rod and cone degeneration in the *rd/rd, rd/rd cl* and *cl,* as well as in a novel *Opn1sw* knockout model lacking UVS opsin. Our results indicate that the UVS opsin is the dominant photoreceptor driving these responses to UV light in the mouse. Although the loss of UVS was accompanied by a ~15 fold decrease in sensitivity, the residual phase-shifts in both the *rd/rd cl* (3% residual sensitivity) and *Opn1sw* KO (6.8% residual sensitivity) demonstrate that melanopsin, and likely rhodopsin, are able to contribute some degree of UV sensitivity through the residual absorption of the α-band but there is no indication of β-band contribution to phase-shifting behavior. Mouse PLR was also demonstrated to receive a strong input from UVS opsin sensitivity that, combined with melanopsin input, drives PLR responses to UV light.

Furthermore, we find that the UVS opsin is primarily responsible for driving retinal c-fos induction to UV as the distinct dorsal-ventral gradient seen in the wildtype mouse retina

following UV light pulses is dependent on the presence of the UVS opsin. c-fos expression in the retina is induced in pRGCs following light exposure in a manner that follows circadian system sensitivity to light and is dependent on photoreceptor input (Hannibal et al., 2001; Masana et al., 1996; Pickard et al., 2009; Semo et al., 2003). Thus, while expression also occurs in other RGCs and amacrine cells as a result of rod and cone signaling, c-fos activation is a well established indicator of retinal sensitivity and cellular activation by light as well as being linked to NIF responses in the SCN (Kornhauser et al., 1990).

As expected with its absorption mainly in the UV we did not observe any significant role for UVS in IF or NIF responses to white light. No differences were found between *Opn1sw* KO and wildtype in a circadian activity screen or in pupil responses to 480nm light. White light c-fos induction was also similar between the genotypes.

Work in conjunction to that presented here was completed by others in our group and describes expanded NIF UV sensitivity. Published alongside this data on phase-shifting in retinal degenerate models, UVS is further shown to drive acute sleep responses to UV light and is linked to distinct SCN input (van Oosterhout et al., 2012). In a comparison of acute sleep induction during a 1hr pulses of 363nm UV light at ZT16, analysis of EEG/ EMG recordings found UV light was as effective as white light in inducing sleep (Lupi et al., 2008). Also, despite studies of visible wavelengths that find that melanopsin is the dominant photopigment (Lupi et al., 2008; Tsai et al., 2009), under UV light, comparable levels of NREM sleep were induced in *Opn4* $^{+/+}$ and *Opn4*$^{-/-}$ animals (van Oosterhout et al., 2012). Furthermore, UV light was found to drive intensity and phase-dependent increases in firing

in the SCN that are retained in the melanopsin knockout. Both transient and sustained components were observed in the SCN response under UV light. When a stimulus was superimposed on a level of white light (lacking UV wavelengths) intended to saturate rods and all other photoreceptor classes excepting UVS cones, additional blue light elicited no further increase in SCN response but UV light resulted in a marked increase in the magnitude of both the transient and sustained responses (van Oosterhout et al., 2012). While there is growing evidence pointing to the difficulty of fully saturating photoreceptors, with rods found to signal through cones at levels thought to be saturating to support entrainment (Altimus et al., 2010), the lack of melanopsin dependence in both sleep and SCN responses suggests further UVS cone involvement. However, conclusive evidence that these responses are due to UVS opsin awaits future experiments in the *Opn1sw* KO. We are now in the process of examining acute sleep induction in the *Opn1sw* KO and have also sent animals to our collaborators in Leiden, Netherlands for in-vivo SCN recordings in this model.

9.2 Resolving contradictory indications of cone contributions –evidence of distinct roles for m- and s-cones in the mouse NIF system

As UVS opsin is expressed in m-cones, which co-express MWS and UVS to varying extents across the retina, and s-cones, which express only UVS, the question remains whether one or both of these classes of cones contribute to those UV sensitive behaviors that have been shown to have significant UVS opsin input. Our data indicates that the contributions of cones to NIF behaviors are not homogenous and there may be specific roles for each cone class.

Differences in UVS and MWS phase-shifting responses

Our investigation of phase-shifting sensitivity under UV light supports a role for UVS cones in this response that greatly exceeds that previously established for MWS cones (Altimus et al., 2010; Dkhissi-Benyahya et al., 2007; Freedman et al., 1999; Lall et al., 2010). As melanopsin overlaps to a great extent with MWS absorption, a greater contribution from MWS cones may not be necessary for the mouse under visible wavelengths. In this view, as the sensitivity of melanopsin, and indeed rhodopsin and MWS opsin, are so limited in the UV, mechanisms for greater sensitivity to UVS input may have evolved that would explain the large contribution from UVS to this response. This in turn suggests significant selection pressures favoring UV sensitivity in mice at similar levels to visible light, leading to the high levels of UV phase-shifting observed in a number of rodent species with and without UVS cones (Provencio and Foster, 1995; von Schantz et al., 1997). Similarly, although analysis of outer retinal contributions to the maintenance of acute sleep is complicated by many factors including the length of light exposure and individual response variation between mice (for recent review see (Muindi et al., 2014)), for 1hr light pulses current evidence suggests that UVS cones provide a greater input to acute sleep induction for UV light than does MWS in m-cones under visible wavelengths (Lupi et al., 2008; van Oosterhout et al., 2012). As with phase-shifting, this does not in and of itself necessarily require different cone class roles, as it could be that melanopsin is able to drive nearly maximal or saturating responses to bright light. Thus additional input from MWS in m-cones processing a similar absorption spectrum has limited impact on sleep induction. Under UV light, however, melanopsin sensitivity is

much lower and the UVS signals from m-cones might contribute a larger proportion of the total signal response.

Cone mediated inhibition

Apart from the UVS inputs to behavioral outputs, we also found a number of indications of a cone inhibition effect that is inconsistent with previous results from studies focused on MWS opsin responses. We observed UV light in the presence of UVS cones resulted in lower dorsal retinal c-fos induction than in their absence in the *Opn1sw*. Even though overall retinal response was greater with UVS opsin present due to larger increases in ventral responses, the unexpected decrease in dorsal retina response suggested that an inhibitory input from one of the UVS expressing cone-classes is exerted on one or more of the residual photopigments in the *Opn1sw* KO retina. Further evidence of this inhibitory influence under UV light was found in analysis of c-fos responses of different pRGC subtypes in light-pulsed retina presented in Chapter 4. We observed greater dorsal responses in M1, but not M2, pRGCs in *rd/rd cl* animals relative to wildtype following UV light exposure, indicating greater melanopsin responses in the absence of outer-retinal signals (Hughes et al., 2013). A third piece of evidence that did not emerge under UV light conditions, but may still be connected to this issue, was the lower entrainment threshold we observed with complete loss of cones in the rodless, coneless *rd/rd cl* mice relative to the rodless. This yet again implicates an inhibitory signal from cones acting on melanopsin signals from pRGCs. Such inhibition has also been previously suggested for NIF responses (Figueiro et al., 2004) but,

despite the considerable evidence in our studies, no similar evidence was found for m-cone related inhibition under visible wavelengths in the red-shifted cone model (Lall et al., 2010).

While the presence of distinct pathways or differential influence of UVS and MWS signals from m-cones on pRGCs may be possible, a simpler explanation both for UVS contributions beyond those of MWS and the contradictory indications for cone-based inhibitory influences is that they are related to the UVS only s-cones and a separate blue-cone signaling pathway in the retina (Haverkamp et al., 2005). Such a pathway might provide input to the pRGCs to drive sustained signals in the SCN (van Oosterhout et al., 2012) and other NIF areas, as they have been found to do in the PON (Allen et al., 2011), and thus support NIF functions in a manner distinct from m-cone input. In terms of inhibitory signals, that the presence of the s-cone pathway, even un-activated, might have an inhibitory influence on pRGCs is supported by primate data from the macaque. In this model a population of pRGCs were found to display ON- signals from MWS and LWS cone classes but OFF signals from SWS cones (Dacey et al., 2005). Dacey et al., suggested that the cone circuitry they observed might have evolved to more precisely set the clock during the large and abrupt changes in light intensity at dawn and dusk. Recently recordings in the mouse PON found evidence that pRGCs received excitatory inputs from s- and m-cones but that s-cones also drive a clear OFF-inhibition of some pRGC responses (Allen et al., 2011). Combined with our data here, a model (Figure 9.1) where intrinsic melanopsin-derived signals in a subtype of pRGCs (likely M1 from the analysis of our c-fos *rd/rd cl* data) are inhibited by the s-cone pathway fits well with the evidence. Unfortunately our UVS knockout lacks UVS expression in both m and s-cone classes, making it difficult to separate m- and s-cone influence. Further investigation,

perhaps including discovery of S-cone specific markers in the mouse to allow better characterization or targeted ablation of individual cone classes, will be a fascinating area for future research in understanding the mouse visual system and how it might relate to our own.

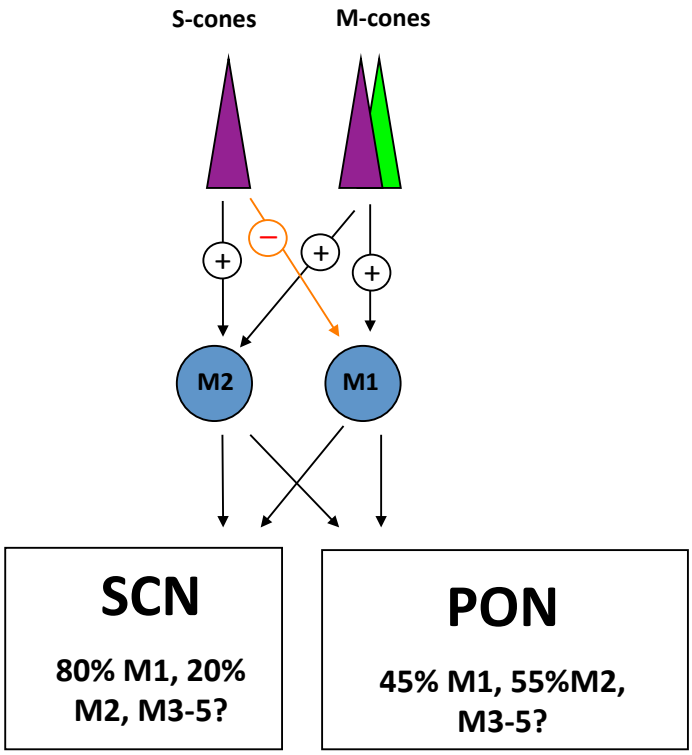

Figure 9.1 Model for s-cone mediated inhibition of melanopsin expressing pRGC Based on the three lines of evidence of cone-derived inhibitory influence on melanopsin signaling discussed in this thesis from threshold of entrainment (Chapter 3) and c-fos induction changes in *rd/rd cl* (Chapter 3) and *Opn1sw* KO (Chapter 8) as well as existing evidence of s-cone based OFF-inhibition (Allen et al., 2011; Dacey et al., 2005), we suggest a model of s-cone inhibitory influence of M1 type pRGCs in the mouse. Here m-cone co-expressing MWS (green) and UVS (violet) opsins provide excitatory input while s-cones provide both excitatory input to M2 and inhibitory signals to M1 pRGCs. Included in this model are the differential projections of M1 and M2 subtypes to the SCN and PON (Baver et al., 2008) to illustrate the implications that this inhibition would have different effects on various NIF outputs based on the balance on pRGC subtype projection.

9.3 Summary of photoreceptor contributions to UV light NIF input compared to visible light

To summarize the similarities and differences in photoreceptor contributions under visible and UV wavelengths as well as indicating areas that require further investigation, we have generated the following figures to illustrate the situation for visible (Figure 9.2) and UV (Figure 9.3) light respectively. The primary sources used for conclusions regarding photopigment contribution are listed with each NIF output.

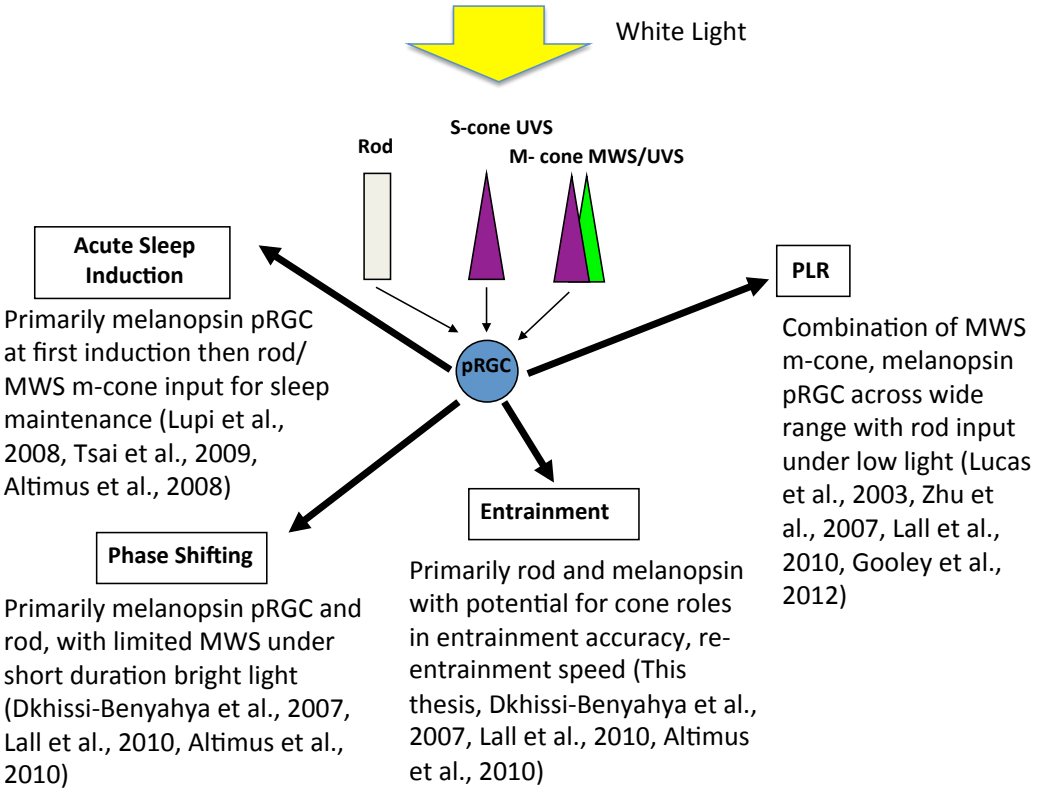

Figure 9.2 Photoreceptor contributions under white light to NIF functions A summary of the contributions to various NIF behaviors in the mouse under white light (<440nm light spectrum of most white light sources) including acute sleep induction, phase-shifting, entrainment and the PLR are presented along with the lines of evidence used to categorise rod, melanopsin and cone class roles. These differ from suggested roles under UV light in terms of acute sleep induction and phase-shifting but not PLR (Figure 9.3 below).

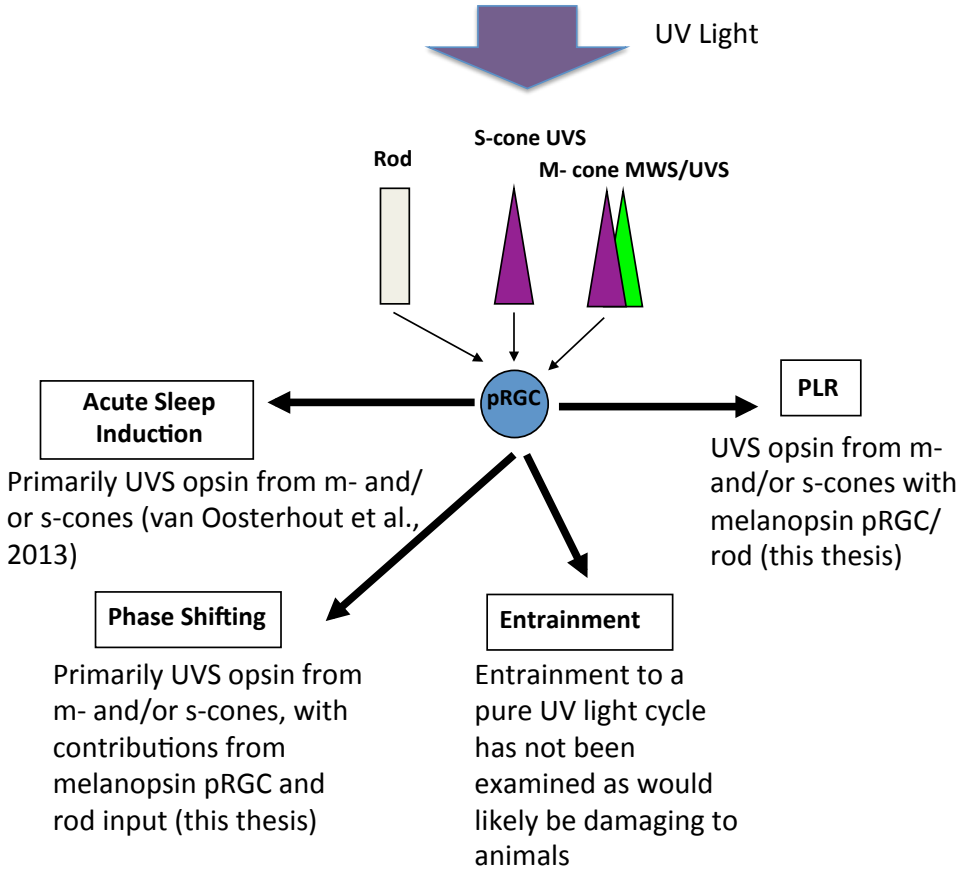

Figure 9.3 Photoreceptor contributions under UV light to NIF functions A summary of the contributions to various NIF behaviors in the mouse under UV wavelengths including acute sleep induction, phase-shifting and the PLR are presented along with the lines of evidence used to categorise rod, melanopsin and cone class roles. These differ from suggested roles under UV light in terms of acute sleep induction and phase-shifting but not PLR (Figure 9.3 below).

9.4 Explaining the UVS expression in the mouse: Image versus non-image forming functions

The discovery of UV sensitivity in rodents was unanticipated. This was a surprise both because it was thought that UVS pigments were absent from mammalian species and

because the lenses of mammals were thought to all possesses a wavelength filter (identified in human eyes) to protect the retina against the harmful impacts of UV radiation. However, while the retinas of primates and a number of other diurnal species do indeed possess molecular compounds to stop UV transmission (Bova et al., 1999), having lenses that transmit wavelengths well into the UV is not at all uncommon, especially amongst rodents (Cooper and Robson, 1969; Gorgels and van Norren, 1992; Lei and Yao, 2006) and UV transmission sufficient for vision has also been found in many species including reindeer (Hogg et al., 2011), hedgehogs, dogs, cats and ferrets (Douglas and Jeffery, 2014). Specific UVS cone photopigments have been identified in species of bats (Fujun et al., 2012) and marsupials (Arrese et al., 2005, 2006) in addition to those in many rodents but photopigments with λ-max above the UV can still allow UV sensitivity given lens transmission.

Examination of which species have lenses transmitting significant amounts of UV light reveals patterns that help to explain some of the major costs and benefits influencing the selection pressures that drive evolution either towards or away from UV sensitivity in a species. As a general trend, nocturnal species generally possess UV sensitivity, as wide spectral sensitivity is important, while diural species that rely on high acuity vision from cone-rich retina would be more affected by the increased chromatic aberration of shorter wavelengths and so UV transmission is more costly (Douglas and Jeffery, 2014). Of course, nocturnal animals would be exposed to far less intense UV radiation during their active period and thus would also be less likely to experience ocular damage due to UV light. However, the sensory trade-offs may be a more important factor as nocturnal species of bat

with more specialized auditory abilities have lost UVS photopigments whilst those that rely more on visual abilities have not (Fujun et al., 2012).

The discussion of trends in UV sensitivity is relevant to our question of what pressures have primarily led to the cone opsin gradients and extensive ultraviolet sensitivity in the mouse. Care must be taken not to focus too much on the UV sensitivity as a specialized ability given its demonstrated prevalence across the animal kingdom (see Chapter 1). Also considering, where it has been viewed as a special channel for example in bird mate choice, sensitivity in other parts of the spectrum has often been found to be at least equally important (Hunt et al., 2001b). However, there can be little doubt that, compared to closely related species in similar environmental niches like the rat, the increased level of UVS opsin expression (Applebury et al., 2000) and sensitivity in the mouse, as well as the presence of such a strong dorsal ventral gradient of UVS, raise the question of which factors have led to selection pressure in this species.

Given previous reports of ERG recordings and behavioral assays (Jacobs et al., 1991, 2004) in addition to the data from visual tasks presented in this thesis, it is clear that mice are able to use UV light for visual perception. While we did not find any role for UVS cones in the optokinetic response, there was an impairment of performance in the visuospatial recognition task under UV light associated with the loss of UVS opsin. However, similar to the findings from the previous behavioral assays of Jacobs et al., we did not find any indication of the particular enhancement of UV visual sensitivity suggested by ERG data with stronger performance of the task under white light in both *Opn1sw* KO and wildtype

genotypes. With most mouse cones being m-cones co-expressing MWS and UVS, only very limited colour discrimination abilities have been found in the mouse (Jacobs et al., 2004). So there is no current evidence that spectral sensitivity into the UV range is particularly useful for the mouse in its natural habit with the majority of its active time occurring during the night when the amount of UV irradiance is extremely low (Hut et al., 2000).

While there might be a role for UV visual sensitivity yet to be observed in mouse ecology, the evidence for NIF functions seems to provide a better explanation for the observed opsin organization in the mouse. With effects of UV light demonstrated for many NIF behaviours including phase-shifting/ photic entrainment, PLR and sleep induction there is little doubt of a strong role of UV sensitivity in this species. As to the particular importance of one of these factors, the Syrian hamster is an interesting point of comparison as a related rodent species without UVS cones that was found to possess a retinal mechanism capable of driving phase-shifting responses to UV light equal in magnitude to visible wavelengths (von Schantz et al., 1997). However, the UV impact on another NIF function in this species, suppression of melatonin, has a 10x lower UV sensitivity compared to visible light, a reduction that would be expected in an animal possessing only photopigments with maximal absorption far from the UV (Podolin et al., 1987). This particular enrichment of UV phase-shifting sensitivity suggests that UV sensitivity is of particular importance for entrainment. In mice, we also observed that phase-shifting sensitivity to UV light matched that of visible wavelengths and that the UVS opsin seems to play a greater role in this response than the MWS opsin. While primarily nocturnal, mice are active around dusk and dawn when there is a relative enrichment of UV wavelengths (Hut et al., 2000) and it is plausible that sensitivity to UV

wavelengths is of particular importance to stable entrainment in mice. The importance of entrainment to coordination of gene expression, physiological processes and behavior is clear and indeed the retina of the mouse with an expression gradient and UV sensitivity biased towards the upwards-facing ventral retina (Applebury et al., 2000; Calderone and Jacobs, 1995) appears ideally suited to gather UV irradiation to input to the circadian system in a way that it is not for visual perception. Interestingly, the disruption of the central clock through loss-of function mutations in both *Per1* and *Per2* genes was found to disrupt UVS expression and in particular affect the dorsal-ventral gradient, implying that clock function has a role in driving the establishment of the UVS cone gradient (Ait-Hmyed et al., 2013).

While photo-entrainment thus seems a plausible explanation for selection pressure that would favor a retina with greater UVS expression than MWS and the dorsal-ventral expression, there remain several arguments against this theory. Firstly, the question arises of why a similar organization is not observed in rats with similar activity timing and natural visual environments (Szél et al., 1996). In addition, if s-cones are responsible for driving sustained responses to UV light seen in the PON and SCN (Allen et al., 2011; van Oosterhout et al., 2012), thus explaining the particularly large UVS contribution to entrainment responses as we suggested in Chapter 8, one would expect s-cones to also show a dorsal-ventral gradient instead of their even pattern across the retina (Haverkamp et al., 2005). This could be because s-cones do not have any particularly important adaptation for NIF input or that there are other advantages to even sampling across the retina. Finally, it should be noted that the presence of a particular trait in a species might not be due to strong positive selection pressure but the lack of negative selection against a given mutation.

Genetic linkage to some other positive trait can result in the propagation of such a neutral mutation. Given the demonstrated potential negative impacts of UV light sensitivity and strong expression gradients this seems unlikely in this case.

While it is clearly not conclusive, the current evidence points to the importance of circadian entrainment input as a plausible explanation for the unique UVS cone opsin organization in the mouse.

9.5 Conclusions and Future Work

In this work the first of our primary aims was to confirm the basis of ultraviolet sensitivity in mice and our examination has confirmed roles for UVS cone mediated sensitivity in both image and non-image forming behaviors.

We further investigated the role of UV in both IF and NIF visual systems. Ultraviolet sensitivity was found in image forming assays of light/dark box, OKR and in a novel visual application of the object recognition task. This adds to the forced-choice discrimination task used by Jacobs et al. (Jacobs et al., 2004) as behavioral proof of ultraviolet vision in mice. While the light/dark box and visuospatial task were affected by the loss of UVS cones, the performance in the OKR drum assay was found to depend primarily on rod performance under the conditions examined here. Performance of the OKR was comparable to white light under bright UV irradiance while visuospatial performance was slightly lower under the brighter UV irradiance condition.

While a primary role for rods was confirmed in determining entrainment threshold under white light, a primary role for UVS cone input was identified as driving phase-shifting to ultraviolet light by comparing phase-shifting IRCs of rod and cone mutants and then of a novel *Opn1sw* KO model lacking UVS expression. No role was found for β-band involvement from other photopigments although residual α-band expression from melanopsin was able to drive limited phase-shifts in the rodless-coneless model and rods appeared to make a significant contribution to phase-shifting under low intensity UV light. UV phase-shifting sensitivity was determined to be at the same level as that of visible wavelengths and the contribution of UVS cones was at a level inconsistent with recent evidence of MWS cone input. With data suggesting that the UVS cones are also capable of acute sleep induction thought to be determined largely by melanopsin under white light, there are indications of differences in MWS and UVS input despite widespread co-expression in cones of the mouse retina. The greater input from UVS opsin may indicate the use of different pathways or processing of UVS signals from m-cones or of a distinct role for UVS-only s-cones. We further found UVS contributions to PLR under UV light and that UVS cones were primarily responsible for driving c-fos induction in the retina under UV light.

The final major aim of this work was to support a hypothesis as to why the mouse retina contains such unique UVS opsin expression and UV sensitivity. Combined, our results support the view that the strong dorsal-ventral expression gradient and relative enrichment of

UVS opsin compared to related species are best explained by a critical input to entrainment responses.

Much of the focus of our work and the interpretation of the results has considered the significance of the data from the behavioural perspective. To expand on these results, one of the key areas for future study is further investigation and separation of the cone classes in the mouse. If a specific marker of s-cones was identified it may be possible to perform a targeted ablation of s-cones and examine if the sustained responses to UV light in the PON and SCN are lost. This could also be used to further characterize the s-cone retinal signaling pathway and examine the evidence of cone-inhibition we observed. Given the gradual loss of cone outer-segments reported in a different *Opn1sw*$^{-/-}$ model published as this work was written (Greenwald et al., 2014), the β-gal reporter expression throughout the normally UVS-expressing cones in our *Opn1sw* KO would also provide an excellent tool to examine cone structural changes in aged animals and gain insight into the impact of opsin loss on photoreceptors.

With mice currently employed as the most common mammalian research model, and with the growing application of mice in the investigation of the visual system and ocular disease, it is vital to fully understand the spectral sensitivity and photoreceptor input to both image and non-image forming visual systems to allow accurate interpretation of results.

Bibliography

Abdeljalil, J., Hamid, M., Abdel-Mouttalib, O., Stéphane, R., Raymond, R., Johan, A., José, S., Pierre, C., and Serge, P. (2005). The optomotor response: a robust first-line visual screening method for mice. Vision Res. *45*, 1439–1446.

Abe, H., Rusak, B., and Robertson, H.A. (1991). Photic induction of Fos protein in the suprachiasmatic nucleus is inhibited by the NMDA receptor antagonist MK-801. Neurosci. Lett. *127*, 9–12.

Acevedo-Arozena, A., Wells, S., Potter, P., Kelly, M., Cox, R.D., and Brown, S.D.M. (2008). ENU Mutagenesis, a Way Forward to Understand Gene Function. Annu. Rev. Genomics Hum. Genet. *9*, 49–69.

Aggleton, J.P., Albasser, M.M., Aggleton, D.J., Poirier, G.L., and Pearce, J.M. (2010). Lesions of the rat perirhinal cortex spare the acquisition of a complex configural visual discrimination yet impair object recognition. Behav. Neurosci. *124*, 55–68.

Albasser, M.M., Davies, M., Futter, J.E., and Aggleton, J.P. (2009). Magnitude of the object recognition deficit associated with perirhinal cortex damage in rats: Effects of varying the lesion extent and the duration of the sample period. Behav. Neurosci. *123*, 115–124.

Albasser, M.M., Amin, E., Iordanova, M.D., Brown, M.W., Pearce, J.M., and Aggleton, J.P. (2011). Separate but interacting recognition memory systems for different senses: the role of the rat perirhinal cortex. Learn. Mem. Cold Spring Harb. N *18*, 435–443.

Albrecht, U., and Foster, R.G. (2002). Placing ocular mutants into a functional context: a chronobiological approach. Methods *28*, 465–477.

Albrecht, U., Sun, Z.S., Eichele, G., and Lee, C.C. (1997). A differential response of two putative mammalian circadian regulators, mper1 and mper2, to light. Cell *91*, 1055–1064.

Allen, A.E., Brown, T.M., and Lucas, R.J. (2011). A distinct contribution of short wavelength sensitive cones to light evoked activity in the mouse pretectal olivary nucleus (PON). J. Neurosci. *31*, 16833–16843.

Altimus, C.M., Güler, A.D., Villa, K.L., McNeill, D.S., Legates, T.A., and Hattar, S. (2008). Rods-cones and melanopsin detect light and dark to modulate sleep independent of image formation. Proc. Natl. Acad. Sci. U. S. A. *105*, 19998–20003.

Altimus, C.M., Güler, A.D., Alam, N.M., Arman, A.C., Prusky, G.T., Sampath, A.P., and Hattar, S. (2010). Rod photoreceptors drive circadian photoentrainment across a wide range of light intensities. Nat. Neurosci. *13*, 1107–1112.

Amir, S., and Robinson, B. (1995). Ultraviolet light entrains rodent suprachiasmatic nucleus pacemaker. Neuroscience *69*, 1005–1011.

Andermann, M.L., Kerlin, A.M., Roumis, D.K., Glickfeld, L.L., and Reid, R.C. (2011). Functional specialization of mouse higher visual cortical areas. Neuron *72*, 1025–1039.

Applebury, M.L., Antoch, M.P., Baxter, L.C., Chun, L.L., Falk, J.D., Farhangfar, F., Kage, K., Krzystolik, M.G., Lyass, L.A., and Robbins, J.T. (2000). The murine cone photoreceptor:

a single cone type expresses both S and M opsins with retinal spatial patterning. Neuron *27*, 513–523.

Arrese, C.A., Oddy, A.Y., Runham, P.B., Hart, N.S., Shand, J., Hunt, D.M., and Beazley, L.D. (2005). Cone topography and spectral sensitivity in two potentially trichromatic marsupials, the quokka (Setonix brachyurus) and quenda (Isoodon obesulus). Proc. Biol. Sci. *272*, 791–796.

Arrese, C.A., Beazley, L.D., and Neumeyer, C. (2006). Behavioural evidence for marsupial trichromacy. Curr. Biol. CB *16*, R193–R194.

Aschoff, J. (1952). [Changes of frequency of periods of activity of mice in constant light and lasting darkness]. Pflüg. Arch. Eur. J. Physiol. *255*, 197–203.

Aschoff, J. (1984). Circadian Timinga. Ann. N. Y. Acad. Sci. *423*, 442–468.

Asteriti, S., Gargini, C., and Cangiano, L. (2014). Mouse rods signal through gap junctions with cones. eLife *3*.

Aton, S.J., Colwell, C.S., Harmar, A.J., Waschek, J., and Herzog, E.D. (2005). Vasoactive intestinal polypeptide mediates circadian rhythmicity and synchrony in mammalian clock neurons. Nat. Neurosci. *8*, 476–483.

Bae, K., Jin, X., Maywood, E.S., Hastings, M.H., Reppert, S.M., and Weaver, D.R. (2001). Differential functions of mPer1, mPer2, and mPer3 in the SCN circadian clock. Neuron *30*, 525–536.

Baker, M. (2013). Neuroscience: Through the eyes of a mouse. Nature *502*, 156–158.

Barlow, C.M., and Root, W.S. (1949). The ocular sympathetic path between the superior cervical ganglion and the orbit in the cat. J. Comp. Neurol. *91*, 195–207, illust.

Barlow, H.B., Hill, R.M., and Levick, W.R. (1964). Retinal ganglion cells responding selectively to direction and speed of image motion in the rabbit. J. Physiol. *173*, 377–407.

Barnard, A.R., Hattar, S., Hankins, M.W., and Lucas, R.J. (2006). Melanopsin regulates visual processing in the mouse retina. Curr. Biol. CB *16*, 389–395.

Baver, S.B., Pickard, G.E., Sollars, P.J., and Pickard, G.E. (2008). Two types of melanopsin retinal ganglion cell differentially innervate the hypothalamic suprachiasmatic nucleus and the olivary pretectal nucleus. Eur. J. Neurosci. *27*, 1763–1770.

Belenky, M.A., Smeraski, C.A., Provencio, I., Sollars, P.J., and Pickard, G.E. (2003). Melanopsin retinal ganglion cells receive bipolar and amacrine cell synapses. J. Comp. Neurol. *460*, 380–393.

Bennett, A.T., and Cuthill, I.C. (1994). Ultraviolet vision in birds: what is its function? Vision Res. *34*, 1471–1478.

Benshoff, H.M., Brainard, G.C., Rollag, M.D., and Lynch, G.R. (1987). Suppression of pineal melatonin in Peromyscus leucopus by different monochromatic wavelengths of visible and near-ultraviolet light (UV-A). Brain Res. *420*, 397–402.

Berson, D.M., Dunn, F.A., and Takao, M. (2002). Phototransduction by Retinal Ganglion Cells That Set the Circadian Clock. Science *295*, 1070–1073.

Berson, D.M., Castrucci, A.M., and Provencio, I. (2010). Morphology and mosaics of melanopsin-expressing retinal ganglion cell types in mice. J. Comp. Neurol. *518*, 2405–2422.

Bevins, R.A., and Besheer, J. (2006). Object recognition in rats and mice: a one-trial non-matching-to-sample learning task to study "recognition memory." Nat. Protoc. *1*, 1306–1311.

Biral, G.P., Cavazzuti, M., Ferrari, R., and Corazza, R. (1982). Optokinetic visual detection in the rat visual centres. A [14C]-2-deoxy-D-glucose study. Arch. Int. Physiol. Biochim. *90*, 141–144.

Blazquez, P.M., Hirata, Y., Heiney, S.A., Green, A.M., and Highstein, S.M. (2003). Cerebellar signatures of vestibulo-ocular reflex motor learning. J. Neurosci. *23*, 9742–9751.

Borbély, A.A. (1976). Sleep and motor activity of the rat during ultra-short light-dark cycles. Brain Res. *114*, 305–317.

Born, R.T., and Bradley, D.C. (2005). Structure and function of visual area MT. Annu. Rev. Neurosci. *28*, 157–189.

Bourin, M., and Hascoët, M. (2003). The mouse light/dark box test. Eur. J. Pharmacol. *463*, 55–65.

Bova, L.M., Wood, A.M., Jamie, J.F., and Truscott, R.J. (1999). UV filter compounds in human lenses: the origin of 4-(2-amino-3-hydroxyphenyl)-4-oxobutanoic acid O-beta-D-glucoside. Invest. Ophthalmol. Vis. Sci. *40*, 3237–3244.

Bowes, C., Li, T., Danciger, M., Baxter, L.C., Applebury, M.L., and Farber, D.B. (1990). Retinal degeneration in the rd mouse is caused by a defect in the β subunit of rod cGMP-phosphodiesterase. Nature *347*, 677–680.

Bowmaker, J.K., and Kunz, Y.W. (1987). Ultraviolet receptors, tetrachromatic colour vision and retinal mosaics in the brown trout (Salmo trutta): age-dependent changes. Vision Res. *27*, 2101–2108.

Brainard, G.C., Vaughan, M.K., and Reiter, R.J. (1986). Effect of light irradiance and wavelength on the Syrian hamster reproductive system. Endocrinology *119*, 648–654.

Brainard, G.C., Barker, F.M., Hoffman, R.J., Stetson, M.H., Hanifin, J.P., Podolin, P.L., and Rollag, M.D. (1994). Ultraviolet regulation of neuroendocrine and circadian physiology in rodents. Vision Res. *34*, 1521–1533.

Briscoe, A.D., and Chittka, L. (2001). The evolution of color vision in insects. Annu. Rev. Entomol. *46*, 471–510.

Brown, T.M., Gias, C., Hatori, M., Keding, S.R., Semo, M., Coffey, P.J., Gigg, J., Piggins, H.D., Panda, S., and Lucas, R.J. (2010). Melanopsin Contributions to Irradiance Coding in the Thalamo-Cortical Visual System. PLoS Biol *8*, e1000558.

Brown, T.M., Wynne, J., Piggins, H.D., and Lucas, R.J. (2011). Multiple hypothalamic cell populations encoding distinct visual information. J. Physiol. *589*, 1173–1194.

Buckmaster, C.A., Eichenbaum, H., Amaral, D.G., Suzuki, W.A., and Rapp, P.R. (2004). Entorhinal cortex lesions disrupt the relational organization of memory in monkeys. J. Neurosci. *24*, 9811–9825.

Bunger, M.K., Wilsbacher, L.D., Moran, S.M., Clendenin, C., Radcliffe, L.A., Hogenesch, J.B., Simon, M.C., Takahashi, J.S., and Bradfield, C.A. (2000). Mop3 is an essential component of the master circadian pacemaker in mammals. Cell *103*, 1009–1017.

Bunger, M.K., Walisser, J.A., Sullivan, R., Manley, P.A., Moran, S.M., Kalscheur, V.L., Colman, R.J., and Bradfield, C.A. (2005). Progressive arthropathy in mice with a targeted disruption of the Mop3/Bmal-1 locus. Genes. N. Y. N 2000 *41*, 122–132.

Burns, S., and Wallman, J. (1981). Relation of single unit properties to the oculomotor function of the nucleus of the basal optic root (accessory optic system) in chickens. Exp. Brain Res. *42*, 171–180.

Busino, L., Bassermann, F., Maiolica, A., Lee, C., Nolan, P.M., Godinho, S.I.H., Draetta, G.F., and Pagano, M. (2007). SCFFbxl3 controls the oscillation of the circadian clock by directing the degradation of cryptochrome proteins. Science *316*, 900–904.

Butler, M.P., and Silver, R. (2010). Divergent photic thresholds in the non-image-forming visual system: entrainment, masking and pupillary light reflex. Proc. R. Soc. B Biol. Sci. rspb20101509.

Calderone, J.B., and Jacobs, G.H. (1995). Regional variations in the relative sensitivity to UV light in the mouse retina. Vis. Neurosci. *12*, 463–468.

Calderone, J.B., and Jacobs, G.H. (1999). Cone receptor variations and their functional consequences in two species of hamster. Vis. Neurosci. *16*, 53–63.

Cameron, M.A., Barnard, A.R., and Lucas, R.J. (2008). The electroretinogram as a method for studying circadian rhythms in the mammalian retina. J. Genet. *87*, 459–466.

Carter-Dawson, L.D., LaVail, M.M., and Sidman, R.L. (1978). Differential effect of the rd mutation on rods and cones in the mouse retina. Invest. Ophthalmol. Vis. Sci. *17*, 489–498.

Cermakian, N., Monaco, L., Pando, M.P., Dierich, A., and Sassone-Corsi, P. (2001). Altered behavioral rhythms and clock gene expression in mice with a targeted mutation in the Period1 gene. EMBO J. *20*, 3967–3974.

Chalupa, L.M., and Thompson, I. (1980). Retinal ganglion cell projections to the superior colliculus of the hamster demonstrated by the horseradish peroxidase technique. Neurosci. Lett. *19*, 13–19.

Chambille, I., Doyle, S., and Servie`re, J. (1993). Photic induction and circadian expression of Fos-like protein. Immunohistochemical study in the retina and suprachiasmatic nuclei of hamster. Brain Res. *612*, 138–150.

Chang, B., Grau, T., Dangel, S., Hurd, R., Jurklies, B., Sener, E.C., Andreasson, S., Dollfus, H., Baumann, B., Bolz, S., et al. (2009). A homologous genetic basis of the murine cpfl1 mutant and human achromatopsia linked to mutations in the PDE6C gene. Proc. Natl. Acad. Sci. *106*, 19581–19586.

Chávez, A.E., Bozinovic, F., Peichl, L., and Palacios, A.G. (2003). Retinal spectral sensitivity, fur coloration, and urine reflectance in the genus octodon (rodentia): implications for visual ecology. Invest. Ophthalmol. Vis. Sci. *44*, 2290–2296.

Chen, S.-K., Badea, T.C., and Hattar, S. (2011). Photoentrainment and pupillary light reflex are mediated by distinct populations of ipRGCs. Nature *476*, 92–95.

Cheng, H.-Y.M., Papp, J.W., Varlamova, O., Dziema, H., Russell, B., Curfman, J.P., Nakazawa, T., Shimizu, K., Okamura, H., Impey, S., et al. (2007). MicroRNA modulation of circadian-clock period and entrainment. Neuron *54*, 813–829.

Chittka, L., Stelzer, R.J., and Stanewsky, R. (2013). Daily changes in ultraviolet light levels can synchronize the circadian clock of bumblebees (Bombus terrestris). Chronobiol. Int. *30*, 434–442.

Clark, R.E., Zola, S.M., and Squire, L.R. (2000). Impaired recognition memory in rats after damage to the hippocampus. J. Neurosci. *20*, 8853–8860.

Coleman, D.L., and Hummel, K.P. (1973). The influence of genetic background on the expression of the obese (ob) gene in the mouse. Diabetologia *9*, 287–293.

Colwell, C.S., and Foster, R.G. (1992). Photic regulation of Fos-like immunoreactivity in the suprachiasmatic nucleus of the mouse. J. Comp. Neurol. *324*, 135–142.

Colwell, C.S., Foster, R.G., and Menaker, M. (1991). NMDA receptor antagonists block the effects of light on circadian behavior in the mouse. Brain Res. *554*, 105–110.

Coombs, J., van der List, D., Wang, G.-Y., and Chalupa, L.M. (2006). Morphological properties of mouse retinal ganglion cells. Neuroscience *140*, 123–136.

Cooper, G.F., and Robson, J.G. (1969). The yellow colour of the lens of the grey squirrel (sciurus carolinensis leucotis). J. Physiol. *203*, 403–410.

Cowey, A., and Franzini, C. (1979). The retinal origin of uncrossed optic nerve fibres in rats and their role in visual discrimination. Exp. Brain Res. *35*, 443–455.

Crawley, J., and Goodwin, F.K. (1980). Preliminary report of a simple animal behavior model for the anxiolytic effects of benzodiazepines. Pharmacol. Biochem. Behav. *13*, 167–170.

Crouch, R.K. (2009). The Visual Cycle: Generation of 11-cis Retinal for Photoreceptors. In Photobiological Sciences Online, K.C. Smith, ed. (American Society for Photobiology),.

Crozier, W.J., and Pincus, G. (1927). Phototropism in young rats. J. Gen. Physiol. *10*, 407–417.

Czeisler, C.A., and Klerman, E.B. (1999). Circadian and sleep-dependent regulation of hormone release in humans. Recent Prog. Horm. Res. *54*, 97–130; discussion 130–132.

Czeisler, C.A., Shanahan, T.L., Klerman, E.B., Martens, H., Brotman, D.J., Emens, J.S., Klein, T., and Rizzo, J.F., 3rd (1995). Suppression of melatonin secretion in some blind patients by exposure to bright light. N. Engl. J. Med. *332*, 6–11.

Dacey, D.M., Liao, H.-W., Peterson, B.B., Robinson, F.R., Smith, V.C., Pokorny, J., Yau, K.-W., and Gamlin, P.D. (2005). Melanopsin-expressing ganglion cells in primate retina signal colour and irradiance and project to the LGN. Nature *433*, 749–754.

Daniele, L.L., Insinna, C., Chance, R., Wang, J., Nikonov, S.S., and Pugh, E.N. (2011). A mouse M-opsin monochromat: retinal cone photoreceptors have increased M-opsin expression when S-opsin is knocked out. Vision Res. *51*, 447–458.

David-Gray, Z.K., Cooper, H.M., Janssen, J.W., Nevo, E., and Foster, R.G. (1999). Spectral tuning of a circadian photopigment in a subterranean "blind" mammal (Spalax ehrenbergi). FEBS Lett. *461*, 343–347.

DeBruyne, J.P., Noton, E., Lambert, C.M., Maywood, E.S., Weaver, D.R., and Reppert, S.M. (2006). A Clock Shock: Mouse CLOCK Is Not Required for Circadian Oscillator Function. Neuron *50*, 465–477.

DeBruyne, J.P., Weaver, D.R., and Reppert, S.M. (2007). CLOCK and NPAS2 have overlapping roles in the suprachiasmatic circadian clock. Nat. Neurosci. *10*, 543–545.

Deegan, J., and Jacobs, G. (1993). On the Identity of the Cone Types of the Rat Retina. Exp. Eye Res. *56*, 375–377.

Desjardins, C., Maruniak, J.A., and Bronson, F.H. (1973). Social rank in house mice: differentiation revealed by ultraviolet visualization of urinary marking patterns. Science *182*, 939–941.

Dkhissi-Benyahya, O., Sicard, B., and Cooper, H.M. (2000). Effects of irradiance and stimulus duration on early gene expression (Fos) in the suprachiasmatic nucleus: temporal summation and reciprocity. J. Neurosci. *20*, 7790–7797.

Dkhissi-Benyahya, O., Gronfier, C., De Vanssay, W., Flamant, F., and Cooper, H.M. (2007). Modeling the Role of Mid-Wavelength Cones in Circadian Responses to Light. Neuron *53*, 677–687.

Do, M.T.H., Kang, S.H., Xue, T., Zhong, H., Liao, H.-W., Bergles, D.E., and Yau, K.-W. (2009). Photon capture and signalling by melanopsin retinal ganglion cells. Nature *457*, 281–287.

Doi, M., Cho, S., Yujnovsky, I., Hirayama, J., Cermakian, N., Cato, A.C.B., and Sassone-Corsi, P. (2007). Light-inducible and clock-controlled expression of MAP kinase phosphatase 1 in mouse central pacemaker neurons. J. Biol. Rhythms *22*, 127–139.

Dollet, A., Albrecht, U., Cooper, H.M., and Dkhissi-Benyahya, O. (2010). Cones are required for normal temporal responses to light of phase shifts and clock gene expression. Chronobiol. Int. *27*, 768–781.

Douglas, R.H., and Jeffery, G. (2014). The spectral transmission of ocular media suggests ultraviolet sensitivity is widespread among mammals. Proc. R. Soc. B Biol. Sci. *281*, 20132995.

Douglas, R.M., Alam, N.M., Silver, B.D., McGill, T.J., Tschetter, W.W., and Prusky, G.T. (2005). Independent visual threshold measurements in the two eyes of freely moving rats and mice using a virtual-reality optokinetic system. Vis. Neurosci. *22*, 677–684.

Doyle, S.E., Castrucci, A.M., McCall, M., Provencio, I., and Menaker, M. (2006). Nonvisual light responses in the Rpe65 knockout mouse: Rod loss restores sensitivity to the melanopsin system. Proc. Natl. Acad. Sci. *103*, 10432–10437.

Dräger, U.C., and Olsen, J.F. (1980). Origins of crossed and uncrossed retinal projections in pigmented and albino mice. J. Comp. Neurol. *191*, 383–412.

Dräger, U.C., and Olsen, J.F. (1981). Ganglion cell distribution in the retina of the mouse. Invest. Ophthalmol. Vis. Sci. *20*, 285–293.

Dreher, B., Sefton, A.J., Ni, S.Y., and Nisbett, G. (1985). The morphology, number, distribution and central projections of Class I retinal ganglion cells in albino and hooded rats. Brain. Behav. Evol. *26*, 10–48.

Dresp, B., and Langley, K. (2006). Fine structural dependence of ultraviolet reflections in the King Penguin beak horn. Anat. Rec. A. Discov. Mol. Cell. Evol. Biol. *288*, 213–222.

Drouyer, E., Rieux, C., Hut, R.A., and Cooper, H.M. (2007). Responses of suprachiasmatic nucleus neurons to light and dark adaptation: relative contributions of melanopsin and rod-cone inputs. J. Neurosci. *27*, 9623–9631.

Duffield, G.E. (2003). DNA microarray analyses of circadian timing: the genomic basis of biological time. J. Neuroendocrinol. *15*, 991–1002.

Dunlap, J.C. (1999). Molecular bases for circadian clocks. Cell *96*, 271–290.

Earnest, D.J., Iadarola, M., Yeh, H.H., and Olschowka, J.A. (1990). Photic regulation of c-fos expression in neural components governing the entrainment of circadian rhythms. Exp. Neurol. *109*, 353–361.

Ebihara, S., and Tsuji, K. (1980). Entrainment of the circadian activity rhythm to the light cycle: effective light intensity for a Zeitgeber in the retinal degenerate C3H mouse and the normal C57BL mouse. Physiol. Behav. *24*, 523–527.

Ebihara, S., Marks, T., Hudson, D.J., and Menaker, M. (1986). Genetic control of melatonin synthesis in the pineal gland of the mouse. Science *231*, 491–493.

Ecker, J.L., Dumitrescu, O.N., Wong, K.Y., Alam, N.M., Chen, S.-K., LeGates, T., Renna, J.M., Prusky, G.T., Berson, D.M., and Hattar, S. (2010). Melanopsin-expressing retinal ganglion-cell photoreceptors: cellular diversity and role in pattern vision. Neuron *67*, 49–60.

Edelstein, K., and Amir, S. (1999). The Role of the Intergeniculate Leaflet in Entrainment of Circadian Rhythms to a Skeleton Photoperiod. J. Neurosci. *19*, 372–380.

Ellenbogen, J.M. (2005). Cognitive benefits of sleep and their loss due to sleep deprivation. Neurology *64*, E25–E27.

Ennaceur, A. (2010). One-trial object recognition in rats and mice: methodological and theoretical issues. Behav. Brain Res. *215*, 244–254.

Ennaceur, A., and Delacour, J. (1988). A new one-trial test for neurobiological studies of memory in rats. 1: Behavioral data. Behav. Brain Res. *31*, 47–59.

Faulstich, M., van Alphen, A.M., Luo, C., du Lac, S., and De Zeeuw, C.I. (2006). Oculomotor plasticity during vestibular compensation does not depend on cerebellar LTD. J. Neurophysiol. *96*, 1187–1195.

Field, G.D., and Chichilnisky, E.J. (2007). Information processing in the primate retina: circuitry and coding. Annu. Rev. Neurosci. *30*, 1–30.

Figueiro, M.G., Bullough, J.D., Parsons, R.H., and Rea, M.S. (2004). Preliminary evidence for spectral opponency in the suppression of melatonin by light in humans. Neuroreport *15*, 313–316.

Fleishman, L.J., Loew, E.R., and Leal, M. (1993). Ultraviolet vision in lizards. Nature *365*, 397–397.

Forrester, J.V., Dick, A.D., McMenamin, P.G., and Lee, W.R. (2002a). Embryology and Early Development of the Eye and Adnexa. In The Eye: Basic Sciences in Practice, (Saunders),.

Forrester, J.V., Dick, A.D., McMenamin, P.G., and Lee, W.R. (2002b). Anatomy of the Eye and Orbit. In The Eye: Basic Sciences in Practice, (Saunders),.

Forrester, J.V., Dick, A.D., McMenamin, P.G., and Lee, W.R. (2002c). Biochemistry and Cell Biology. In The Eye: Basic Sciences in Practice, (Saunders),.

Forrester, J.V., Dick, A.D., McMenamin, P.G., and Lee, W.R. (2002d). Physiology of Vision and the Visual System. In The Eye: Basic Sciences in Practice, (Saunders),.

Foster, R.G. (1998). Shedding light on the biological clock. Neuron *20*, 829–832.

Foster, R.G. (2002). Keeping an Eye on the Time The Cogan Lecture. Invest. Ophthalmol. Vis. Sci. *43*, 1286–1298.

Foster, R.G., and Hankins, M.W. (2002). Non-rod, non-cone photoreception in the vertebrates. Prog. Retin. Eye Res. *21*, 507–527.

Foster, R.G., and Helfrich-Forster, C. (2001). The regulation of circadian clocks by light in fruitflies and mice. Philos. Trans. R. Soc. Lond. Ser. B *356*, 1779–1789.

Foster, R.G., Provencio, I., Hudson, D., Fiske, S., Grip, W.D., and Menaker, M. (1991). Circadian photoreception in the retinally degenerate mouse (rd/rd). J. Comp. Physiol. A *169*, 39–50.

Frasson, M., Sahel, J.A., Fabre, M., Simonutti, M., Dreyfus, H., and Picaud, S. (1999). Retinitis pigmentosa: rod photoreceptor rescue by a calcium-channel blocker in the rd mouse. Nat. Med. *5*, 1183–1187.

Freedman, M.S., Lucas, R.J., Soni, B., Schantz, M. von, Muñoz, M., David-Gray, Z., and Foster, R. (1999). Regulation of Mammalian Circadian Behavior by Non-rod, Non-cone, Ocular Photoreceptors. Science *284*, 502–504.

Frisch, K. v (1924). Sinnesphysiologie und „Sprache“ der Bienen. Naturwissenschaften *12*, 981–987.

Von Frisch, K. (1967). The dance language and orientation of bees. Harv. Univ. Press.

Froy, O., Gotter, A.L., Casselman, A.L., and Reppert, S.M. (2003). Illuminating the Circadian Clock in Monarch Butterfly Migration. Science *300*, 1303–1305.

Fu, Y., Liao, H.-W., Do, M.T.H., and Yau, K.-W. (2005). Non-image-forming ocular photoreception in vertebrates. Curr. Opin. Neurobiol. *15*, 415–422.

Fujun, X., Kailiang, H., Tengteng, Z., Paul, R., Xuzhong, W., and Yi, S. (2012). Behavioral evidence for cone-based ultraviolet vision in divergent bat species and implications for its evolution. Zool. Curitiba *29*, 109–114.

Gall, A.J., Smale, L., Yan, L., and Nunez, A.A. (2013). Lesions of the Intergeniculate Leaflet Lead to a Reorganization in Circadian Regulation and a Reversal in Masking Responses to Photic Stimuli in the Nile Grass Rat. PLoS ONE *8*, e67387.

Gau, D., Lemberger, T., von Gall, C., Kretz, O., Le Minh, N., Gass, P., Schmid, W., Schibler, U., Korf, H.W., and Schütz, G. (2002). Phosphorylation of CREB Ser142 regulates light-induced phase shifts of the circadian clock. Neuron *34*, 245–253.

Gekakis, N., Staknis, D., Nguyen, H.B., Davis, F.C., Wilsbacher, L.D., King, D.P., Takahashi, J.S., and Weitz, C.J. (1998). Role of the CLOCK protein in the mammalian circadian mechanism. Science *280*, 1564–1569.

Ghosh, K.K., Bujan, S., Haverkamp, S., Feigenspan, A., and Wässle, H. (2004). Types of bipolar cells in the mouse retina. J. Comp. Neurol. *469*, 70–82.

Ginty, D.D., Kornhauser, J.M., Thompson, M.A., Bading, H., Mayo, K.E., Takahashi, J.S., and Greenberg, M.E. (1993). Regulation of CREB phosphorylation in the suprachiasmatic nucleus by light and a circadian clock. Science *260*, 238–241.

Giolli, R.A., Blanks, R.H.I., and Lui, F. (2006). The accessory optic system: basic organization with an update on connectivity, neurochemistry, and function. Prog. Brain Res. *151*, 407–440.

Glickfeld, L.L., Reid, R.C., and Andermann, M.L. (2014). A mouse model of higher visual cortical function. Curr. Opin. Neurobiol. *24*, 28–33.

Godinho, S.I.H., Maywood, E.S., Shaw, L., Tucci, V., Barnard, A.R., Busino, L., Pagano, M., Kendall, R., Quwailid, M.M., Romero, M.R., et al. (2007). The after-hours mutant reveals a role for Fbxl3 in determining mammalian circadian period. Science *316*, 897–900.

Goldman, B.D. (2001). Mammalian photoperiodic system: formal properties and neuroendocrine mechanisms of photoperiodic time measurement. J. Biol. Rhythms *16*, 283–301.

Goldsmith, T.H. (1994). Ultraviolet receptors and color vision: Evolutionary implications and a dissonance of paradigms. Vision Res. *34*, 1479–1487.

Gooley, J.J., Lu, J., Chou, T.C., Scammell, T.E., and Saper, C.B. (2001). Melanopsin in cells of origin of the retinohypothalamic tract. Nat. Neurosci. *4*, 1165.

Gooley, J.J., Lu, J., Fischer, D., and Saper, C.B. (2003). A Broad Role for Melanopsin in Nonvisual Photoreception. J. Neurosci. *23*, 7093–7106.

Gooley, J.J., Rajaratnam, S.M.W., Brainard, G.C., Kronauer, R.E., Czeisler, C.A., and Lockley, S.W. (2010). Spectral responses of the human circadian system depend on the irradiance and duration of exposure to light. Sci. Transl. Med. *2*, 31ra33.

Gooley, J.J., Ho Mien, I., St Hilaire, M.A., Yeo, S.-C., Chua, E.C.-P., van Reen, E., Hanley, C.J., Hull, J.T., Czeisler, C.A., and Lockley, S.W. (2012). Melanopsin and rod-cone photoreceptors play different roles in mediating pupillary light responses during exposure to continuous light in humans. J. Neurosci. *32*, 14242–14253.

Gorgels, T.G., and van Norren, D. (1992). Spectral transmittance of the rat lens. Vision Res. *32*, 1509–1512.

Gouras, P., and Ekesten, B. (2004). Why do mice have ultra-violet vision? Exp. Eye Res. *79*, 887–892.

Govardovskii, V.I., Fyhrquist, N., Reuter, T., Kuzmin, D.G., and Donner, K. (2000). In search of the visual pigment template. Vis. Neurosci. *17*, 509–528.

Göz, D., Studholme, K., Lappi, D.A., Rollag, M.D., Provencio, I., and Morin, L.P. (2008). Targeted Destruction of Photosensitive Retinal Ganglion Cells with a Saporin Conjugate Alters the Effects of Light on Mouse Circadian Rhythms. PLoS ONE *3*, e3153.

Greenwald, S.H., Kuchenbecker, J.A., Roberson, D.K., Neitz, M., and Neitz, J. (2014). S-opsin knockout mice with the endogenous M-opsin gene replaced by an L-opsin variant. Vis. Neurosci. *31*, 25–37.

Grozdanic, S., Betts, D.M., Allbaugh, R.A., Sakaguchi, D.S., Kwon, Y.H., Kardon, R.H., and Sonea, L.M. (2003). Characterization of the pupil light reflex, electroretinogram and tonometric parameters in healthy mouse eyes. Curr. Eye Res. *26*, 371–378.

Guerin, M.B., McKernan, D.P., O'Brien, C.J., and Cotter, T.G. (2006). Retinal ganglion cells: dying to survive. Int. J. Dev. Biol. *50*, 665–674.

Güler, A.D., Ecker, J.L., Lall, G.S., Haq, S., Altimus, C.M., Liao, H.-W., Barnard, A.R., Cahill, H., Badea, T.C., Zhao, H., et al. (2008). Melanopsin cells are the principal conduits for rod-cone input to non-image-forming vision. Nature *453*, 102–105.

Hack, I., Frech, M., Dick, O., Peichl, L., and Brandstätter, J.H. (2001). Heterogeneous distribution of AMPA glutamate receptor subunits at the photoreceptor synapses of rodent retina. Eur. J. Neurosci. *13*, 15–24.

Haeseleer, F., Huang, J., Lebioda, L., Saari, J.C., and Palczewski, K. (1998). Molecular characterization of a novel short-chain dehydrogenase/reductase that reduces all-trans-retinal. J. Biol. Chem. *273*, 21790–21799.

Hammond, R.S., Tull, L.E., and Stackman, R.W. (2004). On the delay-dependent involvement of the hippocampus in object recognition memory. Neurobiol. Learn. Mem. *82*, 26–34.

Hankins, M.W., and Lucas, R.J. (2002). The primary visual pathway in humans is regulated according to long-term light exposure through the action of a nonclassical photopigment. Curr. Biol. CB *12*, 191–198.

Hannibal, J., and Fahrenkrug, J. (2002). Melanopsin: a novel photopigment involved in the photoentrainment of the brain's biological clock? Ann. Med. *34*, 401–407.

Hannibal, J., and Fahrenkrug, J. (2004). Target areas innervated by PACAP-immunoreactive retinal ganglion cells. Cell Tissue Res. *316*, 99–113.

Hannibal, J., Møller, M., Ottersen, O.P., and Fahrenkrug, J. (2000). PACAP and glutamate are co-stored in the retinohypothalamic tract. J. Comp. Neurol. *418*, 147–155.

Hannibal, J., Vrang, N., Card, J.P., and Fahrenkrug, J. (2001). Light-Dependent Induction of cFos during Subjective Day and Night in PACAP-Containing Ganglion Cells of the Retinohypothalamic Tract. J. Biol. Rhythms *16*, 457–470.

Hannibal, J., Hindersson, P., Knudsen, S.M., Georg, B., and Fahrenkrug, J. (2002). The photopigment melanopsin is exclusively present in pituitary adenylate cyclase-activating polypeptide-containing retinal ganglion cells of the retinohypothalamic tract. J. Neurosci. *22*, RC191.

Hannibal, J., Hindersson, P., Ostergaard, J., Georg, B., Heegaard, S., Larsen, P.J., and Fahrenkrug, J. (2004). Melanopsin is expressed in PACAP-containing retinal ganglion cells of the human retinohypothalamic tract. Invest. Ophthalmol. Vis. Sci. *45*, 4202–4209.

Hastings, M.H., and Goedert, M. (2013). Circadian clocks and neurodegenerative diseases: time to aggregate? Curr. Opin. Neurobiol. *23*, 880–887.

Hastings, M.H., and Herzog, E.D. (2004). Clock genes, oscillators, and cellular networks in the suprachiasmatic nuclei. J. Biol. Rhythms *19*, 400–413.

Hastings, M., O'Neill, J.S., and Maywood, E.S. (2007). Circadian clocks: regulators of endocrine and metabolic rhythms. J. Endocrinol. *195*, 187–198.

Hatori, M., and Panda, S. (2010). The emerging roles of melanopsin in behavioral adaptation to light. Trends Mol. Med. *16*, 435–446.

Hatori, M., Le, H., Vollmers, C., Keding, S.R., Tanaka, N., Schmedt, C., Jegla, T., and Panda, S. (2008). Inducible Ablation of Melanopsin-Expressing Retinal Ganglion Cells Reveals Their Central Role in Non-Image Forming Visual Responses. PLoS ONE *3*, e2451.

Hattar, S., Liao, H.W., Takao, M., Berson, D.M., and Yau, K.W. (2002). Melanopsin-containing retinal ganglion cells: architecture, projections, and intrinsic photosensitivity. Science *295*, 1065–1070.

Hattar, S., Lucas, R.J., Mrosovsky, N., Thompson, S., Douglas, R.H., Hankins, M.W., Lem, J., Biel, M., Hofmann, F., Foster, R.G., et al. (2003). Melanopsin and rod-cone photoreceptive systems account for all major accessory visual functions in mice. Nature *424*, 76–81.

Hattar, S., Kumar, M., Park, A., Tong, P., Tung, J., Yau, K.-W., and Berson, D.M. (2006). Central projections of melanopsin-expressing retinal ganglion cells in the mouse. J. Comp. Neurol. *497*, 326–349.

Haverkamp, S., and Wässle, H. (2000). Immunocytochemical analysis of the mouse retina. J. Comp. Neurol. *424*, 1–23.

Haverkamp, S., Wässle, H., Duebel, J., Kuner, T., Augustine, G.J., Feng, G., and Euler, T. (2005). The primordial, blue-cone color system of the mouse retina. J. Neurosci. *25*, 5438–5445.

Hayhow, W.R., Webb, C., and Jervie, A. (1960). The accessory optic fiber system in the rat. J. Comp. Neurol. *115*, 187–215.

Hendrickson, A.E., Wagoner, N., and Cowan, W.M. (1972). An autoradiographic and electron microscopic study of retino-hypothalamic connections. Z. Für Zellforsch. Mikrosk. Anat. *135*, 1–26.

Ait-Hmyed, O., Felder-Schmittbuhl, M.-P., Garcia-Garrido, M., Beck, S., Seide, C., Sothilingam, V., Tanimoto, N., Seeliger, M., Bennis, M., and Hicks, D. (2013). Mice lacking Period 1 and Period 2 circadian clock genes exhibit blue cone photoreceptor defects. Eur. J. Neurosci. *37*, 1048–1060.

Hobbelen, J.F., and Collewijn, H. (1971). Effect of cerebro/cortical and collicular ablations upon the optokinetic reactions in the rabbit. Doc. Ophthalmol. *30*, 227–236.

Hofbauer, A., and Dräger, U.C. (1985). Depth segregation of retinal ganglion cells projecting to mouse superior colliculus. J. Comp. Neurol. *234*, 465–474.

Hogg, C., Neveu, M., Stokkan, K.-A., Folkow, L., Cottrill, P., Douglas, R., Hunt, D.M., and Jeffery, G. (2011). Arctic reindeer extend their visual range into the ultraviolet. J. Exp. Biol. *214*, 2014–2019.

Honkavaara, J., Koivula, M., Korpimäki, E., Siitari, H., and Viitala, J. (2002). Ultraviolet vision and foraging in terrestrial vertebrates. Oikos *98*, 505–511.

Van der Horst, G.T., Muijtjens, M., Kobayashi, K., Takano, R., Kanno, S., Takao, M., de Wit, J., Verkerk, A., Eker, A.P., van Leenen, D., et al. (1999). Mammalian Cry1 and Cry2 are essential for maintenance of circadian rhythms. Nature *398*, 627–630.

Huang, N., Chelliah, Y., Shan, Y., Taylor, C.A., Yoo, S.-H., Partch, C., Green, C.B., Zhang, H., and Takahashi, J.S. (2012). Crystal Structure of the Heterodimeric CLOCK:BMAL1 Transcriptional Activator Complex. Science *337*, 189–194.

Huberman, A.D., and Niell, C.M. (2011). What can mice tell us about how vision works? Trends Neurosci. *34*, 464–473.

Huerta, J.J., Llamosas, M.M., Cernuda-Cernuda, R., and García-Fernández, J.M. (1997). Fos expression in the retina of rd/rd mice during the light/dark cycle. Neurosci. Lett. *232*, 143–146.

Huerta, J.J., Llamosas, M.M., Cernuda-Cernuda, R., and García-Fernández, J.M. (1999). Spatio-temporal analysis of light-induced Fos expression in the retina of rd mutant mice. Brain Res. *834*, 122–127.

Hughes, R.J., and Badia, P. (1997). Sleep-promoting and hypothermic effects of daytime melatonin administration in humans. Sleep *20*, 124–131.

Hughes, S., Hankins, M.W., Foster, R.G., and Peirson, S.N. (2012a). Melanopsin phototransduction: slowly emerging from the dark. Prog. Brain Res. *199*, 19–40.

Hughes, S., Welsh, L., Katti, C., González-Menéndez, I., Turton, M., Halford, S., Sekaran, S., Peirson, S.N., Hankins, M.W., and Foster, R.G. (2012b). Differential expression of

melanopsin isoforms Opn4L and Opn4S during postnatal development of the mouse retina. PloS One *7*, e34531.

Hughes, S., Pothecary, C.A., Jagannath, A., Foster, R.G., Hankins, M.W., and Peirson, S.N. (2012c). Profound defects in pupillary responses to light in TRPM-channel null mice: a role for TRPM channels in non-image-forming photoreception. Eur. J. Neurosci. *35*, 34–43.

Hughes, S., Watson, T.S., Foster, R.G., Peirson, S.N., and Hankins, M.W. (2013). Nonuniform distribution and spectral tuning of photosensitive retinal ganglion cells of the mouse retina. Curr. Biol. CB *23*, 1696–1701.

Hunt, D.M., Wilkie, S.E., Bowmaker, J.K., and Poopalasundaram, S. (2001a). Vision in the ultraviolet. Cell. Mol. Life Sci. CMLS *58*, 1583–1598.

Hunt, S., Bennett, A.T.D., Cuthill, I.C., and Griffiths, R. (1998). Blue tits are ultraviolet tits. Proc. R. Soc. B Biol. Sci. *265*, 451–455.

Hunt, S., Cuthill, I.C., Bennett, A.T.D., Church, S.C., and Partridge, J.C. (2001b). Is the ultraviolet waveband a special communication channel in avian mate choice? J. Exp. Biol. *204*, 2499–2507.

Hut, R.A., Scheper, A., and Daan, S. (2000). Can the circadian system of a diurnal and a nocturnal rodent entrain to ultraviolet light? J. Comp. Physiol. [A] *186*, 707–715.

Illing, R.B., and Wässle, H. (1981). The retinal projection to the thalamus in the cat: a quantitative investigation and a comparison with the retinotectal pathway. J. Comp. Neurol. *202*, 265–285.

Ito, M. (1982). Cerebellar Control of the Vestibulo-Ocular Reflex–Around the Flocculus Hypothesis. Annu. Rev. Neurosci. *5*, 275–297.

Jacobs, G.H. (1983). Within-species variations in visual capacity among squirrel monkeys (Saimiri sciureus): Sensitivity differences. Vision Res. *23*, 239–248.

Jacobs, G.H. (1992). Ultraviolet Vision in Vertebrates. Am. Zool. *32*, 544–554.

Jacobs, G.H., and Williams, G.A. (2007). Contributions of the mouse UV photopigment to the ERG and to vision. Doc. Ophthalmol. Adv. Ophthalmol. *115*, 137–144.

Jacobs, G., Fenwick, J., and Williams, G. (2002). Evaluating the Prospects for Color Vision in the Mouse. ARVO Meet. Abstr. *43*, 1780.

Jacobs, G.H., Neitz, J., and Deegan, J.F. (1991). Retinal receptors in rodents maximally sensitive to ultraviolet light. Nature *353*, 655–656.

Jacobs, G.H., Fenwick, J.C., Calderone, J.B., and Deeb, S.S. (1999). Human cone pigment expressed in transgenic mice yields altered vision. J. Neurosci. *19*, 3258–3265.

Jacobs, G.H., Fenwick, J.A., and Williams, G.A. (2001). Cone-based vision of rats for ultraviolet and visible lights. J. Exp. Biol. *204*, 2439–2446.

Jacobs, G.H., Williams, G.A., and Fenwick, J.A. (2004). Influence of cone pigment coexpression on spectral sensitivity and color vision in the mouse. Vision Res. *44*, 1615–1622.

Jacobs, G.H., Williams, G.A., Cahill, H., and Nathans, J. (2007). Emergence of Novel Color Vision in Mice Engineered to Express a Human Cone Photopigment. Science *315*, 1723–1725.

Jagannath, A., Butler, R., Godinho, S.I.H., Couch, Y., Brown, L.A., Vasudevan, S.R., Flanagan, K.C., Anthony, D., Churchill, G.C., Wood, M.J.A., et al. (2013). The CRTC1-SIK1 pathway regulates entrainment of the circadian clock. Cell *154*, 1100–1111.

Jaissle, G.B., May, C.A., Reinhard, J., Kohler, K., Fauser, S., Lütjen–Drecoll, E., Zrenner, E., and Seeliger, M.W. (2001). Evaluation of the Rhodopsin Knockout Mouse as a Model of Pure Cone Function. Invest. Ophthalmol. Vis. Sci. *42*, 506–513.

Jeon, C.-J., Strettoi, E., and Masland, R.H. (1998). The Major Cell Populations of the Mouse Retina. J. Neurosci. *18*, 8936–8946.

Jud, C., Schmutz, I., Hampp, G., Oster, H., and Albrecht, U. (2005). A guideline for analyzing circadian wheel-running behavior in rodents under different lighting conditions. Biol. Proced. Online *7*, 101–116.

Keeler, C.E. (1924). The Inheritance of a Retinal Abnormality in White Mice. Proc. Natl. Acad. Sci. U. S. A. *10*, 329–333.

Kevan, P.G., Chittka, L., and Dyer, A.G. (2001). Limits to the salience of ultraviolet: lessons from colour vision in bees and birds. J. Exp. Biol. *204*, 2571–2580.

King, D.P., Vitaterna, M.H., Chang, A.M., Dove, W.F., Pinto, L.H., Turek, F.W., and Takahashi, J.S. (1997). The mouse Clock mutation behaves as an antimorph and maps within the W19H deletion, distal of Kit. Genetics *146*, 1049–1060.

Klooster, J., Beckers, H.J., Vrensen, G.F., and van der Want, J.J. (1993). The peripheral and central projections of the Edinger-Westphal nucleus in the rat. A light and electron microscopic tracing study. Brain Res. *632*, 260–273.

Klooster, J., Vrensen, G.F., Müller, L.J., and van der Want, J.J. (1995). Efferent projections of the olivary pretectal nucleus in the albino rat subserving the pupillary light reflex and related reflexes. A light microscopic tracing study. Brain Res. *688*, 34–46.

Knüttel, H., and Fiedler, K. (2001). Host-plant-derived variation in ultraviolet wing patterns influences mate selection by male butterflies. J. Exp. Biol. *204*, 2447–2459.

Ko, C.H., and Takahashi, J.S. (2006). Molecular components of the mammalian circadian clock. Hum. Mol. Genet. *15 Spec No 2*, R271–R277.

Koistinaho, J., and Sagar, S.M. (1995). Light-induced c-fos expression in amacrine cells in the rabbit retina. Mol. Brain Res. *29*, 53–63.

Kojima, D., Mori, S., Torii, M., Wada, A., Morishita, R., and Fukada, Y. (2011). UV-Sensitive Photoreceptor Protein OPN5 in Humans and Mice. PLoS ONE *6*.

Kolb, H. (1979). The inner plexiform layer in the retina of the cat: electron microscopic observations. J. Neurocytol. *8*, 295–329.

Kornhauser, J.M., Nelson, D.E., Mayo, K.E., and Takahashi, J.S. (1990). Photic and circadian regulation of c-fos gene expression in the hamster suprachiasmatic nucleus. Neuron *5*, 127–134.

Kott, O., Šumbera, R., and Němec, P. (2010). Light Perception in Two Strictly Subterranean Rodents: Life in the Dark or Blue? PLoS ONE *5*, e11810.

Krause, M., Distler, C., and Hoffmann, K.-P. (2014). Retinal ganglion cells projecting to the accessory optic system in optokinetic blind albinotic rats are direction-selective. Eur. J. Neurosci. *40*, 2274–2282.

Kühn, H., and Wilden, U. (1987). Deactivation of photoactivated rhodopsin by rhodopsin-kinase and arrestin. J. Recept. Res. *7*, 283–298.

Lall, G.S., Revell, V.L., Momiji, H., Al Enezi, J., Altimus, C.M., Güler, A.D., Aguilar, C., Cameron, M.A., Allender, S., Hankins, M.W., et al. (2010). Distinct contributions of rod, cone, and melanopsin photoreceptors to encoding irradiance. Neuron *66*, 417–428.

Lamb, T.D., and Pugh, E.N. (2006). Phototransduction, Dark Adaptation, and Rhodopsin Regeneration The Proctor Lecture. Invest. Ophthalmol. Vis. Sci. *47*, 5138–5152.

Larsen, P.J., Enquist, L.W., and Card, J.P. (1998). Characterization of the multisynaptic neuronal control of the rat pineal gland using viral transneuronal tracing. Eur. J. Neurosci. *10*, 128–145.

Leamey, C.A., Protti, D.A., and Dreher, B. (2008). Comparative Survey of the Mammalian Visual System with Reference to the Mouse. In Eye, Retina, and Visual System of the Mouse, L.M. Chalupa, and R.W. Williams, eds. (Massachusetts Institute od Technology),.

Lee, H., Chen, R., Kim, H., Etchegaray, J.-P., Weaver, D.R., and Lee, C. (2011). The period of the circadian oscillator is primarily determined by the balance between casein kinase 1 and protein phosphatase 1. Proc. Natl. Acad. Sci. 201107178.

Lei, B., and Yao, G. (2006). Spectral attenuation of the mouse, rat, pig and human lenses from wavelengths 360 nm to 1020 nm. Exp. Eye Res. *83*, 610–614.

Lewy, A.J., Wehr, T.A., Goodwin, F.K., Newsome, D.A., and Markey, S.P. (1980). Light suppresses melatonin secretion in humans. Science *210*, 1267–1269.

Lin, B., Koizumi, A., Tanaka, N., Panda, S., and Masland, R.H. (2008). Restoration of visual function in retinal degeneration mice by ectopic expression of melanopsin. Proc. Natl. Acad. Sci. U. S. A. *105*, 16009–16014.

Lin, J.T., Kornhauser, J.M., Singh, N.P., Mayo, K.E., and Takahashi, J.S. (1997). Visual sensitivities of nur77 (NGFI-B) and zif268 (NGFI-A) induction in the suprachiasmatic nucleus are dissociated from c-fos induction and behavioral phase-shifting responses. Brain Res. Mol. Brain Res. *46*, 303–310.

Lind, O., Mitkus, M., Olsson, P., and Kelber, A. (2013). Ultraviolet sensitivity and colour vision in raptor foraging. J. Exp. Biol. *216*, 1819–1826.

Ling, C., Schneider, G.E., and Jhaveri, S. (1998). Target-specific morphology of retinal axon arbors in the adult hamster. Vis. Neurosci. *15*, 559–579.

Liu, A.C., Welsh, D.K., Ko, C.H., Tran, H.G., Zhang, E.E., Priest, A.A., Buhr, E.D., Singer, O., Meeker, K., Verma, I.M., et al. (2007). Intercellular coupling confers robustness against mutations in the SCN circadian clock network. Cell *129*, 605–616.

Liu, A.C., Tran, H.G., Zhang, E.E., Priest, A.A., Welsh, D.K., and Kay, S.A. (2008). Redundant function of REV-ERBalpha and beta and non-essential role for Bmal1 cycling in transcriptional regulation of intracellular circadian rhythms. PLoS Genet. *4*, e1000023.

Liu, J., Itagaki, Y., Ben-Shabat, S., Nakanishi, K., and Sparrow, J.R. (2000). The biosynthesis of A2E, a fluorophore of aging retina, involves the formation of the precursor, A2-PE, in the photoreceptor outer segment membrane. J. Biol. Chem. *275*, 29354–29360.

Lockley, S.W., Evans, E.E., Scheer, F.A.J.L., Brainard, G.C., Czeisler, C.A., and Aeschbach, D. (2006). Short-wavelength sensitivity for the direct effects of light on alertness, vigilance, and the waking electroencephalogram in humans. Sleep *29*, 161–168.

Loew, E.R., McFarland, W.N., Mills, E.L., and Hunter, D. (1993). A chromatic action spectrum for planktonic predation by juvenile yellow perch, Perca flavescens. Can. J. Zool. *71*, 384–386.

Longbottom, R., Fruttiger, M., Douglas, R.H., Martinez-Barbera, J.P., Greenwood, J., and Moss, S.E. (2009). Genetic ablation of retinal pigment epithelial cells reveals the adaptive response of the epithelium and impact on photoreceptors. Proc. Natl. Acad. Sci. U. S. A. *106*, 18728–18733.

Lovejoy, L.P., and Krauzlis, R.J. (2010). Inactivation of primate superior colliculus impairs covert selection of signals for perceptual judgments. Nat. Neurosci. *13*, 261–266.

Lowrey, P.L., and Takahashi, J.S. (2004). Mammalian circadian biology: elucidating genome-wide levels of temporal organization. Annu. Rev. Genomics Hum. Genet. *5*, 407–441.

Lucas, R.J., Freedman, M.S., Muñoz, M., Garcia-Fernández, J.M., and Foster, R.G. (1999). Regulation of the mammalian pineal by non-rod, non-cone, ocular photoreceptors. Science *284*, 505–507.

Lucas, R.J., Douglas, R.H., and Foster, R.G. (2001). Characterization of an ocular photopigment capable of driving pupillary constriction in mice. Nat. Neurosci. *4*, 621–626.

Lucas, R.J., Hattar, S., Takao, M., Berson, D.M., Foster, R.G., and Yau, K.-W. (2003). Diminished pupillary light reflex at high irradiances in melanopsin-knockout mice. Science *299*, 245–247.

Lucas, R.J., Lall, G.S., Allen, A.E., and Brown, T.M. (2012). How rod, cone, and melanopsin photoreceptors come together to enlighten the mammalian circadian clock. Prog. Brain Res. *199*, 1–18.

Lupi, D., Cooper, H.M., Froehlich, A., Standford, L., McCall, M.A., and Foster, R.G. (1999). Transgenic ablation of rod photoreceptors alters the circadian phenotype of mice. Neuroscience *89*, 363–374.

Lupi, D., Oster, H., Thompson, S., and Foster, R.G. (2008). The acute light-induction of sleep is mediated by OPN4-based photoreception. Nat. Neurosci. *11*, 1068–1073.

Lutz, F.E. (1920). Apparently Non-Selective Characters and Combinations of Characters, Including a Study of Ultraviolet in Relation to the Flower-Visiting Habits of Insects. Ann. N. Y. Acad. Sci. *29*, 181–283.

Lyubarsky, A.L., Falsini, B., Pennesi, M.E., Valentini, P., and Pugh, E.N. (1999). UV- and midwave-sensitive cone-driven retinal responses of the mouse: a possible phenotype for coexpression of cone photopigments. J. Neurosci. *19*, 442–455.

Lyubarsky, A.L., Daniele, L.L., and Pugh, E.N. (2004). From candelas to photoisomerizations in the mouse eye by rhodopsin bleaching in situ and the light-rearing dependence of the major components of the mouse ERG. Vision Res. *44*, 3235–3251.

Lyubarsky, A.L., Nikonov, S.S., Daniele, L.L., and Pugh, E.N., Jr (2008). Recent Advances in the Investigation of Mouse Cone Photoreceptors. In Eye, Retina, and Visual System of the Mouse, L.M. Chalupa, and R.W. Williams, eds. (Massachusetts Institute od Technology),.

Madronich, S., McKenzie, R.L., Björn, L.O., and Caldwell, M.M. (1998). Changes in biologically active ultraviolet radiation reaching the Earth's surface. J. Photochem. Photobiol. B *46*, 5–19.

Marshel, J.H., Garrett, M.E., Nauhaus, I., and Callaway, E.M. (2011). Functional specialization of seven mouse visual cortical areas. Neuron *72*, 1040–1054.

Martin Schaefer, H., Schaefer, V., and Vorobyev, M. (2007). Are fruit colors adapted to consumer vision and birds equally efficient in detecting colorful signals? Am. Nat. *169 Suppl 1*, S159–S169.

Masana, M.I., Benloucif, S., and Dubocovich, M.L. (1996). Light-induced c-fos mRNA expression in the suprachiasmatic nucleus and the retina of C3H/HeN mice. Brain Res. Mol. Brain Res. *42*, 193–201.

Masu, M., Iwakabe, H., Tagawa, Y., Miyoshi, T., Yamashita, M., Fukuda, Y., Sasaki, H., Hiroi, K., Nakamura, Y., and Shigemoto, R. (1995). Specific deficit of the ON response in visual transmission by targeted disruption of the mGluR6 gene. Cell *80*, 757–765.

McCall, M.J., Robinson, S.R., and Dreher, B. (1987). Differential retinal growth appears to be the primary factor producing the ganglion cell density gradient in the rat. Neurosci. Lett. *79*, 78–84.

McDougal, D.H., and Gamlin, P.D. (2010). The influence of intrinsically-photosensitive retinal ganglion cells on the spectral sensitivity and response dynamics of the human pupillary light reflex. Vision Res. *50*, 72–87.

McGuire, R.A., Rand, W.M., and Wurtman, R.J. (1973). Entrainment of the body temperature rhythm in rats: effect of color and intensity of environmental light. Science *181*, 956–957.

McNeill, D.S., Sheely, C.J., Ecker, J.L., Badea, T.C., Morhardt, D., Guido, W., and Hattar, S. (2011). Development of melanopsin-based irradiance detecting circuitry. Neural Develop. *6*, 8.

Meijer, J.H., and Schwartz, W.J. (2003). In search of the pathways for light-induced pacemaker resetting in the suprachiasmatic nucleus. J. Biol. Rhythms *18*, 235–249.

Melyan, Z., Tarttelin, E.E., Bellingham, J., Lucas, R.J., and Hankins, M.W. (2005). Addition of human melanopsin renders mammalian cells photoresponsive. Nature *433*, 741–745.

Métin, C., Irons, W.A., and Frost, D.O. (1995). Retinal ganglion cells in normal hamsters and hamsters with novel retinal projections. I. Number, distribution, and size. J. Comp. Neurol. *353*, 179–199.

Miyamoto, M., Aoki, M., Hirai, K., Sugimoto, S., Kawasaki, K., and Imai, R. (2010). A nonsense mutation in Gnat1, encoding the α subunit of rod transducin, in spontaneous mouse models of retinal dysfunction. Exp. Eye Res. *90*, 63–69.

Montgomery, N., Fite, K.V., Taylor, M., and Bengston, L. (1982). Neural correlates of optokinetic nystagmus in the mesencephalon of Rana pipiens: a functional analysis. Brain. Behav. Evol. *21*, 137–150.

Moore, R.Y., Speh, J.C., and Card, J.P. (1995). The retinohypothalamic tract originates from a distinct subset of retinal ganglion cells. J. Comp. Neurol. *352*, 351–366.

Morin, L.P., and Allen, C.N. (2006). The circadian visual system, 2005. Brain Res. Rev. *51*, 1–60.

Morris, M.E., Viswanathan, N., Kuhlman, S., Davis, F.C., and Weitz, C.J. (1998). A screen for genes induced in the suprachiasmatic nucleus by light. Science *279*, 1544–1547.

Morris, R.G.M., Garrud, P., Rawlins, J.N.P., and O'Keefe, J. (1982). Place navigation impaired in rats with hippocampal lesions. Nature *297*, 681–683.

Motulsky, H.J., and Christopoulos, A. (2003). Fitting models to biological data using linear and nonlinear regression. A practical guide to curve fitting (San Diego CA: GraphPad Software Inc.).

Mrosovsky, N. (1999). Masking: history, definitions, and measurement. Chronobiol. Int. *16*, 415–429.

Mrosovsky, N. (2003). Contribution of classic photoreceptors to entrainment. J. Comp. Physiol. A Neuroethol. Sens. Neural. Behav. Physiol. *189*, 69–73.

Mrosovsky, N., and Hampton, R.R. (1997). Spatial responses to light in mice with severe retinal degeneration. Neurosci. Lett. *222*, 204–206.

Mrosovsky, N., and Hattar, S. (2003). Impaired Masking Responses to Light in Melanopsin-Knockout Mice. Chronobiol. Int. *20*, 989–999.

Mrosovsky, N., and Thompson, S. (2008). Negative and positive masking responses to light in retinal degenerate slow (rds/rds) mice during aging. Vision Res. *48*, 1270–1273.

Mrosovsky, N., Foster, R.G., and Salmon, P.A. (1999). Thresholds for masking responses to light in three strains of retinally degenerate mice. J. Comp. Physiol. [A] *184*, 423–428.

Mrosovsky, N., Salmon, P.A., Foster, R.G., and McCall, M.A. (2000). Responses to light after retinal degeneration. Vision Res. *40*, 575–578.

Muindi, F., Zeitzer, J.M., and Heller, H.C. (2014). Retino-hypothalamic regulation of light-induced murine sleep. Front. Syst. Neurosci. *8*.

Müller, L.P. de S., Do, M.T.H., Yau, K.-W., He, S., and Baldridge, W.H. (2010). Tracer coupling of intrinsically photosensitive retinal ganglion cells to amacrine cells in the mouse retina. J. Comp. Neurol. *518*, 4813–4824.

Mure, L.S., Rieux, C., Hattar, S., and Cooper, H.M. (2007). Melanopsin-dependent nonvisual responses: evidence for photopigment bistability in vivo. J. Biol. Rhythms *22*, 411–424.

Naarendorp, F., Esdaille, T.M., Banden, S.M., Andrews-Labenski, J., Gross, O.P., and Pugh, E.N. (2010). Dark Light, Rod Saturation, and the Absolute and Incremental Sensitivity of Mouse Cone Vision. J. Neurosci. *30*, 12495–12507.

Natarajan, V.T., Ganju, P., Ramkumar, A., Grover, R., and Gokhale, R.S. (2014). Multifaceted pathways protect human skin from UV radiation. Nat. Chem. Biol. *10*, 542–551.

Nathans, J., Thomas, D., and Hogness, D.S. (1986). Molecular genetics of human color vision: the genes encoding blue, green, and red pigments. Science *232*, 193–202.

Neitz, J., and Neitz, M. (2011). The genetics of normal and defective color vision. Vision Res. *51*, 633–651.

Neitz, M., and Neitz, J. (2001). The uncommon retina of the common house mouse. Trends Neurosci. *24*, 248–250.

Nelson, R. (1977). Cat cones have rod input: A comparison of the response properties of cones and horizontal cell bodies in the retina of the cat. J. Comp. Neurol. *172*, 109–135.

Nelson, D.E., and Takahashi, J.S. (1999). Integration and saturation within the circadian photic entrainment pathway of hamsters. Am. J. Physiol. *277*, R1351–R1361.

Nelson, R.J., and Zucker, I. (1981). Absence of extraocular photoreception in diurnal and nocturnal rodents exposed to direct sunlight. Comp. Biochem. Physiol. A Physiol. *69*, 145–148.

Newman, L.A., Walker, M.T., Brown, R.L., Cronin, T.W., and Robinson, P.R. (2003). Melanopsin forms a functional short-wavelength photopigment. Biochemistry (Mosc.) *42*, 12734–12738.

Ng, L., Hurley, J.B., Dierks, B., Srinivas, M., Saltó, C., Vennström, B., Reh, T.A., and Forrest, D. (2001). A thyroid hormone receptor that is required for the development of green cone photoreceptors. Nat. Genet. *27*, 94–98.

Niell, C.M., and Stryker, M.P. (2008). Highly Selective Receptive Fields in Mouse Visual Cortex. J. Neurosci. *28*, 7520–7536.

Nikonov, S.S., Kholodenko, R., Lem, J., and Pugh, E.N., Jr (2006). Physiological features of the S- and M-cone photoreceptors of wild-type mice from single-cell recordings. J. Gen. Physiol. *127*, 359–374.

Van Norren, D., and Schellekens, P. (1990). Blue light hazard in rat. Vision Res. *30*, 1517–1520.

O'Brien, J.J., Chen, X., Macleish, P.R., O'Brien, J., and Massey, S.C. (2012). Photoreceptor coupling mediated by connexin36 in the primate retina. J. Neurosci. Off. J. Soc. Neurosci. *32*, 4675–4687.

Ohta, H., Yamazaki, S., and McMahon, D.G. (2005). Constant light desynchronizes mammalian clock neurons. Nat. Neurosci. *8*, 267–269.

Ölveczky, B.P., Baccus, S.A., and Meister, M. (2003). Segregation of object and background motion in the retina. Nature *423*, 401–408.

Omri, S., Omri, B., Savoldelli, M., Jonet, L., Thillaye-Goldenberg, B., Thuret, G., Gain, P., Jeanny, J.C., Crisanti, P., and Behar-Cohen, F. (2010). The outer limiting membrane (OLM) revisited: clinical implications. Clin. Ophthalmol. Auckl. NZ *4*, 183–195.

Van Oosterhout, F., Fisher, S.P., van Diepen, H.C., Watson, T.S., Houben, T., VanderLeest, H.T., Thompson, S., Peirson, S.N., Foster, R.G., and Meijer, J.H. (2012). Ultraviolet light provides a major input to non-image-forming light detection in mice. Curr. Biol. CB *22*, 1397–1402.

Packer, O., Hendrickson, A.E., and Curcio, C.A. (1989). Photoreceptor topography of the retina in the adult pigtail macaque (Macaca nemestrina). J. Comp. Neurol. *288*, 165–183.

Paigen, K. (1995). A miracle enough: the power of mice. Nat. Med. *1*, 215–220.

Panda, S. (2008). Photoentrainment of the Circadian Oscillator. In Eye, Retina, and Visual System of the Mouse, L.M. Chalupa, and R.W. Williams, eds. (Massachusetts Institute od Technology),.

Panda, S., Antoch, M.P., Miller, B.H., Su, A.I., Schook, A.B., Straume, M., Schultz, P.G., Kay, S.A., Takahashi, J.S., and Hogenesch, J.B. (2002a). Coordinated transcription of key pathways in the mouse by the circadian clock. Cell *109*, 307–320.

Panda, S., Sato, T.K., Castrucci, A.M., Rollag, M.D., DeGrip, W.J., Hogenesch, J.B., Provencio, I., and Kay, S.A. (2002b). Melanopsin (Opn4) requirement for normal light-induced circadian phase shifting. Science *298*, 2213–2216.

Panda, S., Provencio, I., Tu, D.C., Pires, S.S., Rollag, M.D., Castrucci, A.M., Pletcher, M.T., Sato, T.K., Wiltshire, T., Andahazy, M., et al. (2003). Melanopsin is required for non-image-forming photic responses in blind mice. Science *301*, 525–527.

Panda, S., Nayak, S.K., Campo, B., Walker, J.R., Hogenesch, J.B., and Jegla, T. (2005). Illumination of the melanopsin signaling pathway. Science *307*, 600–604.

Partch, C.L., Shields, K.F., Thompson, C.L., Selby, C.P., and Sancar, A. (2006). Posttranslational regulation of the mammalian circadian clock by cryptochrome and protein phosphatase 5. Proc. Natl. Acad. Sci. U. S. A. *103*, 10467–10472.

Partch, C.L., Green, C.B., and Takahashi, J.S. (2014). Molecular architecture of the mammalian circadian clock. Trends Cell Biol. *24*, 90–99.

Peichl, L., and González-Soriano, J. (1994). Morphological types of horizontal cell in rodent retinae: a comparison of rat, mouse, gerbil, and guinea pig. Vis. Neurosci. *11*, 501–517.

Peirson, S.N., Thompson, S., Hankins, M.W., and Foster, R.G. (2005). Mammalian photoentrainment: results, methods, and approaches. Methods Enzymol. *393*, 697–726.

Pendergast, J.S., and Yamazaki, S. (2011). Masking responses to light in period mutant mice. Chronobiol. Int. *28*, 657–663.

Peng, C., Rich, E.D., and Varnum, M.D. (2004). Subunit configuration of heteromeric cone cyclic nucleotide-gated channels. Neuron *42*, 401–410.

Perez-Leon, J.A., Warren, E.J., Allen, C.N., Robinson, D.W., and Brown, R.L. (2006). Synaptic inputs to retinal ganglion cells that set the circadian clock. Eur. J. Neurosci. *24*, 1117–1123.

Perry, V.H., and Cowey, A. (1985). The ganglion cell and cone distributions in the monkey's retina: implications for central magnification factors. Vision Res. *25*, 1795–1810.

Petruno, S.K., Clark, R.E., and Reinagel, P. (2013). Evidence That Primary Visual Cortex Is Required for Image, Orientation, and Motion Discrimination by Rats. PLoS ONE *8*, e56543.

Pickard, G.E., Baver, S.B., Ogilvie, M.D., and Sollars, P.J. (2009). Light-Induced Fos Expression in Intrinsically Photosensitive Retinal Ganglion Cells in Melanopsin Knockout (Opn4−/−) Mice. PLoS ONE *4*, e4984.

Pinto, L.H., and Enroth-Cugell, C. (2000). Tests of the mouse visual system. Mamm. Genome *11*, 531–536.

Pinto, L.H., and Troy, J.B. (2008). Survey of the Research Opportunities Afforded by Genetic Variation in the Mouse Visual System. In Eye, Retina, and Visual System of the Mouse, L.M. Chalupa, and R.W. Williams, eds. (Massachusetts Institute od Technology),.

Pinto, L.H., Vitaterna, M.H., Shimomura, K., Siepka, S.M., Balannik, V., McDearmon, E.L., Omura, C., Lumayag, S., Invergo, B.M., Glawe, B., et al. (2007). Generation, identification and functional characterization of the nob4 mutation of Grm6 in the mouse. Vis. Neurosci. *24*, 111–123.

Pires, S.S., Hughes, S., Turton, M., Melyan, Z., Peirson, S.N., Zheng, L., Kosmaoglou, M., Bellingham, J., Cheetham, M.E., Lucas, R.J., et al. (2009). Differential expression of two distinct functional isoforms of melanopsin (Opn4) in the mammalian retina. J. Neurosci. *29*, 12332–12342.

Pittendrigh, C.S., and Daan, S. (1976). A functional analysis of circadian pacemakers in nocturnal rodents. J. Comp. Physiol. *106*, 223–252.

Podolin, P.L., Rollag, M.D., and Brainard, G.C. (1987). The suppression of nocturnal pineal melatonin in the Syrian hamster: dose-response curves at 500 and 360 nm. Endocrinology *121*, 266–270.

Pohl, H. (1992). Ultraviolet radiation: A zeitgeber for the circadian clock in birds. Naturwissenschaften *79*, 227–229.

Porterfield, V.M., Piontkivska, H., and Mintz, E.M. (2007). Identification of novel light-induced genes in the suprachiasmatic nucleus. BMC Neurosci. *8*, 98.

Preitner, N., Damiola, F., Lopez-Molina, L., Zakany, J., Duboule, D., Albrecht, U., and Schibler, U. (2002). The orphan nuclear receptor REV-ERBalpha controls circadian transcription within the positive limb of the mammalian circadian oscillator. Cell *110*, 251–260.

Provencio, I., and Foster, R.G. (1995). Circadian rhythms in mice can be regulated by photoreceptors with cone-like characteristics. Brain Res. *694*, 183–190.

Provencio, I., Jiang, G., De Grip, W.J., Hayes, W.P., and Rollag, M.D. (1998a). Melanopsin: An opsin in melanophores, brain, and eye. Proc. Natl. Acad. Sci. U. S. A. *95*, 340–345.

Provencio, I., Cooper, H.M., and Foster, R.G. (1998b). Retinal projections in mice with inherited retinal degeneration: implications for circadian photoentrainment. J. Comp. Neurol. *395*, 417–439.

Provencio, I., Rollag, M.D., and Castrucci, A.M. (2002). Photoreceptive net in the mammalian retina. This mesh of cells may explain how some blind mice can still tell day from night. Nature *415*, 493.

Prusky, G.T., and Douglas, R.M. (2004). Characterization of mouse cortical spatial vision. Vision Res. *44*, 3411–3418.

Prusky, G.T., and Douglas, R.M. (2008). Measuring Vision in the Awake Behaving Mouse. In Eye, Retina, and Visual System of the Mouse, L.M. Chalupa, and R.W. Williams, eds. (Massachusetts Institute od Technology),.

Prusky, G.T., Alam, N.M., Beekman, S., and Douglas, R.M. (2004). Rapid quantification of adult and developing mouse spatial vision using a virtual optomotor system. Invest. Ophthalmol. Vis. Sci. *45*, 4611–4616.

Prusky, G.T., Alam, N.M., and Douglas, R.M. (2006). Enhancement of Vision by Monocular Deprivation in Adult Mice. J. Neurosci. *26*, 11554–11561.

Prusky, G.T., Silver, B.D., Tschetter, W.W., Alam, N.M., and Douglas, R.M. (2008). Experience-dependent plasticity from eye opening enables lasting, visual cortex-dependent enhancement of motion vision. J. Neurosci. *28*, 9817–9827.

Pugh, E.N., Jr, and Lamb, T.D. (2000). Chapter 5: Phototransduction in Vertebrate Rods and Cones: Molecular Mechanisms of Amplification, Recovery and Light Adaptation. In Handbook of Biological Physics, D.G. Stavenga, W.D. Grip, and E.N. Pugh Jr, eds. (Elsevier), pp. 183–255.

Purves, D. (2001a). Chapter 11. Vision: The Eye. In Neuroscience, G. Augustine, D. Fitzpatrick, L.C. Katz, A.-S. LaMantia, J.O. McNamara, and S.M. Williams, eds. (Sinauer Associates),.

Purves, D. (2001b). Central Projections of Retinal Ganglion Cells. In Neuroscience, G. Augustine, D. Fitzpatrick, L.C. Katz, A.-S. LaMantia, J.O. McNamara, and S.M. Williams, eds. (Sinauer Associates),.

Qiu, X., Kumbalasiri, T., Carlson, S.M., Wong, K.Y., Krishna, V., Provencio, I., and Berson, D.M. (2005). Induction of photosensitivity by heterologous expression of melanopsin. Nature *433*, 745–749.

Rajaratnam, S.M.W., Middleton, B., Stone, B.M., Arendt, J., and Dijk, D.-J. (2004). Melatonin advances the circadian timing of EEG sleep and directly facilitates sleep without altering its duration in extended sleep opportunities in humans. J. Physiol. *561*, 339–351.

Rajchard, J. (2009). Ultraviolet (UV) light perception by birds: a review. Vet. Med. (Praha) *54*, 351–359.

Ralph, M.R., Foster, R.G., Davis, F.C., and Menaker, M. (1990). Transplanted suprachiasmatic nucleus determines circadian period. Science *247*, 975–978.

Raviola, E., and Gilula, N.B. (1975). Intramembrane organization of specialized contacts in the outer plexiform layer of the retina. A freeze-fracture study in monkeys and rabbits. J. Cell Biol. *65*, 192–222.

Rea, M.A. (1992). Different populations of cells in the suprachiasmatic nuclei express c-fos in association with light-induced phase delays and advances of the free-running activity rhythm in hamsters. Brain Res. *579*, 107–112.

Redman, J., Armstrong, S., and Ng, K.T. (1983). Free-running activity rhythms in the rat: entrainment by melatonin. Science *219*, 1089–1091.

Redmond, T.M., Poliakov, E., Yu, S., Tsai, J.-Y., Lu, Z., and Gentleman, S. (2005). Mutation of key residues of RPE65 abolishes its enzymatic role as isomerohydrolase in the visual cycle. Proc. Natl. Acad. Sci. U. S. A. *102*, 13658–13663.

Reischl, S., Vanselow, K., Westermark, P.O., Thierfelder, N., Maier, B., Herzel, H., and Kramer, A. (2007). Beta-TrCP1-mediated degradation of PERIOD2 is essential for circadian dynamics. J. Biol. Rhythms *22*, 375–386.

René Misslin, C.B. (1989). Behavioural validation of a light/dark choice procedure for testing anti-anxiety agents. Behav. Processes 119–132.

Reppert, S.M., and Weaver, D.R. (2002). Coordination of circadian timing in mammals. Nature *418*, 935–941.

Revell, V.L., and Skene, D.J. (2007). Light-induced melatonin suppression in humans with polychromatic and monochromatic light. Chronobiol. Int. *24*, 1125–1137.

Richards, J., and Gumz, M.L. (2012). Advances in understanding the peripheral circadian clocks. FASEB J. Off. Publ. Fed. Am. Soc. Exp. Biol. *26*, 3602–3613.

Robinson, L., Bridge, H., and Riedel, G. (2001). Visual discrimination learning in the water maze: a novel test for visual acuity. Behav. Brain Res. *119*, 77–84.

Robinson, L., Harbaran, D., and Riedel, G. (2004). Visual acuity in the water maze: sensitivity to muscarinic receptor blockade in rats and mice. Behav. Brain Res. *151*, 277–286.

Rodieck, R.W., and Watanabe, M. (1993). Survey of the morphology of macaque retinal ganglion cells that project to the pretectum, superior colliculus, and parvicellular laminae of the lateral geniculate nucleus. J. Comp. Neurol. *338*, 289–303.

Röhlich, P., van Veen, T., and Szél, A. (1994). Two different visual pigments in one retinal cone cell. Neuron *13*, 1159–1166.

Ross, M.R., Gillespie, K.L., Hopper, L.M., Bloomsmith, M.A., and Maple, T.L. (2013). Differential preference for ultraviolet light among captive birds from three ecological habitats. Appl. Anim. Behav. Sci. *147*, 278–285.

Ruan, G.-X., Zhang, D.-Q., Zhou, T., Yamazaki, S., and McMahon, D.G. (2006). Circadian organization of the mammalian retina. Proc. Natl. Acad. Sci. U. S. A. *103*, 9703–9708.

Ruby, N.F., Brennan, T.J., Xie, X., Cao, V., Franken, P., Heller, H.C., and O'Hara, B.F. (2002). Role of melanopsin in circadian responses to light. Science *298*, 2211–2213.

Rudic, R.D., McNamara, P., Curtis, A.-M., Boston, R.C., Panda, S., Hogenesch, J.B., and FitzGerald, G.A. (2004). BMAL1 and CLOCK, Two Essential Components of the Circadian Clock, Are Involved in Glucose Homeostasis. PLoS Biol. *2*.

Rusak, B., Robertson, H.A., Wisden, W., and Hunt, S.P. (1990). Light pulses that shift rhythms induce gene expression in the suprachiasmatic nucleus. Science *248*, 1237–1240.

Saari, J.C., and Bredberg, D.L. (1989). Lecithin:retinol acyltransferase in retinal pigment epithelial microsomes. J. Biol. Chem. *264*, 8636–8640.

Saari, J.C., Bredberg, L., and Garwin, G.G. (1982). Identification of the endogenous retinoids associated with three cellular retinoid-binding proteins from bovine retina and retinal pigment epithelium. J. Biol. Chem. *257*, 13329–13333.

Saari, J.C., Nawrot, M., Kennedy, B.N., Garwin, G.G., Hurley, J.B., Huang, J., Possin, D.E., and Crabb, J.W. (2001). Visual cycle impairment in cellular retinaldehyde binding protein (CRALBP) knockout mice results in delayed dark adaptation. Neuron *29*, 739–748.

Sack, R.L., Lewy, A.J., and Hughes, R.J. (1998). Use of melatonin for sleep and circadian rhythm disorders. Ann. Med. *30*, 115–121.

Sagar, S.M., and Sharp, F.R. (1990). Light induces a Fos-like nuclear antigen in retinal neurons. Mol. Brain Res. *7*, 17–21.

Sakamoto, K., Oishi, K., Shiraishi, M., Hamano, S., Otsuka, H., Miyake, Y., and Ishida, N. (2000). Two circadian oscillatory mechanisms in the mammalian retina. Neuroreport *11*, 3995–3997.

Sakurai, K., Onishi, A., Imai, H., Chisaka, O., Ueda, Y., Usukura, J., Nakatani, K., and Shichida, Y. (2007). Physiological properties of rod photoreceptor cells in green-sensitive cone pigment knock-in mice. J. Gen. Physiol. *130*, 21–40.

Saper, C.B., Scammell, T.E., and Lu, J. (2005). Hypothalamic regulation of sleep and circadian rhythms. Nature *437*, 1257–1263.

Sato, T.K., Panda, S., Miraglia, L.J., Reyes, T.M., Rudic, R.D., McNamara, P., Naik, K.A., FitzGerald, G.A., Kay, S.A., and Hogenesch, J.B. (2004). A functional genomics strategy reveals Rora as a component of the mammalian circadian clock. Neuron *43*, 527–537.

Schaeffel, F. (2008). The Mouse as a Model for Myopia and Optics of Its Eye. In Eye, Retina, and Visual System of the Mouse, L.M. Chalupa, and R.W. Williams, eds. (Massachusetts Institute od Technology),.

Von Schantz, M., Argamaso-Hernan, S.M., Szél, A., and Foster, R.G. (1997). Photopigments and photoentrainment in the Syrian golden hamster. Brain Res. *770*, 131–138.

Schmidt, T.M., and Kofuji, P. (2009). Functional and morphological differences among intrinsically photosensitive retinal ganglion cells. J. Neurosci. *29*, 476–482.

Schmidt, T.M., and Kofuji, P. (2010). Differential cone pathway influence on intrinsically photosensitive retinal ganglion cell subtypes. J. Neurosci. *30*, 16262–16271.

Schmidt, T.M., and Kofuji, P. (2011). Structure and function of bistratified intrinsically photosensitive retinal ganglion cells in the mouse. J. Comp. Neurol. *519*, 1492–1504.

Schmidt, T.M., Taniguchi, K., and Kofuji, P. (2008). Intrinsic and Extrinsic Light Responses in Melanopsin-Expressing Ganglion Cells During Mouse Development. J. Neurophysiol. *100*, 371–384.

Schmidt, T.M., Do, M.T.H., Dacey, D., Lucas, R., Hattar, S., and Matynia, A. (2011). Melanopsin-Positive Intrinsically Photosensitive Retinal Ganglion Cells: From Form to Function. J. Neurosci. *31*, 16094–16101.

Schmucker, C., Seeliger, M., Humphries, P., Biel, M., and Schaeffel, F. (2005). Grating acuity at different luminances in wild-type mice and in mice lacking rod or cone function. Invest. Ophthalmol. Vis. Sci. *46*, 398–407.

Schwartz, W.J., Tavakoli-Nezhad, M., Lambert, C.M., Weaver, D.R., and de la Iglesia, H.O. (2011). Distinct patterns of Period gene expression in the suprachiasmatic nucleus underlie circadian clock photoentrainment by advances or delays. Proc. Natl. Acad. Sci. U. S. A. *108*, 17219–17224.

Sekaran, S., Foster, R.G., Lucas, R.J., and Hankins, M.W. (2003). Calcium imaging reveals a network of intrinsically light-sensitive inner-retinal neurons. Curr. Biol. CB *13*, 1290–1298.

Sekaran, S., Lupi, D., Jones, S.L., Sheely, C.J., Hattar, S., Yau, K.-W., Lucas, R.J., Foster, R.G., and Hankins, M.W. (2005). Melanopsin-dependent photoreception provides earliest light detection in the mammalian retina. Curr. Biol. CB *15*, 1099–1107.

Semo, M., Lupi, D., Peirson, S.N., Butler, J.N., and Foster, R.G. (2003). Light-induced c-fos in melanopsin retinal ganglion cells of young and aged rodless/coneless (rd/rd cl) mice. Eur. J. Neurosci. *18*, 3007–3017.

Semo, M., Gias, C., Ahmado, A., Sugano, E., Allen, A.E., Lawrence, J.M., Tomita, H., Coffey, P.J., and Vugler, A.A. (2010). Dissecting a role for melanopsin in behavioural light aversion reveals a response independent of conventional photoreception. PloS One *5*, e15009.

Sexton, T., Buhr, E., and Gelder, R.N.V. (2012). Melanopsin and Mechanisms of Non-visual Ocular Photoreception. J. Biol. Chem. *287*, 1649–1656.

Shanahan, T.L., and Czeisler, C.A. (1991). Light exposure induces equivalent phase shifts of the endogenous circadian rhythms of circulating plasma melatonin and core body temperature in men. J. Clin. Endocrinol. Metab. *73*, 227–235.

Sharma, V.K., Chandrashekaran, M.K., Singaravel, M., and Subbaraj, R. (1998). Ultraviolet-light-evoked phase shifts in the locomotor activity rhythm of the field mouse Mus booduga. J. Photochem. Photobiol. B *45*, 83–86.

Sharma, V.K., Chandrashekaran, M.K., Singaravel, M., and Subbaraj, R. (1999). Relationship between light intensity and phase resetting in a mammalian circadian system. J. Exp. Zool. *283*, 181–185.

Sharma, V.K., Chidambaram, R., Singh, T.J., Lingakumar, K., Subbaraj, R., and Chandrashekaran, M.K. (2000). Irradiance dependency of UV-A induced phase shifts in the locomotor activity rhythm of the field mouse Mus booduga. Chronobiol. Int. *17*, 777–782.

Sharpe, L.T., and Stockman, A. (1999). Rod pathways: the importance of seeing nothing. Trends Neurosci. *22*, 497–504.

Shearman, L.P., Jin, X., Lee, C., Reppert, S.M., and Weaver, D.R. (2000). Targeted disruption of the mPer3 gene: subtle effects on circadian clock function. Mol. Cell. Biol. *20*, 6269–6275.

Shi, G., Yau, K.-W., Chen, J., and Kefalov, V.J. (2007). Signaling Properties of a Short-Wave Cone Visual Pigment and Its Role in Phototransduction. J. Neurosci. *27*, 10084–10093.

Shimba, S., Ishii, N., Ohta, Y., Ohno, T., Watabe, Y., Hayashi, M., Wada, T., Aoyagi, T., and Tezuka, M. (2005). Brain and muscle Arnt-like protein-1 (BMAL1), a component of the molecular clock, regulates adipogenesis. Proc. Natl. Acad. Sci. U. S. A. *102*, 12071–12076.

Shirogane, T., Jin, J., Ang, X.L., and Harper, J.W. (2005). SCFbeta-TRCP controls clock-dependent transcription via casein kinase 1-dependent degradation of the mammalian period-1 (Per1) protein. J. Biol. Chem. *280*, 26863–26872.

Siepka, S.M., Yoo, S.-H., Park, J., Song, W., Kumar, V., Hu, Y., Lee, C., and Takahashi, J.S. (2007). Circadian mutant Overtime reveals F-box protein FBXL3 regulation of cryptochrome and period gene expression. Cell *129*, 1011–1023.

Silvers, J.M., Harrod, S.B., Mactutus, C.F., and Booze, R.M. (2007). Automation of the novel object recognition task for use in adolescent rats. J. Neurosci. Methods *166*, 99–103.

Simpson, J.I. (1984). The Accessory Optic System. Annu. Rev. Neurosci. *7*, 13–41.

Sirotin, Y.B., and Das, A. (2010). Zooming in on mouse vision. Nat. Neurosci. *13*, 1045–1046.

Smallwood, P.M., Olveczky, B.P., Williams, G.L., Jacobs, G.H., Reese, B.E., Meister, M., and Nathans, J. (2003). Genetically engineered mice with an additional class of cone photoreceptors: implications for the evolution of color vision. Proc. Natl. Acad. Sci. U. S. A. *100*, 11706–11711.

Smith, R.G., Freed, M.A., and Sterling, P. (1986). Microcircuitry of the dark-adapted cat retina: functional architecture of the rod-cone network. J. Neurosci. *6*, 3505–3517.

Soucy, E., Wang, Y., Nirenberg, S., Nathans, J., and Meister, M. (1998). A novel signaling pathway from rod photoreceptors to ganglion cells in mammalian retina. Neuron *21*, 481–493.

Sperling, H.G., and Mills, S.L. (1991). Red-green interactions in the spectral sensitivity of primates as derived from ERG and behavioral data. Vis. Neurosci. *7*, 75–86.

Stein, B.E., and Wallace, M.T. (1996). Comparisons of cross-modality integration in midbrain and cortex. Prog. Brain Res. *112*, 289–299.

Stein, B.E., Wallace, M.W., Stanford, T.R., and Jiang, W. (2002). Book Review: Cortex Governs Multisensory Integration in the Midbrain. The Neuroscientist *8*, 306–314.

Stolz, G., Aschoff, J.C., Aschoff, J., and Born, J. (1987). Circadian variation in the visual evoked potential (VEP). Electroencephalogr. Clin. Neurophysiol. Suppl. *40*, 279–283.

Stone, J. (1978). The number and distribution of ganglion cells in the cat's retina. J. Comp. Neurol. *180*, 753–771.

Straif, K., Baan, R., Grosse, Y., Secretan, B., El Ghissassi, F., Bouvard, V., Altieri, A., Benbrahim-Tallaa, L., and Cogliano, V. (2007). Carcinogenicity of shift-work, painting, and fire-fighting. Lancet Oncol. *8*, 1065–1066.

Strettoi, E. (2008). Synaptic Organization of the Mouse Retina. In Eye, Retina, and Visual System of the Mouse, L.M. Chalupa, and R.W. Williams, eds. (Massachusetts Institute od Technology),.

Strettoi, E., Raviola, E., and Dacheux, R.F. (1992). Synaptic connections of the narrow-field, bistratified rod amacrine cell (AII) in the rabbit retina. J. Comp. Neurol. *325*, 152–168.

Szél, Á., and Röhlich, P. (1992). Two cone types of rat retina detected by anti-visual pigment antibodies. Exp. Eye Res. *55*, 47–52.

Szél, A., Röhlich, P., Caffé, A.R., Juliusson, B., Aguirre, G., and Van Veen, T. (1992). Unique topographic separation of two spectral classes of cones in the mouse retina. J. Comp. Neurol. *325*, 327–342.

Szél, A., Röhlich, P., Mieziewska, K., Aguirre, G., and van Veen, T. (1993). Spatial and temporal differences between the expression of short- and middle-wave sensitive cone pigments in the mouse retina: a developmental study. J. Comp. Neurol. *331*, 564–577.

Szél, A., Röhlich, P., Caffé, A.R., and van Veen, T. (1996). Distribution of cone photoreceptors in the mammalian retina. Microsc. Res. Tech. *35*, 445–462.

Taglialatela, G., Hogan, D., Zhang, W.-R., and Dineley, K.T. (2009). Intermediate- and long-term recognition memory deficits in Tg2576 mice are reversed with acute calcineurin inhibition. Behav. Brain Res. *200*, 95–99.

Tam, S.K.E., Robinson, J., Jennings, D.J., and Bonardi, C. (2014). Dissociations in the effect of delay on object recognition: evidence for an associative model of recognition memory. J. Exp. Psychol. Anim. Learn. Cogn. *40*, 106–115.

Tarttelin, E.E., Bellingham, J., Bibb, L.C., Foster, R.G., Hankins, M.W., Gregory-Evans, K., Gregory-Evans, C.Y., Wells, D.J., and Lucas, R.J. (2003). Expression of opsin genes early in ocular development of humans and mice. Exp. Eye Res. *76*, 393–396.

Teclemariam-Mesbah, R., Ter Horst, G.J., Postema, F., Wortel, J., and Buijs, R.M. (1999). Anatomical demonstration of the suprachiasmatic nucleus-pineal pathway. J. Comp. Neurol. *406*, 171–182.

Thaung, C., Arnold, K., Jackson, I.J., and Coffey, P.J. (2002). Presence of visual head tracking differentiates normal sighted from retinal degenerate mice. Neurosci. Lett. *325*, 21–24.

Thompson, S., Foster, R.G., Stone, E.M., Sheffield, V.C., and Mrosovsky, N. (2008). Classical and melanopsin photoreception in irradiance detection: negative masking of locomotor activity by light. Eur. J. Neurosci. *27*, 1973–1979.

Toda, K., Bush, R.A., Humphries, P., and Sieving, P.A. (1999). The electroretinogram of the rhodopsin knockout mouse. Vis. Neurosci. *16*, 391–398.

Travis, G.H., Golczak, M., Moise, A.R., and Palczewski, K. (2007). Diseases caused by defects in the visual cycle: retinoids as potential therapeutic agents. Annu. Rev. Pharmacol. Toxicol. *47*, 469–512.

Tsai, J.W., Hannibal, J., Hagiwara, G., Colas, D., Ruppert, E., Ruby, N.F., Heller, H.C., Franken, P., and Bourgin, P. (2009). Melanopsin as a Sleep Modulator: Circadian Gating of the Direct Effects of Light on Sleep and Altered Sleep Homeostasis in Opn4−/− Mice. PLoS Biol *7*, e1000125.

Tu, D.C., Zhang, D., Demas, J., Slutsky, E.B., Provencio, I., Holy, T.E., and Van Gelder, R.N. (2005). Physiologic diversity and development of intrinsically photosensitive retinal ganglion cells. Neuron *48*, 987–999.

Ukai-Tadenuma, M., Yamada, R.G., Xu, H., Ripperger, J.A., Liu, A.C., and Ueda, H.R. (2011). Delay in feedback repression by cryptochrome 1 is required for circadian clock function. Cell *144*, 268–281.

Umino, Y., Solessio, E., and Barlow, R.B. (2008). Speed, spatial, and temporal tuning of rod and cone vision in mouse. J. Neurosci. *28*, 189–198.

Underwood, T., and Sealy, S. (2008). UV reflectance of eggs of brown-headed cowbirds (Molothrus ater) and accepter and rejecter hosts. J Ornithol *149*, 313–321.

vanderLeest, H.T., Rohling, J.H.T., Michel, S., and Meijer, J.H. (2009). Phase shifting capacity of the circadian pacemaker determined by the SCN neuronal network organization. PloS One *4*, e4976.

Vecino, E., Hernández, M., and García, M. (2004). Cell death in the developing vertebrate retina. Int. J. Dev. Biol. *48*, 965–974.

Vindlacheruvu, R.R., Ebling, F.J.P., Maywood, E.S., and Hastings, M.H. (1992). Blockade of Glutamatergic Neurotransmission in the Suprachiasmatic Nucleus Prevents Cellular and Behavioural Responses of the Circadian System to Light. Eur. J. Neurosci. *4*, 673–679.

Viney, T.J., Balint, K., Hillier, D., Siegert, S., Boldogkoi, Z., Enquist, L.W., Meister, M., Cepko, C.L., and Roska, B. (2007). Local retinal circuits of melanopsin-containing ganglion cells identified by transsynaptic viral tracing. Curr. Biol. CB *17*, 981–988.

Vitaterna, M.H., King, D.P., Chang, A.M., Kornhauser, J.M., Lowrey, P.L., McDonald, J.D., Dove, W.F., Pinto, L.H., Turek, F.W., and Takahashi, J.S. (1994). Mutagenesis and mapping of a mouse gene, Clock, essential for circadian behavior. Science *264*, 719–725.

Vitaterna, M.H., Selby, C.P., Todo, T., Niwa, H., Thompson, C., Fruechte, E.M., Hitomi, K., Thresher, R.J., Ishikawa, T., Miyazaki, J., et al. (1999). Differential regulation of mammalian Period genes and circadian rhythmicity by cryptochromes 1 and 2. Proc. Natl. Acad. Sci. *96*, 12114–12119.

Vitaterna, M.H., Ko, C.H., Chang, A.-M., Buhr, E.D., Fruechte, E.M., Schook, A., Antoch, M.P., Turek, F.W., and Takahashi, J.S. (2006). The mouse Clock mutation reduces circadian pacemaker amplitude and enhances efficacy of resetting stimuli and phase-response curve amplitude. Proc. Natl. Acad. Sci. U. S. A. *103*, 9327–9332.

Völgyi, B., Deans, M.R., Paul, D.L., and Bloomfield, S.A. (2004). Convergence and segregation of the multiple rod pathways in mammalian retina. J. Neurosci. *24*, 11182–11192.

Völgyi, B., Chheda, S., and Bloomfield, S.A. (2009). Tracer coupling patterns of the ganglion cell subtypes in the mouse retina. J. Comp. Neurol. *512*, 664–687.

Vugler, A.A., Redgrave, P., Semo, M., Lawrence, J., Greenwood, J., and Coffey, P.J. (2007). Dopamine neurones form a discrete plexus with melanopsin cells in normal and degenerating retina. Exp. Neurol. *205*, 26–35.

Wang, J.-S., and Kefalov, V.J. (2011). The cone-specific visual cycle. Prog. Retin. Eye Res. *30*, 115–128.

Wang, L., Sarnaik, R., Rangarajan, K., Liu, X., and Cang, J. (2010). Visual Receptive Field Properties of Neurons in the Superficial Superior Colliculus of the Mouse. J. Neurosci. *30*, 16573–16584.

Wang, Y., Macke, J.P., Merbs, S.L., Zack, D.J., Klaunberg, B., Bennett, J., Gearhart, J., and Nathans, J. (1992). A locus control region adjacent to the human red and green visual pigment genes. Neuron *9*, 429–440.

Waterhouse, J.M., and DeCoursey, P.J. (2004). The relevance of circadian rhythms for human welfare. In Chronobiology: Biological Timekeeping, (Sunderland, MA: Sinauer), pp. 325–358.

Weaver, D.R. (1998). The suprachiasmatic nucleus: a 25-year retrospective. J. Biol. Rhythms *13*, 100–112.

Wehner, R. (1989). Neurobiology of polarization vision. Trends Neurosci. *12*, 353–359.

Weitz, D., Ficek, N., Kremmer, E., Bauer, P.J., and Kaupp, U.B. (2002). Subunit stoichiometry of the CNG channel of rod photoreceptors. Neuron *36*, 881–889.

Welsh, D.K., Logothetis, D.E., Meister, M., and Reppert, S.M. (1995). Individual neurons dissociated from rat suprachiasmatic nucleus express independently phased circadian firing rhythms. Neuron *14*, 697–706.

Whishaw, I.Q. (1995). A comparison of rats and mice in a swimming pool place task and matching to place task: some surprising differences. Physiol. Behav. *58*, 687–693.

Whitt, E., and Robinson, J. (2013). Improved spontaneous object recognition following spaced preexposure trials: evidence for an associative account of recognition memory. J. Exp. Psychol. Anim. Behav. Process. *39*, 174–179.

Wilden, U., Hall, S.W., and Kühn, H. (1986). Phosphodiesterase activation by photoexcited rhodopsin is quenched when rhodopsin is phosphorylated and binds the intrinsic 48-kDa protein of rod outer segments. Proc. Natl. Acad. Sci. U. S. A. *83*, 1174–1178.

Wilks, T.A., Harvey, A.R., and Rodger, J. (2013). Chapter 12: Seeing with Two Eyes: Integration of Binocular Retinal Projections in the Brain. In Functional Brain Mapping and the Endeavor to Understand the Working Brain, F. Signorelli, and D. Chirchiglia, eds.

Winters, B.D., and Reid, J.M. (2010). A Distributed Cortical Representation Underlies Crossmodal Object Recognition in Rats. J. Neurosci. *30*, 6253–6261.

Wollnik, F., Brysch, W., Uhlmann, E., Gillardon, F., Bravo, R., Zimmermann, M., Schlingensiepen, K.H., and Herdegen, T. (1995). Block of c-Fos and JunB expression by antisense oligonucleotides inhibits light-induced phase shifts of the mammalian circadian clock. Eur. J. Neurosci. *7*, 388–393.

Wong, K.Y. (2012). A Retinal Ganglion Cell That Can Signal Irradiance Continuously for Ten Hours. J. Neurosci. *32*, 11478–11485.

Wong, K.Y., Dunn, F.A., Graham, D.M., and Berson, D.M. (2007). Synaptic influences on rat ganglion-cell photoreceptors. J. Physiol. *582*, 279–296.

Wyatt, J.K., Dijk, D.-J., Ritz-de Cecco, A., Ronda, J.M., and Czeisler, C.A. (2006). Sleep-facilitating effect of exogenous melatonin in healthy young men and women is circadian-phase dependent. Sleep *29*, 609–618.

Van Wyk, M., Taylor, W.R., and Vaney, D.I. (2006). Local edge detectors: a substrate for fine spatial vision at low temporal frequencies in rabbit retina. J. Neurosci. *26*, 13250–13263.

Xu, J., Morris, L.M., Michalakis, S., Biel, M., Fliesler, S.J., Sherry, D.M., and Ding, X.-Q. (2012). CNGA3 deficiency affects cone synaptic terminal structure and function and leads to secondary rod dysfunction and degeneration. Invest. Ophthalmol. Vis. Sci. *53*, 1117–1129.

Yam, J.C.S., and Kwok, A.K.H. (2014). Ultraviolet light and ocular diseases. Int. Ophthalmol. *34*, 383–400.

Yao, G., Zhang, K., Bellassai, M., Chang, B., and Lei, B. (2006). Ultraviolet light-induced and green light-induced transient pupillary light reflex in mice. Curr. Eye Res. *31*, 925–933.

Yokoyama, S., Radlwimmer, F.B., and Kawamura, S. (1998). Regeneration of ultraviolet pigments of vertebrates. Febs Lett. *423*, 155–158.

Yokoyama, S., Radlwimmer, F.B., and Blow, N.S. (2000). Ultraviolet pigments in birds evolved from violet pigments by a single amino acid change. Proc. Natl. Acad. Sci. *97*, 7366–7371.

Yoshida, K., Kawamura, K., and Imaki, J. (1993). Differential expression of c-fos mRNA in rat retinal cells: regulation by light/dark cycle. Neuron *10*, 1049–1054.

Yu, D.-Y., Cringle, S., Valter, K., Walsh, N., Lee, D., and Stone, J. (2004). Photoreceptor death, trophic factor expression, retinal oxygen status, and photoreceptor function in the P23H rat. Invest. Ophthalmol. Vis. Sci. *45*, 2013–2019.

Zaidi, F.H., Hull, J.T., Peirson, S.N., Wulff, K., Aeschbach, D., Gooley, J.J., Brainard, G.C., Gregory-Evans, K., Rizzo, J.F., 3rd, Czeisler, C.A., et al. (2007). Short-wavelength light sensitivity of circadian, pupillary, and visual awareness in humans lacking an outer retina. Curr. Biol. CB *17*, 2122–2128.

Zhang, D.-Q., Wong, K.Y., Sollars, P.J., Berson, D.M., Pickard, G.E., and McMahon, D.G. (2008). Intraretinal signaling by ganglion cell photoreceptors to dopaminergic amacrine neurons. Proc. Natl. Acad. Sci. U. S. A. *105*, 14181–14186.

Zhao, X., Stafford, B.K., Godin, A.L., King, W.M., and Wong, K.Y. (2014). Photoresponse diversity among the five types of intrinsically photosensitive retinal ganglion cells. J. Physiol. *592*, 1619–1636.

Zheng, B., Albrecht, U., Kaasik, K., Sage, M., Lu, W., Vaishnav, S., Li, Q., Sun, Z.S., Eichele, G., Bradley, A., et al. (2001). Nonredundant roles of the mPer1 and mPer2 genes in the mammalian circadian clock. Cell *105*, 683–694.

Zhu, Y., Tu, D.C., Denner, D., Shane, T., Fitzgerald, C.M., and Gelder, R.N.V. (2007). Melanopsin-Dependent Persistence and Photopotentiation of Murine Pupillary Light Responses. Invest. Ophthalmol. Vis. Sci. *48*, 1268–1275.

Zuclich, J.A., Previc, F.H., Novar, B.J., and Edsall, P.R. (2005). Near-UV/blue light-induced fluorescence in the human lens: potential interference with visual function. J. Biomed. Opt. *10*, 044021–044021 – 7.

(2008). Eye, Retina, and Visual System of the Mouse (Massachusetts Institute od Technology).